# Identification of the extent of artisanal coal mining and related acid mine water hazards using remote sensing and field sampling: A case study in Jaiñtia Hills of North-eastern India

Bantehsonglang Blahwar
January, 2010

# Identification of the extent of artisanal coal mining and related acid mine water hazards using remote sensing and field sampling: A case study in Jaiñtia Hills of North-eastern India

by

Bantehsonglang Blahwar

Thesis submitted to the International Institute for Geo-information Science and Earth Observation and the Indian Institute of Remote Sensing in partial fulfilment of the requirements for the degree of Master of Science in Geo-information Science and Earth Observation, Specialization: Geo-hazards

**Thesis Assessment Board**
Chairman: Prof. Dr. Victor Jetten
External Examiner: Dr. Saumitra Mukherjee, JNU, New Delhi
IIRS Member: Dr. P. K. Champatiray
IIRS Member: Dr. S.K. Srivastava
ITC Member: Drs. Michiel Damen

**Thesis Supervisors**
Dr. S. K. Srivastava, IIR
Drs. J. B. de Smeth, ITC

**INTERNATIONAL INSTITUTE FOR GEO-INFORMATION SCIENCE AND EARTH OBSERVATION**
**ENSCHEDE, THE NETHERLANDS**
**&**
**INDIAN INSTITUTE OF REMOTE SENSING, NATIONAL REMOTE SENSING CENTRE,**
**I.S.R.O., DEPARTMENT OF SPACE, GOVT. 0F INDIA, DEHRADUN, INDIA**

# Disclaimer

*"Commit to the LORD whatever you do, and your plans will succeed."*

*Proverbs 16:3*

# Abstract

Coal is being mined in several districts in the state of Meghalaya, India with the highest production coming from the Jaiñtia Hills district. Due to Constitutional rights allowing the indigenous tribal population to have the complete ownership of their land, including its subsurface resources, coal mining in the State has been carried out by many individuals at a cottage scale level. Coal is extracted using an artisanal method of underground mining which is called as "rat-hole" mining. The mining of coal in this district has brought about several environmental changes including degradation in surface water quality due to *acid mine drainage* (AMD) as reported in literature. AMD is caused by the oxidation and hydrolysis of metal sulphides, particularly pyrites, found in coal, deposit over-burden and in the waste dumps releasing large quantities of sulphates and protons, thereby lowering the pH of the water bodies. Highly acidic water leaches metals from surrounding rocks and soils adding to the deterioration of water quality in the mining areas. Metals stay in solution till the pH rises further downstream in a water course through dilution from incoming non-polluted tributaries and they precipitate out or get adsorbed by water colloidal particles and stream bed sediments. This creates another environmental problem with stream beds coated with amorphous iron oxide/hydroxide precipitates and high metal concentrations in the sediments which make the streams toxic.

The main objectives of this study are: (1) to use remote sensing to identify and map the extent of artisanal coal mines in the Umiurem-Umtarang watershed in the central Jaiñtia Hills district, (2) to carry out an object based classification for semi-automatic identification and mapping of the coal mines, (3) to determine the hydro-chemical characteristics of AMD in surface water by field survey, sampling and analysis, (4) to assess the presence of undesirably high heavy metal concentrations in water samples and sediments in the watershed, and (5) to map the spatial variability of concentrations of different pollutants along the streams in the watershed.

Visual analysis of the merged CARTOSAT-1 and RESOURCESAT-1 (IRS-P6) LISS-IV image shows high density of coal mines in the southern portion of the study area comprising of Tura sandstones of Jaiñtia Group. This map, when compared with that interpreted from a pan-sharpened QuickBird (PAN – spatial resolution 0.61m at nadir and multi-spectral – spatial resolution 2.44m at nadir) image, yielded an accuracy of 46% by polygon count and 59% by area comparison. The lower accuracy is primarily because of the lower spatial resolution of the merged CARTOSAT-1/RESOURCESAT-1 image whereby clusters of many mines seen on the QuickBird image appeared as a single big mine. Further, several older mines with darker overburden signatures due to overgrowth merged with the background vegetation or barren land and their identification was missed out in the visual interpretation of merged CARTOSAT-1/RESOURCESAT-1 image.

An algorithm is developed to semi-automatically classify the coal mines through an *object oriented classification* (OOC) approach using the Definiens Developer 7 software. OOC results are found to be much superior over pixel-based supervised classification using Maximum Likelihood Classifier (MXL) since OOC approach considers spectral, textural and shape characters of each segmented image object for classification. While MXL produced inconclusive results, the OOC approach produced an overall accuracy of 67% when compared with the visually interpreted merged CARTOSAT-1/RESOURCESAT-1 image. The error of omission is 33% but the error of commission is quite high at 54%. The high error of commission is mainly because of the misclassification of many

objects of roads and settlements as they had similar spectral, textural and shape (due to *quadtree* method of segmentation) characteristics as that of coal mines. These were the main reasons for a high error of commission. The OOC algorithm developed on CARTOSAT-1/RESOURCESAT-1 data is also tested on pan-sharpened QuickBird data in a small subset of the study area. The overall accuracy of OOC based output on QuickBird data is found as 72% with commission and omission errors of 15% and 28% respectively.

Field sampling and analysis of streamwater samples during the monsoon and post-monsoon periods reveal that at many locations in proximity to coal mines, water quality is affected by AMD. While water is generally of acidic nature (pH ranging between 2.74 and 7.4) throughout the study area because of intense leaching, the effect of AMD is observed in the southern portion of the watershed where there is high density of coal mines, as seen through remote sensing data. It is also observed that at locations affected by AMD (characterized by low pH and high acidity) streamwaters also contain high concentration of sulphate, iron and manganese. Concentrations of heavy metals in streamwaters and sediments, on the other hand, have not reached alarming levels in the study area. These results show that oxidation and dissolution of pyrites associated with coal and overburden material is the primary reason for AMD in the study area. It is also concluded that the coal/coal bearing formations do not contain appreciable amounts of trace metals in the sulphide minerals. The evidence of AMD is also seen in the form of presence of iron oxide/hydroxide precipitates on the stream beds downstream of coal mining activity. Such precipitates can also be seen through pan-sharpened QuickBird image (true color composite) and color ratio composites of Landsat ETM+.

Heavy metals, barring iron and manganese, are found to be within permissible limits in water samples. In the stream sediments, except for cadmium, they are also found to be less than the Threshold Effect Concentrations (TEC's), below which harmful effects on sediment-dwelling organisms are not expected. However, in no cases are the heavy metals or other metals higher than the Probable Effect Concentrations (PEC's), above which harmful effects on sediment-dwelling organisms are expected to occur frequently. The predicted incidence of toxicity in the stream sediments during monsoon varies from 9% to 23% and during post-monsoon varies from 4% to 32%, indicating low impact on sediment-dwelling organisms.

# Acknowledgements

First and foremost, I would like to thank The Almighty, for giving me the opportunity and the health and strength to be here and to complete my degree from this reputed institute.

I wish to express my profound gratitude to my supervisors, Dr.S.K.Srivastava, IIRS and Drs.J.B.de Smeth, ITC, for their guidance and constant help throughout the course of this study. Their useful suggestions and meticulous scrutiny of the work are gratefully acknowledged. I would like to specially thank Drs.J.B.de Smeth for analysing the sediment samples.

I extend my gratitude to Mr.H.Prasad, former Chairman, Mr.A.Biswa, Chairman, and Mr.D.Hooroo, Member Secretary, Meghalaya State Pollution Control Board, Shillong, without whose approval and grant of necessary leave, I would not have been here in the first place. I would also like to thank Dr.V.K.Dadhwal, Dean, IIRS and his colleagues who found me competent to study this course.

Special mention has to be made of Dr.V.Hari Prasad, former Programme Co-ordinator, Geo-hazards, for all his guidance, help and advice; especially before my trip to ITC. I also extend my gratitude to Dr.Suresh Kumar, Programme Co-ordinator and Mr.I.C.Das, Course Co-ordinator, Geo-hazards for their help throughout the course.

Special thanks go out to my colleagues and friends at the Meghalaya State Pollution Control Board, especially Shai, Deswyn, Jonathan, Malvin, Sandrew, Arches, Donnycia, Lurshai, Scoling, Con and Kalita, for their help and assistance during my field work and analysis. I wish to express my thanks and gratitude to my senior colleagues Mr.J.H.Nengnong, Dr.(Ms)B.Nongbri, Mr.W.R.Kharkrang, Mrs.B.Majaw and Mrs.J.Sawian for their useful guidance and advice.

I would like to thank Ms.Minakshi Kumar, PRSD, IIRS for her help with the object oriented classification and Mr.Ram Mohan Rao, GID, IIRS for providing me with computer facilities at his Division to carry out image segmentation.

I would like to express sincere gratitude to Mr.F.Blah, Chief Forest Officer, Jaiñtia Hills Autonomous District Council, Jowai for all his help and for allowing his staff to guide me during my field work. I wish to thank Dr.M.K.Sarma, Deputy Director, Directorate of Mineral Resources, Government of Meghalaya for sparing his time to go out of his way to provide me with all the data in his department.

I am grateful to my senior Mahendra Singh, for helping me with the pre-field laboratory preparations. I also thank my friends, Don, for all the data and information from NEHU; Daniel, Wet, Hope and Len for their help during monsoon sampling; Nitajan for guiding me in the field during post-monsoon sampling.

I wish to extend my gratitude to all my teachers at IIRS and ITC for the wealth of information they have imparted to me throughout the course. Special thanks to the Computer Management staff at IIRS, who have kept our desktops in perfect condition for the past 18 months.

I would like to thank my friends, Richa, Vikas, Jagannath, Tuba, Veena, Sananda, Arnab, Dipanwita, S.P.Singh and my other batch-mates for a fabulous 18 months together.

Last but not least, I am eternally indebted to my parents for their love, prayers, constant support and encouragement. I thank my brothers for their company during my field work and my sisters for all the encouragement and support. I thank Gracel for being there always.

(BANTEHSONGLANG BLAHWAR)

# Table of contents

# List of figures

# List of tables

# 1. Introduction

## 1.1. Introduction

The mining and use of coal has been in existence for ages. Though it is not clear who first discovered the uses of coal, but its history can be traced back several centuries before the birth of Christ. Theophrastus, a pupil of Aristotle, who lived nearly three hundred years before Christ, was perhaps the first ancient author to have mentioned about coal (Bank, 1883). Bank (1883) also wrote that the Romans knew about the uses of coal since the time of Julius Caesar’s invasion of Great Britain (55 – 54 BC) and that the coalfields of Great Britain were, perhaps, the first to be opened during the time of the Roman occupation (AD 43 till AD 410). The Encyclopædia Britannica Online (2009) reported that the Hopi Indians of the present day’s south-western United States of America used coal for heating, cooking and in ceremonial chambers since the 12th century AD. Marco Polo wrote in his memoirs that there was widespread use of coal by the Chinese in the 13th century AD (Britannica, 2009).

Initially, coal was mined for domestic purpose only. It was not till the Industrial Revolution that the mining of coal was carried out on a large and commercial scale. Coal mines were opened up in several parts of Europe and America to feed the steam powered engines and machines of the time. Along with industrialization came development. Railroads were laid and steamboats were used to transport coal from the mines to the trading centres. Bank (1883) wrote that the first railroads in America were made for the sole purpose of coal transportation. The large scale mining of coal as the primary fuel was carried out till the mid 1950s, after which alternative fuels like oil, electricity, nuclear power and renewable energy sources started becoming popular. By the 1970s, environmental concerns over coal mining slowed down its extraction in the West. However, coal still remains an important fuel, especially for generation of electricity.

Coal mining in India was started by the British in the late 18th century. Production remained minimal due to want of demand. It was till the introduction of steam locomotives in the mid 19th century that production started steadily rising. After attaining Independence in 1947, the Government made 5-year plans for the development of the coal industry and to make it more scientific and systematic. By the mid 1950s the Government had two coal mining companies with the collieries owned by the Railways as the main hub. With the burgeoning steel industry, the requirement of coal increased manifold. However, the private companies were not able to cope with the demand. The unscientific practices and poor working conditions that these mines presented prompted the Government to nationalize coal production in the country. Taking over of the private coal mines was carried out in phases with enactment of, firstly, the Coking Coal Mines (Emergency Provisions) Act, 1971 followed by the Coking Coal Mines (Nationalisation) Act, 1972 and the Coal Mines (Taking Over of Management) Act, 1973 wherein the coking coal mines and the coke oven plants, except those of the Tata Iron & Steel Company Limited and Indian Iron & Steel Company Limited, were nationalized on 1st May 1972 and brought under the Bharat Coking Coal Limited (BCCL), a new

Central Government Undertaking. The enactment of the Coal Mines (Nationalisation) Act, 1973 finally brought about the nationalization of all mines on 1st May 1973. This Act has remained the main Central legislation determining the eligibility of coal mining in India (Ministry of Coal, Government of India website).

The state of Meghalaya, located in North-eastern India, is rich in natural resources like coal, limestone, uranium, kaolin, clay, etc. The most widely exploited of these is coal. The occurrence of coal was first reported by H. B. Medlicott in 1869 (GSI, 1974; NEC 1991). Its subsequent mining, initially confined to the Khasi Hills only, was carried out at a very small scale level for domestic consumption. The thickness of the coal seams range between 30cms and 200cms (Sarma, 2005) and were highly inconsistent for large scale mining. The commercial extraction of coal started to increase only after 1978-79 (De, 2007). From the Khasi Hills, mining slowly started in the other districts also. Presently, mining is being actively carried out in various places in the Jaiñtia Hills District and as much as 74% of the total production of the state is presently generated from this district (Sarma, 2005).

After Independence, Jaiñtia Hills became a part of the United Khasi and Jaiñtia Hills Autonomous District under the Sixth Schedule of the Indian Constitution (Payal, 2002). Under Clause 3 of the Schedule, the District Council can make laws for management and allotment of land in the district (Payal, 2002). However, land is solely owned by the people, either individually or by the clans. Neither the Central nor the State Governments have any control on the land (Das Gupta *et al.* 2002) except by acquisition or lease from the land owners. This land holding system allowed the owners to exploit their land, including underground resources, in whatever way they deemed fit and profitable. Thus, thousands of private mines exist in all the coal and limestone rich areas of the state.

Coal in Jaiñtia Hills is extracted by an artisanal method of underground mining that differs from that in the rest of the country. This method is called as “rat-hole” mining. In this type of mining, wherever the land owner suspects that coal is present, the forest cover is cleared and a shaft of diameter varying from 3m to 10m is sunk. Holes are then dug into the coal seam and the holes go deeper and deeper with coal extraction. These holes are just big enough to accommodate a man to crawl in with his tools and a basket or wheeled cart on which he transports the coal to the outside (Fig.1.1). These holes or “burrows” go in all directions and for several kilometres following the coal seam (Wangdi, 2004). When the coal is brought to the surface, it is collected near the mine or loaded directly onto trucks which carry it to the depots located near the main roads. These road side depots are a major source of air, water and soil pollution and, coupled with the off-road movement of heavy vehicles, the ecological balance of the area has been adversely affected (Swer and Singh, 2003).

As mentioned earlier, because of the peculiar land holding system and coal seams not profitable for large scale mining, the Government has turned a blind eye to the unplanned and unscientific coal mining in Meghalaya and has not imposed any of the provisions of the Acts of Parliament which are enforced in other parts of the country. Mining in Meghalaya, be it coal or limestone, has been left entirely to the individuals to carry out while the State Government sat back and collected revenue in the form of royalty and transportation taxes from the mine owners.

(a) A cliff adit near Khlieh Myntriang.

(b) A mine shaft at Khlieh Myntang.

(c) Close-up of mine shaft at Khlieh Myntang.

(d) A mine near Khloo Kynring.

(e) Miners hard at work at Khlieh Myntang.

(f) More miners at a mine on Narwan Road.

(g) A new mine being dug near Byrwai.

(h) A new mine being dug on Narwan Road.

**Figure 1.1: The "rat-hole" mines of Jaiñtia Hills.**

## 1.2. Environmental problems associated with coal mining

Without a doubt, coal mining has brought about development and employment opportunities (Swer and Singh, 2003; 2004) and immense wealth to the few who can afford large land holdings and sink many mines. However, it has brought about gross changes demographically and environmentally. Cheap labor from Nepal and Bangladesh form the core group of miners who live in the most despicable conditions in the labor camps. Inter-racial and inter-religion marital alliances have resulted in demographical changes in the district. The landscape of Jaiñtia Hills has been completely changed due to coal mining. Mine shafts have been dug almost everywhere from forests, agricultural fields and grasslands. All types of land uses can be seen around the coal mining areas with mine shafts and mine spoils mixed with agricultural fields, pine groves and human habitation (Das Gupta *et al.* 2002) (Fig.1.2). Sarma (2005) reports a loss of 40% of forest area in a span of 26 years while, at the same time, mining area increased at the rate of 1.2 sq.km. per annum (Fig.1.3). Abandoned and exhausted mines are never backfilled and this has led to submergence and landslides at several places (Fig.1.4). It is common practice to never refill an abandoned mine as that would cost money (Fig.1.4). These have become a big danger to humans and life stock, especially after they become overgrown with vegetation (Fig.1.4(c)). The mine shafts are also never refilled after work is completed and this makes it very dangerous to walk around in the coal mining areas of Jaiñtia Hills.

**Figure 1.2: Mixed land use around a mine at Khlieh Myntang Village.**

**Figure 1.3: Forests cut down to make way for a coal depot.**

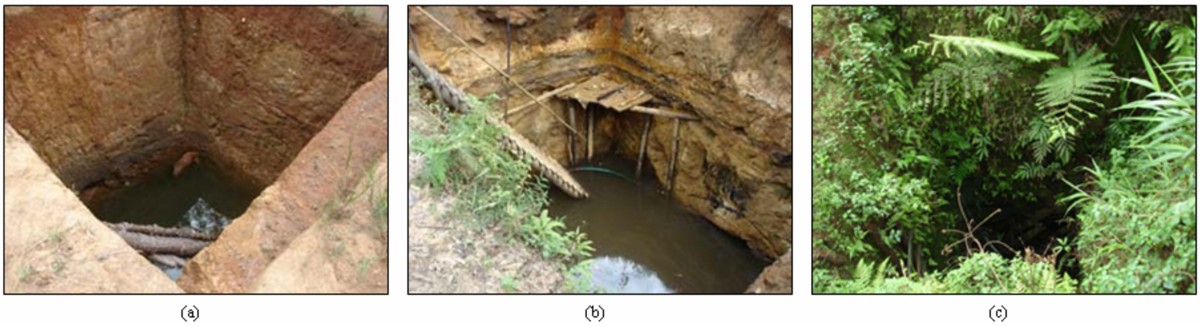

**Figure 1.4: Photographs of abandoned mines.**
**(a) near Khlieh Mynthang (b) at Khloo Kynring (c) at a road side in Byrwai.**

On the contrary, Shankar *et al.* (1993) opined that rat-hole type artisanal mining has proved to be a big success in the Jaiñtia Hills and other parts of Meghalaya because of the close proximity of the coal seam to the surface. They argued that this type of mining was not only cost-effective and did not require skilled man-power, but also caused less land degradation as the direct soil structure damage from it was limited to only the size of the mine shaft, the overburden heaps and spoils. However, they also found that the two major problems associated with this type of mining were (i) the formation of colliery spoils with no structure due to the upside down change of the soil horizons and mixing with coal particles and (ii) deposition of coal particles though water seepage and wind action during wet and dry seasons respectively, thereby affecting areas which were not under the direct influence of coal mining.

But, on the whole, coal mining, especially if carried out as in Meghalaya, leads to all round environmental degradation (Fig. 1.5 and 1.6). The common impacts include land degradation, loss of forest cover, topsoil and agricultural land, changes in topography and hydrologic conditions, pollution of surface and ground waters, retarded vegetation growth, destruction of ecological balance; and land subsidence, temperature rise and loss of coal resources in places where there are mine fires (Chatterjee *et al.* 1994). Underground coal mines are particularly damaging to water quality because they get flooded easily and water has to be continuously pumped to the surface bringing along with it various pollutants, especially dissolved minerals from the rocks it comes in contact with (Ghose and Sinha, 1990).

**Figure 1.5: Environmental degradation at Sohkynphor Village.**

**Figure 1.6: A coal depot near Mynska Village.**

## 1.3. Acid Mine Drainage (AMD)

Coal mining is associated with Acid Mine Dainage (AMD) which is caused by the oxidation and hydrolysis of metal sulphides found in coal, over-burdens and in the waste dumps (Gray, 1996). The oxidation of iron pyrites releasing sulphuric acid from coal mines can be represented by the following equations (Singer and Stumm, 1970):

$FeS_2\ (s) + 7/2\ O_2\ (aq) + H_2O = Fe^{2+}, Fe^{3+} + 2SO_4^{2-} + 2H^+$ (1)

$Fe^{2+} + ¼\ O_2\ (aq) + H^+ = Fe^{3+} + ½\ H_2O$ (2)

$Fe^{3+} + 3H_2O = Fe(OH)_3\ (s) + 3H^+$ (3)

$FeS_2\ (s) + 14Fe^{3+} + 8H_2O = 15Fe^{2+} + 2SO_4^{2-} + 16H^+$ (4)

The oxidation of pyrite is generally accelerated by the presence of bacteria such as *Thiobacillus ferrooxidans* in waters of low pH (Kim and Chon, 2001). The presence of high acidity in the water causes the degradation of surface water quality and impacts stream aquatic biota (Chon and Hwang, 2000). Further, iron hydroxide/sulphate minerals forms a yellowish coating at the bottom of streams and makes it difficult for aquatic life to survive in streams affected by acid mine drainage (Kim and Chon, 2001).

The leaching of AMD leads to surface water contamination by soluble heavy metals present in the coal deposits and other acid soluble weathered materials which add to the deterioration of water quality in the mining areas (Singh, 1987). Heavy metals such as lead, zinc, copper, arsenic, selenium, mercury and cadmium are released into the surface water (da Silva *et al.*, 2006) which becomes unsuitable for aquatic life, destroys mining equipment and render the water unfit for drinking and recreation (Singh, 1987).

Metals are necessary not only for the development of a society but are also essential in life functions. One of the pathways by which metals enter into the environment is through mining activities. These activities may affect relatively small areas but they may have larger impacts on the environment as a whole (Salem and El-Fouly, 2000). Metal contamination of water can persist for many years even after the source has been eliminated. Boult *et al.* (1994) stated that metal contamination of the Afon Goch stream flowing through a mining site at Anglesey, U.K. persisted even after mining operations stopped almost a century ago.

AMD has been a major cause of concern in various parts of the world where mining has been carried out for several decades and centuries now. The full extent of the environmental pollution caused by mine water discharges is difficult to assess accurately, however, in 1989, an estimate was made that about 19,300 km of streams and rivers, and about 72,000 ha of lakes and reservoirs worldwide had been seriously damaged by mine effluents (Johnson and Hallberg, 2005). Robb and Robinson (1995) reported that as per the National Rivers Authority report in 1994, there were 96 discharges from abandoned mines into the rivers of England and Wales which, when combined with discharges from working mines, altogether cause significant pollution to 198 km of natural water courses.

## 1.4. Research Motivation

In the Jaiñtia Hills, coal mining has left its once beautiful landscape scarred and deformed forever (Fig.1.7). Artisanal rat-hole mines dot the whole district making it look like a bad case of chicken pox. Forests have slowly dwindled. Even agricultural land and fruit orchards have not been spared. One can catch a glimpse of lush green paddy fields or an orchard of citrus fruits with a gaping black hole right in their midst (Fig.1.8). Mining is usually carried out in the dry winter months upto around May, before the monsoon sets in. During monsoon, the mine shafts and burrows fill up with water. When work resumes after the monsoon, huge quantities of water are pumped out and discharged into the nearest surface water-body thus, contributing to AMD contamination of the water-body. Water that percolates into the soil during monsoon enters into the mines and comes in contact with the metals, oxidizing them. Cliff adits spew this red colored acidic water which eventually end up in a water body nearby (Fig.1.9). It is commonly seen that coal laden trucks are washed on the river banks adding acidic water into the rivers and streams (MSPCB, 1997). Rain water leaching through the coal dumps at the road-side depots also generates highly acidic leachate which flows into the water-bodies.

**Figure 1.7: Jaiñtia Hills scarred forever.**

**Figure 1.8: Mine in the middle of a paddy field at Khloo Kynring.**

**Figure 1.9: Cliff adits spewing acidic mine water into the river below.**

**Figure 1.10: The red colored Chyrmang River.**

AMD has caused untold deterioration to the water quality of many streams and rivers of Jaiñtia Hills District (Fig.1.10). Swer and Singh (2003; 2004) report pH value as low as 2.31 recorded in one of the streams in the coal mining areas. Water with pH as low as this leads to weathering and dissolution of silicate and other rock minerals causing the release of trace elements like aluminium, manganese, copper, cadmium, lead, etc. into the water (Gray, 1996; Swer and Singh, 2003; 2004). The iron hydroxide precipitate makes the water very turbid and changes its color to reddish brown or brownish orange thereby affecting aquatic life by blocking out the sunlight (Swer and Singh, 2003; 2004). The overall impact of AMD on the ecology is the elimination of species, simplification of the food chain and reduction in ecological stability (Gray, 1997). Swer and Singh (2003; 2004) have reported that the rivers in the coal mining areas lack commonly found aquatic life-forms like fish, frogs and crustaceans.

The Meghalaya State Pollution Control Board, Shillong (MSPCB, 2007) reported a case of massive fish death along the Lukha River, on the eastern border of Jaiñtia Hills, and its waters turning into a deep blue color, a white precipitate covering the entire river bed and all aquatic life coming to an end (Fig.1.11). This phenomenon was attributed to AMD brought into this river by its tributary, Lunar River. Low pH and high acidity were recorded from their point of confluence and downstream. The changing of color of the river from green to blue color indicated the presence of metals. This can be seen from the higher content of metals found in the sediments than in the water samples collected at the same locations.

Shankar *et al.* (1993) have found that mining has brought about decrease in soil fertility because of lower pH, carbon, nitrogen and phosphorus content and higher manganese, zinc, iron and sulphur concentrations. The physico-chemical properties of coal mine spoils have been completely altered and their ability to sustain plant growth has diminished due to low soil moisture, organic carbon and nutrients (Das Gupta *et al.*, 2002). Sarma (2005) observed that the number of trees and shrubs have decreased and forest cover upto 40.5 sq.km. (40%) lost in 26 years while at the same time, mining has been steadily increasing at the rate of 1.2 sq.km. per annum. The Meghalaya State Pollution Control Board, Shillong (MSPSB, 1997) has observed that the pH of water from rivers, streams, mine drains and even drinking water from taps and hand pumps exceeded the permissible limit for drinking water prescribed by the Bureau of Indian Standards (BIS). The movement of heavy vehicles overloaded with coal and coal dust flying about from the depots has caused tremendous air pollution along the roads (MSPCB, 1997).

**Figure 1.11: The blue Lukha River.**
(courtesy: Meghalaya State Pollution Control Board)

**Figure 1.12: The red colored Umbon River (Station R13).**

Thus, unregulated and unplanned mining of coal has led to widespread environmental problems, particularly of AMD contamination which has resulted in the deterioration of the quality of many water bodies in Jaiñtia Hills District rendering them to almost dead rivers and streams with absolutely no signs of aquatic life (Fig1.12). The primary reason why this study is being taken up is to find upto what extent remote sensing, coupled with field sampling, can help in locating AMD affected areas and to serve as an eye-opener to the state's decision makers.

## 1.5. Research Objectives

To carry out the study, the following objectives have been framed:

- To identify and map spatial extent of rat-hole type coal mines in relation to geological setting using RESOURCESAT-1 (IRS-P6) LISS-IV, CARTOSAT-1, Landsat ETM+ and ASTER images.
- To identify mines through object oriented classification (OOC)
- To determine the hydro-chemical characteristics of AMD in surface water in the watershed by field survey, sampling and analysis.
- To assess the presence of undesirably high heavy metal concentrations in water samples and sediments in the watershed.
- To map the spatial variability of concentrations of different pollutants along the rivers in the watershed.

## 1.6. Research Questions

To meet the aforementioned objectives, the following research questions have been framed:

- Can the rat-hole mines be identified and mapped through RESOURCESAT-1 (IRS-P6) LISS-IV, CARTOSAT-1, ETM+ and ASTER images?
- Can the mines be identified using OOC?
- What are the hydro-chemical characteristics of AMD in the watershed?
- Are the mines the main cause of AMD in the watershed or are there other plausible causes?
- What is the extent of the presence of heavy metals in the watershed?

## 1.7. Thesis outline

This thesis consists of six chapters, a brief outline of which is given below:

Chapter 1 : This chapter gives an introduction to the study including the background of the problem, research motivation and the research objectives and questions.

Chapter 2 : This chapter deals with a review of literature relevant to the study and it includes literature on AMD problems, band ratio calculation, object oriented image classification and previous studies conducted in the Jaiñtia Hills district.

Chapter 3 : This chapter describes the study area in terms of location, geology, physiography, etc. and it also gives an idea about the coal belt of the Jaiñtia Hills district.

Chapter 4 : In this chapter, the materials used, i.e. software, satellite imagery and instruments, have been enumerated and the methodology of every step of the study have been discussed.

Chapter 5 : This chapter displays the results attained, through image interpretation, image processing and from field sampling and analysis, and discusses the outcome of these results.

Chapter 6 : In this chapter, conclusions are drawn from the attained results and discusses if the research questions have been answered and research objectives met.

# 2. Literature Review

## 2.1. Acid Mine Drainage

The problem of acid mine drainage (AMD) is a widely studied and documented subject. Almost all the industrialized nations have been through a phase of unplanned and unorganized coal mining to meet the ever increasing demand for fuel to power their development and have all been victims to AMD. AMD is a persistent problem, the effects of which can be seen long after mining activities have ceased. The presence of AMD can still be observed in mining areas of Europe that were opened by ancient Romans prior to A.D. 476 (CSS, 2000).

AMD is basically the outflow of acidic water from metal or coal mines. Metal mines associated with sulphide minerals often generate highly acidic discharges which can cause a lot of environmental damage. Acid rock drainage (ARD) is a naturally occurring phenomenon within rocks containing sulphide minerals as part of the rock weathering process which is increased by large scale earth disturbances like mining activities and large constructions (Wikipedia). Sulphide ores are widely used as raw materials in several industrial processes. Common sulphide ores are pyrite and marcasite, which are also constituents of coal; and pyrrhotite. In the former two, iron and sulphur are in reduced forms and other metals, such as cobalt, nickel and copper, may partially replace iron and arsenic can replace sulphur to some extent (Murad and Rojik, 2004). Iron is contained as an “essential” element in numerous sulphides like chalcopyrite, pentlandite and arsenopyrite (Murad and Rojik, 2004). Exposure of iron bearing sulphide ores to the atmosphere results in the oxidation of both iron and sulphide releasing large quantities of sulphuric acid and the formation of ochreous ferric oxyhydroxide precipitates. In areas affected by AMD, the most common end products of ferrous sulphide oxidation have been observed to be jarosite, schwertmannite, goethite and ferrihydrite (Murad and Rojik, 2004). Sediments in acidic waters mainly contained schwertmannite and goethite while those of near neutral waters contained ferrihydrite (Williams *et al.* 2002).

The United Kingdom (U.K.) has a long track record of mining activities dating back several centuries. The standard method for treating mine drainage has been to pump out the water, treat it with lime to precipitate the iron before discharging it into water courses. The impact of AMD is being felt more acutely now that many mines are closing and pumping of water has reduced. Another problem being faced is the breach of sealed adits and sudden release of acid water laden with metals into water courses. An important example of such an accident happened in 1992 when the flooded Wheal Jane metal mine, an ancient mine worked since the 18th century producing copper, zinc, tin and lead, breached its seal and released high levels of zinc, cadmium and iron into the adjoining estuary turning it orange with iron deposits (McGinness, 1999). AMD is one of the biggest liabilities of the British Government. In 1998-99, the Government through the Coal Authority spent £3 million in tackling the problem of water pollution from abandoned mines and this has been projected to rise in years to come (McGinness, 1999). An important law enacted in the U.K. in this regard is the Water Resources Act (1991) which provides for the prosecution of river polluters, and allows the National Rivers Authority

(NRA) to recover from the polluter the cost of cleaning up. A working mine is the responsibility of the owners, and if pollution is taking place then the NRA can make the owner deal with the pollution. However, abandoned mines have been exempted from the purview of this law with the Coal Authority assuming ownership of such mines to undertake monitoring of and to deal with mine water and other emissions (McGinness, 1999).

In western U.S.A., small abandoned mines that were worked long before modern environmental control machineries were established still cause devastating effects to 8,000 to 16,000 kms. of streams (Jennings, 2008). The U.S. Environmental Protection Agency (USEPA) has identified 188 sites where human health and environmental damages are caused by mining and mineral processing waste management activities (EPA, 1995a). Several laws have been enacted to check environmental pollution caused by the mining industry. One of the most significant enactments is the Comprehensive Environmental Response, Compensation, and Liability Act (CERCLA) of 1980 which is commonly known as Superfund. This law authorizes the EPA to respond to releases, or threatened releases, of hazardous substances that may endanger public health, welfare or the environment. EPA can also force parties responsible for environmental contamination to clean it up or to reimburse the Superfund for response costs incurred by EPA (EPA, 1995b).

Australia has a large number of historic mines scattered all over its length and breadth. There are about 83,000 mines, including abandoned, “small scrapings” and large scale operating mines recorded in New South Wales, Tasmania and Queensland alone, and it is estimated that between 10% to 30% of these mines are potential generators of acidic wastes (Harries, 1997). It has now become a priority to characterize and manage mine wastes for their acid generating potential. The Australian and New Zealand Mineral and Energy Council (ANZMEC) in 1995, issued baseline environmental guidelines considered to be the minimum appropriate for operating mines in Australia. These guidelines stipulated the prediction of development of acid generating processes and resultant drainage water quality for evaluating long term environmental impacts of waste dumps, tailings impoundment structures and mine excavations, and to use the information obtained for developing appropriate mine closure structures (Harries, 1997).

The Canadian mining industry has identified AMD as its single largest environmental problem. The Mine Environment Neutral Drainage (MEND) programme was established in 1989 with a view to tackle this nagging problem. MEND is a cooperative programme financed and administered by the Canadian mining industry, the Canadian government and provincial governments with an estimate of C$18 million for its first phase ending in 1997 (Harries, 1997).

India, too, has a long history of mining with the first recorded coal mine opened in 1774. Now, more than two centuries later, there is a realization that for environmentally sustainable development, unplanned exploitation of mineral resources should be curbed and a system put into place whereby progress is achieved through eco-friendly methods (ENVIS, 2003). The Constitution of India has made it a Directive for the State (Article 48A) and a Fundamental Duty for every citizen (Article 51A) to protect and improve the environment and to safeguard forests and wildlife (COI, 2007). Several laws regulating mining activities and providing for environment preservation and protection have been put into place by the Government. Notable amongst these are the Mines and Minerals (Development & Regulation) Act, 1957, amended in 1994; Mineral Concession Rules, 1960; and the Mineral Conservation and Development Rules, 1988 which regulate mining of minerals other than coal, lignite, natural gas and petroleum. Besides these, the mining industry is also covered by the environmental Acts like the Water (Prevention and Control of Pollution) Act, 1974 (amended in 1988), the Air (Prevention and Control of Pollution) Act, 1981 (amended in 1988), the Environment (Protection) Act, 1986 (with Rules 1986 and 1987), the Forest (Conservation) Act, 1980 (amended in 1988) and the Wildlife (Protection) Act, 1972 (amended in 1991) (ENVIS, 2003).

However, the Constitutional machinery for mining does not apply to Meghalaya, as it falls under the provision of the Sixth Schedule of the Constitution, which provides for the administration of Tribal Areas in the States of Assam, Meghalaya, Tripura and Mizoram. An official note on coal mining activities in Meghalaya obtained from the Directorate of Mineral Resources, Government of Meghalaya, states that “the peculiar land tenure system existing in the state has encouraged the local people that mining of minerals occurring in their land is their customary right. Land to the local tribals does not construe to mean only the surface, but it includes everything on and under it. Land, in the state, does not belong to the Government except by acquisition or lease from the land owners”. Due to this reason, mining in the state is being carried out by individuals in their own private premises on a cottage scale level and in a very unplanned and unorganized setting which has proved to be detrimental to the environment.

Gray (1997) has recognized AMD as a multi-factor pollutant which affects aquatic eco-systems in several direct and indirect pathways; and because of its complexity, its impact on riverine systems is difficult to quantify and predict. He has categorized the major effects of AMD on a riverine system as chemical, physical, biological and ecological (Fig. 2.1).

Cotter and Bridgen (2006) have attributed the environmental and ecological effects of AMD to:

***Acidity and metal toxicity***: high acidity and the high concentrations of dissolved heavy metals make acid mine drainage extremely toxic to most organisms which is why AMD affected streams are largely devoid of life for a long way downstream.

***Sedimentation***: precipitation of iron oxides and hydroxides, called ochre, covers the river bed with a very fine silt preventing benthic organisms from feeding, thus, leading to their disappearance. This has a domino effect on the organisms higher on the food chain. Ochre also affects fish breeding by reducing the amount of gravel for them to lay their eggs.

The detrimental effects of AMD on the environment, particularly on river systems, have been studied and documented all over the world. The effects of AMD can be felt long after mining operations have ceased at a particular place. Gray (1996, 1997, 1998) has extensively studied the AMD draining from the abandoned copper and sulphur mines at Avoca, Ireland and its impact on the surroundings. He has come up with a comprehensive management approach for remediation of the affected area for successful rehabilitation of affected sites and long term protection of the environment. Boult *et al.* (1994) have found that the Afon Goch in Anglesey, U.K., which rises from the metal mining area of Parys Mountain, carries metal concentration that is much higher than other Welsh rivers of similar size and have called the stream as one of the most metal and acid contaminated streams in the U.K. In Scotland, one of the world’s first industrialized countries and one of the first to face post-industrial dereliction, AMD due to abandoned coal mines is second only to sewage as the main source of fresh water pollution; and in catchments within coal mining areas, it stands first (Younger, 2001).

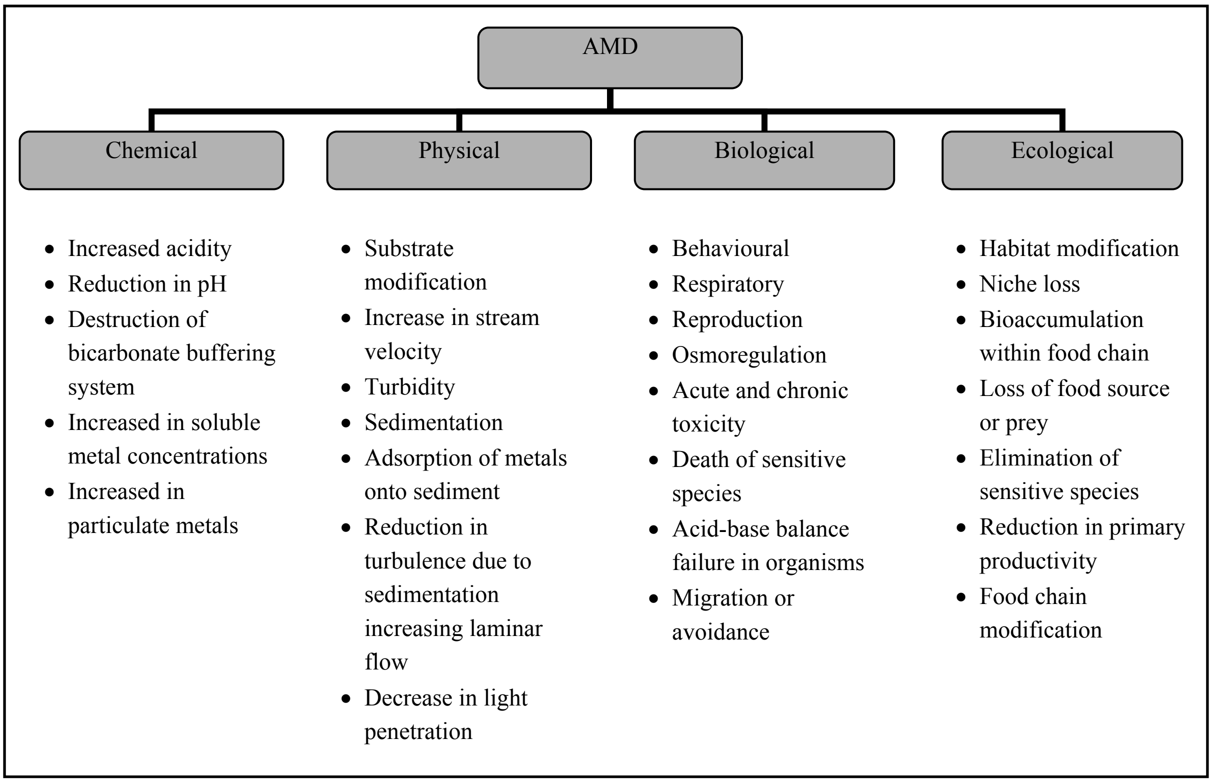

**Figure 2.1: The major effects of AMD on a riverine system.**
**(after Gray, 1997)**

Ezeigbo and Ezeanyim (1993) reported that AMD caused by coal mining in Enugu, Nigeria, which has been mined since 1916, has caused a major problem to supply of drinking water to the city with the continuous pumping out of mine water into the nearby streams and rivers, including the Ekulu River, the water of which is used to partly supply drinking water to the city. In South Africa, mining has caused a lot of environmental problems at several places. An old abandoned metalliferrous mine, the working of which ceased in the 1980s, continues to release a considerable amount of dark, reddish-brown water with pH values as low as 2.5 into the surface environment and surface sinkholes resulting from the collapse of old coal mines have affected groundwater and surface water quality (Akcil and Koldas, 2006). AMD is responsible for an environmental problem at the Loubert coal mine, in the eastern Transvaal. Water from the mine is collected in three pollution control reservoirs. However, spillage and seepage from these reservoirs flow into the Human Spruit, a nearby river, and have considerably affected the soils around and the water quality in the stream (Geldenhuis and Bell, 1998). The water quality in and around Johannesburg, South Africa has been impacted by AMD from gold mine tailings dumps that are disused or are undergoing retreatment to extract remaining gold in the Witwatersrand gold mines which have been worked since 1886 (Tutu *et al.*, 2008).

Lottermoser *et al.* (1999) have reported that AMD from a relic copper mine in New South Wales, Australia, worked between 1894 and 1912 is still causing environmental problems with its low pH and metal rich waters. Stream sediments have metal concentration exceeding background values by one or two orders of magnitude. Bioaccumulation and biomagnification processes have been observed at the mine and smelter sites and algae growing in the polluted streams in the vicinity have been found to display bioaccumulation of metals. Harris *et al.* (2003) studied the Montalbion silver mining area in north Queensland, Australia, which has been abandoned since 1922, and have observed that water sampling during their study period in 2002 showed the release of AMD from the waste dumps which have affected the receiving stream by making it acidic and coating its bed with a layer of ochre or “yellow boy”.

The estuary of the Tinto and Odiel Rivers in south west Spain has been badly affected by AMD from one the most important sulphur deposits in Europe which has been worked for at least 4500 years. The problem has been intensified since 1966 after the establishment of paper and fertilizer industries along the banks which add to the pollution in the estuary making it one of the most polluted locations in Western Europe (Borrego *et al.*, 2002; Grande *et al.*, 2003; Sainz *et al.*, 2003; Chica-Olmo *et al.*, 2004; Olías *et al.*, 2004; Sainz *et al.*, 2005; Sarmiento *et al.* 2009). Elsewhere in Europe, Rukezo (2003) has studied AMD due to mining of volcanogenic sulphide ore deposits in the Recsk-Lahoca mining area in the Matra Mountains, Hungary. da Silva *et al.* (2006) investigated the geochemical characteristics of the AMD discharged from the abandoned mine and tailing piles of the polymetallic massive sulphide Lousal Mine in southern Portugal. Gemici (2008) evaluated the environmental effects of metal pollution in the water, mine wastes and stream sediments around the Alaşehir mercury mine in Turkey.

Korea has been having its share of AMD problems with mining having been going on for several decades now. Chon and Hwang (2000) have cited a report by the Coal Industry Promotion Board which states that 41 coal mines discharged AMD in Korea with a total discharge of over 141,000m$^3$ per day. Their study in the vicinity of the Dogye coal mine shows a definite AMD problem which gets diluted downstream by mixing with inflow waters of higher pH and precipitation of metals. Lee *et al.* (2001) found high levels of cadmium, copper, lead and zinc in the soils sampled in the paddy fields and in the forest area around the abandoned polymetallic Daduk Mine. Similarly high levels of metals was observed in plants sampled in their study area vis-à-vis those in a control site. High concentration of metals was also seen in the stream sediments and water samples which they concluded was due to the mine tailings in the vicinity. Similar reports of positive AMD contamination from improperly disposed mineral waste piles and untreated mine drainage have been given by Lee and Lee (2001) and Kim and Chon (2001).

In India, Rawat and Singh (1982) and Singh (1987) have reported AMD problems in the coalfields of Assam in the North-eastern part of India where the mine water has been severely affected. The Damodar river basin contains 46% of India’s coal reserve, but due to the low sulphur content of the coal, this area does not have an acute AMD problem, as observed by Tiwary and Dhar (1994). The main problem here is the bacterial contamination of the Damodar River, which is the main source of water supply, and lowering of groundwater table due to underground coal mining. Tiwary (2001) carried out a study of water quality of different mines of major Indian coalfields, selecting both acidic and non-acidic mines. He found that mines of the Western, Northern and North-eastern coalfields are the prime contributors of AMD to the surrounding water bodies. However, the waters around non-acidic mines of Central India suffer most from bacterial contamination through anthropogenic sources. Pandey *et al.* (2007) conducted a comprehensive study of contamination caused by toxic mine drainage from Asia’s biggest copper mine at Malanjkhand, Central India. They studied the AMD affected water bodies, stream sediments and metal accumulation in plants. They also conducted bio-monitoring of the affected areas with the help of benthic macro-invertebrates. Their result proves a very significant impact on environmental health.

An interesting study on environmental degradation due to coal mining has been conducted by Sharma *et al.* (2009) wherein an attempt was made to determine environment liability directly in terms of economy. They have classified the main pollutants due to mining and processing of coal as green house gases, coal dust and acid mine drainage and the financial liabilities due to these as greenhouse liabilities, coal dust liability and sulphur liability respectively. Their study found that greenhouse liabilities accounted for US$12.07, coal dust liability US$5.0 and sulphur liability US$101.97. When the total liabilities are compared with the annual coal production in India, which is US $5,000 million, 2.4% of the total economic gain is lost to environmental pollution. Though this is a significant amount, it remains unaccounted for and unnoticed in India.

## 2.2. Remote Sensing and its use in mining related studies

Surface mining has been seen to be the cause of several environmental problems like land degradation, erosion, land subsidence, loss of forest cover and agricultural land, increased acidity of soil, AMD causing pollution to surface and ground waters and destruction of ecological balance (Chatterjee *et al.*, 1994), to cite a few. To remediate these areas, continuous monitoring is required so as to come up with suitable solutions for reclamation and environmental management (Rathore and Wright, 1993). Remote sensing, with its advantages of having a synoptic view of the Earth, ability to collect data from even inaccessible locations, relatively cheap, rapid and repetitive data acquisition, and ease to manipulate and integrate in a Geographical Information System (GIS), has been extensively used to study mining related environmental degradation. Rathore and Wright (1993) have made an extensive review of the integration of remote sensing in monitoring environmental impacts of surface coal mining. They have reviewed various studies which have used remote sensing for monitoring land disruption in coal mining areas, for detection of mine fires, for monitoring of mine revegetation and reclamation, for water pollution assessment and for detection of subsidence.

Repic *et al.* (1991) used multispectral videography in the yellow-green, red and near infrared regions to study selected water quality parameters in two abandoned coal mine lakes affected by AMD. Water samples from 14 locations were also collected simultaneously with the acquisition of the video imagery. They found that the yellow-green band had the highest positive and the highest negative correlation with iron ion content and pH respectively. High correlation with iron was attributed to the presence of “yellow boy” $Fe(OH)_3$ flocs in the lakes and that with pH was because of increased iron in solution caused by increased acidity. The authors, thus, demonstrated that water color induced by presence of iron ions significantly influenced the spectral values of the lakes.

Chatterjee *et al.* (1994) used a Landsat TM data to construct a model to assess the environmental impacts of opencast and underground coal mining at Jharia coalfield, Jharkhand (eastern India). Digital image processing was carried out to generate a standard False Color Composite FCC 432 (R-G-B) and hybrid FCC’s 742 and 754 (R-G-B). They also generated a TM band 6 density sliced image to identify areas with thermal anomalies. TM band 7 data was edge enhanced, using a Laplacian operator, and a second hybrid FCC 754 was generated using this enhanced data. NDVI was also calculated for delineating and differentiating vegetation classes and, finally, a supervised land use classification using Maximum Likelihood Classifier (MLC) was prepared and verified through field investigations. From the standard FCC, the authors could not identify many features. However, from the hybrid FCC 742, the authors were able to distinguish coal from water bodies as the former appeared in darker shades of purple and the latter in blue. Linear features and drainage lines became prominent in this hybrid. The authors succeeded in showing that different combinations of landsat TM bands could yield hybrid FCCs that can be very useful for studying the various environmental impacts of coal mining.

Saha *et al.* (2005) opined that land cover classification on the basis of spectral remote sensing data, in high mountainous regions, like the Himalayas, is fraught with difficulties because of the presence of shadows due to high altitude of the terrain, cloud cover, deep narrow valleys and ravines, low sun angles, steep slopes and differential vegetation cover. To overcome these difficulties, they have come up with an approach which incorporates data from other sources, along with remote sensing data, to make their classification more accurate. For their study in Rudraprayag and Chamoli districts of Uttarakhand (north India), in addition to IRS LISS-3 data, they have used an NDVI (Normalized Difference Vegetation Index) layer and a DEM (Digital Elevation Model). The authors used several five-band combinations to find which combination gave the highest separability so as to be appropriate for classification. They found that all the five-band combinations and also the complete data set were equally good, but the best combination was that of the four LISS-3 bands and the DEM. The overall accuracy of classification using LISS-3 bands only turned out to be 86.94% and it increased to 91% when the whole data set was used. The best accuracy of 92.06% was achieved for a combination of LISS-3 bands 1, 2 and 4, NDVI and DEM. This proved that the use of ancillary data, in addition to remote sensing data, had improved the classification accuracy by reducing the number of misclassified classes and the shadow effect.

Sometimes topographic slope and aspect, shadows or seasonal variations in sunlight illumination angle and intensity cause differences in brightness values from identical surface materials which can cause misclassification of features. In such situations, Jensen (1996) writes that band ratio calculation may be applied to reduce these differences. Lillesand and Kiefer (2000) have defined band ratio calculation as an image enhancement resulting from the division of DN (digital number) values in one spectral band by the corresponding values in another band. Ratio images have an added advantage by conveying the spectral or color characteristics of image features regardless of variations in scene illumination conditions (Lillesand and Kiefer, 2000). Ratios also provide unique information that may not be discernable in any single band but is useful in classification (Jensen, 1996). Ratio images can be used to produce a color composite by combining any three and assigning each image with a separate primary color (Sabins, 1987).

Band ratio calculation has been considered to be a relatively rapid method for carrying out land use and land cover studies (Rahman, 1997). Several studies have been carried out using band ratios for land use land cover classification and also for mineral exploration. Sabins (1987) found that ratio image of Landsat Thematic Mapper (TM) bands 3 and 1 enhanced places with high content of iron oxide, which have maximum reflectance in band 3.

Rahman (1997) used a Landsat TM image for classification into various LULC classes by selecting ten band ratios from the total of thirty possible ratios using Landsat TM. The discernable LULC features using the various band ratios were described in detail. The author also found that in the color composites of (i) TM5/TM7, TM4/TM3, TM3/TM2 (RGB), (ii) TM4/TM3, TM3/TM2, TM3/TM4 (RGB) and (iii) TM3/TM2, TM5/TM3, TM5/TM6 (RGB), the LULC features were revealed in different colors uniquely. The author concluded by saying that although band ratio calculation was an effective and rapid method to identify LULC features, by enhancing or subduing the brightness values of pixels of different classes, especially in the fields of mineral identification, drought, vegetation canopy change, etc, it fell short by not being able to assign the pixels into classes.

Salem and El-Fouly (2000) have used the band ratios of Landsat TM bands 5/7 and 3/1 to enhance the spectral reflectance of hydrothermal alteration and iron enrichment respectively, in their study of mineral reconnaissance in Egypt. Iron oxide has been successfully detected along the coast of south Myanmar by using band ratios of VNIR (Visible Near Infra Red) B2/B1 in ASTER (Advanced Space-borne Thermal Emission Reflection Radiometer) and VNIR B3/B1 and SWIR (Short Wave Infra Red) B5/B4 in Landsat TM images (Soe *et al.*, 2005). Trinh *et al.* (2005) have successfully used band ratios, particularly the ratio red/near infrared, of Landsat MSS (Multispectral Scanner System) and Landsat TM images to map the land use and soil degradation in a district in Vietnam.

Rajendran and Thirunavukkarasu (2007) in their analysis of uncertainties in visualizing remote sensing data have found that Landsat TM band ratio of band 5/band 4 and IRS-P6 LISS-IV band ratio of band 3/band 2 yield good results in indicating the outcrop of iron bearing silicates in their study area. Nasipuri and Chatterjee (2009) have used the popular band ratios Normalized Difference Vegetation Index (NDVI), Normalized Difference Water Index (NDWI) and Normalized Difference Bareness Index (NDBI) to classify land use around the Maithon reservoir in east India.

With the advent of high spatial resolution imagery in the past decade, there has been a growing consensus that traditional pixel-based classification methods have inherent drawbacks (Devereux *et al.*, 2004; Song *et al.*, 2005; Yan *et al.*, 2006; Barille and Bilotta, 2008; Durieux *et al.*, 2008; Moine *et al.*, 2009). As these classifiers basically depend on the spectral reflectance of the features, they often “produce maps that lack spatial coherence because of spectral heterogeneity and spatial variance that lead to the well-known salt and pepper effect” (Durieux *et al.*, 2008). With high spatial resolution, each pixel gets classified uniquely from the surrounding area and homogeneous regions are not generated, except by using filters (Durieux *et al.*, 2008). Further, each pixel of high resolution images may contain several land cover types, i.e. the mixed pixel problem, which is difficult to solve with pixel-based classification (Song *et al.*, 2005). Due to such drawbacks, the trend has now shifted towards object oriented image analysis (OOIA) which is based on image segmentation.

Object-oriented classification (OOC) has been introduced to remote sensing only recently (Song *et al.*, 2005). This has been made possible with the advent of high resolution imagery and the availability of powerful software that can handle both image processing and GIS functionalities in an object based environment (Blaschke, 2009). The first step of OOC involves image segmentation which partitions the image into non-intersecting, homogeneous regions or objects, with all contiguous regions being dissimilar, and this is followed by classification of these objects based on spectral, spatial and contextual information using common classifiers (Song *et al.*, 2005). Thus, OOC does not operate directly on single pixels, but objects consisting of many pixels that have been grouped together in a certain way by the user using image segmentation (Yan *et al.*, 2006). This helps OOC attain higher classification accuracy vis-à-vis pixel-cased classification.

Generally, image segmentation is carried out by one of the following techniques: clustering, edge detection and region growing (Song *et al.*, 2005; Yan *et al.*, 2006). The accuracy of image segmentation directly affects the performance of OOC (Yan *et al.*, 2006).

Barlow *et al.* (2003, 2006) have used OOC on an input of a number of layers, like multispectral and panchromatic images, a DEM and its derivatives and NDVI of the study area, to identify landslide scars and classify them into different types of slides by using a step-wise elimination of the undesired land use and land cover. Yan *et al.* (2006) compared the pixel-based and OOIA approaches in studying a coal fire area in China and found that the OOC scored a much higher accuracy than the pixel-based classification. Song *et al.* (2005) used a “competitive pixel-object classification approach” using Bayesian neural network to classify an area into nine land cover classes and found that their approach had the highest accuracy as compared to both pixel-based and object-based approaches using Bayesian neural networks. Barille and Bilotta (2008) classified burnt vegetation by using OOC on very high resolution IKONOS images. Durieux *et al.* (2008) used OOIA to extract buildings and monitor urban sprawl change detection. Moine *et al.* (2009) have used an OOC based semi-automatic method to detect landslides using high resolution satellite imagery.

Song *et al.* (2005) write that despite its increasing use as a classification tool, OOC has its disadvantages which they have listed as:

- Classification accuracy depends on the quality of image segmentation.
- Classification error accumulates due to the error in both image segmentation and classification process.
- A misclassified object will lead to all pixels in that object being misclassified.

In recent years, hyperspectral remote sensing and ground based spectroscopy have been successfully used to estimate the extent of AMD by assessing the mineralogy of the stream sediments. The typical yellow to reddish-brown color of the precipitates make them very obvious and they can even be observed in aerial or satellite imagery. Williams *et al.* (2002) observed that the sediments occurring at each pH mode were spectrally separable and they have successfully used spectral angle difference mapping to correlate sediment color with stream water pH. Choe *et al.* (2008) tested the possibility of using spectral indicators obtained from a field sample in estimating heavy metals and also to extend their use in mapping heavy metal distributions. The parameters derived from the spectra of sediment samples were linked to heavy metals and extended to hyperspectral remote sensing using HyMap images. Montero *et al.* (2005) have used a digital mapping system in combination with a portable reflectance spectrometer to characterize abandoned mines in order to assess their potential for AMD discharge. They mapped minerals occurring on the surface of waste-rock piles and their surroundings, stressing on minerals that are indicators of sub-aerial oxidation of pyrite and the subsequent formation of AMD. The mineral maps enabled the generation of remediation-priority maps, in which the piles that contained high concentrations of low-pH minerals are assumed to have the highest potential to release AMD and more priority can be given for necessary remediation.

## 2.3. Previous studies conducted in Jaiñtia Hills District

Shankar *et al.* (1993) conducted a study in Bapung and Sutnga to quantify the impact of coal mining on soil fertility through assessment of the chemical characteristics of soil under different land uses in both an un-mined control area and mine affected area. They also determined the physical and chemical properties of an undisturbed native forest soil, pre-mined over-burden and an age series of colliery spoils in order to be able to predict the natural pattern of nutrient recovery with time. They found that the soil in mine affected areas had lower pH, carbon, nitrogen and phosphorus and higher manganese, zinc, iron and sulphur vis-à-vis the un-mined control area. They also found that the physical and chemical properties of colliery spoils showed partial recovery over a period of 20 years. Nutrients and pH increased with age, while, at the same time, concentrations of calcium, manganese, iron, and sulphur decreased.

Lyngdoh (1995) studied the edaphic changes and community characteristics of naturally recovering coal mine spoils in the Jaraiñ area of Jaiñtia Hills. The main observations were that soil was acidic in all locations, including the control site which had a soil pH of 4.2; cation exchange capacity was very low at all sites; organic matter, total Kjeldahl nitrogen, nutrients and phosphorus increased with spoil age; and there were more species observed in the control site than in the mining sites.

The Meghalaya State Pollution Control Board, Shillong conducted a study of the environmental impacts of coal mining in Jaiñtia Hills (MSPCB, 1997) in which water and ambient air quality at several locations in the district were monitored for two years in pre-monsoon, monsoon and post-monsoon seasons. Water samples were collected from rivers, streams and mine drains and ambient air quality was monitored at the mining areas and at coal depots. The study revealed that the water quality is highly acidic, with lowest pH recorded being 2.7. There was no distinction between the water quality from the different locations and there was only a slight seasonal variation. Iron content was found to be very high and no variation in the water quality was observed in the two year period. The ambient air quality was found to exceed the National Ambient Air Quality Standards prescribed by the Government of India on a few occasions and this was mainly attributed to vehicular emissions and dust generated due to movement of these vehicles on unpaved forest tracks.

Das Gupta (1999) and Das Gupta *et al.* (2002) investigated the physico-chemical properties of coal mine spoils to study the colonization, establishment and growth of plants on these spoils and to enumerate soil microbial population and measure the activity of soil micro-organisms. Their study was conducted in Bapung coal mining area from where they selected mine spoils of ages varying from 0-2 years up to 12-14 years and a control site undisturbed by mining. Their study revealed that mining activities had adversely affected the physico-chemical and biological properties of soil making it less suitable for plant growth and development. With soil moisture content and organic carbon being the least in the youngest mine spoil, there was very less plant growth on them. Nutrients were found to be deficient in the youngest spoils and showed an increasing trend with age. Similar observations were also made with the cation exchange capacity of the soil. The number of plant species also showed an increasing trend from the youngest mine spoil to the control site and also with age of the mine spoils. Though mining had altered the soil properties, a slow natural recovery process was observed by the authors.

Swer and Singh (2003, 2004) conducted water quality studies in Jaiñtia Hills to assess the impacts of coal mining on surface water and aquatic biodiversity. Their studies have revealed that AMD has affected several rivers in the mining areas of the district with the color of these rivers being a perpetual orange or red and pH varying from 2.31 to 4.01. High concentrations of metals, sulphates, electrical conductivity, suspended solids and silt in these rivers has rendered them unusable by humans and has wiped out almost all aquatic life except for a few resistant species. The polluted water, combined with deposition of silt and coal dust on the river beds, has impaired the ecosystem of benthic macro-invertebrates which in turn has affected the supply of food to higher organisms leading to their disappearance from these rivers. AMD also directly affected fish by causing various physiological disturbances leading to death by anoxia. It was observed that most of the rivers lack commonly found aquatic life-forms like fish, frogs and crustaceans.

Sarma (2005) studied the effects of coal mining on vegetation cover in a part of the Jaiñtia Hills district. It was found that coal mining had greatly affected the plant growth in the district. While normal growth and species distribution was observed in undisturbed areas, the mined areas showed reduced plant species and dominance of one or two species. In the study area, in a period of 26 years, there was a loss of 40.5 sq.km. of forest cover and 48% dense forests. While mining area increased at the rate of 1.2 sq.km. per year, cropped areas reduced by about 5 sq.km.

Jeeva (2007) in his study on impact of mining on plant diversity and community structure of aquatic and terrestrial ecosystems in Jaiñtia Hills has observed that despite having similar edapho-climatic conditions, the different study sites showed high differences in species composition which he has attributed to AMD discharge. There were more terrestrial species in the undisturbed areas and soil was found to be acidic in all sites. Water quality was degraded to the extent that streams have lost their life sustaining role and have become devoid of aquatic life.

The soil types present in the study area are also of importance to see if they contribute to acidity of the water bodies. Soil acidification is a natural process that is accelerated by certain plants and human activities, like industrial and mining activities (Bolan *et al.*, 2005). Soil acidification is caused mainly by (1) production of carbonic and organic acids in the soil which dissolves earth alkali cations from soil minerals leading to it acidification, (2) the uptake of basic earth alkali cations by plants and their release of protons ($H^+$) to maintain electroneutrality, (3) the accumulation of organic nitrogen which is a large source of protons and during the transformation and cycling of carbon, nitrogen and sulphur, and (4) the addition of dissolved strong acids through atmospheric activities (Blake, 2005).

The entire north-eastern region of India has the largest stretch of acid soils in India with the main cause being the humid tropical climate along with severe soil erosion due to rugged topography, high rainfall and shifting cultivation (Sen *et al.*, 1997). Both surface and subsurface soils are highly leached exhibiting poor base saturation with low cation exchange capacity (Sen *et al.*, 1997a). Acid soils of North-east India have been studied earlier by Sen *et al.* (1994, 1996, 1997a, 1997b) and Nayak *et al.* (1996). The soils have thick solum and free drainage with red color and high clay content. The color pattern of soils indicates the dominance of iron oxides in the pedogenic environment. The soils are acidic (pH 4.0 to 5.6) and highly leached, having poor base saturation and low cation exchange capacity (Sen *et al.*, 1997).

Singh *et al.* (1999) have written that the variation in topography and landform in Meghalaya, coupled with climatic and rainfall variation, has dictated the formation of different soils in the state. The soils have been classified into 4 orders, 8 sub-orders, 14 great-groups and 25 sub-groups. The soil depth in the state is mostly a combination of deep and moderately deep (56.99% of total geographical area), followed by deep soils (27.92%), moderately deep soils (11.3%) and the rest is moderately shallow to moderately deep (Table 2.1). Majority of the soils are loamy with only 8 – 10 % fine clayey and about 8% sandy. Soils of Meghalaya have been found to be acidic in reaction (pH 4.5 – 6.5) with majority of the soils (65%) classified as moderately acidic and the rest are slight acidic (Table 2.1).

**Table 2.1: Soil depth and soil reaction classes.**
**(after Singh *et al.*, 1999)**

| Soil depth | | Soil reaction | |
|---|---|---|---|
| **Class** | **Depth** | **Class** | **pH** |
| Extremely shallow | < 10 cm | Strongly acidic | < 4.5 |
| Very shallow | 10 – 25 cm | Moderately acidic | 4.5 – 5.5 |
| Shallow | 25 – 50 cm | Slightly acidic | 5.5 – 6.5 |
| Slightly deep | 50 – 75 cm | Neutral | 6.5 – 7.5 |
| Moderately deep | 75 – 100 cm | Slightly alkaline | 7.5 – 8.5 |
| Deep | > 100 cm | Moderately alkaline | 8.5 – 9.5 |
| | | Strongly alkaline | > 9.5 |

The Department of Agriculture, Government of Meghalaya (DoA, 2006) has described that the soils of the Meghalaya hills have been derived from gneissic complex parent materials, varying in color from dark brown to dark reddish-brown and in depth from 50-200 cm, rich in organic carbon but deficient in available phosphorous and medium to low in available potassium. The reaction of the soils varies from acidic (pH 5.0 to 6.0) to strongly acidic (pH 4.5 to 5.0). Most of the soils occurring on higher altitudes under high rainfall belt are strongly acidic due to intense leaching and are not suitable for intensive crop production. Base saturation of these soils is less than 35 %. These soils are rated low in available boron and molybdenum and about 40% of the soils of the state contain micronutrients below the critical level.

Shankar *et al.* (1993) and Satapatty (2002) have also mentioned that acidic soil in Jaiñtia Hills has limited the agricultural production of the area.

# 3. Study Area

## 3.1. Introduction

The state of Meghalaya is located in India's North-eastern corner (Fig.3.2) It was granted complete statehood by the Government of India on the 21st January 1972. It has Bangladesh bordering it to the south and west and Assam in the north and east. The name of the state literally means "The Abode of the Clouds" and has been derived from the perpetual cloud cover hovering over the hills during the monsoon season. The state has been divided into seven districts with its capital located at Shillong, fondly called the "Scotland of the East" due to its striking similarity with the Scottish highlands. With its scenic natural beauty and cool climate, Meghalaya is a popular tourist destination with 462,952 foreign and domestic tourists visiting it in 2007 (DES, 2009). The villages of Sohra (Cherrapunjee) and Mawsynram, famous for having the heaviest rainfall in the world, are located in the southern part of the state and are a major tourist attraction.

Meghalaya is also richly endowed with natural resources like coal, limestone, uranium, kaolin, clay, to name a few. Table 3.1 shows the reserves and grades of mineral resources obtained from records of the Directorate of Mineral Resources (DMR), Government of Meghalaya. Good quality limestone deposits with an inferred estimate of 5000 million tonnes exist along the southern part of the state (Meghalaya State Official website). The limestone has been traditionally mined to produce slaked lime which is exported to other states and also to Bangladesh. The Hindustan Paper Corporation Limited, Jagi Road, Assam, is one of the major buyers of slaked lime for its paper production. Lafarge Surma Cement Limited and Chhatak Cement Company Limited, both located in Bangladesh, are totally dependent upon the state's limestone as they rely upon their mines in southern Meghalaya for their cement production. Uranium reserves of around 9.22 million tonnes have been identified in the West Khasi Hills District (MSPCB website). However, till date, its mining has not been approved by the Government due to public opposition.

**Table 3.1: Reserves and Grades of Meghalaya's mineral resources.**

| S.No. | Minerals | Reserves (in million tones) | Grades |
|---|---|---|---|
| 1. | Limestone | 14700.00 | Cement, metallurgical and chemical |
| 2. | Coal | 576.48 | Sub-bituminous, partly caking, medium to high sulphur and calorific value |
| 3. | Kaolin | 5.24 | White ware |
| 4. | Lithomargic Clay | 97.0 | White ware, earthen ware, furnace lining, curing soap, etc. |
| 5. | Glass Sand | 3.0 | Ordinary glass ware |
| 6. | Quartz | 0.5 | Ordinary ceramic grade |
| 7. | Feldspar | 0.127 | Ceramic grade |
| 8. | Iron ore | 3.60 | Low grade |

| | | | |
|---|---|---|---|
| 9. | Sillimanite | 0.045 | High temperature furnace lining |
| 10. | Bauxite | 1.45 | Low grade (40% $Al_2O_3$) |
| 11. | Rock Phosphate | 0.015 | Low grade (15-30% $P_2O_5$) |
| 12. | Phosphatic nodule | Nominal | $P_2O_5$: 5 – 15% |
| 13. | Gypsum | Nominal | Crystals of salanite variety |
| 14. | Granite | 5.0 million $m^3$ | Table top, wall cladding, etc. |
| 15. | Uranium | 9.22 | 0.104%: $U_2O_8$ |
| 16. | Base metal/ Trace metal | 1.14% Cu: 0.80mt; 1.60% Zn: 0.85mt; Pb: 0.88mt, with traces of Cd, Bi, Ag. Tenor of gold encountered in 3 boreholes in Tyrsad. | |

Source: DMR, Govt. of Meghalaya

The occurrence of coal in Meghalaya was first reported by H. B. Medlicott in 1869 (GSI, 1974; NEC 1991). The coal belts are confined to the Tertiary sediments of the Garo, Khasi and Jaiñtia Hills districts and the Lower Gondwana sediments in the western part of the Garo Hills district. The deposition of coal happened under stable shelf condition along the southern periphery of the Shillong Plateau (NEC, 1991). The distribution and concentration of specific trace elements in coal samples indicate that the coals of Meghalaya have a marine influence during their formation and they show a gradual trend of increase in total sulphur from west to east (Mukherjee *et al.*, 1992). The deposits are found in thin seams of thickness ranging from 30 cm to 210 cm embedded in sedimentary rock, sandstone and shale of the Eocene age (Sarma, 2005; GSI, 1981). In the Garo Hills, coal occurs in the Tura sandstone of the Jaiñtia group (Eocene) while in the Jaiñtia Hills, coal deposits in Lakadong, Lumshnong, Malwar, Musiang-Lamare and Mutang are reported to occur in the Lakadong sandstone member and those around Jaraiñ-Shkentalang, Bapung, Sutnga and Iooksi in the Lower Sylhet sandstone member or Therria Formation of Palaeocene Age. Fig. 3.1 shows the location of coal deposits in Meghalaya.

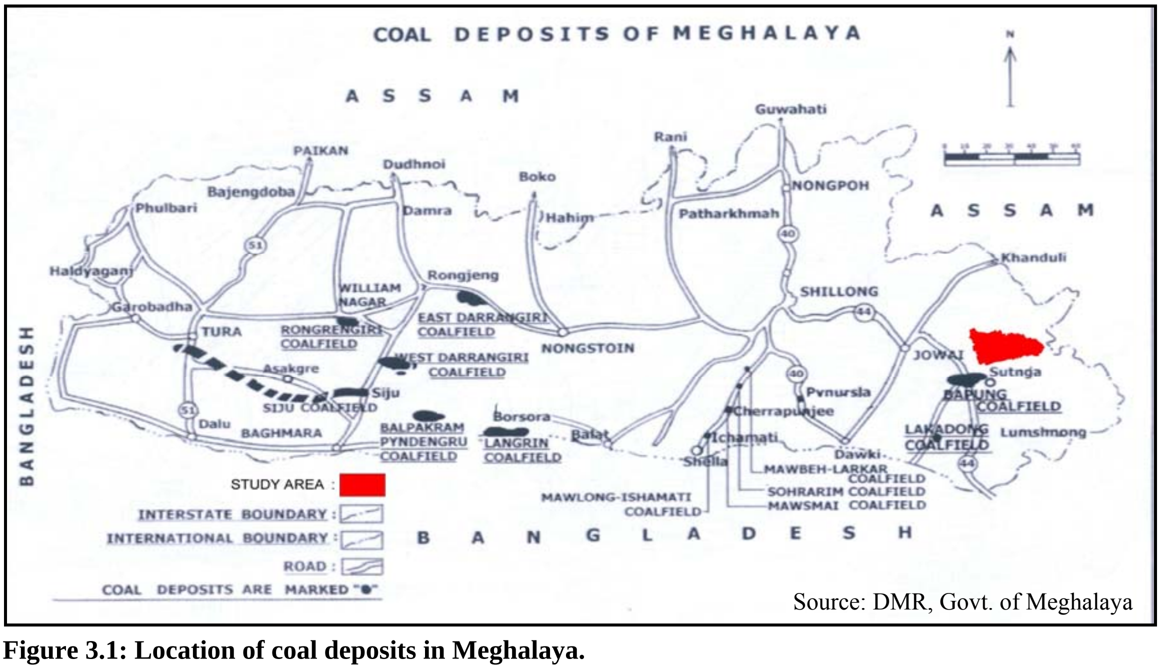

Source: DMR, Govt. of Meghalaya

**Figure 3.1: Location of coal deposits in Meghalaya.**

## 3.2. Jaiñtia Hills District

The Jaiñtia Hills District is the eastern most district of Meghalaya (Fig.3.2). It lies between 91°58’E and 92°50’E longitudes and 25°02’N and 25°45’N latitudes. It is bounded by Cachar and North Cachar Hills Districts of Assam in the east, the Karbi-Anglong District of Assam in the north, the East Khasi Hills District of Meghalaya in the west and it shares the international boundary with Bangladesh in the south. It covers an area of 3819 sq.km. and is home to a population of 299,108 people, with 96% Scheduled Tribes, as per the Census of India 2001 (DES, 2009). The district headquarter, Jowai, is located at a distance of 66 km from Shillong along the National Highway 44. This is a very important highway as it connects the rest of India to the Barak Valley of Assam, Mizoram, Tripura and parts of Manipur (Suchiang, 2002). A summary of the vital statistics of Jaiñtia Hills is given in Table 3.2.

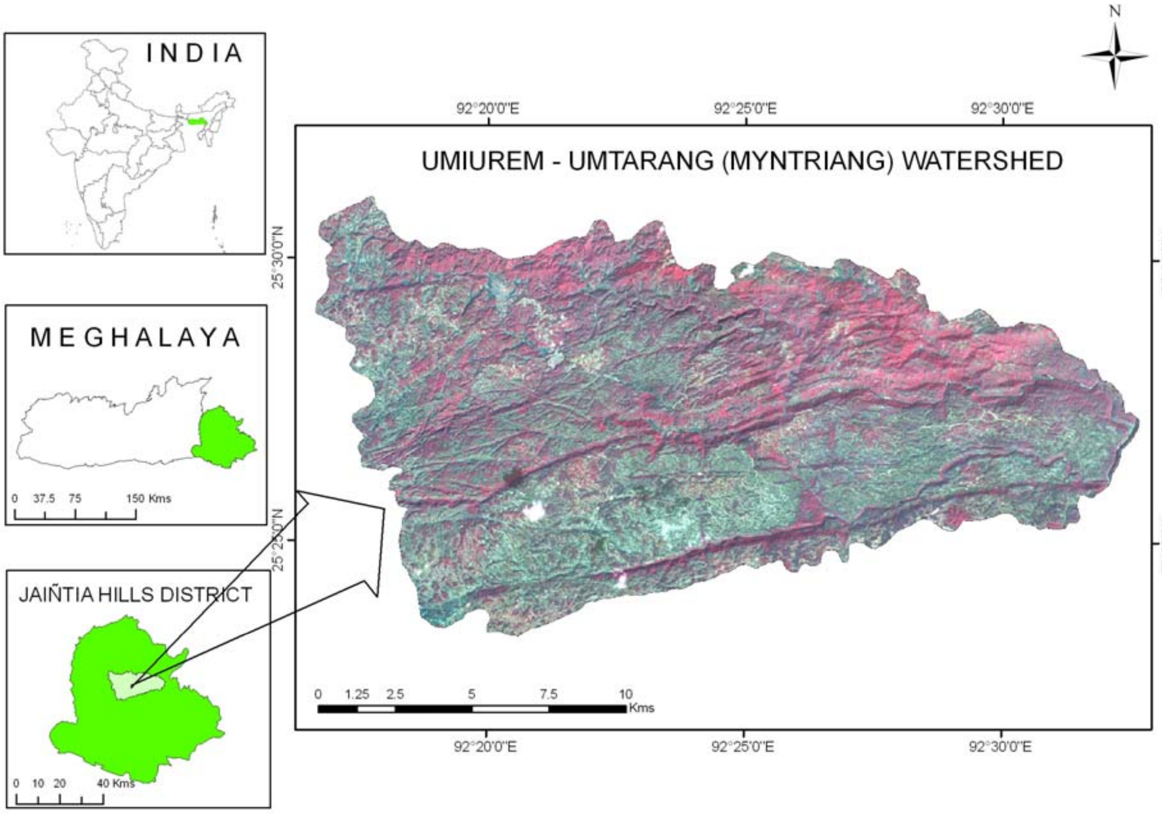

**Figure 3.2: Location of study area (Merged CARTOSAT-1/RESOURCESAT-1 image).**

**Table 3.2: Vital Statistics of Jaiñtia Hills District.**

| S. No. | Items | Units | Year | Jaiñtia Hills District statistics |
|---|---|---|---|---|
| 1. | Area | sq.km | 2001 | 3819 |
| 2. | Sub-divisions (other than district head quarters) | Nos. | 2007 | 2 |
| 3. | Community Development Blocks | ” | 2001 | 5 |
| 4. | No. of towns | ” | 2001 | 1 |
| 5. | No. of villages | ” | 2001 | 499 |
| 6. | Total Population | ’000 Nos. | 2001 | 299.1 |
| 7. | Male Population | ” | 2001 | 149.9 |
| 8. | Female Population | ” | 2001 | 149.2 |
| 9. | Rural Population | ” | 2001 | 274.0 |
| 10. | Urban Population | ” | 2001 | 25.1 |
| 11. | Scheduled Tribes Population | ” | 2001 | 287.0 |
| 12. | Scheduled Castes Population | Nos. | 2001 | 456 |
| 13. | Total Literacy | % | 2001 | 51.9 |
| 14. | Population density | Per sq.km. | 2001 | 78 |
| 15. | Sex ratio | Females per 1000 males | 2001 | 996 |
| 16. | Male Literacy | % | 2001 | 50.1 |
| 17. | Female Literacy | % | 2001 | 53.7 |
| 18. | Total Cropped Area | Hectares | 2004-05 | 30507 |
| | | | | |
| 19. | Population of Cultivators | ’000 Nos. | 2001 | 52.2 |
| 20. | Agricultural laborers | ” | 2001 | 17.1 |
| 21. | Registered small scale industries | Nos. | 2006 | 722 |
| 22. | Medium and large scale industries | ” | 2004-05 | 15 |
| 23. | Coal production | ’000 MT | 2005-06 | 3890 |
| 24. | Limestone production | ” | 2005-06 | 412 |

Source: DES, 2007

### 3.2.1. Geology

The Jaiñtia Hills District is a contiguous part of the Meghalaya plateau which is a remnant of an ancient plateau of Pre-Cambrian Indian Peninsular Shield which has been block uplifted to its present height, and its landscape evolution is closely linked to that of the peninsula (GSI, 1974; Sarma, 2005). The core of the plateau consists of an ancient mass of gneiss, schist and granite formations, exposed in the north but hidden in the south beneath Cretaceous and Tertiary deposits and a Mesozoic trap known as Sylhet Trap (Bhattacharyya, 2002). The general stratigraphic formation of the Jaiñtia Hills is given in Table 3.3.

**Table 3.3: General stratigraphic formation of Jaiñtia Hills District.**

| Age | Group | Formation | Lithology |
|---|---|---|---|
| Recent | - | - | Alluvium, sand, silt and clay |
| ~~~~~~~~~~~~~~~~~~~~~~~~~~~ Unconformity ~~~~~~~~~~~~~~~~~~~~~~~~~~~ | | | |
| Upper Eocene | Jaiñtia | Kopili Formation | Alterations of shales and hard sandstones with a few limestone bands |
| Middle Eocene | Jaiñtia | Sylhet limestone | Prang limestone: Fossiliferous, argillaceous limestone |
| | | | Narpuh sandstone: Sandstone with subordinate calcareous bands |
| Lower Eocene | Jaiñtia | | Umlatdoh sandstone: Foraminiferal limestone containing a few sandstone bands |
| | | | Lakadong sandstone: Coal-bearing quartzitic sandstone |
| | | | Lakadong limestone: Fossiliferous limestone |
| Palaeocene | Jaiñtia | Theria sandstone (lower Sylhet sandstone) | Medium to coarse grained ferruginous, quartzitic sandstones, containing thin coal seams, carbonaceous shales and, at places, clay beds. |
| ~~~~~~~~~~~~~~~~~~~~~~~~~~~ Unconformity ~~~~~~~~~~~~~~~~~~~~~~~~~~~ | | | |
| Pre-Cambrian | - | - | Acid and basic intrusives, quartzites, phyllites, etc. |
| ~~~~~~~~~~~~~~~~~~~~~~~~~~~ Unconformity ~~~~~~~~~~~~~~~~~~~~~~~~~~~ | | | |
| Archaeans | - | - | Granite and gneissic complex |

Source: NEC, 1991

The Archaeans are exposed over an extensive area near Jowai and are also confined to the deep ravines and gorges within the sedimentary rocks. The acid and basic intrusives comprise the Pre-Cambrian stratum. The coal bearing rocks have been deposited over platform areas under stable shelf condition with the Tertiaries of the Jaiñtia Group extensively developed over these areas. These unconformably overlie the Archaeans and Pre-Cambrian formations with sediments ranging in age from Palaeocene to Upper Eocene (NEC, 1991). The rock formations strike ESE-WNW to E-W with a low dip of 2° to 12°, which increases southwards. The predominant structural lineament along the southern fringe of the district is the Dawki fault which continues eastwards into North Cachar Hills District of Assam. The geology map of the district is shown at Fig.3.3.

### 3.2.2. Physiography and Drainage

The Jaiñtia Hills District comprises of flat topped low hills with mild gradient. The mean elevation of the district ranges between 1050m to 1350m with the Maryngksih peak on the eastern part being the highest point at an elevation of 1631m from the mean sea level (Jaiñtia Hills District official website). The physiography can be divided into three parallel zones, viz. (i) the northern hills draining into the Brahmaputra Valley, (ii) the central plateau and (iii) the southern steep slope or escarpment (Bhattacharyya, 2002). The plateau shows a gradual inclination towards the south. The drainage pattern of Jaiñtia Hills shows a spectacular feature of extraordinary straight river and stream courses, evidently along joints and faults (GSI, 1974). The major rivers draining into the Brahmaputra Valley in the north include the Kopili and its tributaries, the main ones being Umiurem, Myntriang, Mynriang, Rimanar, Kharkor, Umtarang, Rashu and Sarbang; and the Umkhen River. The Umngot River forms the boundary between the East Khasi Hills and Jaiñtia Hills Districts of Meghalaya and flows south towards Bangladesh. Another major river is the Myntdu which encircles Jowai on three directions before it is joined by several tributaries, the main ones being Prang, Umlatang and Lynriang, on its way to Bangladesh. The Lubha and its main tributaries, the Umlunar and Lukha, also flow into Bangladesh through Sonapur in the east. Fig. 3.4 shows the drainage map of the coal mining areas of Jaiñtia Hills.

### 3.2.3. Climate

The district experiences tropical monsoon climate with the hottest day never going above 26°C and winter temperatures of around 8°C. The rainfall is very heavy due to orographic uplift of monsoon clouds. The average annual rainfall varied from a lowest of 2898 mm in 2006 to a highest of 5379 mm in 2007 and generally falls in the months of March to October. Table 3.4 shows the minimum and maximum temperature recorded at Jowai in 2007 and Table 3.5 shows the annual rainfall at Jowai from 2001 to 2007.

**Table 3.4: Minimum and Maximum temperature recorded at Jowai in 2007.**

| | Jan | Feb | Mar | Apr | May | Jun | Jul | Aug | Sep | Oct | Nov | Dec |
|---|---|---|---|---|---|---|---|---|---|---|---|---|
| Min (°C) | 8.23 | 9.36 | 12.58 | 15.25 | 18.00 | 18.59 | 18.97 | 19.40 | 19.40 | 19.07 | 17.01 | 9.79 |
| Max (°C) | 18.36 | 17.66 | 22.07 | 23.09 | 24.70 | 24.10 | 22.79 | 25.40 | 24.12 | 22.10 | 21.66 | 18.70 |

Source: DES, 2009

**Table 3.5: Rainfall recorded at Jowai 2001-07.**

| | 2001 | 2002 | 2003 | 2004 | 2005 | 2006 | 2007 |
|---|---|---|---|---|---|---|---|
| Rainfall (mm) | 4909 | 4169 | 3180 | 5374 | 3042 | 2898 | 5379 |

Source: DES, 2009

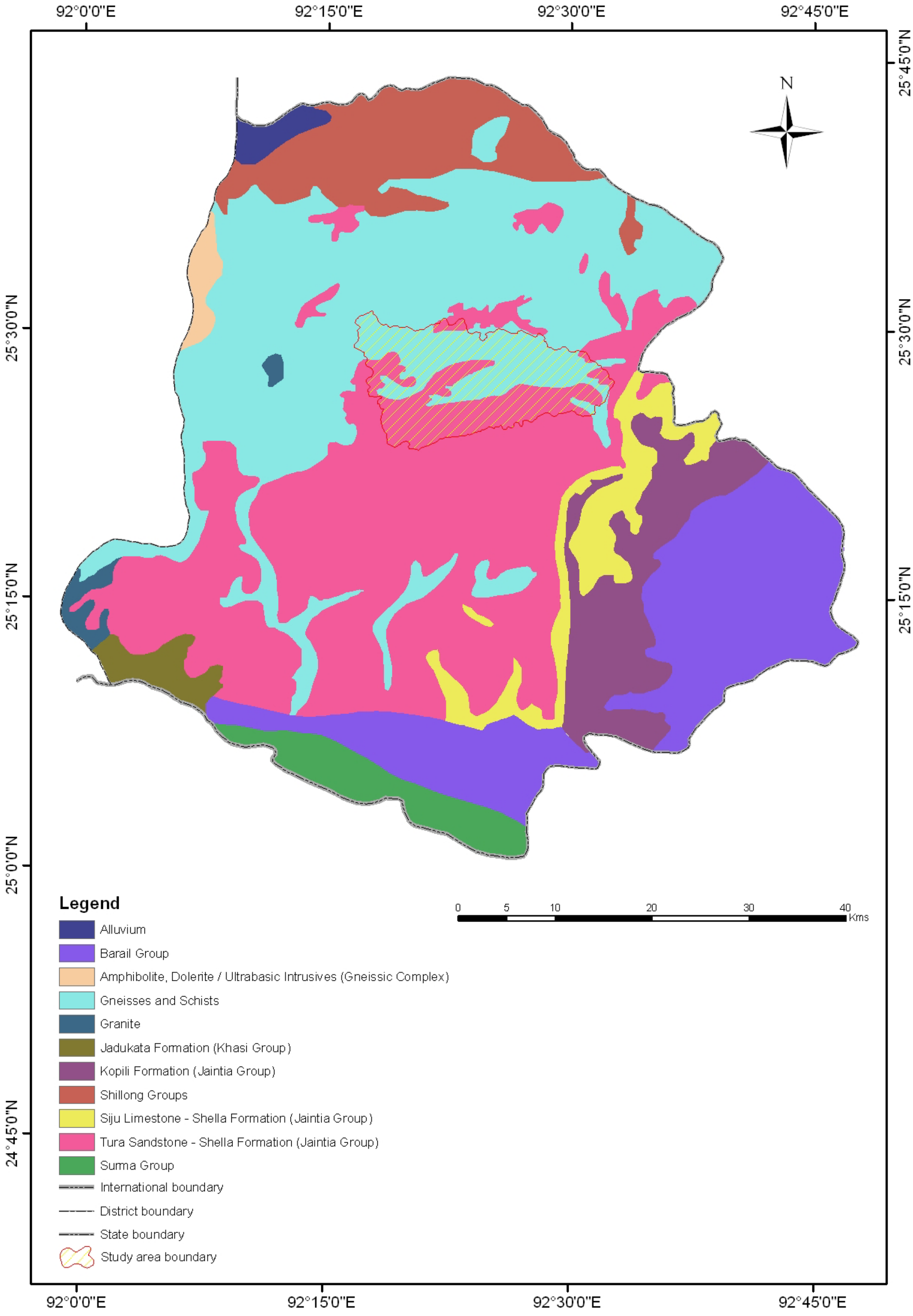

**Figure 3.3: Geology map of Jaiñtia Hills district.
(after NEC, 1991)**

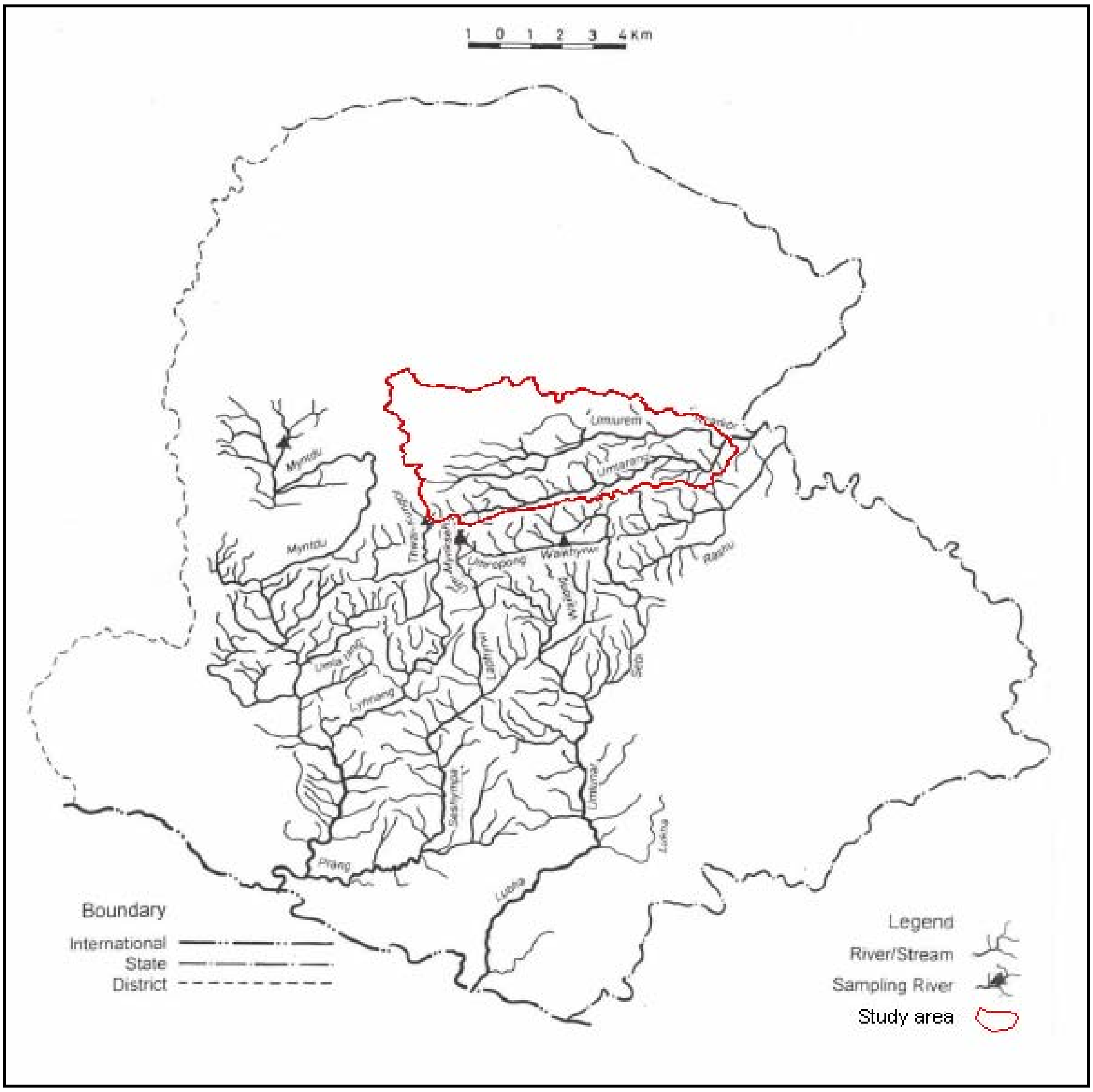

**Figure 3.4: Drainage map of coal mining areas in Jaiñtia Hills.**
**(after Swer & Singh, 2003)**

### 3.2.4. Soil

The prevalent soil types in the district are red loamy soil, red yellow soil and laterite soil. Due to the high rainfall, the top soil is very thin and at some places, the underlying rocks have been completely exposed. The soils are mostly acidic with high organic content and nitrogen but low phosphate and potash content (Bhattcharyya, 2002).

### 3.2.5. Natural vegetation

The official website of Meghalaya reports that Jaiñtia Hills District still has fairly good forest cover with 46.13% of its geographical area still under forest. Depending upon the altitude, the vegetation of Jaiñtia Hills varies from sub-tropical to temperate (Bhattacharyya, 2002). Primary forests have mostly depleted and given way to secondary forests of Pinus kesiya which grows well in the degraded conditions (Das Gupta, 1999). Bhattacharyya (2002) has categorized the vegetation into 3 types, viz. mixed evergreen forests, grasslands and pine forests. The first type are predominant in the hill slopes of the lower part of the district and consists of broad leaved trees and shrubs with scattered bamboos and timber trees. The hill tops with shallow topsoil are generally devoid of vegetation and are covered by grasslands. Temperate vegetation like pine is dominant in the uplands. A summary of the area of forest type classes in the state in given in Table 3.6.

**Table 3.6: Forest Type classes of different districts of Meghalaya.**
**(Area in sq. km.)**

| Class | East Khasi | West Khasi | Jaiñtia | West Garo | South Garo | East Garo | Ri Bhoi | Total |
|---|---|---|---|---|---|---|---|---|
| Sub tropical pine forest | 111.88 | 341.07 | 54.52 | - | - | 34.97 | 542.44 | 542.44 |
| Tropical semi-evergreen | 170.68 | 221.53 | 503.31 | 480.79 | 292.18 | 453.87 | 337.19 | 2459.55 |
| Tropical moist/ Dry deciduous | 781.74 | 1568.67 | 828.39 | 1257.08 | 716.4 | 955.5 | 859.73 | 2459.55 |
| Tropical dry deciduous and bamboo mix | 127.66 | 677.1 | 382.27 | 316.99 | 177.49 | 110.29 | - | 6967.51 |
| Degraded | 577.27 | 852 | 462.97 | 656.3 | 110.67 | 360.27 | 364.3 | 1791.8 |
| Grasslands | 182.74 | 264.72 | 128.95 | - | 28.68 | 34.61 | - | 3383.78 |
| Agriculture/ Non forest | 760.21 | 1301.43 | 1430.93 | 914.04 | 470.68 | 675.42 | 793.19 | 621.7 |
| Built up | 16.46 | - | - | - | - | - | - | 16.46 |
| Sandy area | 4.05 | 18.29 | 13.21 | 33.17 | 38.17 | 9.18 | 13.54 | 129.61 |
| Water bodies | 15.31 | 20.19 | 14.45 | 55.63 | 15.73 | 3.86 | 45.08 | 170.25 |
| **Total** | **2748** | **5247** | **3819** | **3714** | **1850** | **2603** | **2448** | **22429** |

Source: Meghalaya official website

## 3.3. Coalfields of Jaiñtia Hills

Meghalaya has an estimated coal reserve of 559 million tones, which are spread over in an area of 213.9 sq. km. The Garo Hills district has the highest coal reserve of 390 million tones, followed by West Khasi Hills (98 million tones), Jaiñtia Hills (39 million tones) and East Khasi Hills districts (31 million tones) (Fig. 3.5.) (DEF, 2005). Due to inaccessibility of most of the coalfields because of slow development, coal mining in the Garo Hills is still in its nascent stage. Mining of coal in the Jaiñtia Hills started more than 100 years ago, primarily for domestic use, and its commercial extraction started to increase only after 1978-79 (De, 2007). The district produces more than 50% of the state's total production with mining being actively carried in all the identified coalfields. Fig.3.6, details of which are given as Appendix 1, gives the production of coal from 1994 till 2009.

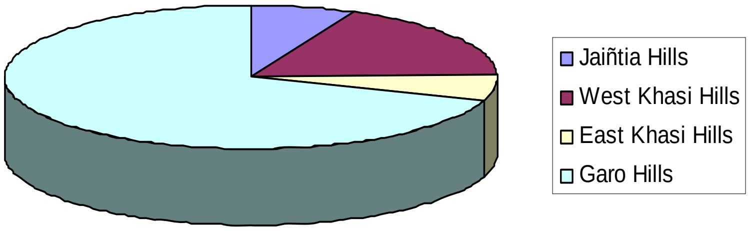

**Figure 3.5: Coal reserves in Meghalaya.**

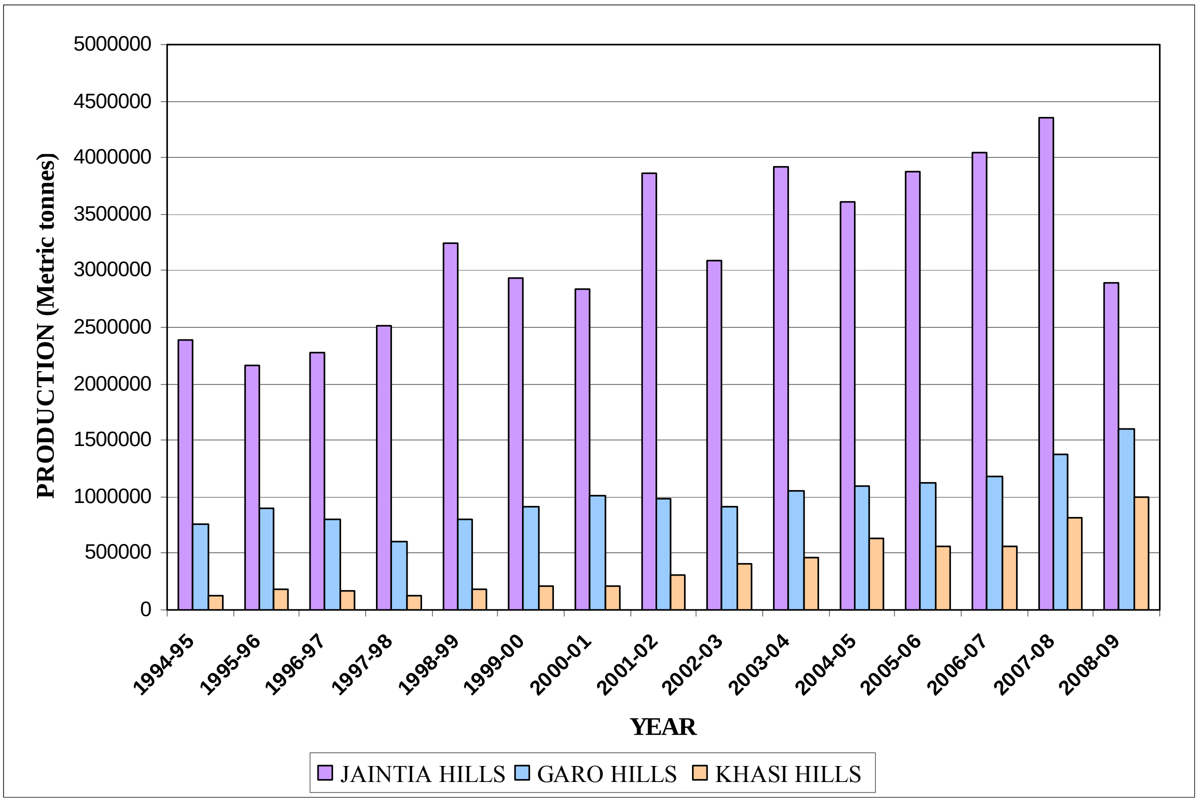

**Figure 3.6: Production of coal in Meghalaya from 1994-95 to 2008-09.**

Source: DMR, Govt. of Meghalaya

The coalfields of Jaiñtia Hills are located in the central and southern part of the district between 25°10’N and 25°28’N latitudes and 92°8’E and 92°33’30”E longitudes. The coal bearing strata covers an area of 70 sq.km. and is spread out in small detached patches. All the coalfields have the same geographical, stratigraphical and structural set-up. The main coal occurrences are Jaraiñ-Skhentalang, Lakadong, Lumshnong, Malwar-Musiang Lamare, Mutang, Bapung, Sutnga and Iooksi. Out of these, the Bapung coalfield is the most important in terms of areal extent and accessibility (NEC, 1991).

### 3.3.1. Jaraiñ-Shkentalang

This field has an inferred coal reserve of 1.1 million tonnes within an area of 2.8 sq.km. The coal seams occur in the Therria Formation (Lower Sylhet Sandstone) of Palaeocene Age. Two seams with thickness varying from 0.10m to 0.15m and from 0.30m to 1.00m have been observed. The coal shows moisture of 1.6%, ash 4.4%, volatile matter 48.1% total sulphur 5% and calorific value of 8450 Kcal/kg (GSI, 1974, 1981; NEC, 1991; DMR office records).

### 3.3.2. Lakadong

The Lakadong plateau covers a large area between the Hari and Prang Rivers. Coal occurrences have been reported from the Umlatdoh and Pamsaru areas with proven reserves of 5 million tonnes. In Umlatdoh a seam of thickness from 0.3m to 2.1m, in the Lakadong sandstone of Eocene Age, has been recorded over an area of 1.04 sq.km. In a few places, a thin seam varying in thickness from 0.1 to 0.3m overlies the lower main seam with a parting of 12m. In Pamsaru, a seam of

0.31 to 1.1m thickness in the Lakadong sandstone has been recorded over an area of 0.5 sq.km. The coal here shows moisture of 1.8% to 4.2% (at 60% RH and 40°C), ash of 3.7% to 17.1% and volatile matter of 32.3% to 36.8%. The coal is strongly caking with Caking Index of 31 to 33. Total sulphur is 3.2% to 5.3% of which organic sulphur is 95.7% to 99.2%. The Lakadong coal is said to be of the best quality available in the Northeast, however, the coal seams are not economical to work (GSI, 1974, 1981; NEC, 1991; DMR office records).

### 3.3.3. Lumshnong

Several isolated exposures are recorded in west and south-west of Lumshnong in an area of 0.6 sq.km. The seam has an E-W trend which dips to the south at 4° to 6° and a thickness of 0.3 to 0.6m. The coal shows moisture 1.6% to 1.8%, ash 3.2%, to 3.8% and total sulphur 1.6% to 4%. The inferred reserve of coal in this area is 0.2 million tones. The area does not offer any prospect for large scale mining (GSI, 1981; NEC, 1991).

### 3.3.4. Malwar-Musiang Lamare

Exposures of coal have been reported around Malwar and Musiang-Lamare villages confined to the Lakadong sandstone over an area of 2.59 and 2.31 sq.km. respectively. In Malwar, there is only one seam with thickness ranging from 0.31 to 1.67m. In Musiang-Lamare, the coal seam shows pinching and swelling and varies in thickness from 0.31 to 1.06m. The general strike of the seams is ENE-WSW and the dip varies from 7° to 10° towards SSE. The analytical data of this coal shows moisture 4.7% (at 60% RH and 40°C), ash 1.4%, and volatile matter 33.4%. The coal is weakly caking with Caking Index being less than 5. The calorific value is around 7400 Kcal/kg and total sulphur is 4.8% of which organic sulphur is most dominant (97.9%). The area contains an inferred reserve of 1.1 million tonnes of coal (GSI, 1981; NEC, 1991; DMR office records).

### 3.3.5. Mutang

A coal seam with a thickness varying from 0.25 too 1.8m has been recorded to the north-west of Mutang village. The seam shows a conspicuous pinching and swelling and as such does not merit any further attention (GSI, 1981).

### 3.3.6. Bapung

The Bapung coalfield is the most important coalfield in the Jaiñtia Hills with inferred reserves of 33.66 million tonnes within an area of 46 sq.km. A coal seam varying in thickness from 0.31m to 1.05m, striking in an ESE-WNW direction with south-westerly rolling dips varying from 4° to 7°, has been reported. The coal on air dried basis analyses 2.02 % to 4.2% moisture, 2.3% to 5.78% ash and 40.54% to 53.84% volatile matter. The sulphur content ranges from 2.77% to 5.21% (GSI, 1981; NEC, 1991; DMR office records).

### 3.3.7. Sutnga

The Sutnga coalfield is an extension of the Bapung coalfield. Outcrops of coal have been recorded within the lower most member of the Sylhet limestone within an area of 0.16 sq.km. Two coal seams have been recorded with the top seam having thickness of 0.1 to 0.2m and the bottom of

0.3 to 1.07m. The seam shows a low regional dip of 3° towards south. The coal shows moisture of 1.5% to 2.3%, ash of 2.2% to 3%, volatile matter of 42.4% to 42.8%, total sulphur of 4% to 4.9% and calorific value of 8050 to 8345 Kcal/kg. The total inferred reserves here are 0.65 million tonnes (GSI, 1981; NEC, 1991; DMR office records).

### 3.3.8. Iooksi

The coal occurrences in Iooksi are found in the Therria sandstone with thickness varying from 0.5 to 0.9m and lying within an area of 3.6 sq.km. The ash content varies from 6.0 to 18.1%, volatiles from 33.0 to 43.4% and the coals are weakly caking. Total sulphur varies from 2.19 to 6.32%. The total inferred reserve is 1.5 million tonnes (NEC, 1991; DMR office records).

## 3.4. Present Study Area

This study is carried out in the watershed of the Umiurem and Umtarang (Myntriang) Rivers (Fig.3.2) which is located towards the central part of the Jaiñtia Hills District between 92°15'E and 92°34'E longitude and between 25°20'N and 25°32'N latitude. The catchment covers an area of 237.44 sq.km. This catchment falls within the Bapung coalfield and encompasses the active coal mine areas of Bapung and Sohkynphor. The two rivers join with the Kopili River, the main feeder of the Kopili Hydro-electricity Project of the North Eastern Electric Power Corporation Limited (NEEPCO) which generates 275 MW of power. This area has been primarily selected because of the availability of RESOURCESAT-1 (IRS-P6) LISS-IV and CARTOSAT-1 images from the National Remote Sensing Centre, Hyderabad. The watershed has an elevation ranging from 746m to 1400m above MSL (Fig. 3.7.). The drainage showing Strahler's stream order 3 onwards is shown in Fig. 3.8.

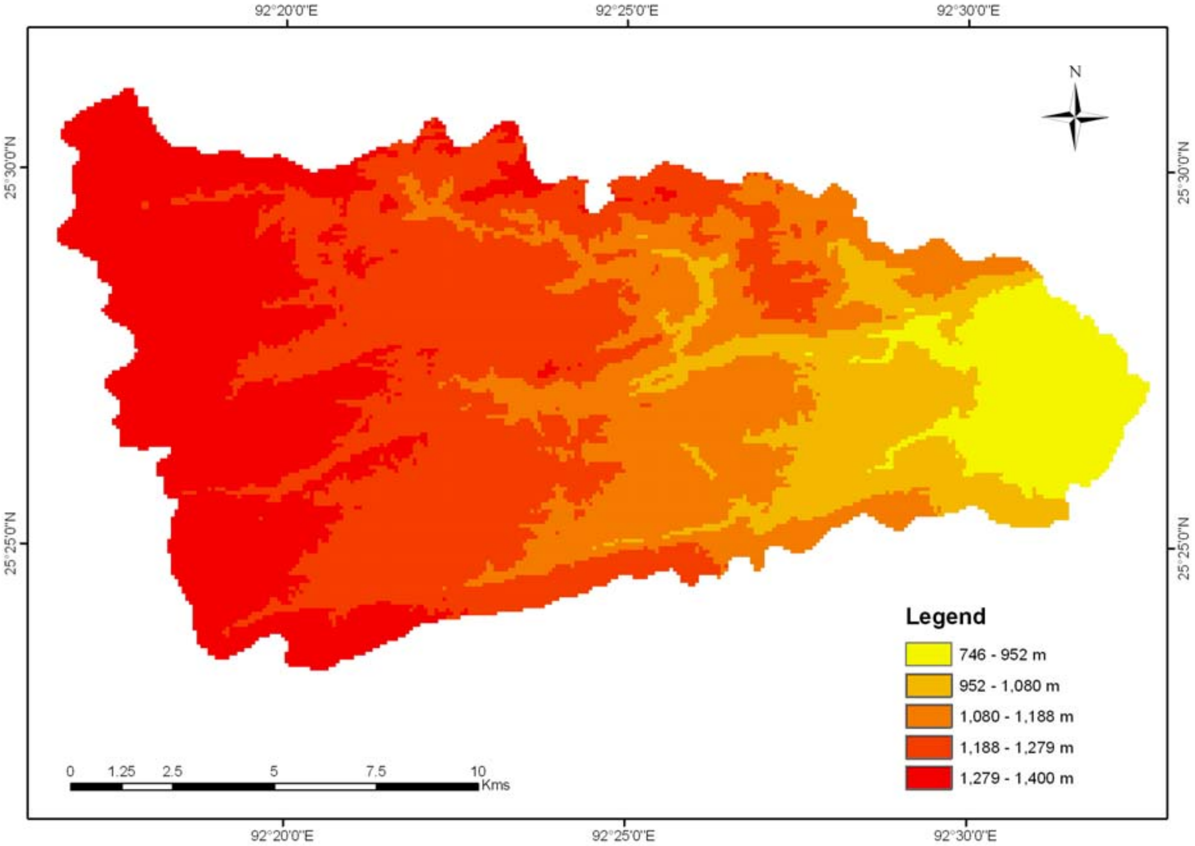

**Figure 3.7: SRTM DEM of study area.**

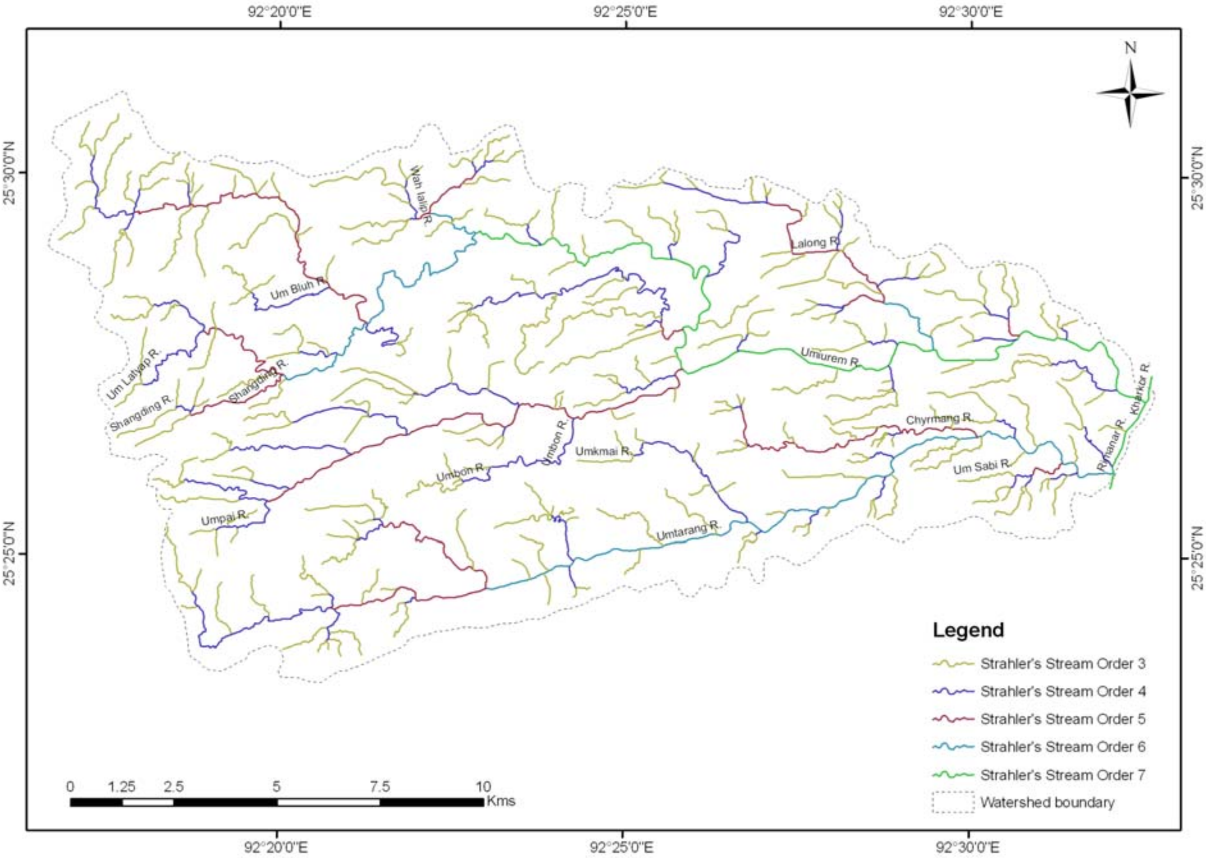

**Figure 3.8: Drainage in study area.**

### 3.4.1. Geology of the study area

The study area consists of only two major lithological groups, the contact of which runs horizontally across and dividing it into almost two equal parts. The geology is shown at Fig.3.9. This map has been extracted from Fig.3.3 with slight modifications done by Dr. S .K. Srivastava, Thesis Supervisor, after field survey and through interpretation of the merged CARTOSAT-1/ RESOURCESAT-1 (IRS P6) LISS-IV image.

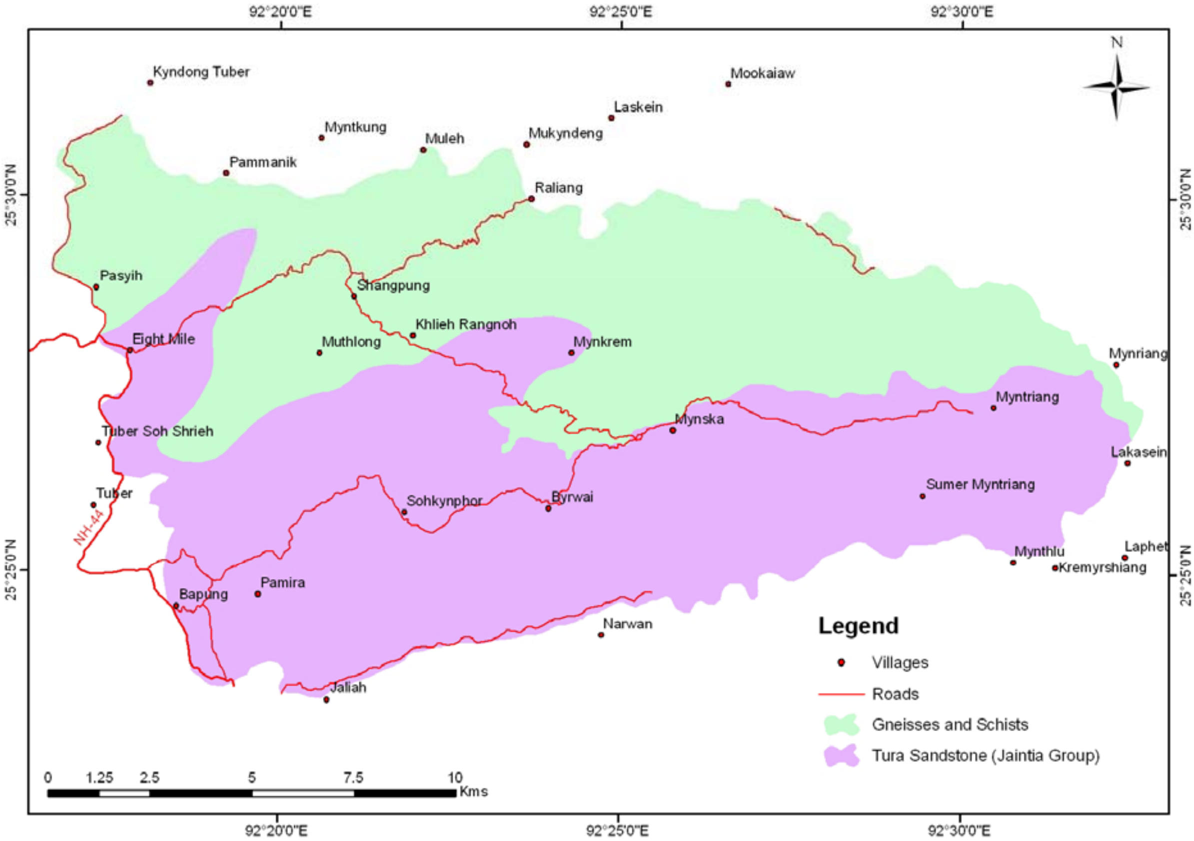

**Figure 3.9: Geology of the study area.**

At 8th Mile village, we first come across gently dipping weathered sandstone (Fig.3.10a) which continues eastwards till Umbluh River (Sampling station R8) where we find an outcrop of gneisses on both banks of the river (Fig.3.10b and Fig.3.10c). After this, we find gneisses all the way to the eastern corner of the study area with another contact at Pyntei Village, located between Raliang and Biar (Sampling station R26), which lies outside the watershed (Fig.3.10d). Granitic gneisses are observed again just to the east of Raliang (Fig. 3.10e). There are also some evidences of spheroidal weathering of granitic gneisses near Raliang (Fig.3.10f).

(a) Gently dipping sandstone at 8th Mile Village.

(b) Gneisses on western bank of Umbluh River.

(c) Gneisses on eastern bank of Umbluh River.

(d) Lithological contact at Pyntei.

(e) Granitic gneisses outside Raliang.

(f) Spheroidal weathering of granitic gneisses near Raliang.

**Figure 3.10: Field photographs depicting the geology of the study area.**

Near Mynska, just to the west along the road, there is a seepage zone (Sampling station A9) with yellow stains seen on the wall and along flow path (Fig.3.11a and Fig.3.11b). The southern part of the study area comprises of sandstone of the Jaiñtia Group with coal bearing strata. Figures 3.11c – 3.11f show the lithology at different places in the southern part of the study area.

(a) Seepage zone near Mynska with yellow stains on wall (sampling location A9).

(b) Seepage zone near Mynska (sampling location A9).

(c) Horizontally bedded sandstone at 8th Mile.

(d) Horizontally bedded sandstone at Mookhep.

(e) Near horizontal thin bedded sandstones with coal horizon.

(f) Close-up of the coal horizon.

**Figure 3.11: Field photographs depicting the geology of the study area.**

### 3.4.2. Soils in the study area

The study area is made up of soils of the Upper Plateau which are mainly of three types (NBSSLUP, 1996):

(1) Deep, excessively drained, fine soils on moderately sloping side-slopes of hills having loamy surface with moderate erosion hazard; *associated with:* Moderately deep, excessively drained, coarse-loamy soils on gently sloping hill tops with very severe erosion hazard and strong stoniness. The soil taxonomies include Typic Kandiudults and Typic Dystrochrepts.

(2) Deep, excessively drained, fine soils on moderately sloping side-slopes of hills having loamy surface with moderate erosion hazard; *associated with:* Deep, poorly drained, fine-loamy soils on very gently sloping valleys with very slight erosion hazard and groundwater table below one metre depth of the surface. The soil taxonomies include Typic Hyplohumults and Humic Haplaquepts.

(3) Deep, excessively drained, fine soils on moderately sloping side-slopes of hills having loamy surface with moderate erosion hazard; *associated with:* Moderately deep, excessively drained, fine-loamy soils on gently sloping hill tops with very severe erosion hazard and strong stoniness. The soil taxonomies include Typic Kandihumults and Typic Dystrochrepts.

# 4. Materials and Methods

This chapter discusses the different inputs used for the study along with the methodology employed to obtain the final results to address the research objectives. The software and instruments used have also been listed.

## 4.1. Materials

### 4.1.1. Satellite Images and Ancillary Data

The different satellite images and ancillary data used for this study are described in Table 4.1.

**Table 4.1: List of data acquired.**

| S. No. | Data | Source | Date of acquisition |
|---|---|---|---|
| 1. | ASTER<br>AST_L1B_00301282003043638_20080519221916_6715 | ITC, Enschede, The Netherlands | 28-01-2003 |
| 2. | ASTER<br>AST_L1B_00301312004043603_20070726053442_27260 | ITC, Enschede, The Netherlands | 31-01-2004 |
| 3. | ASTER<br>AST_L1B_00302162004043602_20080519221946_7637 | ITC, Enschede, The Netherlands | 16-02-2004 |
| 4. | Landsat 7 (ETM+) Path 136, Row 042<br>**Author:** NASA Landsat Program<br>**Publication Date:** 12-02-2004<br>**Collection Name:** Landsat7 ETM+<br>**Image Name:** p136r042_7dx19991219.ETM-GLS2000<br>**Processing Level:** Ortho, GLS2000<br>**Publisher:** USGS<br>**Publisher Location:** Sioux Falls<br>**Product Coverage Date:** 19-12-1999 | Global Land Cover Facility, www.landcover.org. | 19-12-1999 |
| 5. | SRTM WRS2 tile Path 136, Row 042<br>**Author:** USGS<br>**Publication Date:** 2006<br>**Collection Name:** Shuttle Radar Topography Mission<br>**Image Name:** 3 arcsec scene SRTM_ffB03_p136r042<br>**Processing Level:** 3 arcsec, Filled Finished-B<br>**Publisher:** Global Land Cover Facility, University of Maryland<br>**Publisher Location:** College Park, Maryland<br>**Product Coverage Date:** February 2000 | Global Land Cover Facility, www.landcover.org | February 2000 |

| | | | |
|---|---|---|---|
| 6. | IRS P6 (RESOURCESAT-1) LISS 4 Path 101, Row 042 | NRSC, Hyderabad | 30-03-2007 |
| 7. | IRS P6 (RESOURCESAT-1) LISS 4 Path 101, Row 054 | NRSC, Hyderabad | 05-02-2008 |
| 8. | CARTOSAT-1 PAN-A Path 607, Row 280 | NRSC, Hyderabad | 27-01-2006 |
| 9. | CARTOSAT-1 PAN-A Path 608, Row 280 | NRSC, Hyderabad | 16-01-2006 |
| 10. | QuickBird Standard Imagery Bundle (black and white and multispectral), a subset of catalog ID 1010010004C76600 | Digital Globe, USA | 30-01-2006 |
| 11. | Google Earth merged PAN and multispectral image of QB02 sensor of QuickBird | GoogleEarth | 30-01-2006 |
| 12. | ASTER GDEM ASTGTM_N25E092_dem | ASTER GDEM website | -- |
| 13. | Topographic maps: Sheet Number 83-C/6, 7 and 11 ; scale 1:50,000 | Survey of India | -- |
| 14. | Geology map of Meghalaya (scale 1:500,000) | NEC, Shillong | -- |
| 15. | Meghalaya Soil map (scale 1:500,000) | NBSSLUP, Jorhat | -- |

### 4.1.2. Software used

The software used during the course of the study are given below:

- ArcGIS 9.3
- ERDAS Imagine 9.1
- Definiens Developer 7.0

### 4.1.3. Instruments used

The following instruments were used during field survey and for analysis of the water and sediment samples:

- Eutech Cyberscan pH11 pH/mV/°C meter
- Aqualytic SensoDirect CD24 conductivity meter
- Garmin GPS12 GPS meter
- Systronics Spectrophotometer
- Merck ThermoScientific UV10 spectrophotometer
- Shimadzu AA680 and PerkinElmer 2380 Atomic Absorption/Flame Emission Spectrophotometer (AAS)
- Varian Liberty II sequential inductively coupled plasma optical emission spectrometer (ICP-OES)
- Atomic Absorption/Flame Emission Spectrophotometer
- Systronics Digital Nepheloturbidity meter
- Chemito Flame Photometer

## 4.2. Methodology

To meet the desired objectives, the methodology of this study has been divided into the following parts:

- Pre-field data collection and preparation.
- Visual interpretation and digital image processing of satellite images.
- Water and sediments field sampling during two seasons and their analysis.

- Data representation and interpretation.
- Preparation of maps showing the spatial distribution of trace metals due to AMD in the catchment.

A schematic of the methodology has been given at Fig.4.1.

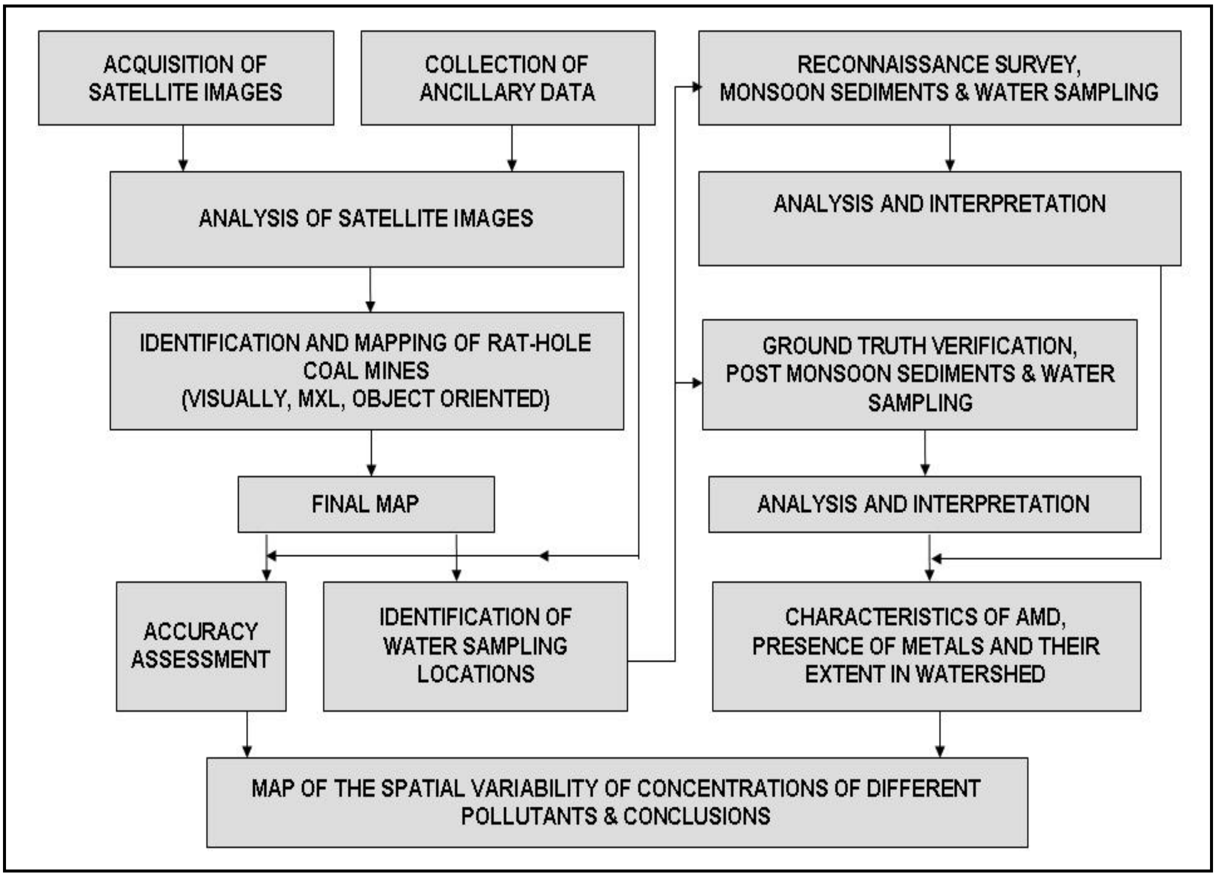

**Figure 4.1: Schematic diagram of methodology.**

### 4.2.1. Pre-field data collection and preparation

- Satellite data acquisition.
- Preparation of base map of the catchment area from Survey of India topo-sheets, including extraction of watershed boundary and drainage in the catchment.
- Collection of ancillary data from various organizations and state government departments.

### 4.2.2. Image processing and interpretation

#### 4.2.2.1. ASTER images

The ASTER images obtained from ITC, the Netherlands consisted of the three VNIR bands only, i.e. band 1 (green), band 2 (red) and band 3N (near infrared). Hence, it was not possible to do any processing by band ratio calculation. Further, with a spatial resolution of 15m, identification of the artisanal coal mines using these images was impossible as the mines have a diameter or a side of about 6 to 8m. These images were shelved and no processing was done on them.

#### 4.2.2.2. Landsat ETM+ images

The Landsat ETM+ images with spatial resolutions of 15m for panchromatic and 30m for multispectral could not be used for identification of the small artisanal “rat-hole” type coal mines even after their fusion (15m spectral resolution). However, because of having seven bands spread through a wide range of the electromagnetic spectrum, Landsat ETM+ is very well suited for carrying out band ratio calculation and stacking different ratio images, using the primary colors, to produce hybrid FCC’s which can give a better idea about the land use and land cover in the study area.

As coal mining is associated with the presence of iron and its oxides, the ETM+ images were used to detect the presence of iron oxides/hydroxides on the stream beds, as a preliminary overview of the presence of AMD in the study area. As stated earlier, the oxidation and hydrolysis of iron pyrites in coal leads to the formation of sulphuric acid and precipitation of iron oxide/hydroxide. The latter forms an orange, yellow or red colored coating at the bottom of stream beds which is often called “yellow boy” or ochre. During the lean season, these ochre-coated stream beds are exposed and, in satellite imagery, show a typical red-orange signature when viewed as true color composite (TCC). Fig. 4.2 and 4.3 show a couple of Google Earth screen shots of parts of the study area to corroborate this.

**Figure 4.2: Google Earth screen shot of Umtarang (Myntriang) River.**

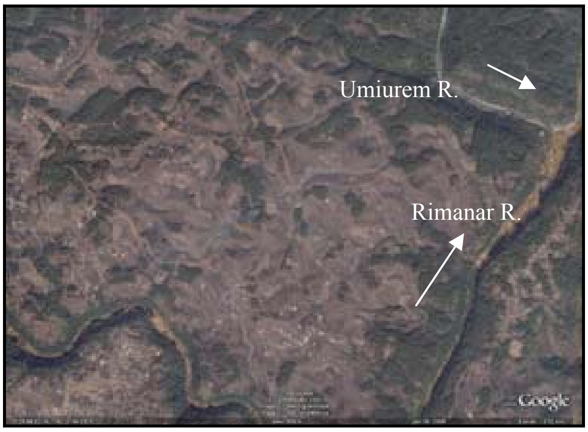

**Figure 4.3: Google Earth screen shot of Rimanar River.**

All thirty possible band ratios were generated using the ERDAS software Model Maker. Three ratio images were taken at a time and hybrid FCC’s were generated by assigning each ratio image a primary color. This way several FCC’s were generated using different ratio combinations. These images were interpreted to detect the presence of iron oxides on stream beds.

#### 4.2.2.3. Merged CARTOSAT-1 and RESOURCESAT-1 (IRS-P6) LISS-IV images

The first step was to merge the 2.5m spatial resolution panchromatic CARTOSAT-1 image with the 5.8m spatial resolution multispectral image of RESOURCESAT-1 (IRS-P6) LISS-IV in the ERDAS Imagine software using the available algorithms with Brovey Transform method and nearest neighbour resampling technique giving the best result (Fig.4.4). In order to improve the classification, along with the merged image, the following layers were added (Saha *et al.*, 2005):

1. NDVI layer generated from the RESOURCESAT-1 (IRS-P6) LISS-IV image,
2. First and second principal components of the RESOURCESAT-1 (IRS-P6) LISS-IV image, and
3. ASTER GDEM.

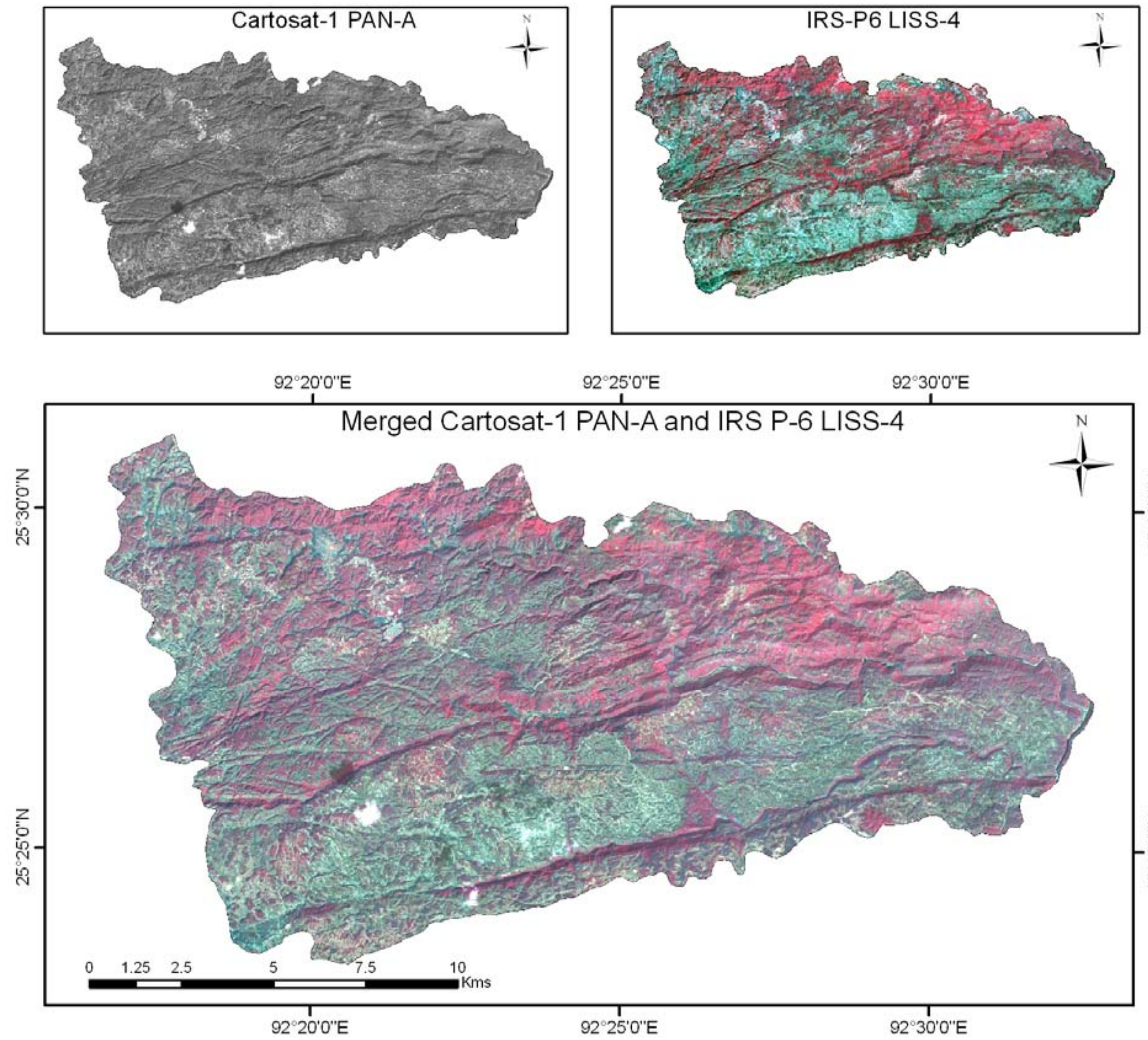

**Figure 4.4: The original images before merging and the merged image.**

A supervised classification using Maximum Likelihood Classifier (MXL) was carried out to classify the study area into five classes:

1. Forest,
2. Fallow and Barren land,
3. Settlements and Roads,
4. Rivers, and
5. Mines.

### 4.2.2.4. Visual interpretation

The merged CARTOSAT-1/RESOURCESAT-1 image was visually interpreted to map the extent of mining area. The mine shafts were identified through their peculiar signature of dark spots surrounded by bright over burden dumps. Fig.4.5 shows a zoomed-in view of a part of the watershed with labels indicating the different features. Fig.4.6 shows how the mines look like on the ground. The mine shafts were digitized as point features, while the entire area of mine and overburden was digitized as polygons and each polygon was treated as a mine.

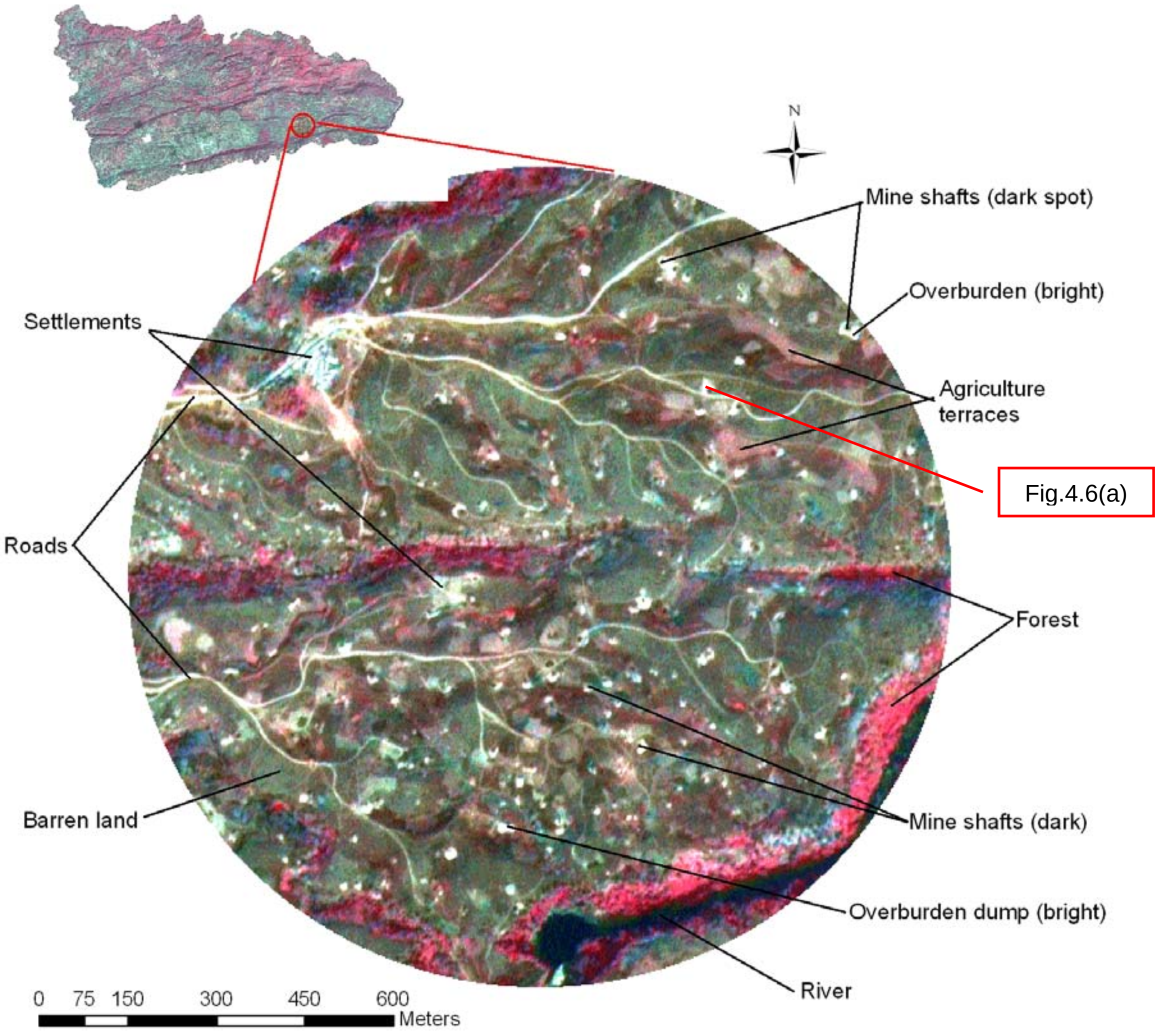

**Figure 4.5: Zoomed-in view of part of the watershed.**
**(as seen in the merged CARTOSAT-1/RESOURCESAT-1 LISS-IV image)**

The QuickBird panchromatic (61cm spatial resolution at nadir) and multi-spectral (2.44m spatial resolution at nadir) were merged so as to serve as a base for accuracy assessment of the interpretation. Merging was done on ERDAS software using the various available algorithms with the best result produced by Principal Component method and cubic convolution resampling. The merged image was visually interpreted in the same way as the merged CARTOSAT-1/RESOURCESAT-1 image. Accuracy assessment was done by comparing the number of intersecting mine polygons between the QuickBird and the merged CARTOSAT-1/RESOURCESAT-1 images.

(a) A mine near Chyrmang. (b) A mine south of Narwan Road.

(c) A new mine being dug south of Narwan Road. (d) A mine east of road to Lakaseiñ.

**Figure 4.6: Views of mines around the study area.**

### 4.2.2.5. Object oriented image classification

The extent of the mining area within the watershed was also mapped in a semi-automatic way by developing an algorithm for OOC in the Definiens Developer 7 software. First of all, the different layers to be used in the process were selected (Fig.4.7). The main image used for the classification was the merged CARTOSAT-1/RESOURCESAT-1 image. Its three layers were given a weight of one each. The other layers added were the CARTOSAT-1 panchromatic image and the NDVI layer generated from the RESOURCESAT-1 LISS-IV image. These layers and those added subsequently were not given any weight for classification. As the main objective was to identify and map the extent of mines in the watershed, features that were not required with this classification were masked out one by one. This procedure has been followed after Barlow *et al.* (2003, 2006).

It was observed that the CARTOSAT-1 panchromatic image contained a few clouds and shadows. Therefore, a layer was created to mask out these features. As mines were not expected to exist along river courses, a layer was created to mask out the river courses also. The slope layer was added in order to mask out the steep land where mines were not expected to exist. It may be mentioned that both ASTER GDEM and SRTM DEM were used to create the drainage and slope maps. It was found that SRTM DEM, even with a spatial resolution of 90 m, produced better results than ASTER GDEM with 15 m resolution. The latter produced a drainage network with several gaps in it and proved useless for the task. The NDVI layer generated from IRS-P6 LISS-IV image was used to mask out vegetation. The CARTOSAT-1 panchromatic texture image was generated through Image Interpreter in ERDAS Imagine software and this, along with the geology layer of the watershed (Fig.3.9), were used to fine tune the classification process.

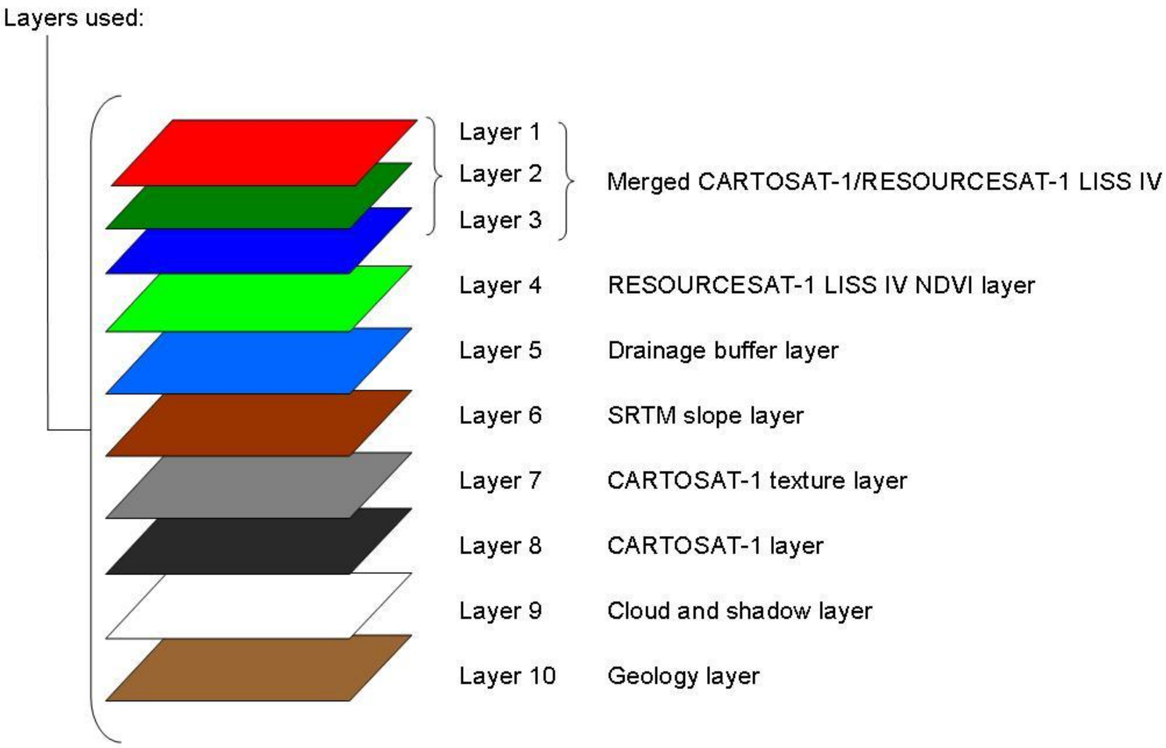

**Figure 4.7: Layers used for OOC of merged CARTOSAT-1/RESOURCESAT-1 image.**

The first and most important step to any OOC is image segmentation. Segmentation is performed by splitting the image into zoned partial areas of differing characteristics called image objects. Each image object is a group of connected pixels representing a definite region in an image (Definiens, 2008b). Image objects are pixels grouped on the basis of their reflectance characteristics, shape criteria, texture and proximity, making OOC a powerful classification tool because it allows the incorporation of texture and areal characteristics, such as the length to width ratio, shape index, etc, to be included for classification (Barlow, 2003; Moine, 2009). The software uses six algorithms for segmentation. However, for the present study only the following two were used (Definiens, 2008a):

***Quadtree based segmentation*** which splits the image into a quadtree grid formed by square objects. Each square firstly has the maximum possible size and secondly must fulfil the homogeneity criteria defined by the mode and scale parameter. Mode defines either the color difference, which should be less than a user defined scale, or the super object form, which stipulates that each square object must completely fit into the super-object. The latter condition works only if there is an upper image level.

***Multi-resolution segmentation*** which applies an optimization procedure that locally minimizes the average heterogeneity of image objects for a given resolution. Image layers can be weighted differently depending on their importance or suitability for the segmentation result. Thematic layers can also be added and weighted for consideration during segmentation process. A scale parameter is defined to determine the maximum allowed heterogeneity for the resulting image objects. The size of image objects can be varied by modifying the value of the scale parameter**.** The homogeneity criterion is calculated as a combination of color and shape properties. These parameters define the percentage to which the spectral values of the image layers will contribute to the entire homogeneity criterion. The user has to assign a weight between 0.1 and 0.9 to shape criterion, which indirectly defines the color criterion (color criterion = 1 – shape criterion). The shape criterion is composed of two complementary parameters, smoothness and compactness. The former is used to optimize image objects with regard to smoothness of borders and the latter with regard to compactness. A weight between 0.1 and 0.9 is given to compactness, which will indirectly define the smoothness (smoothness = 1 – compactness).

After the image has been suitably segmented, the objects are then classified "to give them both a meaning and a label" (Definiens, 2008b). The software generates a host of statistics, including layer mean values, shape, texture, relationships between classes and between levels, etc., for each image object and these statistics are used to discriminate between objects. Each class has to be defined by a set of criteria and the objects are assigned to a class which best fits these criteria. The whole sequence of segmentation and classification is defined in a rule set which consists of a list of processes and commands, organized in a tree-like structure, which can be edited and executed individually and which, when executed entirely, detects the objects of interest as required (Definiens, 2008b).

The present study area has an area of 237.44 sq.km., so, classification rules were first developed for a subset (Definiens, 2008b) which was about 20 sq.km. in area (Fig.4.8). After many trials, it was found that the best segmentation was achieved through multi-resolution segmentation process with a scale factor of 7, shape factor of 0.2 and compactness of 0.1. The classification followed thereafter was taken after Barlow *et al.* (2003, 2006) wherein identification of the mines was done by eliminating the other features one by one. The unclassified background, rivers and steep slope were masked out by taking the mean values in respective layers. Vegetation was masked out by using the NDVI layer and fine tuned by using mean layer value of the CARTOSAT-1 panchromatic layer. The latter layer mean value was also used to mask out barren and fallow land. Roads were classified by using shape properties of length to width ration and shape index. The settlements were classified by using texture after Haralick, grey level co-occurrence matrix (GLCM) dissimilarity in all directions of the CARTOSAT-1 texture image. The unclassified objects were considered to be mines.

Subsequently, this rule set was used to segment and classify the entire image. A problem arose because the study area was relatively big and there was not enough computer memory space for multi-resolution segmentation. To overcome this, it was found fit to combine quadtree based and multi-resolution segmentation processes. Defininens (2008b) suggested that by running a quadtree based segmentation first and then merging the small image objects through multi-resolution, one can save a lot of computing time with no significant differences in the results. Therefore, for the entire study area, a quadtree based segmentation, in the color mode and with a scale factor of 6, was first run on the image. From the resultant objects, the background, clouds, shadows and rivers were classified and masked out. A multi-resolution segmentation was then run on the unclassified objects. This step refined the shape of the objects, particularly that of the roads. The steep slope, vegetation and barren and fallow land and roads were classified by the same rules used for the subset. For settlements, besides the texture rule, the geology of the study area was also used. It was found that there was a lot of confusion between the mines and settlements as both have not only almost the same spectral signature but texture was found to be similar too. Many settlement objects, especially around the central and northern parts of the study area, were misclassified as mines by the rule set. Visually it was observed that there were no mines existing in the areas mapped as gneiss and schist in the central and northern parts of the watershed. The geology layer was used to classify all unclassified objects within gneisses as settlements. The rule set used to classify the entire area is given as Appendix 2. A schematic of the entire process has been summarized in Fig. 4.9.

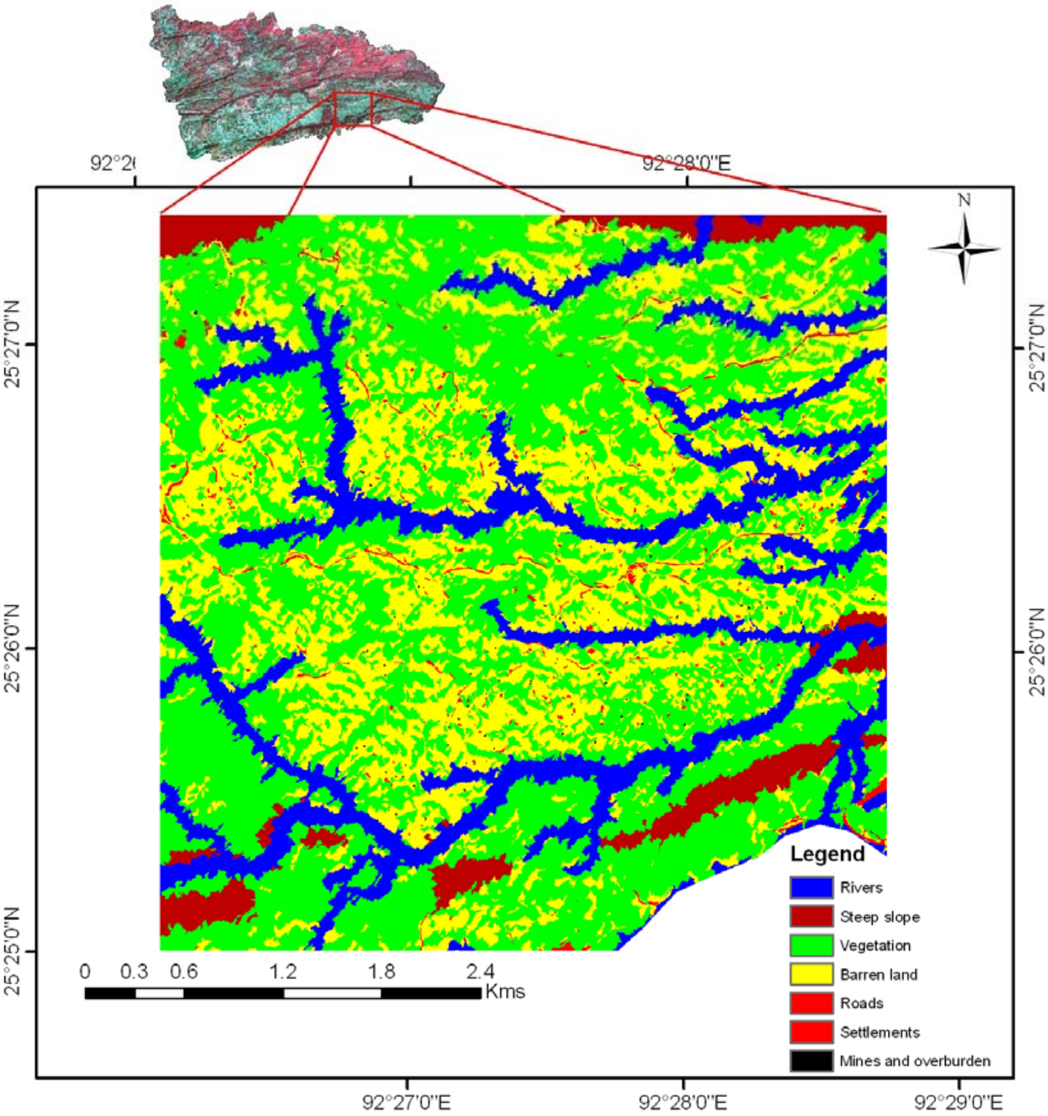

**Figure 4.8: Location of subset used in OOC of merged CARTOSAT-1/RESOURCESAT-1 image.**

To check the accuracy of the semi-automatic classification, it was first exported as a shape file with only the mine polygons. This was compared with the visually interpreted map of mine distribution. An intersection of the two maps gave the correctly identified mines. Over identified mines gave the error of commission while unrecognized mines gave the error of omission.

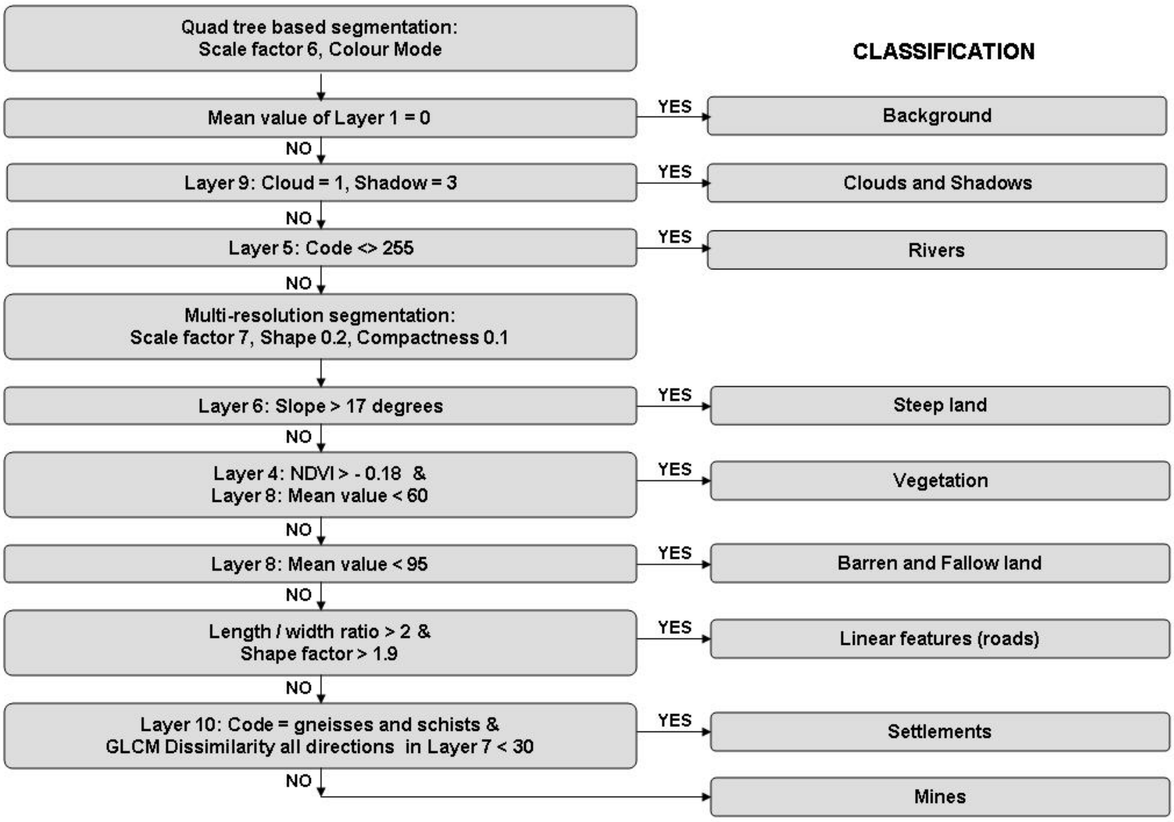

**Figure 4.9: Schematic of OOC process for merged CARTOSAT-1/RESOURCESAT-1 image.**

To validate the OOC process, the rule-set used for the above classification was used for a semi-automatic classification of a 2.4 sq.km. subset of the pan-sharpened QuickBird image. A subset had to be taken as the segmentation process could not be carried out on the whole image because of computer memory problem. The layers that were not used in this OOC were that of (i) geology, because the QuickBird image was only of areas within sedimentary rock, (ii) cloud and shadow, (iii) slope, because it was generated from SRTM whose 90 m spatial resolution was too big to match with the 61cm spatial resolution of the pan-sharpened QuickBird image, (iv) texture image of CARTOSAT-1 panchromatic data generated by using ERDAS Imagine software, and (v) CARTOSAT-1 panchromatic image. The image segmentation parameters were also changed to suitably match with the spatial resolution. For the quadtree segmentation in color mode, a scale factor of 50 was selected and for the multi-resolution segmentation used in the second segmentation step, a scale factor of 25 was used. Shape was given a weight of 0.5 and compactness 0.4. The threshold values used for class description had to be changed also. However, the basic process was the same. A schematic for this process is given at Fig.4.10.

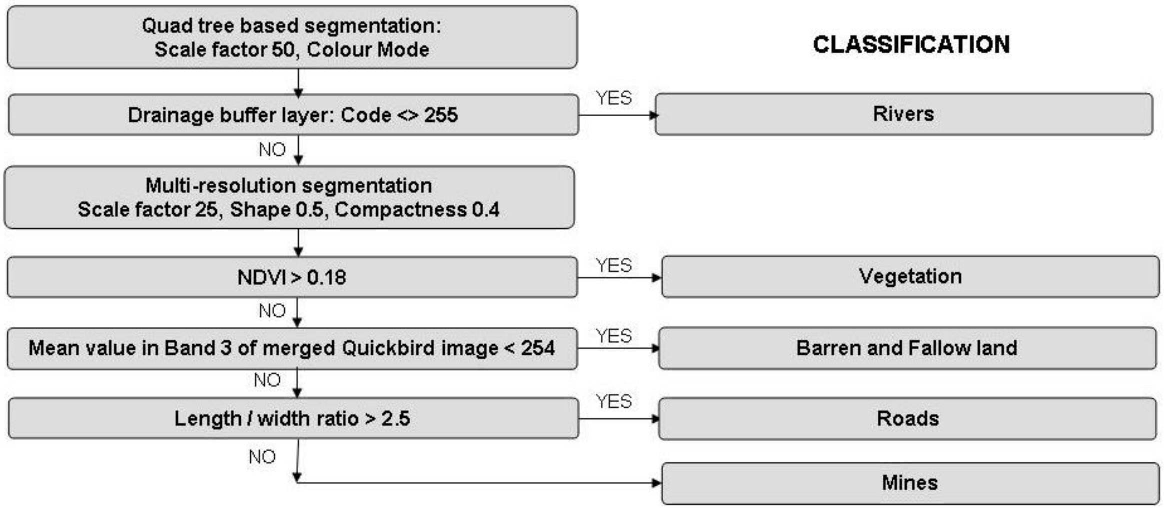

**Figure 4.10: Schematic of OOC process for pan-sharpened QuickBird image.**

### 4.2.3. Field-based steam water and sediment sampling and analysis

Field-based water and stream sediment sampling was carried out for two seasons to determine if there is any seasonal variation in their quality. Monsoon sampling was carried out between 30th June and 16th July, 2009 and post-monsoon sampling between 13th and 27th October, 2009. Grab water samples were collected. Two water samples were collected from every location. One sample was collected in a pre-washed polyethylene container for analysis of anions, iron and other physico-chemical properties; and the other sample was collected in an acid-washed polyethylene container for analysis of trace metals. In addition, a sample for dissolved oxygen (DO) was also collected. Stream sediments were collected in fresh zip-loc polythene packets. Several handfuls of bed sediments were collected from different places around the sampling location and placed in the polythene packet. The parameters measured *in situ* were pH, electrical conductivity, temperature and latitude-longitude of the sampling location by instruments mentioned in Section 4.1.3 earlier in the chapter. For determination of DO, the sample was fixed *in situ* by adding 1 ml each of manganese sulphate and alkali-iodide-azide.

Tentative sampling locations were identified through Survey of India topo-sheets during the pre-field work period. These locations were mainly bridges and stream confluences. However, after reaching the field it was found that most parts of the area were accessible only through unpaved forest roads and, with most of the main streams flowing through steep sided valleys and requiring a lot of walking to reach them, covering all the tentative sites was not possible due to time constraint. Most of the sampling sites were located on streams that were either close to accessible roads or with, at most, two hours walking distance from the road.

The monsoon sampling programme was disrupted by heavy rain and served mostly as a reconnaissance survey only. The daily rainfall recorded at Jowai, the district head quarter, located about 20 km from the northwest corner of the study area, between June and October 2009, obtained from the Meghalaya State Electricity Board (MeSEB) is given in Fig.4.11 details of which are given in Appendix 3.

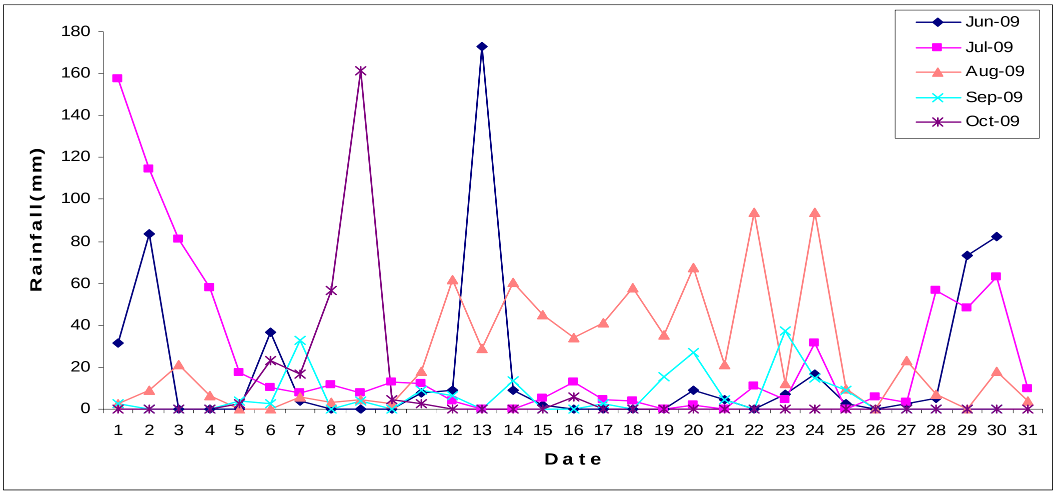

**Figure 4.11: Daily rainfall in Jowai (June-October 2009).**
**(Source: Meghalaya State Electricity Board)**

During the monsoon sampling, 14 water samples were collected along with 8 stream sediment samples. Sediment samples could not be collected from locations where the streams were too deep. Besides these, at 4 other locations, only field measurements were carried out. The sampling locations were designated as "R" for river and "A" for the other locations. Fig.4.12 shows the locations of the monsoon sampling locations. During this period, ancillary data and other necessary information were also collected from various Government departments, organizations and libraries.

The post-monsoon sampling was, in reality, carried out during a "late monsoon" period. There was heavy rainfall the week before the sampling, which started on 13th October. However, a dry spell in the weeks following allowed for a better coverage of the watershed. The areas which require long distance walking were left out once again because of the time constraint. During the post-monsoon programme, 30 water samples were collected, which included 29 river water samples, designated as "R"; and 1 sample of water which was being pumped out from a mine, designated as "M". At the same time, 22 sediment samples were collected and field measurements were carried out at 12 other locations, designated as "A". Again, stream sediment samples were collected only from locations where the stream was not deep. Fig.4.13 shows the locations of the post-monsoon sampling locations and Fig.4.14 shows a few photographs taken during the field work.

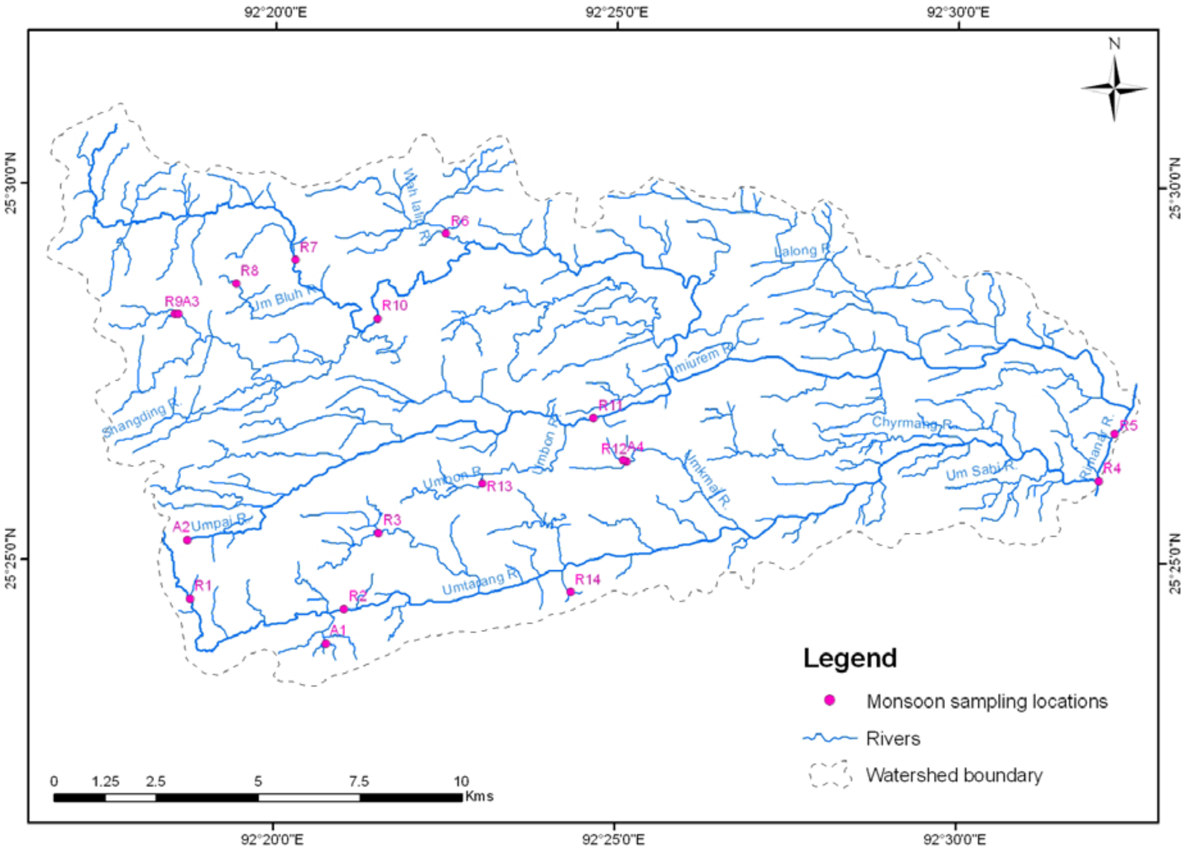

Figure 4.12: Monsoon sampling locations.

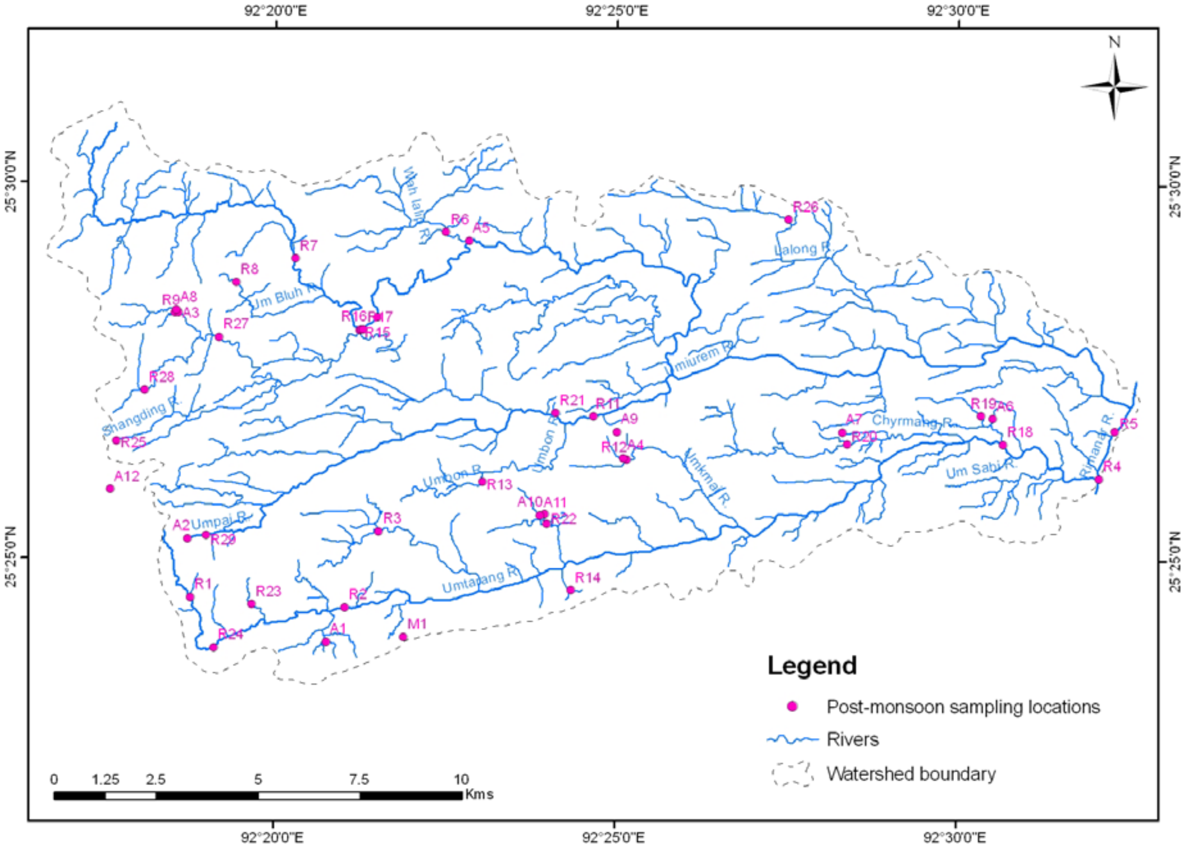

Figure 4.13: Post-monsoon sampling locations.

(a) Khlieh Myntriang (R2).

(b) Wah Ialip (R6).

(c) Um Kmai River (R12).

(d) Umbon River (R13).

(e) Umpai River (R21).

(f) Mine discharge north of Narwan road (M1).

**Figure 4.14: Field photographs.**

The sampling locations were also classified on the basis of provenance so as to correlate the presence of AMD at the location with the geology. The distribution of mines obtained from the remote sensing part of the study can be compared with the laboratory analysis results and the geology of the area to give a fairly good idea about the origin of AMD in the study area. Table 4.2 gives the classification of the sampling locations based on their geological provenance along with a brief description of the activities around each location. Strahler number was used to define the stream order taken from Survey of India topo-sheets.

**Table 4.2: Description of sampling locations.**

| Location_Code | Provenance | Stream order | Remarks | Sediments sampling |
|---|---|---|---|---|
| R1 | S | 2 | Major coal depots of Bapung and mines are observed upstream of the location. | YES |
| R2 | S | 4 | Located in active mining area. | YES |
| R3 | S | 4 | No mining activity in the vicinity but active mining upstream of location. | YES |
| R4 | S | 7 | Located on the Rimanar River which flows northwards and meets the Kopili River north of Lakasein Village. The Rimanar receives discharge from Umtarang-Myntriang River, Umiurem River and several other rivers flowing from active coal mining areas of Sutnga, Jalaphet, etc. | NO |
| R5 | S | 7 | Located on the Rimanar River at Lakasein Village downstream of R4. | YES |
| R6 | M | 4 | Background values for metamorphics (gneisses). | YES |

Table 4.2 contd…

| | | | | |
|---|---|---|---|---|
| R7 | M | 4 | Background values for metamorphics (gneisses). | NO |
| R8 | M+S | 3 | Background values for metamorphics (gneisses). | NO |
| R9 | S | 3 | Located downstream of major coal depot at 8th Mile Village. | YES |
| R10 | M+S | 5 | No mining activity in the vicinity. | NO |
| R11 | S+M | 4 | Located on Umpai River. No mining activity in the vicinity but receives discharge from coal mining areas. | YES |
| R12 | S | 3 | Located downstream of active mining areas. | YES |
| R13 | S | 3 | Located in active mining area. | YES |
| R14 | S | 1 | Background values for sedimentary (sandstone) | NO |
| R15 | M+S | 4 | No mining activity in the vicinity. Coal depot of 8th Mile located upstream. | YES |
| R16 | M+S | 4 | No mining activity in the vicinity. | NO |
| R17 | M+S | 5 | Downstream of confluence of R15 and R16. | YES |
| R18 | S | 5 | Located in active mining area. | YES |
| R19 | S | 2 | Located in active mining area. | YES |
| R20 | S | 3 | Located in active mining area. | YES |
| R21 | S+M | 4 | Located upstream of R11. No mining activity in the vicinity but receives discharge from coal mining areas. | YES |
| R22 | S | 3 | Located in active mining area. | YES |
| R23 | S | 2 | Located in active mining area. | YES |
| R24 | S | 2 | Located downstream of R1 with major coal depots just upstream. | YES |
| R25 | S | 1 | Background values for sedimentary (sandstone) | |
| R26 | M | 3 | Background values for metamorphics (gneisses) | YES |
| R27 | S+M | 3 | Located downstream of R9. No mining activity in the vicinity. Coal depot of 8th Mile located upstream. | YES |
| R28 | S | 3 | No mining activity in the vicinity but major coal depot of 8th Mile Village located upstream. | NO |
| R29 | S | 2 | Background values for sedimentary (sandstone) | YES |
| M1 | S | - | Direct discharge from mine. | NO |
| A1 | S | 1 | Background values for sedimentary (sandstone) | NO |
| A2 | S | 1 | Background values for sedimentary (sandstone) | NO |
| A3 | S | 3 | Located just downstream of R9. | NO |

Table 4.2 contd…

| | | | | |
|---|---|---|---|---|
| A4 | S | 2 | No mining activity in the vicinity but a coal depot is located upstream. | NO |
| A5 | M | 5 | Background values for metamorphics (gneisses). | NO |
| A6 | S | 1 | Located in active mining area. | YES |
| A7 | S | 1 | Located in active mining area. | NO |
| A8 | S | 1 | No mining activity in the vicinity. Coal depot of 8th Mile located upstream. | NO |
| A9 | S | 1 | Seepage zone to the west of Mynska Village. | NO |
| A10 | S | 2 | Located in active mining area. | NO |
| A11 | S | 2 | Located in active mining area. | YES |
| A12 | S | 3 | Background values for sedimentary (sandstone) | NO |

Note: S means provenance lies completely in sedimentary rocks (sandstone)
M means provenance lies completely in metamorphic rocks (gneisses)
M+S means provenance lies mainly in metamorphic rocks and partly in sedimentary rocks
S+M means provenance lies mainly in sedimentary rocks and partly in metamorphic rocks

#### 4.2.3.1. Laboratory work

**(1) Water samples**

All the water samples were analysed at the Laboratory of the Meghalaya State Pollution Control Board, Shillong within 24 hours of their collection. The following water quality parameters were analyzed as per NEERI (1987):

1) ***Turbidity***: Turbidity was directly measured by using the Nepheloturbidity meter.

2) ***Dissolved Oxygen (DO)***: DO was determined by Winkler's Method. A separate water sample was collected in Biological Oxygen Demand (BOD) bottles of 300ml capacity, filled to the brim. To the sample, 1 ml of $MnSO_4$ was added followed by 1 ml of alkali-iodide-azide reagent and the bottle shut immediately. The solution was well mixed by inverting the bottle a few times. A white precipitate forms if the sample is devoid of oxygen and becomes increasingly brown with rising oxygen content. The precipitate was dissolved by adding 1 ml conc. $H_2SO_4$ and mixing well. The sample was then titrated against standard $Na_2S_2O_3$ (0.025N) solution using starch as indicator. The amount of DO is directly proportional to the amount of thiosulphate solution.

3) ***Solids***: Solids in water sample were determined gravimetrically. Total solids were first determined by evaporating to dryness a known volume of sample and calculating by taking initial and final weight of the dish. The total suspended solids (TSS) were determined by filtering the sample through 0.45µm glass fibre filter paper of known initial weight, drying the latter in a muffle furnace, taking its final weight and calculating from the difference in weight. Total dissolved solids (TDS) were determined by subtracting TSS from total solids.

4) ***Total Hardness***: Total hardness was determined by titrating the sample against standard EDTA (Ethylene Diamine Tetra Acetic acid) (0.01M) after adding a buffer solution and using sodium sulphide nonahydrate as inhibitor and calmagite indicator.

5) ***Acidity***: Acidity was determined titrimetrically against standard (0.02N) NaOH solution with phenolphthalein as indicator.

6) ***Alkalinity***: Alkalinity was determined titrimetrically against (0.02N) standard $H_2SO_4$ with phenolphthalein as indicator. Total alkalinity was determined by further adding methyl orange indicator to the same sample and continuing the titration till end point is reached (yellow color changes to orange).

7) ***Calcium***: Calcium was determined by titrating the sample against standard (0.01M) EDTA with NaOH buffer and solochrome indicator.

8) ***Magnesium***: Magnesium was determined through calculation using the following equation (APHA-AWWA-WEF, 1998):

$$\text{Mg (mg/l)} = [\text{Total hardness (as } CaCO_3 \text{ mg/l)} - \text{Calcium hardness (as } CaCO_3 \text{ mg/l)}] \times 0.243$$

9) ***Sodium***: Sodium was determined by using a flame photometer at 589nm wavelength.

10) ***Potassium***: Potassium was determined by using a flame photometer 665nm wavelength.

11) ***Chloride***: Chloride was determined by Argentometric Method which involves titration of the sample with standard silver nitrate, using potassium chromate as indicator, till color changes from yellow to red.

12) ***Nitrate***: Nitrate was determined by Phenol Disulphonic Acid (PDA) Method. The sample was first evaporated to dryness on a water bath and the residue dissolved with phenol disulphonic acid reagent. 10ml of ammonium hydroxide was then added and nitrate was determined by reading the intensity of color developed at 410nm wavelength in a spectrophotometer.

13) ***Sulphate***: Sulphate was also determined colorimetrically using a spectrophotometer. A buffer solution was first mixed properly with the sample before a spatula of barium chloride was added and stirred constantly for 1 minute. Sulphate concentration was then read from a spectrophotometer.

14) ***Iron***: Total iron was determined colorimetrically by the Phenanthroline Method. Iron in the sample was first dissolved by boiling with 2 ml conc. HCl and 1 ml hydroxylamine HCl solution until the volume was reduced to 15 to 20 ml. After cooling to room temperature, 10ml ammonium acetate buffer and 4ml phenanthroline solution were added and the solution was diluted to 100 ml. It was then mixed thoroughly and allowed to stand for around 10 minutes for color development. The concentration was then read from a spectrophotometer.

***Trace elements***: Trace elements analyzed were Zn, Pb, Cd, Cr, Cu, and Mn. These were analyzed as per de Zwart and Trivedi (1994). A flowchart of the analysis procedure is shown at Fig. 4.15.

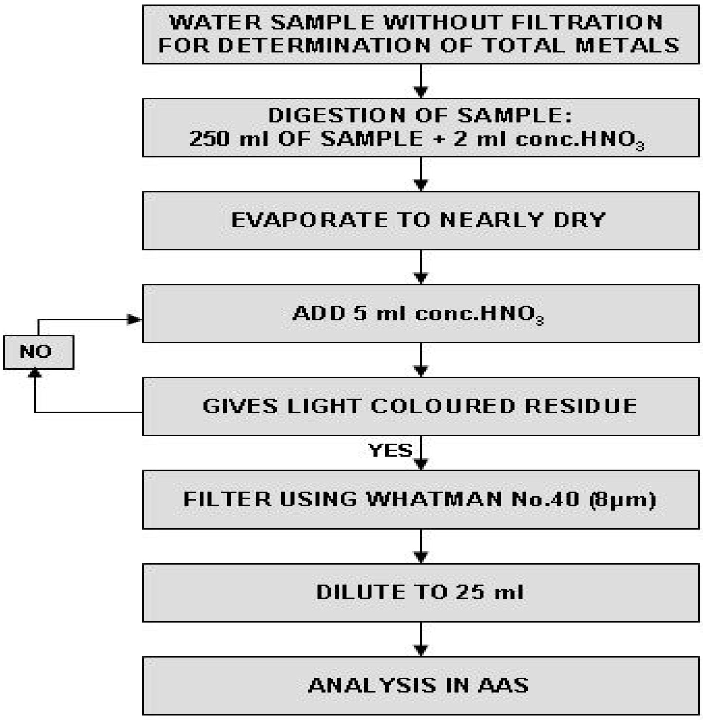

**Figure 4.15: Analysis procedure for trace metals in water samples. (after de Zwart and Trivedi, 1994)**

Table 4.3 gives the operating conditions and detection limits of the different trace metals analyzed in the AAS (de Zwart and Trivedi, 1994; User Manual of AAS):

**Table 4.3: Operating conditions and detection limits of AAS.**

| Element | Wavelength (nm) | Flame gases | Detection limit (mg/l) |
|---|---|---|---|
| Zinc | 213.9 | Air – Acetylene | 0.003 |
| Lead | 283.3 | Air – Acetylene | 0.010 |
| Cadmium | 228.8 | Air – Acetylene | 0.010 |
| Chromium | 357.9 | Air – Acetylene | 0.001 |
| Copper | 324.7 | Air – Acetylene | 0.001 |
| Manganese | 279.5 | Air – Acetylene | 0.010 |
| Nickel | 232.0 | Air – Acetylene | 0.030 |

### (2) Sediment samples

The trace metals in stream sediments were analysed at the ITC laboratory by Drs. J. B. deSmeth. The trace metals analysed were antimony, arsenic, barium, cadmium, cobalt, copper, chromium, iron, manganese, lead, lithium, nickel and zinc. The analysis procedure is given below:

1. The wet samples were first dried. Then they were ground in a mortar and pestle and sieved through a 250 micron mesh. The sieved samples were then left overnight in an oven for complete drying.
2. 500 mg of sample is decomposed in a 30 ml test-tube with a solution 1 ml of Aqua Regia and 1 ml of demineralised water on a shaking water bath at 90°C for two hours. Every 30 minutes the tubes are extra shaken on a Vortex shaker. The sample gets diluted forty times. The batch also includes two repeat samples, two ITC A Reference standard powders and one blank.

3. After two hours, 18.2 ml of demineralised water is added (0.2 extra to compensate average loss through evaporation). The tubes are homogenized and left for 15 minutes on the hot shaking water bath to remove all material attached to the side of the tube.
4. The samples are left to precipitate overnight and next day are decanted in a clean 20 ml Pyrex tube with stopper.
5. Combined calibration standards are prepared for the different trace metals in the same acid strength as the samples.
6. The samples are then analysed on a Varian sequential ICP-OES, model Liberty 2. Analysis starts with a liquid control sample (LCS). After 19 samples again a LCS is analysed followed by remeasurement of the calibration liquids and a new LCS. The samples are analysed in random order and include the repeat samples, ITC reference house standard material and blank.
7. After all the samples are measured, the samples of which repeats were made are reanalyzed after recalibration.

#### 4.2.3.2. Data quality check

Any laboratory analytical work has to produce information that is technically valid, legally defensible and of known quality (APHA-AWWA-WEF, 1998). Errors may creep in right from the sample collection stage and more so during the analysis. The quality check applied in this study is the anion-cation balance. For natural waters, the anion and cation sums, when expressed in milliequivalents per litre, must balance because such waters must be electrically neutral (APHA-AWWA-WEF, 1998). The balance is computed by the following formula (APHA-AWWA-WEF, 1998):

$$\%\text{difference} = 100 * \frac{\sum \text{cations} - \sum \text{anions}}{\sum \text{cations} + \sum \text{anions}} \ldots\ldots\ldots\ldots(1)$$

A positive difference means that there are excess cations or insufficient anions and vice versa. A %difference of ±10% is assumed to be good (APHA-AWWA-WEF, 1998).

In balancing the ions for the monsoon samples, it was found that eight of the fourteen samples were outside the acceptable difference of ±10%. The reasons for this could be either contamination during sample collection or, most likely, error during analysis as it was done very quickly. Since, the monsoon sampling was more like a reconnaissance survey only, more attention was paid during the post-monsoon sampling. However, the monsoon analysis values were used in preparation of the different maps.

The post-monsoon ion balance was found to be much better with all twenty nine river samples being within the acceptable limit. The only sample falling outside the limit was the one collected directly from the mine discharge (M1). This sample was groundwater being pumped out from an underground mine and collected from the outlet of the pumping main. This sample can be expected to be in disequilibrium due to reaction with the surface air. Plots of the cation sum versus the anion sum for both monsoon and post-monsoon samples are shown in Fig. 4.16. As expected, the monsoon plot was more scattered with many points lying far from the trend line. The post-monsoon plot showed a good balance between the cations and anions and they are linearly related.

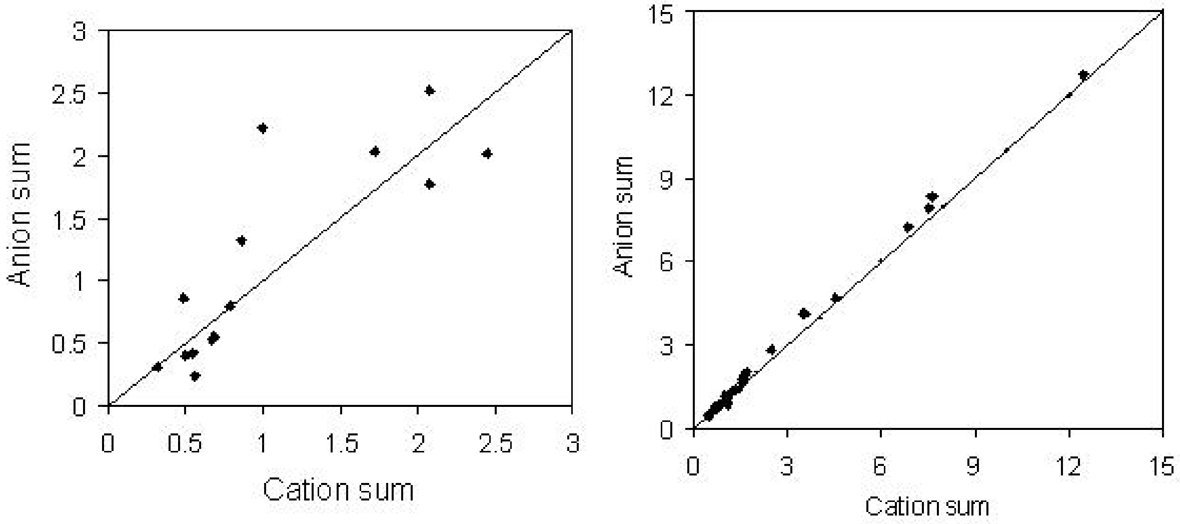

**Figure 4.16: Scatter plot of cation sum versus anion sum (a) monsoon water samples and (b) post-monsoon water samples.**

Another quality check used for the water samples was the collection and analysis of duplicate samples. In general, 10% of water samples have to be collected and analyzed in duplicate (APHA-AWWA-WEF, 1998). During the monsoon sampling, no duplicate sample was collected. However, five water samples of the thirty collected during post-monsoon were collected in duplicate. The relative percent difference (RPD) is given by (APHA-AWWA-WEF, 1998):

$$\text{RPD} = \frac{(\text{sample result} - \text{duplicate result})}{(\text{sample result} + \text{duplicate result})/2} * 100 \ldots\ldots\ldots\ldots(2)$$

The calculation for RPD for the post-monsoon water samples is given in Table 4.4. High RPD for turbidity could be dirty test tube during analysis. Sodium and potassium were analyzed in a flame photometer which has a least count of 1 mg/l. With all the readings rounded up to the nearest whole number, a change of 1 unit of measurement will give a very high percent difference. High RPD for chlorides and other parameters determined titrimetrically will be because of human error during titration. The trace metals have very low concentrations, close to the lower limit of detection where the procentual errors are large and a small change in concentration therefore, leads to high RPD.

**Table 4.4: Calculation of Relative Percent Difference between duplicates of post-monsoon water samples.**

| Code | R2 | | | R4 | | | R5 | | | R13 | | | R26 | | |
|---|---|---|---|---|---|---|---|---|---|---|---|---|---|---|---|
| Sample | (a) | (b) | RPD | (a) | (b) | RPD | (a) | (b) | RPD | (a) | (b) | RPD | (a) | (b) | RPD |
| Turb. | 1.3 | 1.2 | 8 | 0.4 | 0.5 | 22.2 | 0.6 | 0.7 | 15.4 | 1.9 | 2 | 5.1 | 1.7 | 1.9 | 11.1 |
| TDS | 568 | 597 | 5 | 272 | 282 | 3.6 | 497 | 521 | 4.7 | 262 | 276.1 | 5.2 | 20.1 | 18.2 | 9.9 |
| TSS | 10 | 10 | 0 | 5 | 5 | 0.0 | 5 | 5 | 0.0 | 10 | 10 | 0 | 5 | 5 | 0 |
| TH | 117.1 | 115 | 1.8 | 94 | 90 | 4.3 | 95 | 90 | 5.4 | 24 | 24 | 0 | 20 | 21 | 4.9 |
| Acid. | 79 | 82 | 3.7 | 32 | 36 | 11.8 | 68 | 72 | 5.7 | 51 | 56 | 9.3 | 6 | 5 | 18.2 |
| Alk. | 0 | 0 | | 0 | 0 | | 0 | 0 | | 0 | 0 | | 16 | 14 | 13.3 |
| Ca | 60 | 55 | 8.7 | 24 | 25 | 4.1 | 27 | 24 | 11.8 | 14 | 13 | 7.4 | 1 | 1 | 0 |
| Mg | 13.9 | 14.6 | 4.9 | 17 | 15.8 | 7.3 | 16.5 | 16 | 3.1 | 2.4 | 2.7 | 11.8 | 4.6 | 4.9 | 6.3 |
| Na | 7 | 6 | 15.4 | 15 | 14 | 6.9 | 13 | 15 | 14.3 | 11 | 12 | 8.7 | 10 | 11 | 9.5 |
| K | 4 | 5 | 22.2 | 11 | 9 | 20 | 11 | 12 | 8.7 | 6 | 7 | 15.4 | 8 | 7 | 13.3 |
| Cl | 70 | 68 | 2.9 | 3 | 2 | 40 | 5 | 4 | 22.2 | 7 | 8 | 13.3 | 3 | 2 | 40 |
| NO3 | 3.9 | 3.7 | 5.3 | 2.5 | 2.4 | 4.1 | 2.7 | 3 | 10.5 | 2.3 | 2.5 | 8.3 | 1.4 | 1.5 | 6.9 |
| SO4 | 127.4 | 122.7 | 3.8 | 190.4 | 185.8 | 2.5 | 190 | 183.8 | 3.3 | 66.4 | 68.4 | 3. | 28.7 | 31.0 | 7.7 |
| Fe | 9.8 | 9.7 | 1 | 2.1 | 2.3 | 9.1 | 1.1 | 1.2 | 8.7 | 4.6 | 4.4 | 4.4 | 1.26 | 1.30 | 3.1 |
| Cu | BDL | BDL | | 0.01 | 0.01 | 0.0 | BDL | 0.01 | | BDL | BDL | | BDL | BDL | |
| Cd | BDL | BDL | | BDL | BDL | | BDL | BDL | | BDL | BDL | | BDL | BDL | |
| Cr | BDL | BDL | | BDL | BDL | | 0.01 | 0.01 | 0 | BDL | BDL | | BDL | BDL | |
| Mn | 0.13 | 0.11 | 16.7 | 0.31 | 0.31 | 0.0 | 0.28 | 0.29 | 3.5 | 0.06 | 0.06 | 0 | 0.01 | 0.01 | 0 |
| Ni | BDL | BDL | | 0.03 | 0.03 | 0.0 | 0.05 | 0.05 | 0 | BDL | BDL | | BDL | BDL | |
| Pb | BDL | BDL | | 0.01 | 0.01 | 0.0 | 0.01 | 0.01 | 0 | BDL | BDL | | BDL | BDL | |
| Zn | 0.03 | 0.04 | 28.6 | 0.13 | 0.14 | 7.4 | 0.18 | 0.14 | 25.0 | 0.01 | 0.01 | 0 | BDL | BDL | |

### 4.2.3.3. Data representation and interpretation

The basic descriptive statistics – mean, quartiles, standard deviation, minimum and maximum – were generated for all samples. Box plots were used to define the cut-off values for representing in maps showing the spatial distribution of the main pollutants associated with AMD, i.e. pH, sulphates, iron and sum of dissolved trace metals. Graduated symbols along with a color scheme were used to represent the relative concentration of the pollutants in the sampling locations. A correlation matrix showing the relationship of the different pollutants with each other and scatter plots of pH with other pollutants were also generated to interpret the analysis results.

An effective graphical representation of water quality data is the trilinear Piper diagram (Fig.4.17). The Piper diagram is drawn by plotting the proportion (in % milli-equivalents per liter) of the major cations [$Ca^{2+}$, $Mg^{2+}$, ($Na^{+} + K^{+}$)] on one triangular diagram and the proportions of the major anions [alkalinity ($CO_3^{2-} + HCO_3^{1-}$), $Cl^{-}$, $SO_4^{2-}$] on another. These are then projected upwards on a quadrilateral to give an idea about the main features of the water chemistry and to see if the analysis falls into distinct clusters (Drever, 1997). The Piper diagram gives four tentative conclusions about the origin of the water represented by the analysis, viz. water type, precipitation or solution, mixing and ion exchange (Hounslow, 1995). The two main uses of Piper diagrams are that they serve as a visual way of displaying a water analysis in order to classify water into a "type" or "hydrochemical facies” based on the relative proportions of the major ions and as a quick test to see if a series of water compositions can be explained by mixing between two end members, if the compositions will plot along a straight line in each of the fields of the diagram (Drever, 1997). The Piper diagram showing different water types is given in Fig.4.17 and it can be interpreted after Sadashivaiah (2008), Drever (1997) and Hounslow (1995) as given in Table 4.5.

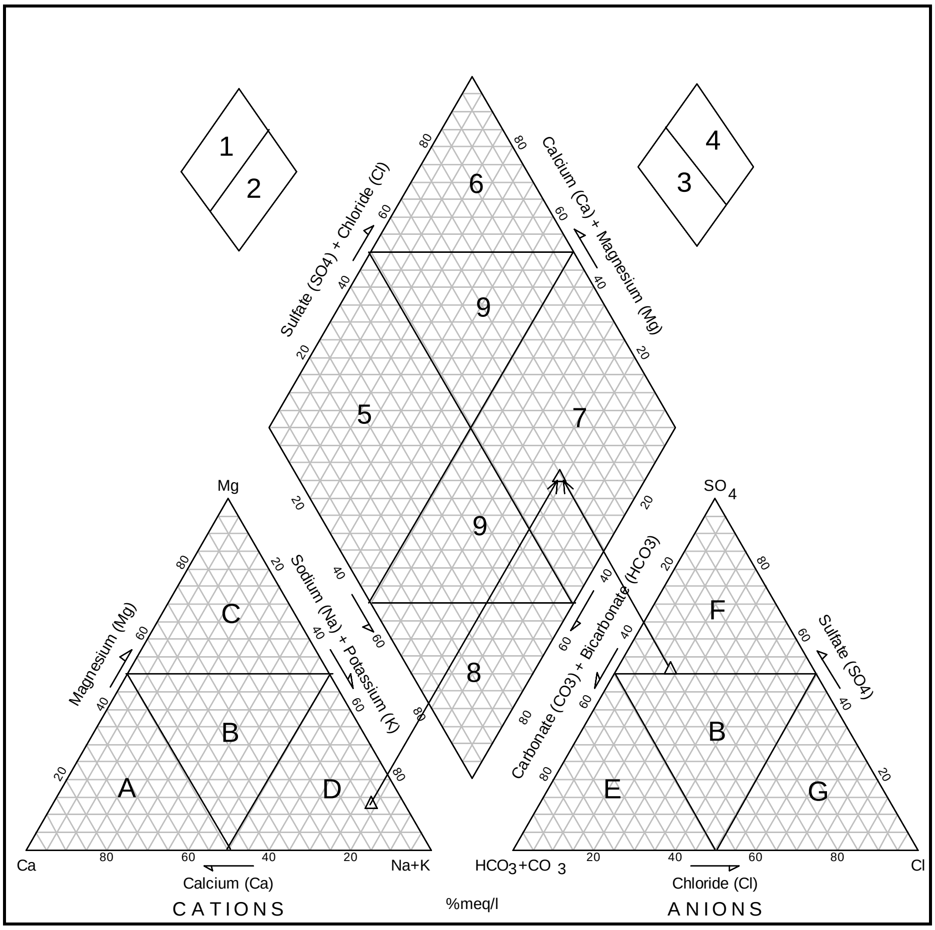

**Figure 4.17: Piper diagram showing different water types. (after Sadashivaiah, 2008)**

**Table 4.5: Interpretation of Piper diagram.**

| | |
|---|---|
| 1: $(Ca^{2+} + Mg^{2+}) > (Na^+ + K^+)$ | A: Calcium type |
| 2: $(Ca^{2+} + Mg^{2+}) < (Na^+ + K^+)$ | B: No dominant type |
| 3: $(CO_3^{2-} + HCO_3^-) > (SO_4^{2-} + Cl^-)$ | C: Magnesium type |
| 4: $(CO_3^{2-} + HCO_3^-) < (SO_4^{2-} + Cl^-)$ | D: Sodium or potassium type |
| 5: Magnesium bicarbonate type (temporary hardness) | E: Bicarbonate type |
| 6: Calcium chloride type (permanent hardness) | F: Sulphate type |
| 7: Sodium chloride type (saline type) | G: Chloride type |
| 8: Sodium bicarbonate type (alkali carbonate) | |
| 9: Mixed type (no dominant cation-anion) | |

### 4.2.4. Pollutant distribution maps

As mentioned earlier in the chapter, maps showing the distribution of selected metal pollutants associated with AMD in water samples were generated by plotting their concentration with graduated symbols and a color scheme. Standards of permissible concentrations for these pollutants have also been prescribed by the Bureau of Indian Standards and the Central Pollution Control Board and can be used to assess the level of pollution in the water. River bed sediments, on the other hand, do not have any prescribed standards in India. Several numerical sediment quality guidelines (SQG's) have been developed in other countries, particularly in the U.S.A. These have been developed using a variety of approaches on the basis of pollution receptors – benthic organisms, wildlife or humans – each having its own advantages and disadvantages for assessing the sediment quality of a river system (MacDonald *et al.*, 2000).

To bring about an agreement and a synthesis between the various SQG's, MacDonald *et al.* (2000) proposed consensus-based SQG's for 28 chemicals of concern in freshwater sediments, viz. metals, polycyclic aromatic hydrocarbons (PAH's), polychlorinated biphenyls (PCB's) and organo-chlorine pesticides. They developed 2 SQG's, from published and existing SQG's, for each pollutant, including a threshold effect concentration (TEC) and a probable effect concentration (PEC). The TEC's were contaminant concentration levels below which harmful effects on sediment-dwelling organisms were not expected. The PEC's, on the other hand, were intended to identify contaminant concentrations above which harmful effects on sediment-dwelling organisms were expected to occur frequently. These consensus-based SQG's were then tested for reliability by applying them to a large data set from all over the U.S.A. and the results were found to be very accurate.

The consensus-based SQG's were developed by firstly scouring through published SQG's and selecting only the "effects-based" ones, which specified both TEC's and PEC's. The consensus-based SQG's were then calculated by taking the geometric mean of those SQG's for which at least 3 or more values were available for each contaminant. Te geometric mean was calculated as it gives an estimate of central tendency which was not unduly affected by extreme values and also because the distributions of the SQG's were not known. The authors developed consensus-based SQG's for 8 trace metals, 10 PAH's, 1 each for total PAH and total PCB, and 9 organo-chlorine pesticides. Table 4.6 shows the calculated consensus-based SQG's proposed by MacDonald *et al.* (2000) for trace metals.

**Table 4.6: Sediment Quality guidelines for trace metals in freshwater ecosystems that reflect threshold effect concentration (TEC) and a probable effect concentration (PEC).**
**(after MacDonald *et al.*, 2000)**

| S.No. | Trace metal (mg/kg dry weight) | Consensus-based TEC | Consensus-based PEC |
|---|---|---|---|
| 1 | Arsenic | 9.79 | 33.0 |
| 2 | Cadmium | 0.99 | 4.98 |
| 3 | Chromium | 43.4 | 111.0 |
| 4 | Copper | 31.6 | 149.0 |
| 5 | Lead | 35.8 | 128.0 |
| 6 | Mercury | 0.18 | 1.06 |
| 7 | Nickel | 22.7 | 48.6 |
| 8 | Zinc | 121.0 | 459 |
| 9 | Iron (%)* | 2.0 | 4.0 |
| 10 | Manganese* | 460.0 | 780.0 |

* after da Silva *et al.* (2006)

The PEC values can further be used to predict the incidence of toxicity to sediment-dwelling organisms due to a combined effect of several contaminants. To do this, firstly, the concentration of each substance in each sediment sample was divided by its respective consensus-based PEC to give the PEC quotient (PEC-Q). The PEC-Q's of all substances in the sample were summed and the mean PEC-Q was calculated for each sample. The authors had then plotted a curve (Fig.4.18), the equation of which was used to estimate the predicted incidence of toxicity at each sampling location.

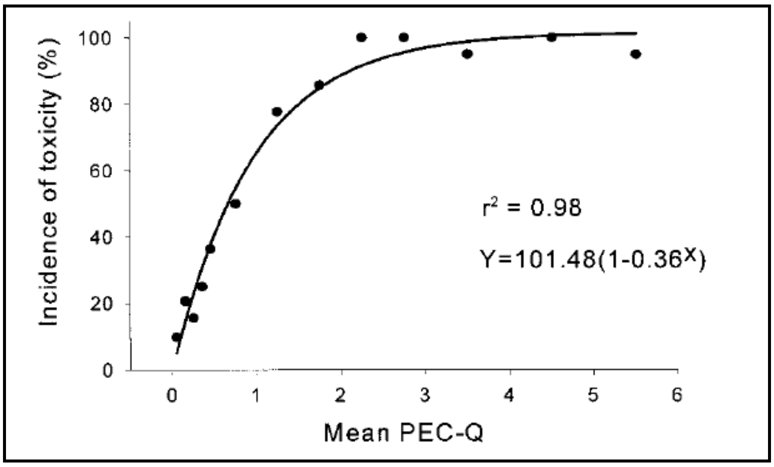

**Figure 4.18: Relationship between mean PEC-Q and incidence of toxicity in freshwater sediments.**

MacDonald *et al.* (2000) gave the following uses for the SQG's developed:

1. to identify hot spots of sediment contamination,
2. to determine the potential for and spatial extent of injury to sediment-dwelling organisms,
3. evaluate the need for sediment remediation, and
4. support the development of monitoring programmes to assess the extent of contamination and effects of contaminated sediments on sediment-dwelling organisms.

These SQG's, however, did not consider the potential for bioaccumulation in aquatic organisms nor the hazards to the higher organisms that consume these aquatic organisms.

In this study, the concentration of trace metals in stream sediments (As, Cd, Cr, Cu, Pb, Ni and Zn) were compared with the TEC and PEC values developed by MacDonald *et al.* (2000) and those of Mn and Fe were compared with TEC and PEC values given by da Silva *et al.* (2006). The mean PEC-Q values were calculated and through them, the incidence of toxicity to sediment-dwelling organisms was calculated for each sampling location for both seasons by using the equation given by MacDonald *et al.* (2000).

The predicted toxicity was then represented in maps to show the distribution of contamination due to a combined effect of trace metals in river bed sediments. Graduated symbols and a color scheme were used to show the levels of toxicity.

# 5. Results and Discussions

## 5.1. Image analysis for identification of rat-hole mines

### 5.1.1. Visual interpretation of merged CARTOSAT-1/RESOURCESAT-1 image

Through visual interpretation and manual digitization of the merged CARTOSAT-1/ RESOURCESAT-1 image, 1281 mines and overburden dumps could be identified in the whole watershed. As expected, the mines were distributed mostly in the coal-bearing sandstone in the central and southern part of the study area. The map showing distribution of mines is given at Fig.5.1. Each mine was digitized as a polygon which included the overburden dump around it. No mining activity could be seen in the northern part, which left the Umiurem River and its tributaries untouched. The major activity could be observed along the northern bank of the Umtarang (Myntriang) River with a few mines scattered on its southern bank.

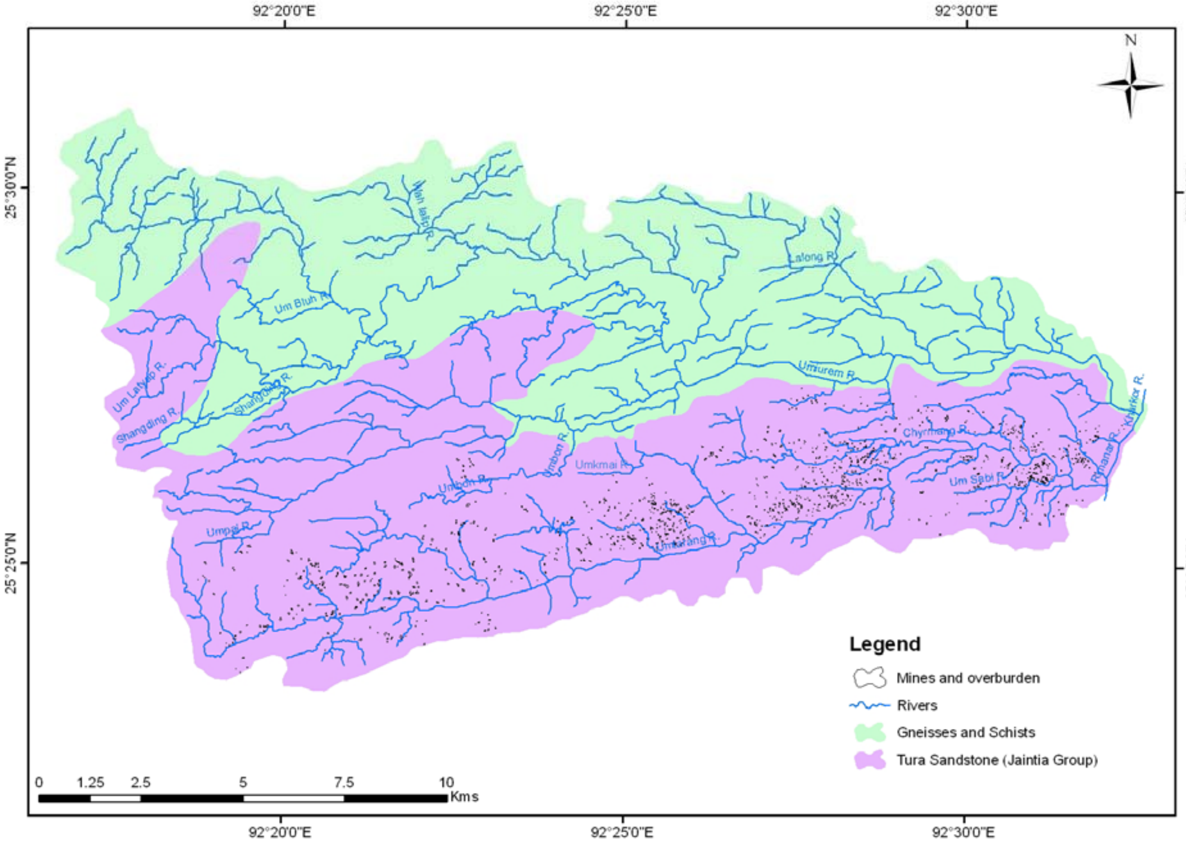

**Figure 5.1: Distribution of mines digitized from merged CARTOSAT-1/RESOURCESAT-1 image.**

As stated earlier, the pan-sharpened QuickBird image was used to assess the accuracy of the visual interpretation. The QuickBird image constituted only about 13% of the total area of the watershed (Fig.5.2), however, manual digitization of the image yielded 1546 mines and overburden dumps within the approximately 30 sq.km. area (Fig.5.3).

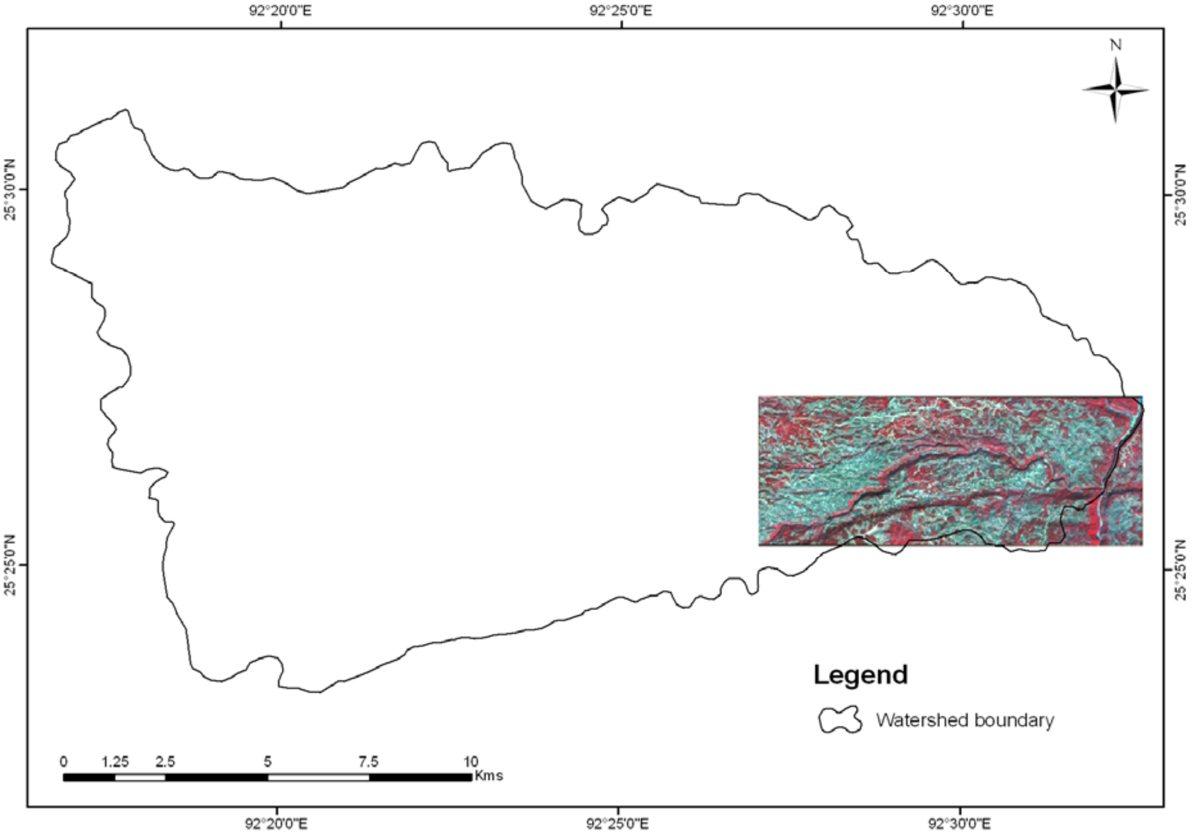

Figure 5.2: QuickBird image with respect to entire study area.

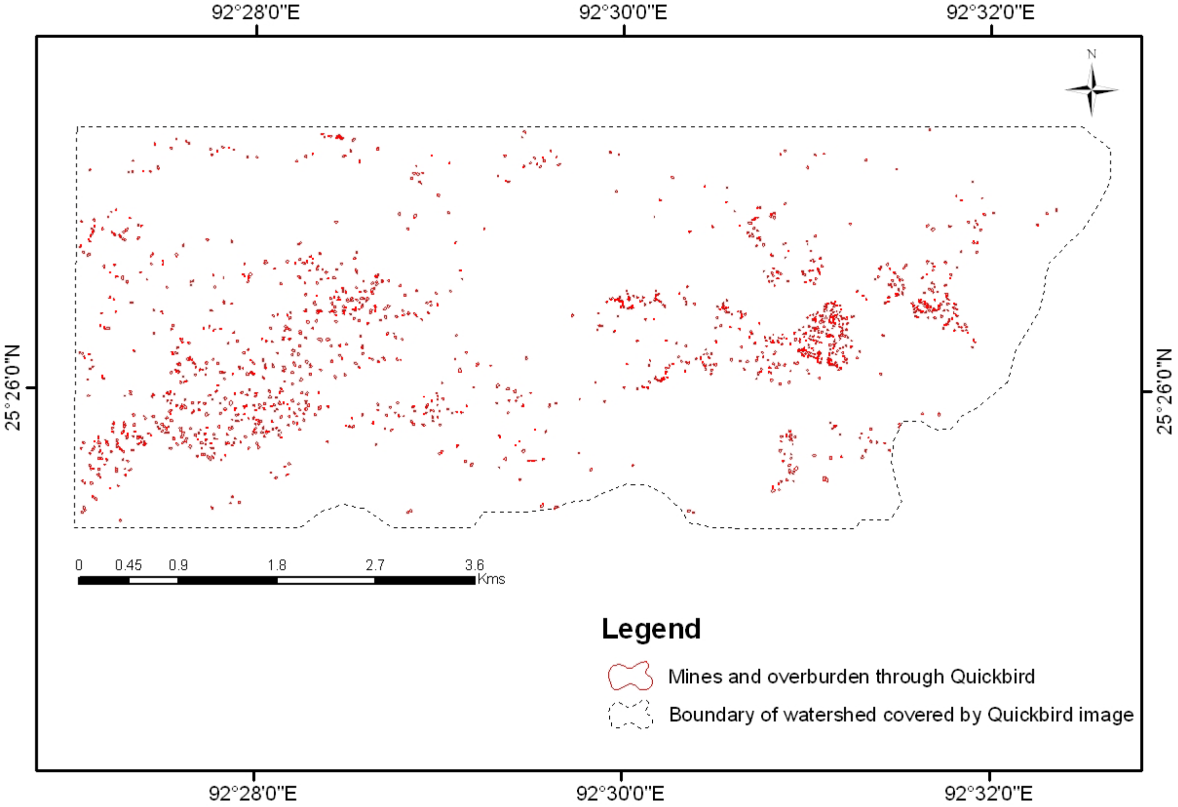

Figure 5.3: Distribution of mines digitized from QuickBird image.

To check the accuracy, the number polygons of the merged CARTOSAT-1/RESOURCESAT-1 image, identified within the area covered by QuickBird only, were compared with those of the latter. It was seen that only 712 polygons were digitized through CARTOSAT-1/RESOURCESAT-1 image within this same area which gave an accuracy of 46%. The accuracy assessment was also carried out in terms of area of the polygons visually mapped through the two different images. The 712 polygons mapped through the CARTOSAT-1/RESOURCESAT-1 image covered an area of 0.16 sq.km. and the 1546 polygons mapped through the pan-sharpened QuickBird image covered 0.27 sq.km. which gives an accuracy of 59.3%. Table 5.1 shows a summary of the accuracy assessment for the merged CARTOSAT-1/RESOURCESAT-1 image.

**Table 5.1: Accuracy assessment calculation of visual interpretation of merged CARTOSAT-1/ RESOURCESAT-1 image.**

| | | **No. of mines** |
|---|---|---|
| a | Visually mapped through merged CARTOSAT-1/RESOURCESAT-1 image | 712 |
| b | Visually mapped through pan-sharpened QuickBird image | 1546 |
| | Overall accuracy (a / b * 100) | **46.05 %** |
| | | **Area (sq.km.)** |
| c | Area of polygons mapped through merged CARTOSAT-1/ RESOURCESAT-1 image | 0.16 |
| d | Area of polygons mapped through pan-sharpened QuickBird image | 0.27 |
| | Overall accuracy (c / d * 100) | **59.26 %** |

The general sizes of the mines vary from 6m to 8m in width. Through the pan-sharpened QuickBird image, with its spatial resolution of only 61 cm, it was possible to see individual mines very clearly. The main reasons for a very low accuracy are given below:

(1) The pan-sharpened QuickBird's very high resolution image made it possible to see and map each and every mine easily. Due to this, many mines, that were either not visible or were missed out during interpretation of the merged CARTOSAT-1/RESOURCESAT-1 image, have been mapped through pan-sharpened QuickBird image. Fig.5.4 (a) and (b) give an example of such a case. In the figure, the background image is that of the merged CARTOSAT-1/RESOURCESAT-1 image and on it shape files of the visual interpretation of this image and of the pan-sharpened QuickBird have been overlaid. The polygons of the former have been shown in red and of the latter in black. The pink rectangles show examples of areas on the image where mines have been mapped through QuickBird but not through merged CARTOSAT-1/ RESOURCESAT-1. Fig.5.4 (a) shows the case where mines were not visible and where mines have been missed out in the CARTOSAT-1/RESOURCESAT-1 image. Fig.5.4 (b) shows where series of small mines have been mapped through pan-sharpened QuickBird image but at the same location only a few bigger mines were discernible through CARTOSAT-1/RESOURCESAT-1 image.

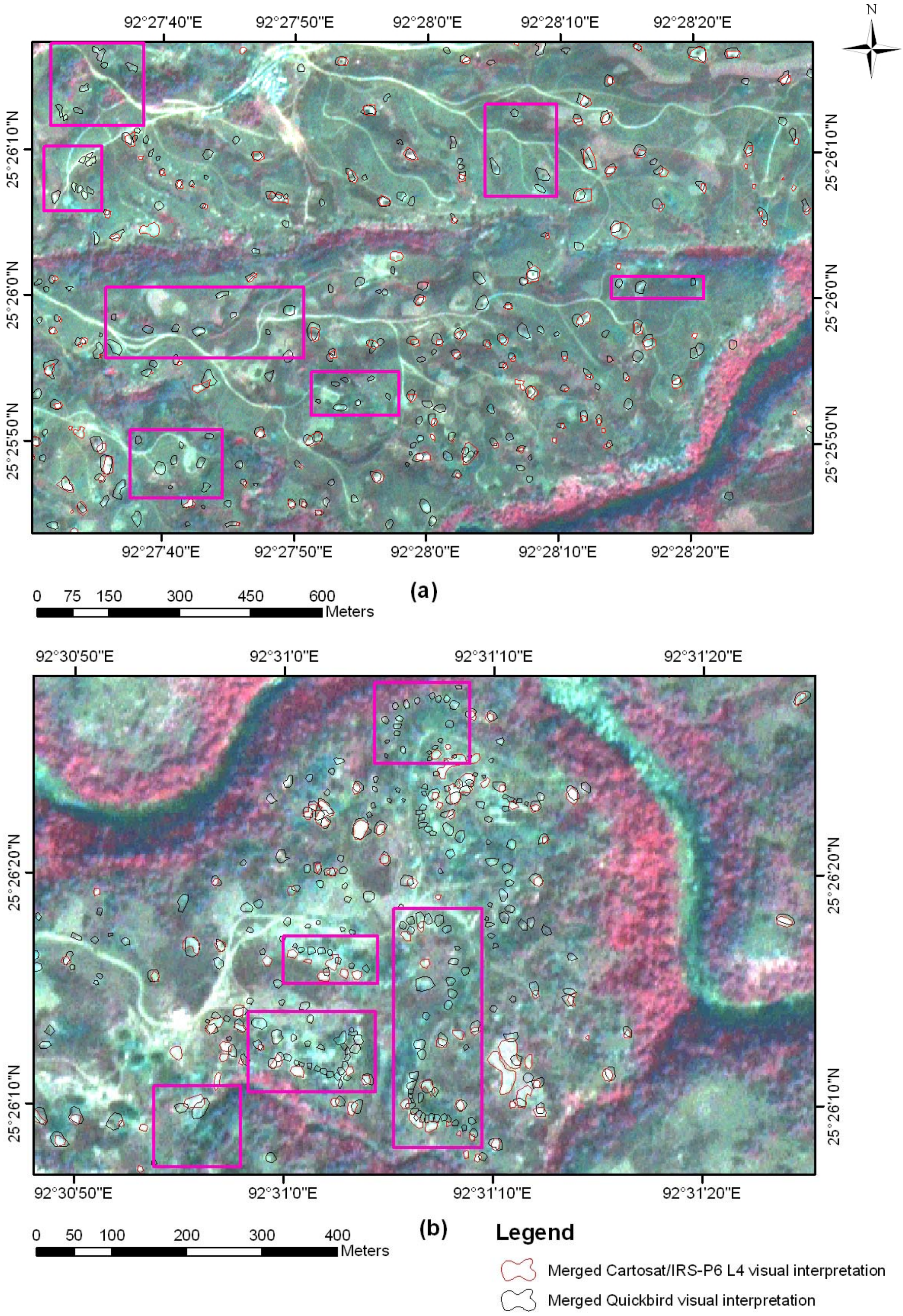

**Figure 5.4: Comparison of visual interpretation of merged CARTOSAT-1/RESOURCESAT-1 and pan-sharpened QuickBird (omission error).**

**The pink rectangles show examples of areas on the image where mines have been mapped through QuickBird but not through merged CARTOSAT-1/ RESOURCESAT-1. (a) shows the case where mines were not visible and where mines have been missed out in the CARTOSAT-1/RESOURCESAT-1 image. (b) shows where series of small mines have been mapped through pan-sharpened QuickBird image but at the same location only a few bigger mines were discernible through CARTOSAT-1/RESOURCESAT-1 image.**

(2) The other reason for low accuracy was the spatial resolution difference. At several places in the merged CARTOSAT-1/RESOURCESAT-1 image, one big polygon had been mapped, whereas, at the same location, not one, but many mine shafts were in existence as seen in the pan-sharpened QuickBird image. This has resulted to the polygon count of the merged CARTOSAT-1/RESOURCESAT-1 image being very less vis-à-vis the pan-sharpened QuickBird image. In Fig.5.5 (a) and (b), the white rectangles show a few examples of areas where through QuickBird many mine shafts could be seen at a location where through merged CARTOSAT-1/ RESOURCESAT-1 image only one mine was identified. The pink rectangles show unmapped mines and the yellow ellipses show mines completely misclassified through the merged CARTOSAT-1/RESOURCESAT-1 image.

The total area of polygons mapped through QuickBird was higher because of more number of polygons. However, the accuracy became higher because the sizes of most of the polygons mapped through the merged CARTOSAT-1/RESOURCESAT-1 image were bigger as stated above.

Although the overall accuracy of the visual interpretation of the merged CARTOSAT-1/ RESOURCESAT-1 image was very low, it was further observed that out of the 712 polygons identified, 635 polygons, i.e. 89%, were found to spatially match with those of the pan-sharpened QuickBird image. Due to lower spatial resolution, the mapping error had occurred but what had been mapped was found to be suitable for the merged CARTOSAT-1/RESOURCESAT-1 image to be used as a reference for accuracy assessment of the OOC.

The merged CARTOSAT-1/RESOURCESAT-1 image, along with the additional layers of LISS-IV NDVI, Principal Component (PC) 1 and PC 2 and ASTER GDEM, were also used in a supervised classification in the ERDAS software. Training sites were taken throughout the image, with the QuickBird image used as a reference. The five classes that were classified were: (1) Forest, (2) Fallow and barren land, (3) Settlements and roads, (4) Rivers, and (5) Mines. The classified image is shown in Fig.5.6. A close-up of the merged CARTOSAT-1/RESOURCESAT-1 has been shown as (a) and that of the corresponding area in the classified image has been shown as (b).

The intention of the classification was to see if the "rat-hole" mines could be classified or not. At a glance, the forest, fallow and barren land and settlements have come out quite well. However, there has been a misclassification of roads, mines and rivers. Point 1 in Fig.5.6 (a) and (b) shows an example where the roads have been classified as mines. Dry stream beds on the eastern corner of the study area have also been misclassified as mines. Settlements have been classified as mines at several places also – Point 2 shows an example. Barren land has been classified as rivers and vice versa at several places – Point 3. This was due to the inherent problem with pixel-based classifiers being used on very high resolution images. Each pixel was classified uniquely with no homogeneous region generated (Durieux *et al.*, 2008). Misclassification also occurred due to the similarity in spectral signatures of the overburden dumps around the mine shafts and other land cover types, particularly roads, settlements and the exposed river beds.

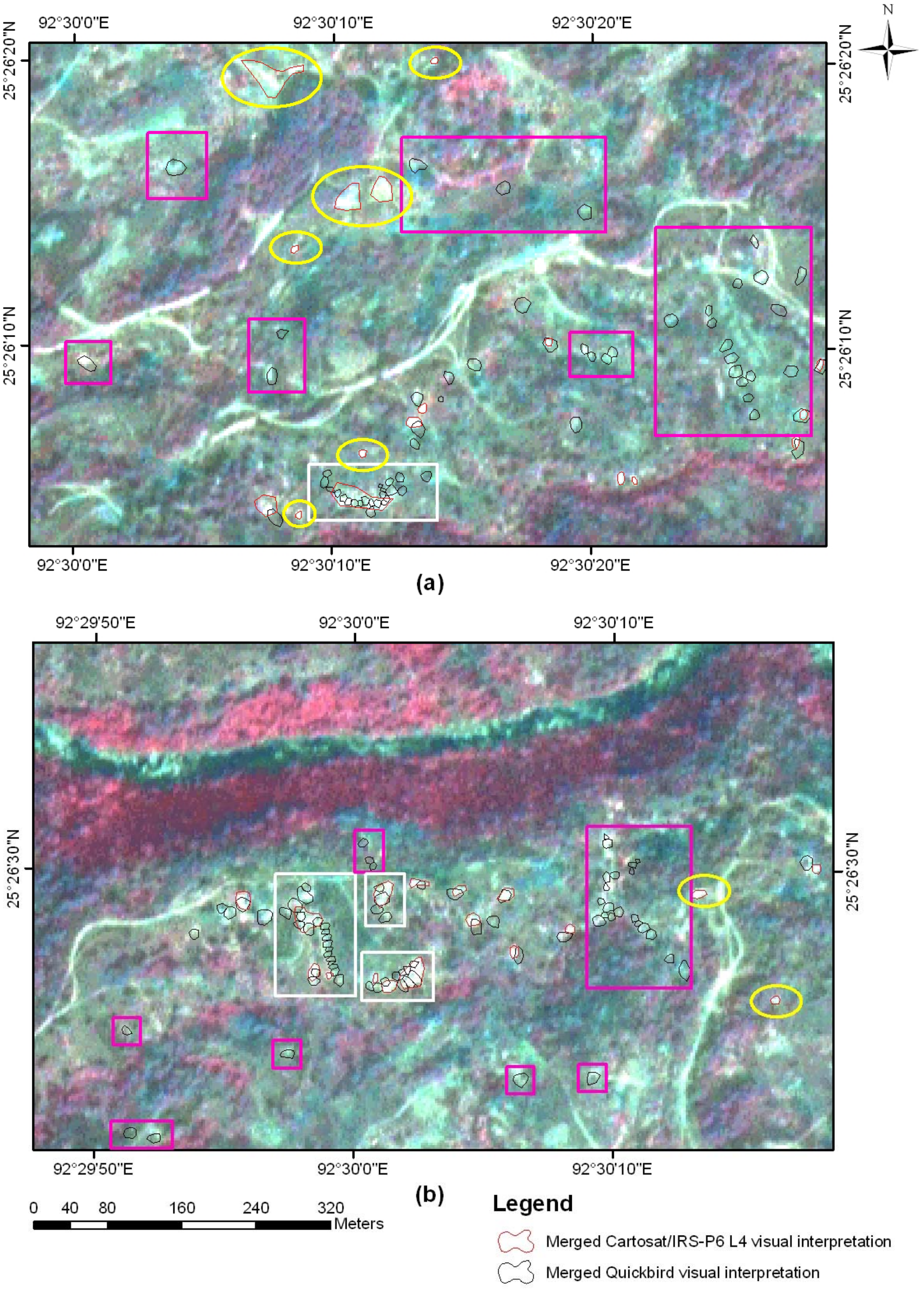

**Figure 5.5: Comparison of visual interpretation of merged CARTOSAT-1/RESOURCESAT-1 and pan-sharpened QuickBird (resolution difference).**

**The white rectangles show a few examples of areas where through pan-sharpened QuickBird many mine shafts could be seen at a location where through merged CARTOSAT-1/RESOURCESAT-1 image only one mine was identified. The pink rectangles show unmapped mines and the yellow ellipses show mines completely misclassified through the merged CARTOSAT-1/RESOURCESAT-1 image.**

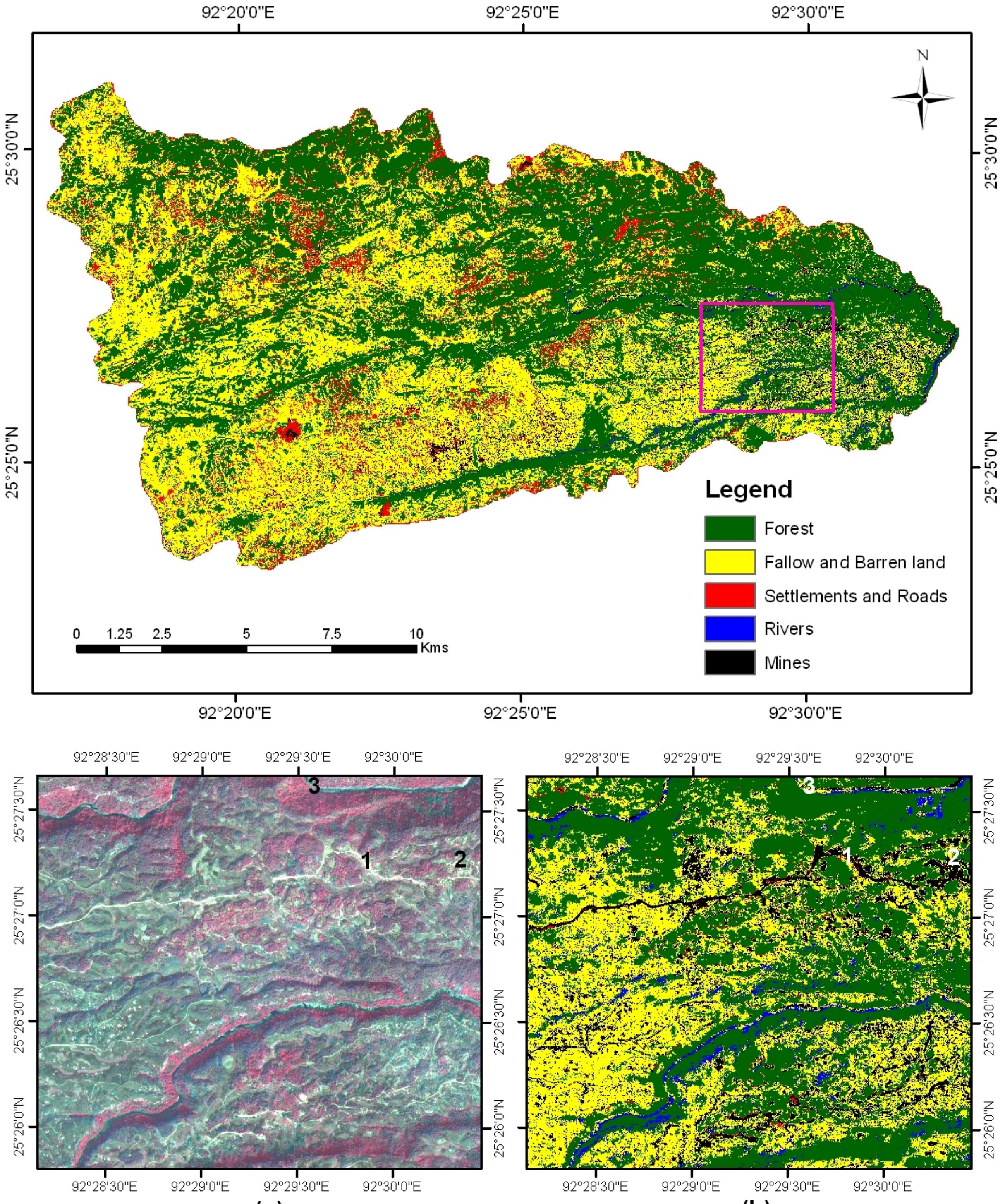

(a) (b)

**Figure 5.6: Land use land cover supervised classification of merged CARTOSAT-1/RESOURCESAT-1 image using Maximum Likelihood classifier.**

**The pink rectangle shows the position of the close-ups taken on (a) CARTOSAT-1/RESOURCESAT-1 image and (b) Corresponding location on classified image. Point 1 shows an example where the roads have been classified as mines. Point 2 shows an example where settlements have been classified as mines. Point 3 shows an example where rivers have been classified as barren land.**

The main reason for this misclassification was because pixel-based classifiers do not consider textural information (Yan *et al.*, 2006). This was another major drawback with such classifiers, especially if used on high spatial resolution images. The addition of layers like ASTER GDEM, LISS-IV NDVI and PC 1 and PC2 did not help produce a good result. Since the classification did not yield any conclusive result, an accuracy assessment was not done. To meet the objective, object-based classification technique was carried out on the image.

### 5.1.2. Object Oriented Classification (OOC)

With the supervised classification using MXL classifier yielding nothing conclusive, it was felt necessary to try out a semi-automatic process to classify the area and map out the mines by using OOC in the Definiens Developer 7 software. By running the rule set given as Appendix 2, we get the output given at Fig.5.7.

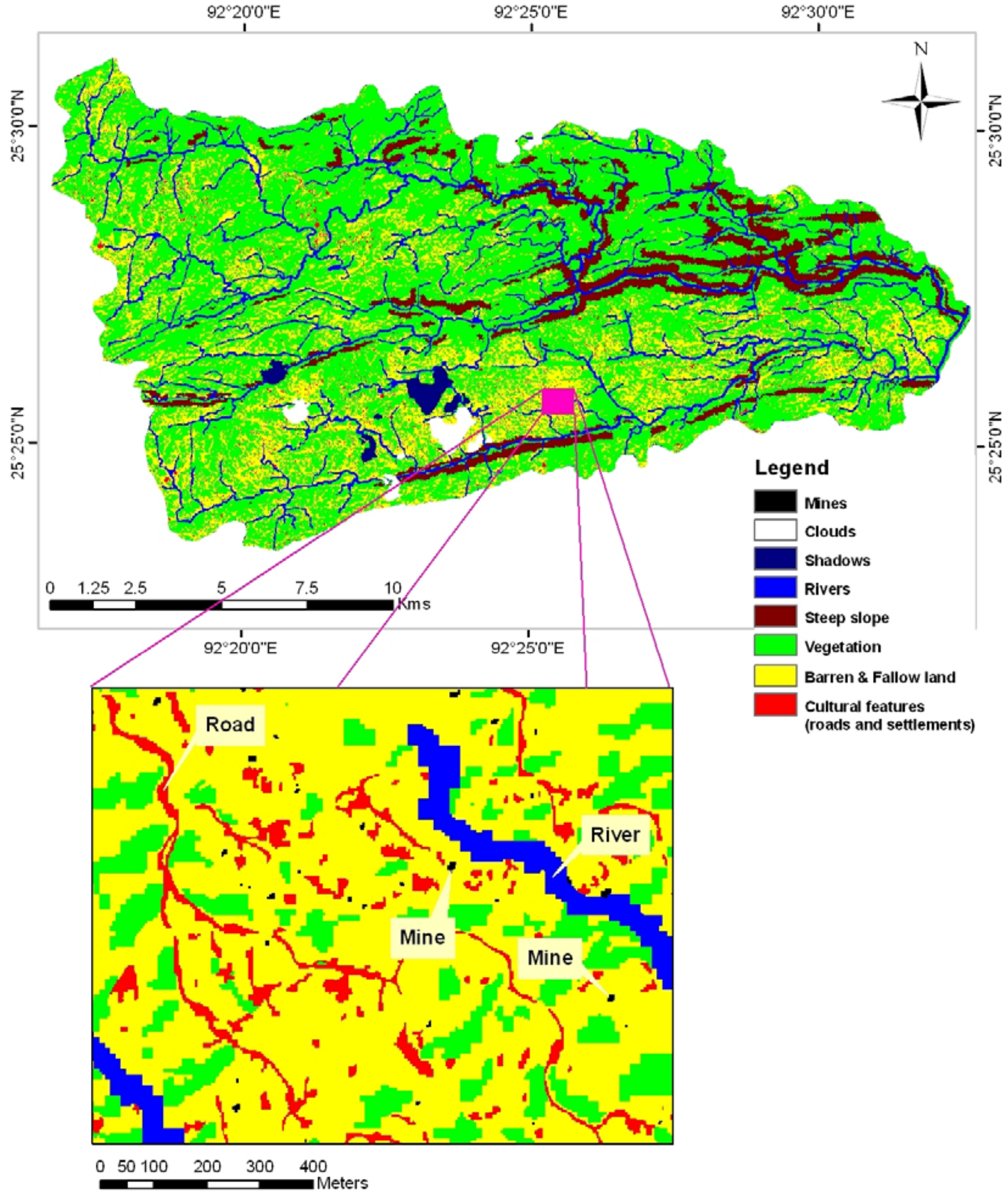

**Figure 5.7: OOC image of merged CARTOSAT-1/RESOURCESAT-1 image and close-up.**

The classified image was exported from the Definiens software as a shape file containing the mine polygons only. There were 1555 polygons (mines) classified through OOC, as compared to 1281 polygons (mines) mapped through visual interpretation. Fig.5.8 shows an overlay of the two shape files with the black ellipses indicating some areas where there has been misclassification of settlements as mines. Both cultural features (settlements and roads) and mines have very similar spectral signatures. Textural information was able to discriminate between the two features to some extent. By masking out the northern gneiss dominant areas using the geology layer and classifying the remaining polygons there as settlements, it has been observed that the number of misclassified polygons was reduced to a big extent. Further processing to fine tune the classification through textural properties did not help. Instead, correctly identified mines got classified as cultural features.

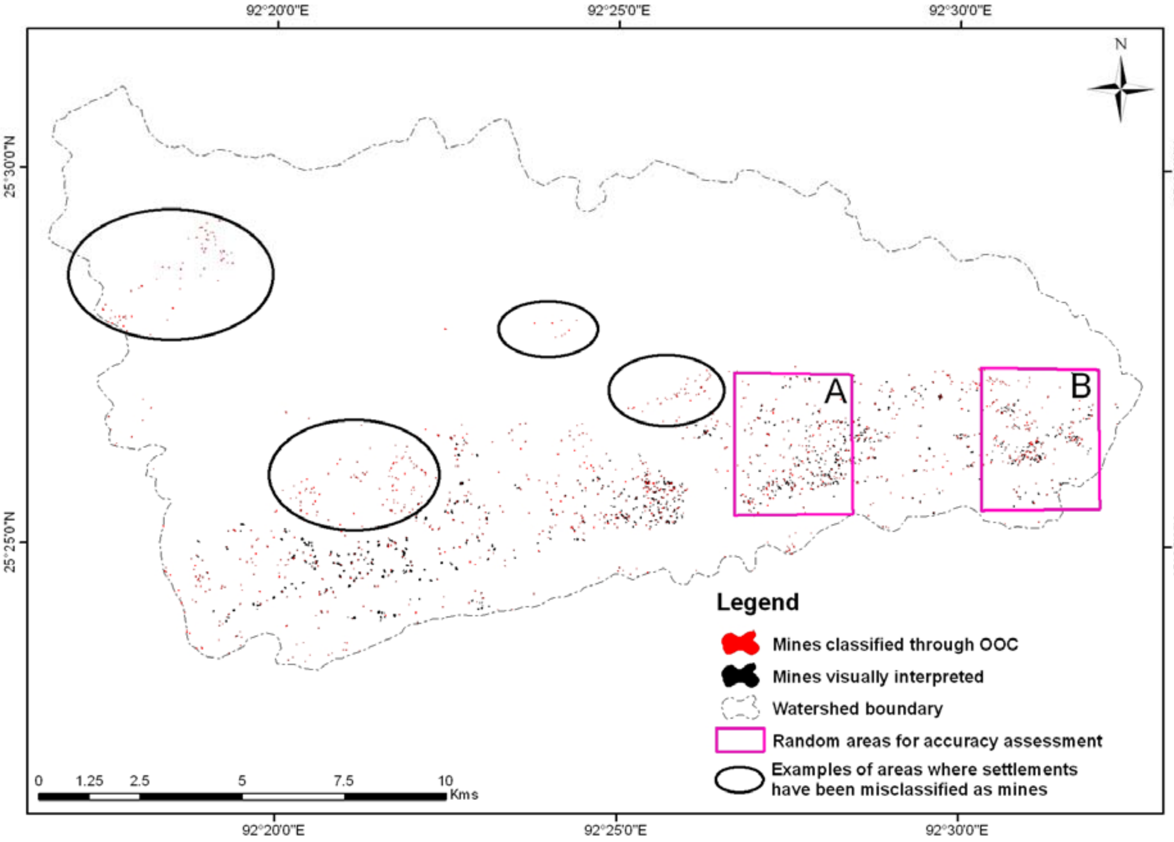

**Figure 5.8: Overlay of mines classified through OOC and through visual interpretation.**

The classification was then checked for accuracy. Two random areas, where the concentration of mines was very high, were selected. These areas are shown in pink rectangles labelled “A” and “B” in Fig.5.8. Each area was about 10 sq.km. in area. The two shape files were intersected and polygons that intersect were considered as correctly identified mines. Those identified through OOC but not visually interpreted were considered as error of commission. Error of omission was considered for those polygons that were visually mapped but missed out through OOC (Fig.5.9). In random area “A”, there were 294 mines that were visually mapped and 274 mines classified through OOC. Out of these 226 mines were found to intersect, which gave an overall accuracy of 76.9%, an error of omission of 23.1% and an error of commission of 16.3%. Random area “B” yielded an overall accuracy of 60.5%, an error of omission of 39.5% and an error of commission of 13%. For the whole watershed, the overall accuracy was calculated to be 67.4%, the error of omission 32.6% and the error of commission 54%.

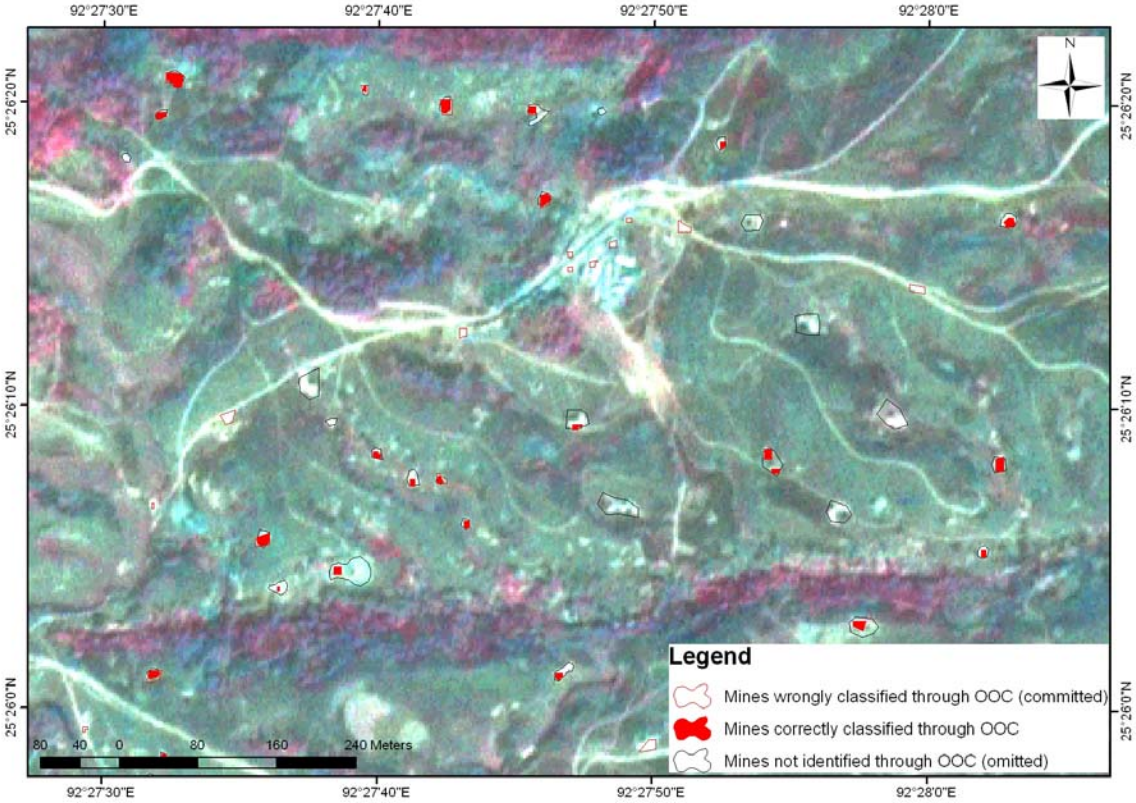

**Figure 5.9: Examples of mine polygons classified through OOC and visually mapped mine polygons. (The background is the merged CARTOSAT-1/RESOURCESAT-1 image).**

Table 5.2 shows the calculation for accuracy assessment. High error of commission for the whole watershed was due to misclassification of cultural features as mines. Similar spectral and textural signatures of these features and similarity in shape due to quadtree segmentation are the main reasons for this misclassification. The addition of the geology layer helped in classifying cultural features in the northern gneissic areas correctly as it was known that there were no mines in these areas. Perhaps, the addition of another contextual layer which depicts the settlement boundaries would have reduced the high error of commission. Moreover, if it had been possible to run multi-resolution segmentation directly on the whole image, this error would have further reduced.

**Table 5.2: Accuracy assessment calculation of object oriented classification of merged CARTOSAT-1/ RESOURCESAT-1 image.**

| | | **No. of mines** | | | **Area (sq.km.)** |
|---|---|---|---|---|---|
| | | **Random area "A"** | **Random area "B"** | **Whole watershed** | |
| a | Visually mapped | 294 | 277 | 1281 | 0.42 |
| b | Classified through OOC | 274 | 203 | 1555 | 0.16 |
| c | Correctly classified (intersecting) | 226 | 167 | 863 | |
| d | Not classified (a - c) | 68 | 110 | 418 | |
| e | Over classified (b - c) | 48 | 36 | 692 | |
| f | Overall accuracy (c/a * 100 %) | **76.9** | **60.3** | **67.4** | **38.1** |
| g | Error of omission (d/a * 100 %) | **23.1** | **39.7** | **32.6** | |
| h | Error of commission (e/a * 100 %) | **16.3** | **13.0** | **54.0** | |

As done earlier with the visual interpretation, the areal extent of the polygons mapped through visual interpretation was compared with that of the polygons obtained through OOC. The total area of the 1281 polygons obtained through visual interpretation was 0.42 sq.km. and that of the 1555 polygons through OOC was 0.16 sq.km which gave an overall accuracy of 38%. Although the number of polygons through OOC was more, the total area they cover was less than half of that obtained visually. This was because the size of the polygons visually mapped was much bigger in size. In Fig.5.9, it can be seen that at several places the red colored mine polygons correctly identified through OOC were much smaller in size than the black colored mine polygons not identified through OOC.

An OOC was also carried out on the pan-sharpened QuickBird image as mentioned at the end of Section 4.2.2.5 using the procedure given at Fig.4.10. The classified image of the subset has been given at Fig.5.10, which also shows the location of the subset. Accuracy assessment of the classification was carried out by intersecting the polygon shape file of mines identified through OOC and that of mines visually mapped through the pan-sharpened QuickBird image. The overall accuracy worked out to be 71.5%, error of commission 14.7% and error of omission 28.5%. In terms of areal extent, the visually mapped polygons covered an area of 0.051 sq.km and the OOC polygons covered an area of 0.029 sq.km. This classification was better than that of the merged CARTOSAT-1/RESOURCESAT-1 image, especially in terms of error of commission. It can be concluded that the process followed was correct as it gave consistent results with both merged CARTOSAT-1/RESOURCESAT-1 image and pan-sharpened QuickBird image. Table 5.3 shows the accuracy assessment calculation of OOC of pan-sharpened QuickBird image.

**Table 5.3: Accuracy assessment calculation of OOC of subset of pan-sharpened QuickBird image and comparison with OOC of merged CARTOSAT-1/RESOURCESAT-1 image at same location.**

| | | **QuickBird** | | **CARTOSAT-1/ RESOURCESAT-1** | |
|---|---|---|---|---|---|
| | | **No. of mines** | **Area (sq.km.)** | **No. of mines** | **Area (sq.m)** |
| a | Visually mapped | 421 | 0.051 | 166 | 23,558.19 |
| b | Classified through OOC | 363 | 0.029 | 95 | 7820.69 |
| c | Correctly classified (intersecting) | 301 | | 90 | |
| d | Not classified (a - c) | 120 | | 76 | |
| e | Over classified (b - c) | 62 | | 5 | |
| f | Overall accuracy (c/a * 100 %) | **71.5** | **56.9** | **54.2** | **33.2** |
| g | Error of omission (d/a * 100 %) | **28.5** | | **45.8** | |
| h | Error of commission (e/a * 100 %) | **14.7** | | **3** | |

The decrease in accuracy by taking areal extent of the mapped polygons was because the number of mine polygons identified through OOC was less than that which was visually mapped. Also, as seen with OOC of the merged CARTOSAT-1/RESOURCESAT-1 image, the size of the mine polygons identified through OOC were smaller in size as compared to those which were visually mapped. In the subset taken, the settlements, which were mostly temporary labor sheds, have merged with the barren and fallow land and vegetation. That was why no settlements were classified in this image. The error of omission was high due to darker signatures of older mines which merged with the vegetation and barren and fallow land and were missed out through OOC. Fig.5.11 shows examples of the different mine polygons visually mapped and classified through OOC.

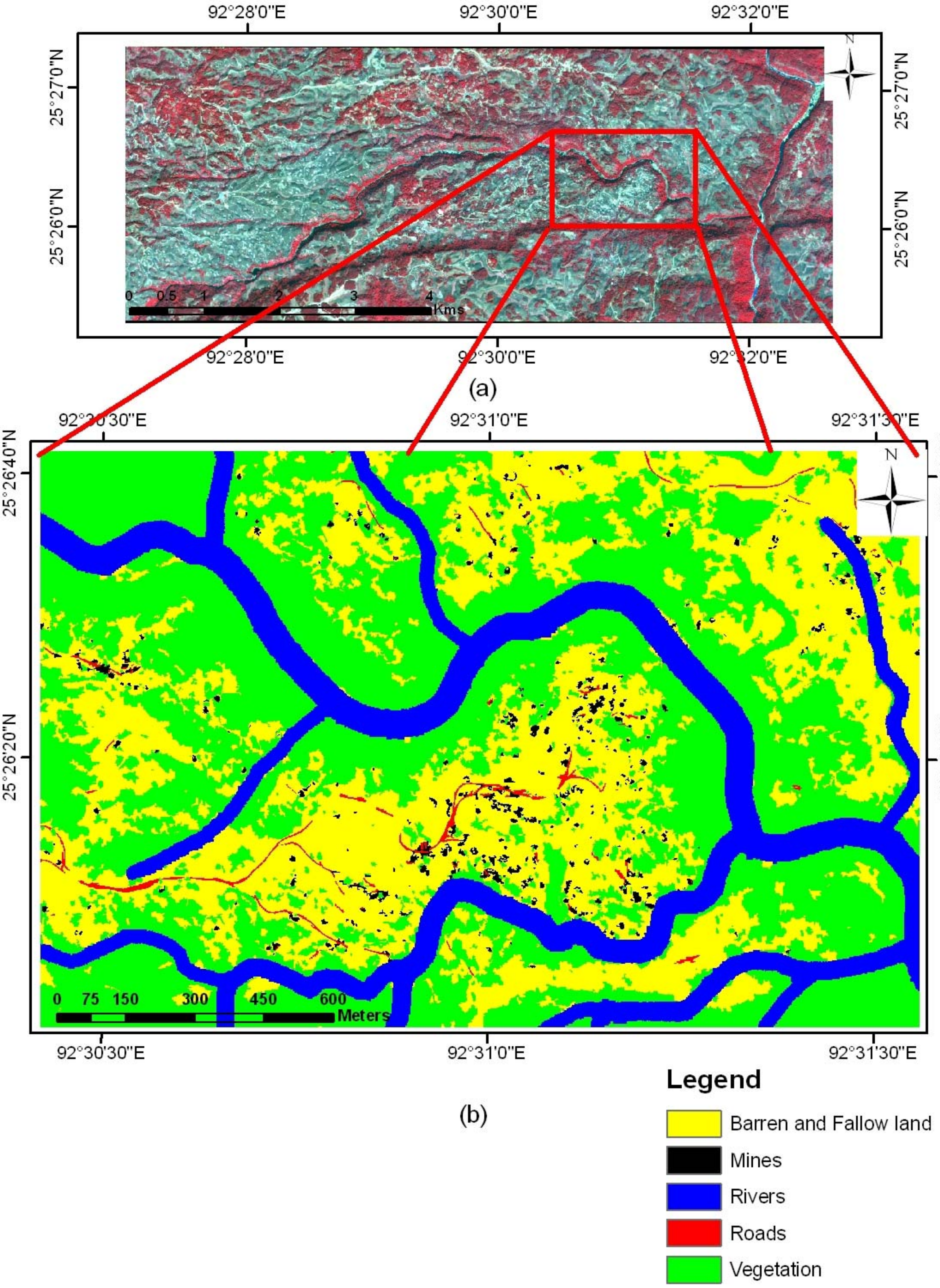

**Figure 5.10: Object oriented classification of pan-sharpened QuickBird image (a) location of the subset (b) classified image.**

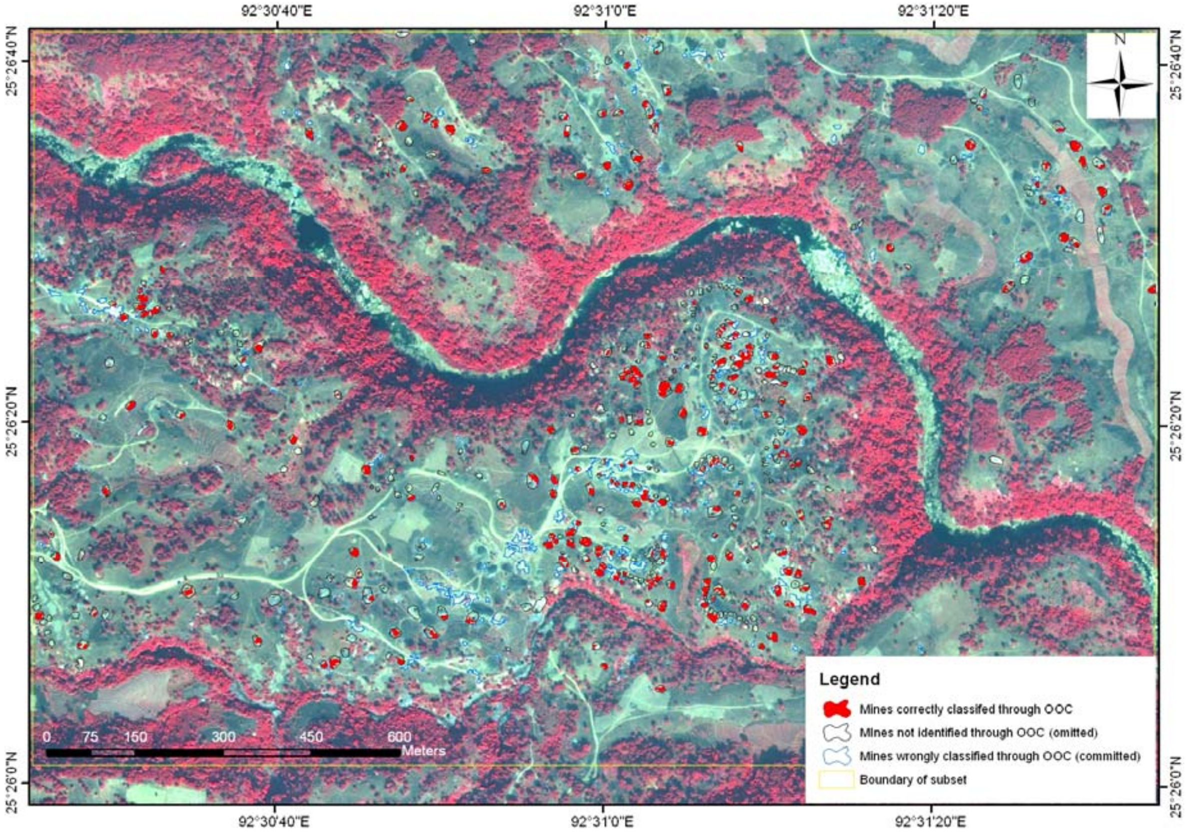

**Figure 5.11: Examples of mine polygons classified through OOC and visually mapped mine polygons. (The background is the pan-sharpened QuickBird image).**

A comparison of the accuracy obtained through OOC of the pan-sharpened QuickBird image and that obtained through the merged CARTOSAT-1/RESOURCESAT-1 image in the same subset is shown in Table 5.3. It is seen that the accuracy is much better in the QuickBird classification which is because of its higher spatial resolution.

In conclusion, it may be said that object-based classification had proven its superiority over pixel-based classification in identification of the artisanal “rat-hole” mines of Jaiñtia Hills. While pixel-based classification resulted in a completely misclassified image, OOC was able to segregate and map out the mines. In the mining area, with overburden dumps, unpaved forest roads, playgrounds, dry river beds and settlements having the same spectral signature, OOC has been able to address this problem to a large extent. Through its added advantage of using textural, contextual and shape parameters of the class objects, OOC was able to discriminate among the classes. Despite having a high error of commission, OOC has proved to be an efficient method for mapping out the extent of mining in the study area.

A general drawback of the OOC is that the rule-set developed for one data or area may not work on another. The image layers used may remain the same. However, values like scale parameter, weights for color and shape and weights for smoothness and compactness in the segmentation process are area specific and need to be modified if used for another data or area. Similarly, the threshold values of different classes used in the classification process have to be modified suitably. These aside, OOC has out-performed pixel-based classification and has shown that in this age of very high resolution imagery, the classification trend has to shift from the pixel to the object.

## 5.2. Image analysis to map iron precipitates on stream bed

Another image analysis that was carried out was on Landsat ETM+ images to identify areas of high iron oxide through band ratio calculation and stacking of these ratio images to produce hybrid FCCs. As mentioned earlier, the Landsat ETM+ images could not be used for identification of the rat-hole mines because of their large spatial resolution. However, because of having more number of spectral bands, these images were used in a different way. From literature several combinations were used to highlight iron oxide rich areas. The combinations that were tried out in red, green and blue order were (B3/B4, B3/B1, B5/B7), (B3/B1, B4, B5/B4), (B3/B1, B4/B2, B1/B7), (B3/B1, B7/B5, B4/B3) and (B3/B1, B5/B4, B5/B7). The best combination that highlighted the iron precipitates on dry stream beds was the last combination and has been described below.

Peters and Hauff (2000) and Vandeberg (2003) have used the combination of B3/B1, B5/B4, B5/B7 (red, green, blue) to identify iron oxides, ferrous minerals and clays. This combination is also given in the ERDAS software as an index for mineral composite. The ratio B3/B1 is generally used for detecting iron oxides, B5/B4 for ferrous minerals and B5/B7 for clay minerals. The composite image obtained is given as Fig.5.12.

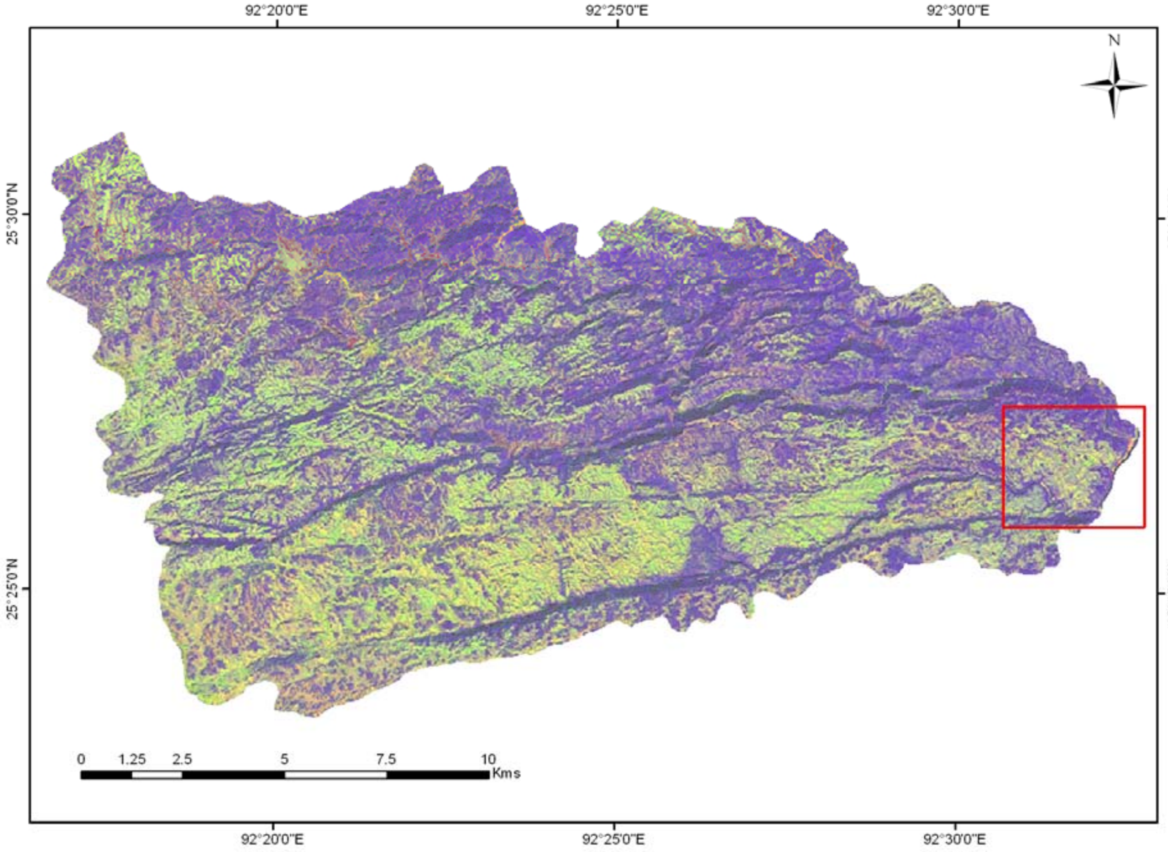

**Figure 5.12: Landsat ETM+ image showing band ratio combinations 3/1-5/4-5/7.**

Here the vegetation appeared in dark blue and the barren and fallow land in yellow to green. However, the feature to be noted is the dry bed of the Rimanar River, in the eastern corner of the image. The river bed here appeared in shades of red and orange which indicated the presence of iron rich materials (Peters and Hauff, 2000). A close-up of the area shown by the red rectangle in Fig.5.12 is shown at Fig.5.13. The inset photographs were taken at the sampling locations indicated.

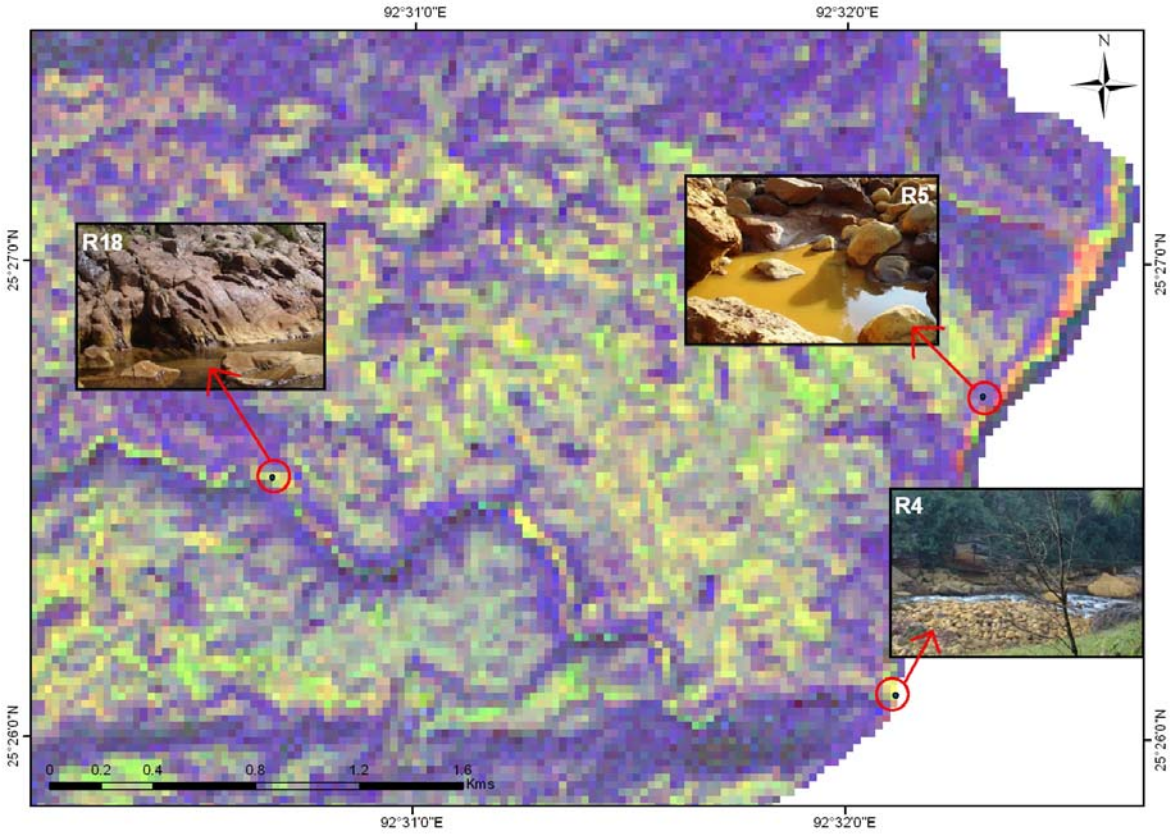

**Figure 5.13: Close-up of area shown by red rectangle in Fig.5.10.**
**(Inset photographs are of sampling locations indicated).**

As mentioned earlier, when viewed as true color composite (TCC), the QuickBird image shows the areas of high iron oxide very clearly. The typical yellow to reddish-brown color of the precipitates make them very obvious and they can be easily picked up in aerial or satellite imagery, especially in very high resolution imagery like that of QuickBird. Fig. 5.14 shows the QuickBird image in TCC with close-ups showing areas with presence of high iron precipitates on the dry stream beds. Insets 1, 4 and 6 show the same locations identified through Landsat ETM+ with presence of high iron precipitates. This shows that areas with potential AMD problems can be identified easily through high resolution satellite or aerial images and can help in the planning and management of remediation of such areas.

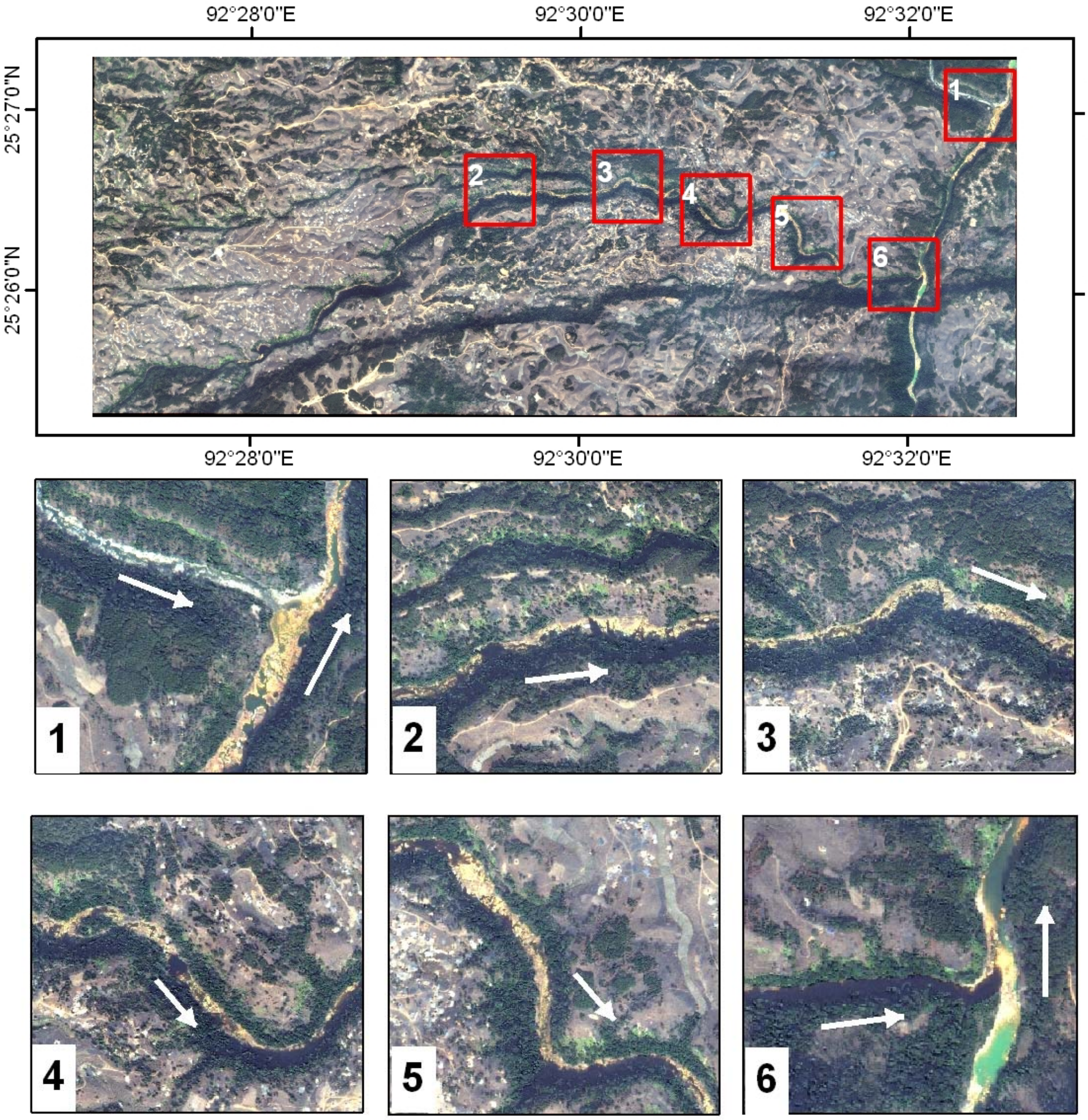

**Figure 5.14: QuickBird image in true color composite (TCC) showing areas with presence of high iron precipitates on dry stream beds.**
**Inset 1 shows the unaffected Umiurem River (flowing eastwards) at its confluence with the affected Rimanar River (flowing northwards); Insets 2, 3, 4 and 5 show the affected Umtarang (Myntriang) River at different locations; Inset 6 shows the confluence of the Umtarang (Myntriang) River and the Rimanar River; Insets 1, 4 and 6 show the same locations identified through Landsat ETM+ as areas with presence of high iron precipitates on the dry stream beds.**

Inset 1 shows the unaffected Umiurem River flowing from west to east with pH of 5.46, iron concentration of 1.26 mg/l and sulphate concentration of 28.7 mg/l measured in the water during post-monsoon at station R26 upstream of this location. The predicted incidence of toxicity in the bed sediments is 12%. However, the Rimanar River, flowing northwards, shows yellow coloration of its exposed bed. At station R5 which is just upstream of the confluence, the pH is 3.08, iron concentration is 1.1 mg/l and sulphate concentration is 190 mg/l in water samples. The predicted incidence of toxicity in the bed sediments is high at 30%. Similarly, station R4 which is located just upstream of inset 6 along the Rimanar River has pH of 3.57, iron concentration of 2.1 mg/l and sulphate concentration of 190.42 mg/l. The predicted incidence of toxicity in the bed sediments is not calculated because sediments could not be collected as the river is very deep at this location.

Even though identification of the mines was not possible through Landsat ETM+ image, a preliminary assessment can be made to identify streams that are facing AMD problems in the watershed. This can help in planning monitoring programmes and to identify which areas need more attention. The main drawback of the Landsat ETM+ image is its coarse spatial resolution which made it possible to identify only the wider streams that have an AMD problem. The red to orange coloration was barely visible for station R4 and R18 on the Myntriang (Umtarang) River but were much clearer at station R5 on the Rimanar River, which is comparatively wider. This has demonstrated that through the simple process of band ratio calculation, remote sensing has helped in identifying rivers affected by AMD.

## 5.3. Field-based stream water and sediment sampling and analysis

### 5.3.1. Water quality

Monsoon water sampling was carried out in June-July 2009. The summary of the analytical results of water samples is given at Table 5.4 and the details are given as Appendixes 4 and 5. When these results were compared with the Indian Standards for drinking water (BIS, 2003), given as Appendix 10, it was observed that almost all the parameters, for which standards have been prescribed, were within the desirable limits for drinking water except for pH, iron and manganese. pH was found to be within the desirable limit (6.5-8.5) at only 4 out of 18 locations. Iron was found to be above the desirable limit (0.3 mg/l) at 11 out of 14 locations and out of these, at 5 locations the values were above the maximum permissible limit (1.0 mg/l), prescribed in the case an alternate drinking water source was absent. Manganese was above the desirable limit (0.1 mg/l) in 4 out of 14 locations, but these were observed to be below the maximum permissible limits.

**Table 5.4: Summary of analytical results of monsoon water samples.**

| Parameter | n | Min | Max | Mean | SD | Q1 | Q2 | Q3 |
|---|---|---|---|---|---|---|---|---|
| pH | 18 | 3.3 | 7.4 | 4.92 | 1.43 | 3.62 | 4.3 | 6.3 |
| EC | 18 | 6.0 | 402.0 | 124.7 | 141.03 | 18.9 | 47.5 | 248.0 |
| Turbidity | 14 | 0.3 | 3.9 | 1.54 | 1.21 | 0.7 | 0.85 | 2.1 |
| D O | 14 | 3.2 | 9.44 | 7.19 | 1.84 | 6.6 | 7.5 | 8.7 |
| TDS | 14 | 9.2 | 361.8 | 127.69 | 126.13 | 17.0 | 80.55 | 223.2 |
| TSS | 14 | 5.0 | 20.0 | 9.64 | 4.58 | 5.0 | 10.0 | 10.0 |
| Total hardness | 14 | 4.0 | 116.0 | 30.14 | 30.98 | 8.0 | 19.0 | 52.0 |
| Acidity | 9 | 16.0 | 108.0 | 59.56 | 32.09 | 30.0 | 60.0 | 80.0 |
| Alkalinity | 5 | 0.8 | 12.0 | 6.16 | 4.21 | 4.0 | 6.0 | 8.0 |
| Ca | 11 | 2.0 | 9.0 | 5.09 | 2.70 | 2.0 | 6.0 | 6.0 |
| Mg | 14 | 0.2 | 23.5 | 4.95 | 7.32 | 0.24 | 0.95 | 9.9 |
| Na | 14 | 2.0 | 14.0 | 6.71 | 2.76 | 5.0 | 6.5 | 8.0 |
| K | 14 | 3.0 | 14.0 | 6.07 | 2.87 | 4.0 | 5.5 | 7.0 |
| Chloride | 14 | 4.0 | 9.0 | 6.57 | 1.83 | 5.0 | 6.5 | 8.0 |

| | | | | | | | | |
|---|---|---|---|---|---|---|---|---|
| Nitrate | 13 | 1.2 | 1.9 | 1.58 | 0.20 | 1.5 | 1.6 | 1.7 |
| Sulphate | 14 | 1.3 | 112.0 | 44.89 | 39.84 | 6.6 | 31.55 | 85.0 |
| Fe | 14 | 0.2 | 4.0 | 1.21 | 1.22 | 0.36 | 0.66 | 1.6 |
| Zn | 13 | 0.0 | 0.22 | 0.06 | 0.07 | 0.02 | 0.03 | 0.06 |
| Pb | 6 | 0.01 | 0.02 | 0.01 | 0.01 | 0.01 | 0.01 | 0.02 |
| Cd | - | BDL | BDL | - | - | - | - | - |
| Cr | 12 | 0.0 | 0.01 | 0.01 | 0.0 | 0.0 | 0.01 | 0.01 |
| Cu | 2 | 0.0 | 0.0 | 0.0 | 0.0 | 0.0 | 0.0 | 0.0 |
| Mn | 13 | 0.02 | 0.2 | 0.09 | 0.05 | 0.05 | 0.09 | 0.12 |
| Σ(metals) | 14 | 0.21 | 4.32 | 1.36 | 1.3 | 0.52 | 0.78 | 1.92 |

**Note:** n = Number of valid samples, SD = Standard deviation, BDL = Below detectable limit
Q1, Q2, Q3 = First, second and third quartiles of the each parameter distribution
All values are in mg/l except pH, EC (µS/cm) and Turbidity (NTU)

The stream water in the study area was generally acidic with pH ranging between 3.3 (R2) and 7.4 (A1). Electrical conductivity ranged from 6 mg/l to 402 mg/l with the highest value recorded at R2. The Central Pollution Control Board, Delhi prescribes that dissolved oxygen (DO) should be 6 mg/l or more for a “drinking water source without conventional treatment but after disinfection” and 4 mg/l or more for “propagation of wild life and fisheries”. Besides R2, where the DO recorded was 3.2 mg/l, all other locations met either one or both of the standards. Total dissolved solids (TDS) ranged between 9.2 mg/l and 361.8 mg/l with the highest value recorded at R2, where the pH was the least. All the major cations and anions, for which standards were available (Ca, Mg, $Cl^-$, $NO_3^-$ and $SO_4^{2-}$), were found to be within desirable limits. Trace metals were found to be within desirable limits, mostly below detectable limits, except for Mn, as discussed earlier. Iron was the major pollutant mainly due to hydrolysis of pyrites in waters of low pH.

To classify the water type for monsoon samples, a Piper diagram was plotted and shown at Fig.5.15. The sampling locations were divided into two types based on the lithology of the location. The circle (○) represented locations in sandstone areas and the triangle (△) represented those in gneisses and schists (metamorphics). The stations located where the river drains through both gneisses and schists and sandstone have been labelled as (□) for locations flowing through more gneisses and schists areas than sandstone areas and (◇) for more sandstone areas than gneisses and schists.

From the figure it can be seen that the main water type was of sodium-potassium type, followed by magnesium type and lastly by calcium type. Sulphate was the dominant anion, followed by chloride. The water types in the study area are dominantly of sodium (potassium) sulphate type, followed by calcium (magnesium) sulphate type. It was also observed that all the water samples from locations in gneisses and schists were of sodium (potassium) sulphate type and most of the samples from sandstone areas were of the calcium (magnesium) sulphate type with only a few falling in the former type. The dominance of sulphate over the other anions can be attributed to presence of pyrite from the coal mines.

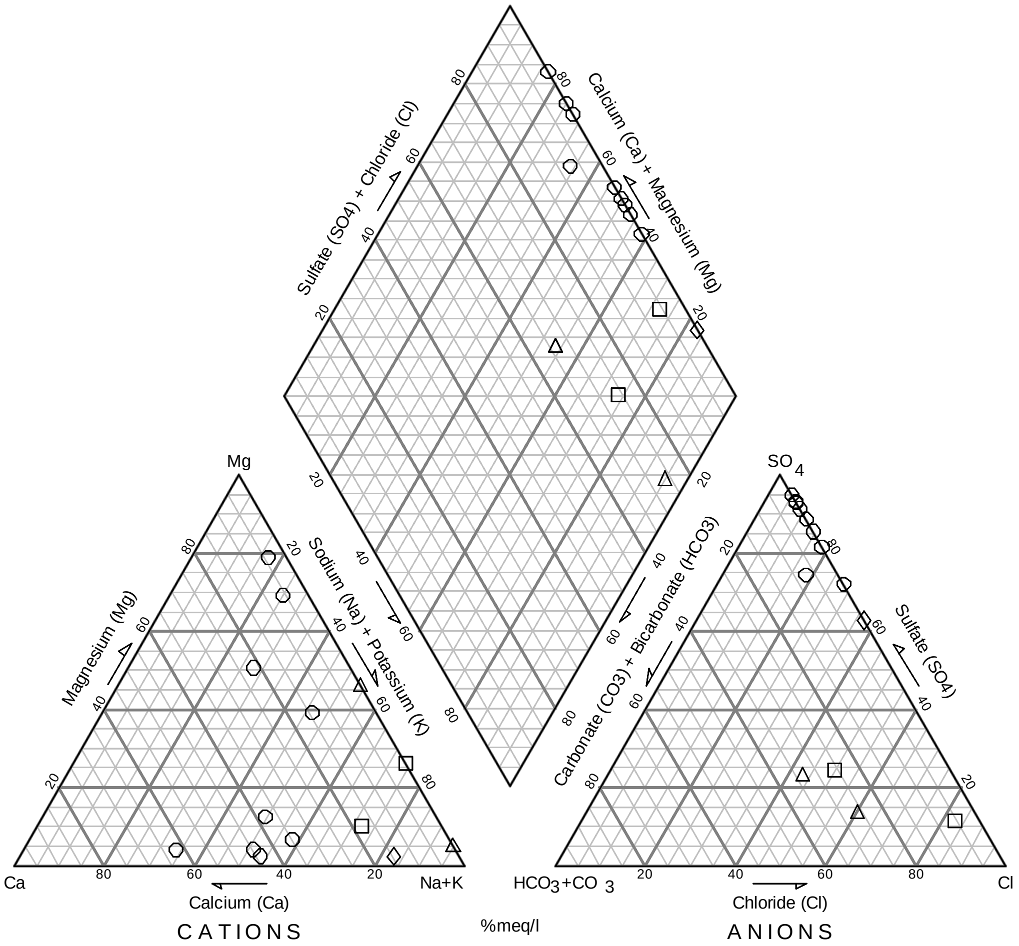

**Figure 5.15: Piper diagram for monsoon water samples.**
**Symbols indicate sampling location in sandstone (○), in metamorphics (△), in metamorphics and sandstone (□) and sandstone and metamorphics (◇).**

Post-monsoon water sampling was carried out in October 2009. The summary of the analytical results of water samples is given at Table 5.5 and the details are given as Appendixes 7 and 8. Comparing these results with the Indian Standards for drinking water (BIS, 2003) (Appendix 10), it was observed that, as with the monsoon samples, almost all the parameters, for which standards have been prescribed, were within the desirable limits for drinking water except for pH, iron and manganese and TDS at a few locations. pH was found to be below the desirable limit (6.5-8.5) at all locations. Iron was found to be above the desirable limit (0.3 mg/l) at 28 out of 30 locations and out of these, at 14 locations the values were above the maximum permissible limit (1.0 mg/l). Manganese was above the desirable limit (0.1 mg/l) in 10 out of 30 locations and in 3 of these locations, it was observed to be above the maximum permissible limit. TDS was above the desirable limit (500 mg/l) in 4 of the locations, but these were observed to be below the maximum permissible limits.

**Table 5.5: Summary of analytical results of post-monsoon water samples.**

| Parameter | n | Min | Max | Mean | SD | Q1 | Q2 | Q3 |
|---|---|---|---|---|---|---|---|---|
| pH | 42 | 2.74 | 6.24 | 4.47 | 1.23 | 3.26 | 4.45 | 5.63 |
| EC | 42 | 6.5 | 1143.0 | 225.48 | 324.42 | 19.75 | 39.45 | 290.5 |
| Turbidity | 30 | 0.3 | 6.2 | 1.72 | 1.54 | 0.6 | 1.2 | 2.3 |
| D O | 10 | 6.2 | 8.0 | 7.3 | 0.48 | 7.2 | 7.2 | 7.6 |
| TDS | 30 | 8.0 | 998.0 | 198.24 | 277.89 | 17.2 | 40.6 | 262.0 |
| TSS | 30 | 5.0 | 15.0 | 8.17 | 3.82 | 5.0 | 5.0 | 10.0 |
| Total hardness | 30 | 3.0 | 271.0 | 49.15 | 66.43 | 7.0 | 20.0 | 58.0 |
| Acidity | 30 | 0.0 | 386.0 | 47.93 | 87.84 | 6.0 | 16.0 | 38.0 |
| Alkalinity | 30 | 0.0 | 24.0 | 6.9 | 7.68 | 0.0 | 2.0 | 14.0 |
| Ca | 30 | 0.05 | 205.0 | 24.9 | 48.43 | 1.0 | 3.5 | 15.0 |
| Mg | 30 | 0.5 | 22.1 | 5.89 | 6.24 | 1.2 | 2.9 | 7.5 |
| Na | 30 | 5.0 | 17.0 | 9.9 | 2.77 | 8.0 | 9.5 | 11.0 |
| K | 30 | 2.0 | 11.0 | 5.87 | 2.33 | 4.0 | 6.0 | 7.0 |
| Cl | 30 | 2.0 | 91.0 | 14.2 | 22.45 | 4.0 | 5.0 | 8.0 |
| Nitrate | 30 | 1.0 | 4.6 | 2.01 | 1.07 | 1.2 | 1.5 | 2.5 |
| Sulphate | 30 | 4.07 | 486.3 | 91.62 | 122.18 | 17.15 | 37.04 | 87.15 |
| Fe | 30 | 0.1 | 13.0 | 2.66 | 3.52 | 0.84 | 1.05 | 2.1 |
| Zn | 16 | 0.01 | 0.19 | 0.07 | 0.06 | 0.03 | 0.05 | 0.11 |
| Pb | 7 | 0.01 | 0.02 | 0.01 | 0.004 | 0.01 | 0.01 | 0.01 |
| Cd | - | BDL | BDL | - | - | - | - | - |
| Cr | 4 | 0.01 | 0.01 | 0.01 | 0.0 | 0.01 | 0.01 | 0.01 |
| Cu | 5 | 0.01 | 0.02 | 0.01 | 0.01 | 0.01 | 0.01 | 0.02 |
| Mn | 29 | 0.01 | 0.46 | 0.11 | 0.11 | 0.03 | 0.08 | 0.13 |
| Ni | 9 | 0.01 | 0.14 | 0.05 | 0.04 | 0.03 | 0.04 | 0.07 |
| Σ(metals) | 30 | 0.13 | 13.49 | 2.83 | 3.63 | 0.9 | 1.18 | 2.59 |

**Note:** n = Number of valid samples, SD = Standard deviation, BDL = Below detectable limit

Q1, Q2, Q3 = First, second and third quartiles of the each parameter distribution

All values are in mg/l except pH, EC (µS/cm) and Turbidity (NTU)

The river water during post-monsoon was acidic with pH ranging between 2.74 (again at R2) and 6.24 (R29). Electrical conductivity was higher in post-monsoon sampling with a highest value of 1143 mg/l, recorded at R24. All the major cations and anions, for which standards were available (Ca, Mg, $Cl^-$, $NO_3^-$ and $SO_4^{2-}$), were found to be within desirable limits. Trace metals were found to be within desirable limits, mostly below detectable limits, except for Mn, as discussed earlier.

A Piper diagram was also plotted for post-monsoon samples (Fig.5.16). The symbols used were the same as for monsoon samples. From the figure it can be seen that the main water type was again of sodium-potassium type, followed by mixed type with no dominant cation and lastly, by calcium type. Sulphate was the dominant anion, followed by mixed type with no dominant anion and one sample in bicarbonate type. The samples taken from areas of gneisses and schists were mostly of sodium (potassium) sulphate type with two falling in the no dominant cation-anion zone. The samples from sandstone areas were mostly of calcium (magnesium) sulphate type with a few sodium (potassium) sulphate types and one falling in the no dominant cation-anion zone. Domination of sulphate ions once again indicate pyrite hydrolysis due to coal mining.

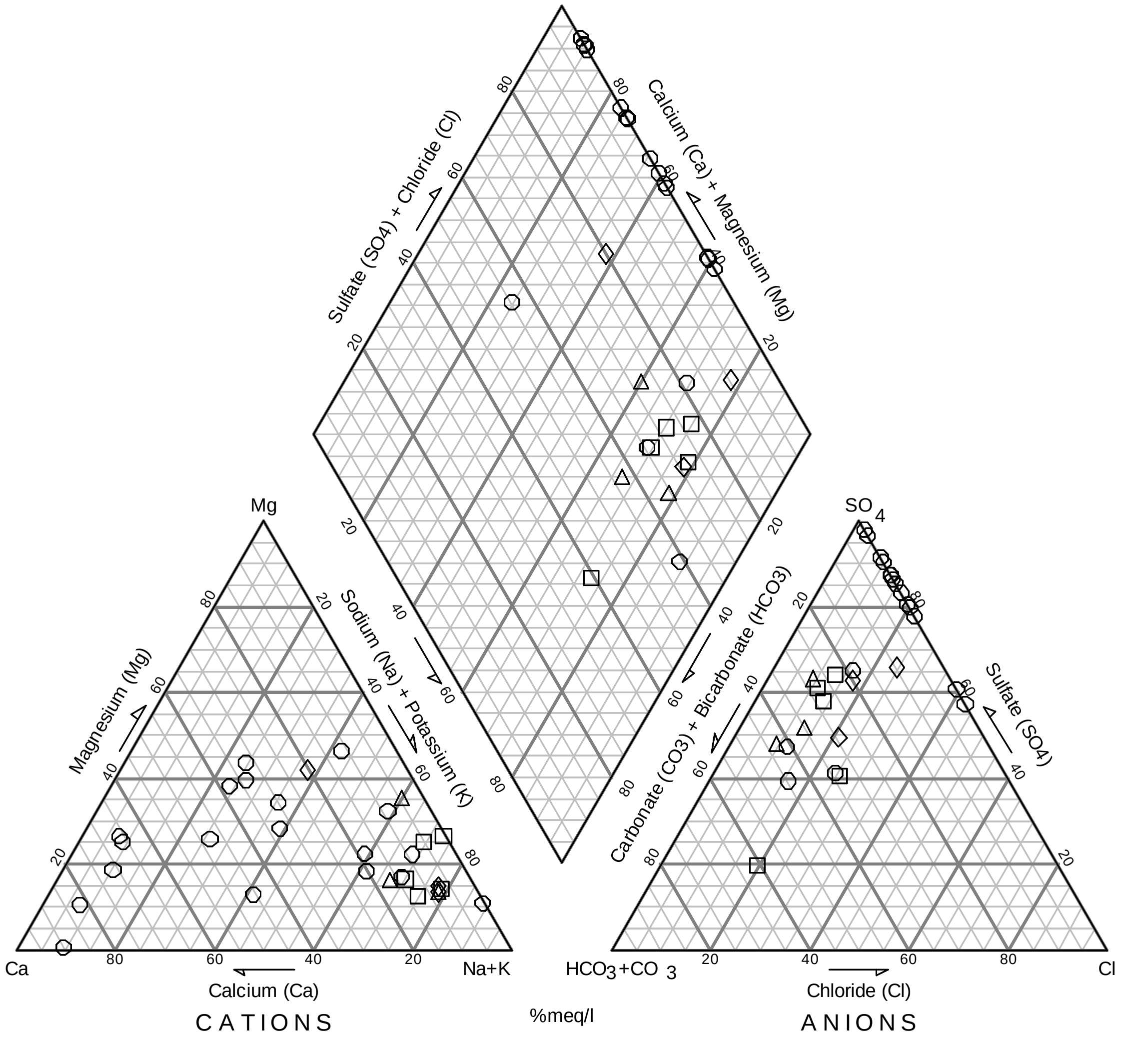

**Figure 5.16: Piper diagram for post-monsoon water samples.**
**Symbols indicate sampling location in sandstone (○), in metamorphics (△), in metamorphics and sandstone (□) and sandstone and metamorphics (◇).**

To examine the relationships of the various parameters analyzed, Pearson correlation coefficient were generated for both monsoon and post-monsoon samples and the resultant matrices have been given at Table 5.6 and Table 5.7 respectively. The correlation was calculated on raw data.

The correlation matrix of the monsoon samples show a high negative correlation between pH and electrical conductivity (EC), total dissolved solids (TDS), sulphates, sodium, potassium and iron which indicates the presence of these pollutants in waters of low pH. EC shows high correlation with TDS, as the latter is a measure of the former and the main constituents of TDS are calcium, sodium, potassium, sulphates, iron, manganese and zinc. Total hardness (TH) correlates very high with magnesium, manganese and sulphates which show that the rivers are generally of permanent hard water. Sulphates have high correlation with iron, zinc and manganese which is also reflected in higher concentration of these metals vis-à-vis the others in water samples. Iron and zinc have a high correlation which shows the solubility of these metals in waters of low pH.

**Table 5.6: Correlation matrix of different parameters for monsoon water samples.**

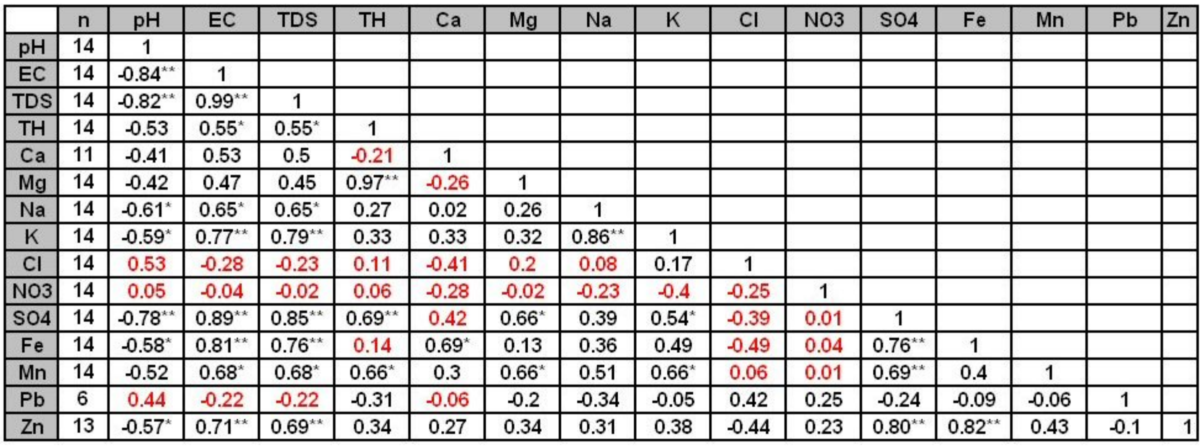

| | n | pH | EC | TDS | TH | Ca | Mg | Na | K | Cl | NO3 | SO4 | Fe | Mn | Pb | Zn |
|---|---|---|---|---|---|---|---|---|---|---|---|---|---|---|---|---|
| pH | 14 | 1 | | | | | | | | | | | | | | |
| EC | 14 | -0.84** | 1 | | | | | | | | | | | | | |
| TDS | 14 | -0.82** | 0.99** | 1 | | | | | | | | | | | | |
| TH | 14 | -0.53 | 0.55* | 0.55* | 1 | | | | | | | | | | | |
| Ca | 11 | -0.41 | 0.53 | 0.5 | -0.21 | 1 | | | | | | | | | | |
| Mg | 14 | -0.42 | 0.47 | 0.45 | 0.97** | -0.26 | 1 | | | | | | | | | |
| Na | 14 | -0.61* | 0.65* | 0.65* | 0.27 | 0.02 | 0.26 | 1 | | | | | | | | |
| K | 14 | -0.59* | 0.77** | 0.79** | 0.33 | 0.33 | 0.32 | 0.86** | 1 | | | | | | | |
| Cl | 14 | 0.53 | -0.28 | -0.23 | 0.11 | -0.41 | 0.2 | 0.08 | 0.17 | 1 | | | | | | |
| NO3 | 14 | 0.05 | -0.04 | -0.02 | 0.06 | -0.28 | -0.02 | -0.23 | -0.4 | -0.25 | 1 | | | | | |
| SO4 | 14 | -0.78** | 0.89** | 0.85** | 0.69** | 0.42 | 0.66* | 0.39 | 0.54* | -0.39 | 0.01 | 1 | | | | |
| Fe | 14 | -0.58* | 0.81** | 0.76** | 0.14 | 0.69* | 0.13 | 0.36 | 0.49 | -0.49 | 0.04 | 0.76** | 1 | | | |
| Mn | 14 | -0.52 | 0.68* | 0.68* | 0.66* | 0.3 | 0.66* | 0.51 | 0.66* | 0.06 | 0.01 | 0.69** | 0.4 | 1 | | |
| Pb | 6 | 0.44 | -0.22 | -0.22 | -0.31 | -0.06 | -0.2 | -0.34 | -0.05 | 0.42 | 0.25 | -0.24 | -0.09 | -0.06 | 1 | |
| Zn | 13 | -0.57* | 0.71** | 0.69** | 0.34 | 0.27 | 0.34 | 0.31 | 0.38 | -0.44 | 0.23 | 0.80** | 0.82** | 0.43 | -0.1 | 1 |

** Correlation is significant at the 0.01 level (2-tailed)

* Correlation is significant at the 0.05 level (2-tailed)

n = Number of valid samples

**Table 5.7: Correlation matrix of different parameters for post-monsoon water samples.**

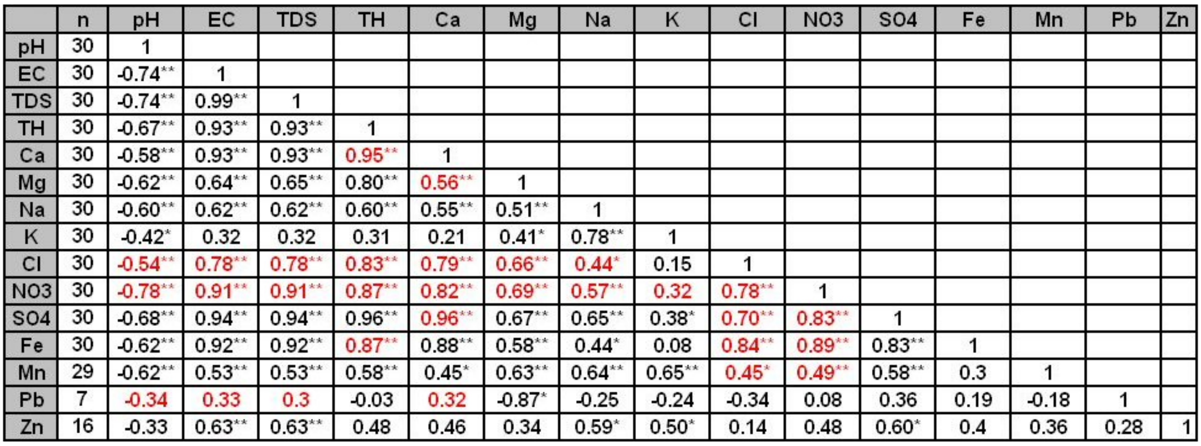

| | n | pH | EC | TDS | TH | Ca | Mg | Na | K | Cl | NO3 | SO4 | Fe | Mn | Pb | Zn |
|---|---|---|---|---|---|---|---|---|---|---|---|---|---|---|---|---|
| pH | 30 | 1 | | | | | | | | | | | | | | |
| EC | 30 | -0.74** | 1 | | | | | | | | | | | | | |
| TDS | 30 | -0.74** | 0.99** | 1 | | | | | | | | | | | | |
| TH | 30 | -0.67** | 0.93** | 0.93** | 1 | | | | | | | | | | | |
| Ca | 30 | -0.58** | 0.93** | 0.93** | 0.95** | 1 | | | | | | | | | | |
| Mg | 30 | -0.62** | 0.64** | 0.65** | 0.80** | 0.56** | 1 | | | | | | | | | |
| Na | 30 | -0.60** | 0.62** | 0.62** | 0.60** | 0.55** | 0.51** | 1 | | | | | | | | |
| K | 30 | -0.42* | 0.32 | 0.32 | 0.31 | 0.21 | 0.41* | 0.78** | 1 | | | | | | | |
| Cl | 30 | -0.54** | 0.78** | 0.78** | 0.83** | 0.79** | 0.66** | 0.44* | 0.15 | 1 | | | | | | |
| NO3 | 30 | -0.78** | 0.91** | 0.91** | 0.87** | 0.82** | 0.69** | 0.57** | 0.32 | 0.78** | 1 | | | | | |
| SO4 | 30 | -0.68** | 0.94** | 0.94** | 0.96** | 0.96** | 0.67** | 0.65** | 0.38* | 0.70** | 0.83** | 1 | | | | |
| Fe | 30 | -0.62** | 0.92** | 0.92** | 0.87** | 0.88** | 0.58** | 0.44* | 0.08 | 0.84** | 0.89** | 0.83** | 1 | | | |
| Mn | 29 | -0.62** | 0.53** | 0.53** | 0.58** | 0.45* | 0.63** | 0.64** | 0.65** | 0.45* | 0.49** | 0.58** | 0.3 | 1 | | |
| Pb | 7 | -0.34 | 0.33 | 0.3 | -0.03 | 0.32 | -0.87* | -0.25 | -0.24 | -0.34 | 0.08 | 0.36 | 0.19 | -0.18 | 1 | |
| Zn | 16 | -0.33 | 0.63** | 0.63** | 0.48 | 0.46 | 0.34 | 0.59* | 0.50* | 0.14 | 0.48 | 0.60* | 0.4 | 0.36 | 0.28 | 1 |

** Correlation is significant at the 0.01 level (2-tailed)

* Correlation is significant at the 0.05 level (2-tailed)

n = Number of valid samples

**N.B.**: Figures in red color indicate major differences between correlation coefficients of the two seasons.

The correlation matrix of the post-monsoon samples also show similar high negative relationship between pH and EC, TDS, the major cations and anions, iron and manganese. pH is observed to have negative relation with all parameters which means that with lower pH there is more dissolution of metals and other pollutants and in water with higher pH either the metals have precipitated or they are not present at all. EC is very highly correlated with TDS and also with almost all the cations, anions and metals analyzed. Calcium and magnesium have high correlation with the anions contributing to the hardness of the water.

Gray (1996) has pointed out that sulphate and EC are important indicators of AMD firstly because both are extremely sensitive to AMD even after large dilutions have occurred and secondly, because sulphate is not removed to a great extent by both sorption and precipitation processes due to fluctuations in pH. In this case, both monsoon and post-monsoon samples show very high correlation between sulphate and EC which indicates the presence of AMD in the study area. As the strength of correlation increases with increase in contamination (Gray, 1996), in this case, with correlation coefficients of 0.89 and 0.94 for monsoon and post-monsoon samples respectively, it can be concluded that the rivers in the study area are being impacted by AMD.

It may be mentioned that in generating the correlation matrices, a few analyzed parameters were left out. Only those parameters which were common to both seasons and which have enough valid samples for a proper correlation calculation were selected.

A comparison of the matrices of the two seasons revealed that some parameters have a big difference in their correlation coefficients. pH generally shows a negative relationship with all parameters which indicates that with increase in pH, the dissolved solids precipitate out or get adsorbed by the bed sediments. However, in the monsoon samples pH showed a positive relationship with chloride, nitrate and lead. The reason could be that for lead, the number of valid samples was relatively less for calculating the correlation. Both chloride and nitrate show high differences in their relationships in both seasons. This is possibly due to human error during analysis in the monsoon samples which yielded inaccurate results which was, however, not the case with post-monsoon samples. The negative relationships of total hardness (TH) with calcium and of calcium and magnesium in the monsoon samples may also be due to inaccuracies in analysis. A big increase was noted in the calcium – sulphate relationship. The former vindicates the findings through the Piper diagram (Fig. 5.16) that in the leaner post-monsoon season, the dominant water was calcium-sulphate type.

As seen from Fig.4.16, there was a lot of variation in the sum of anions and cations in the monsoon samples. The results were dispersed both above and below the trend line. However, the post-monsoon samples fitted well around the trend line. This was also a reason for the major differences in correlation coefficients of the two seasons. Further, the difference in number of samples (14 in monsoon and 30 in post-monsoon) may have also affected the calculation of correlation coefficients in the two seasons which has led to high differences for several parameters.

The scatter plots of pH plotted against a few selected pollutants have been generated and shown in the following figures.

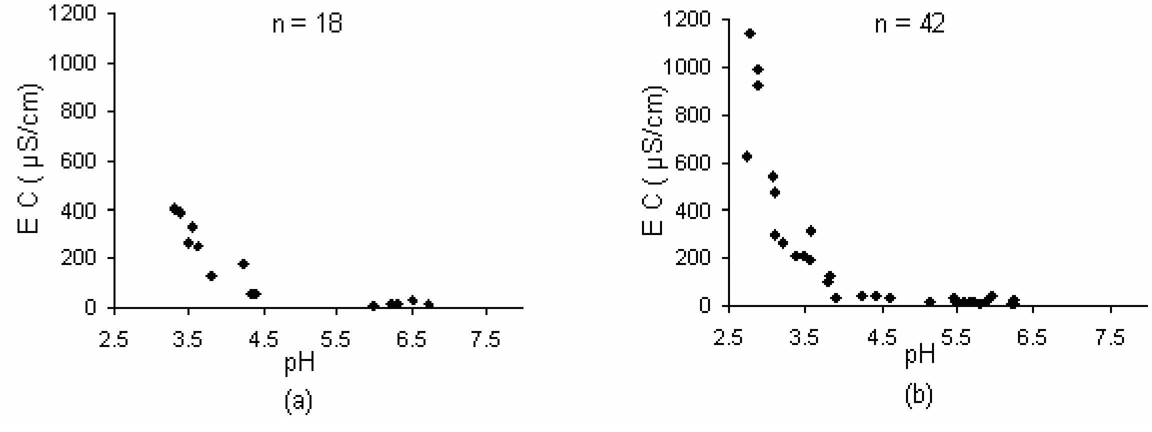

**Figure 5.17: Scatter plot of pH versus EC**
**(a) monsoon water samples (b) post-monsoon water samples.**

Fig.5.17 shows that in waters of low pH, particularly below pH 4, the ion activity increases significantly. This shows that AMD plays a role in reducing the pH and leaching of metals from the surrounding rocks and mine spoils. In low pH, the metals stay in solution and increase the EC.

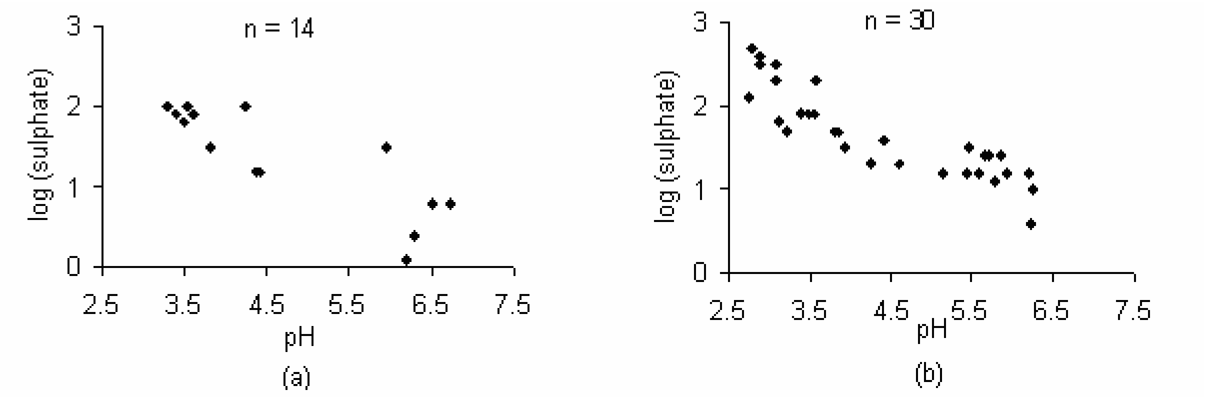

**Figure 5.18: Scatter plot of pH versus log$_{10}$ (sulphate)**
**(a) monsoon water samples (b) post-monsoon water samples.**

Fig. 5.18 shows the relationship of pH with sulphate. By taking sulphate in log scale, a linearly decreasing trend can be observed, especially in the post-monsoon samples. The limited number of samples in monsoon has also showed a more or less similar trend. This is true because in waters of low pH, pyrite hydrolysis releases large quantities of sulphate into the water and this reduces with increase in pH.

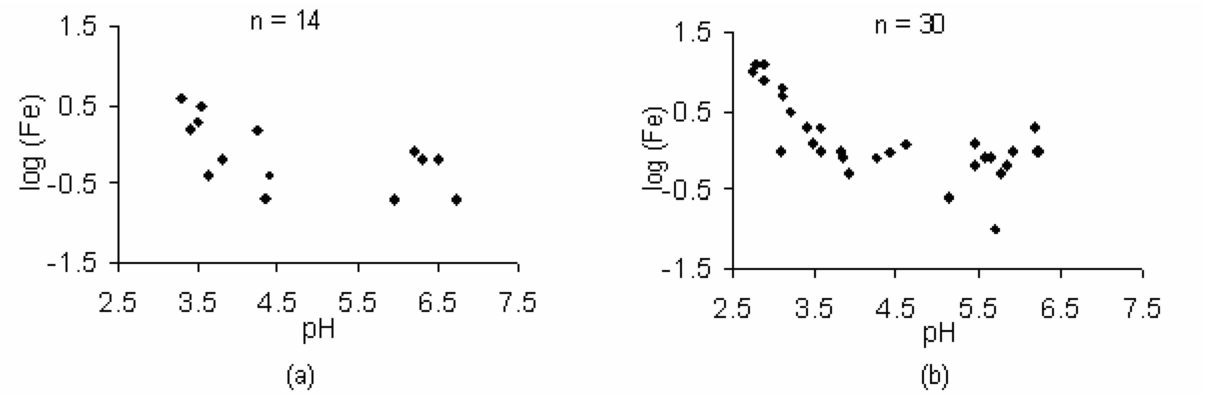

**Figure 5.19: Scatter plot of pH versus log$_{10}$ (iron)**
**(a) monsoon water samples (b) post-monsoon water samples.**

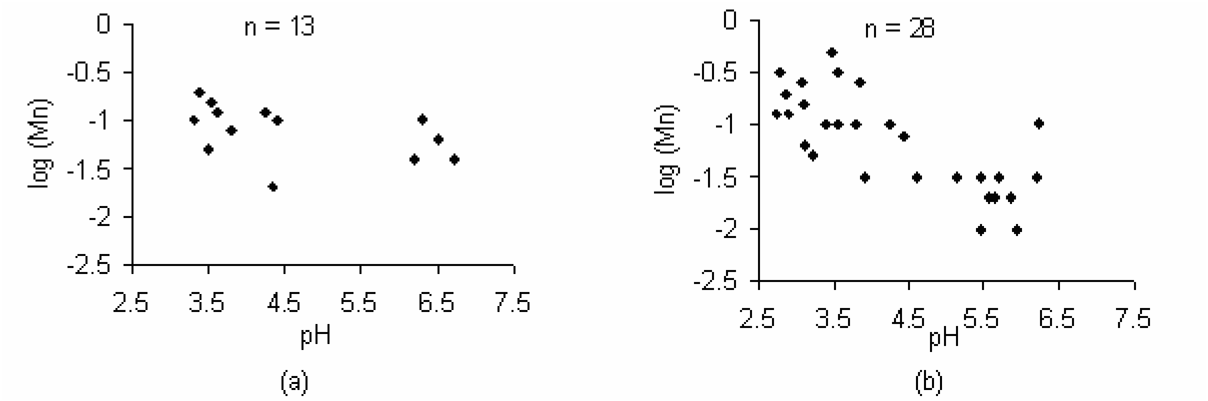

**Figure 5.20: Scatter plot of pH versus $\log_{10}$ (manganese)
(a) monsoon water samples (b) post-monsoon water samples.**

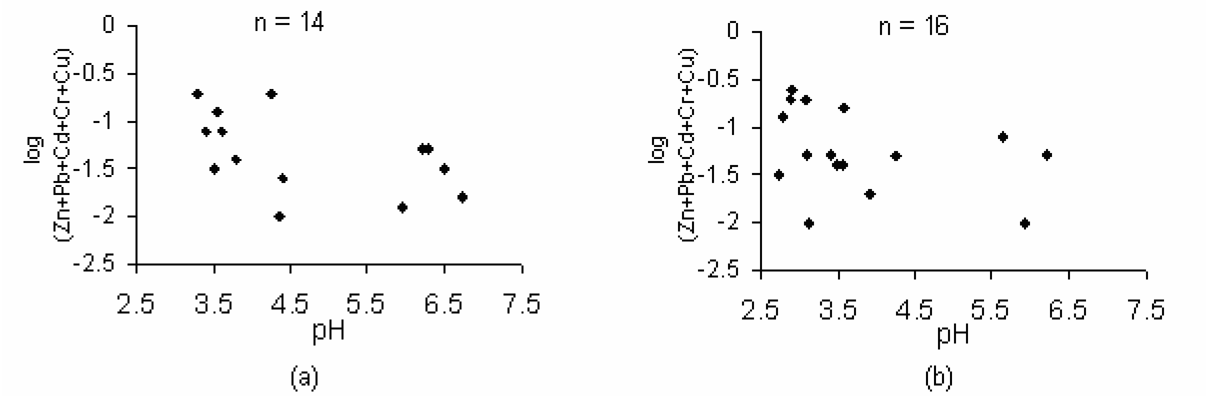

**Figure 5.21: Scatter plot of pH versus $\log_{10}$ (sum of trace metals)
(a) monsoon water samples (b) post-monsoon water samples.**

The scatter plots shown in Fig.5.19 through Fig.5.21 show that in waters of low pH, the solubility of metals increases and they stay in solution as they are leached from the surroundings. As the pH increases the solubility of Fe decreases and oxyhydroxides are formed. At the same time, the capacity of the particles in the water to adsorb metal ions also increases which results in the removal of metals to the particles and bed sediments (Eby, 2004).

The variation of some of the important parameters in the two studied seasons has been plotted as box plots in the following figures.

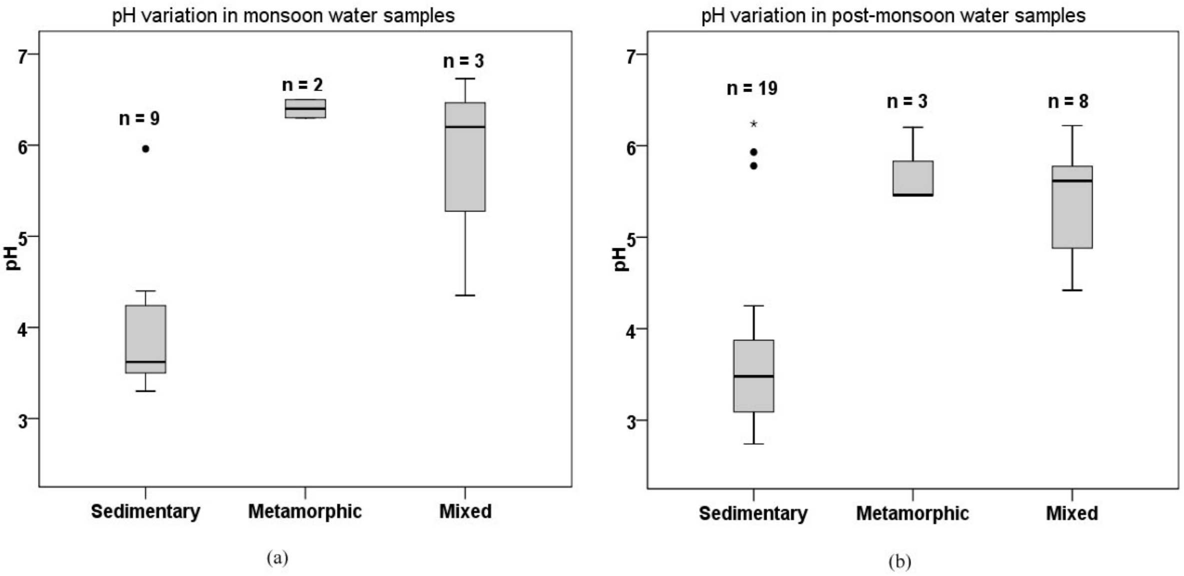

**Figure 5.22: Variation of pH in (a) monsoon (b) post-monsoon.**
**(Stream provenance is shown along X-axis. "n" denotes the number of valid samples)**

From Fig. 5.22 it is obvious that the impacted streams all lie in the sedimentary rock around the coal mining area. However, it can also be seen from the extreme values and outliers in the figure, that locations within sedimentary rock but away from coal mining areas (R14, R29 and A2) show high pH. This shows that pyrite hydrolysis from coal mining is the major cause of AMD in the study area. Overall, there has been a slight decrease of pH in the post-monsoon samples due to reduced dilution in the stream water.

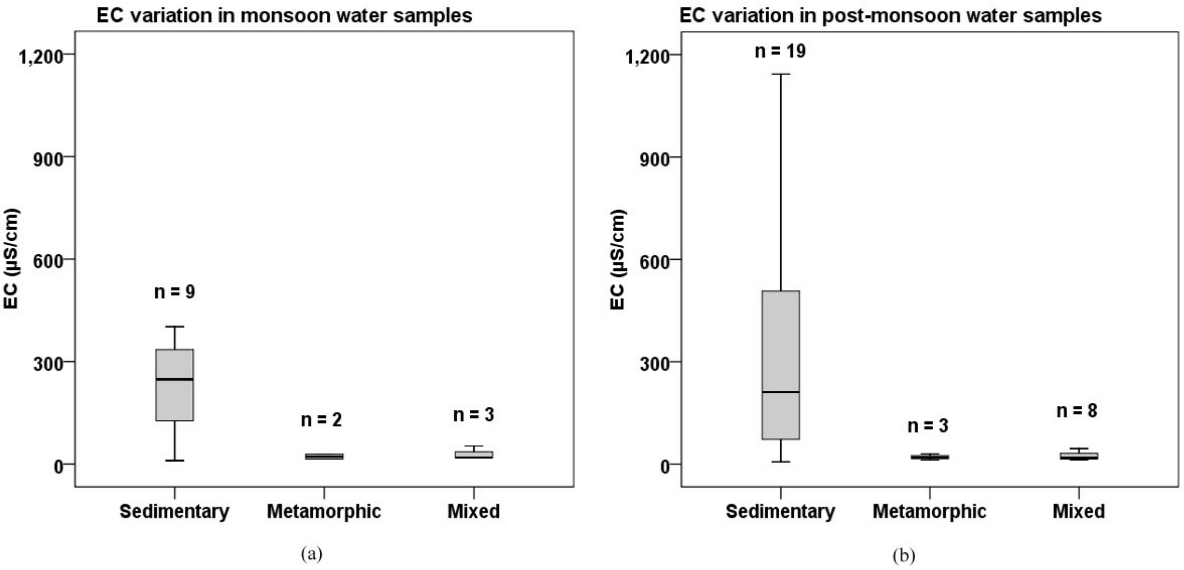

**Figure 5.23: Variation of EC in (a) monsoon (b) post-monsoon.**
**(Stream provenance is shown along X-axis. "n" denotes the number of valid samples)**

From Fig.5.23 it can be seen that EC is high in locations where pH is low. The outlier in monsoon samples from sedimentary rock was recorded at A2, a head stream. EC is seen to be higher in post-monsoon samples with pH being lower.

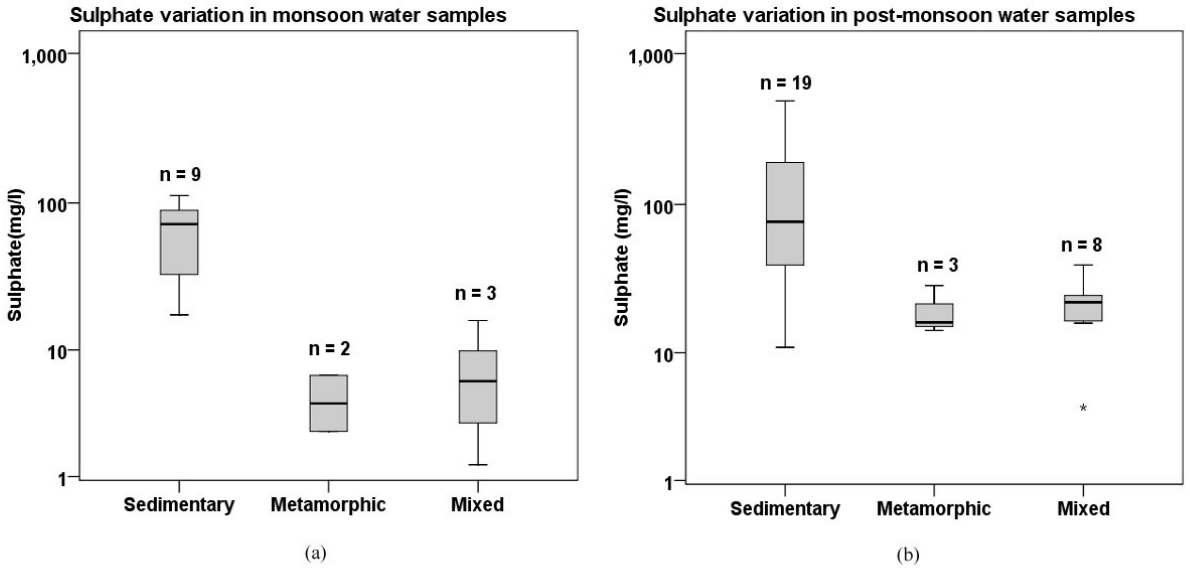

**Figure 5.24: Variation of sulphate in (a) monsoon (b) post-monsoon.**
**(Stream provenance is shown along X-axis. "n" denotes the number of valid samples)**

Sulphates can also be seen to have higher concentration in samples from sedimentary rock where the pH is much lower due to presence of coal mines (Fig.5.24). Similarly, higher sulphate concentration in post-monsoon samples is expected with lower pH and increased hydrolysis of pyrite from the surrounding coal mining areas.

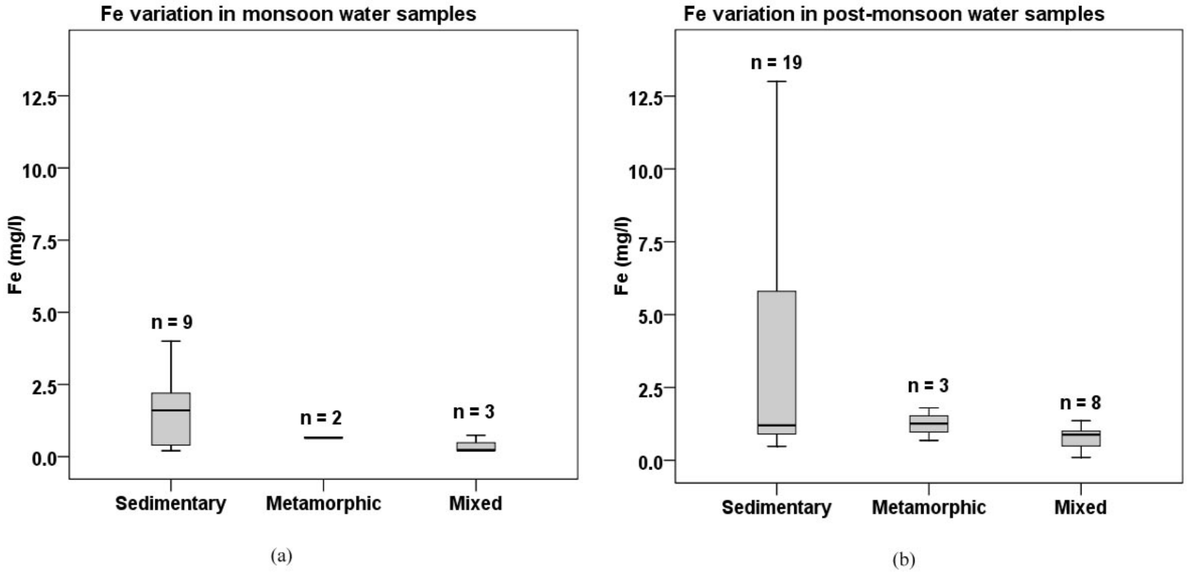

**Figure 5.25: Variation of iron in (a) monsoon (b) post-monsoon.**
**(Stream provenance is shown along X-axis. "n" denotes the number of valid samples)**

The presence of high iron in samples from sedimentary rock (Fig.5.25) shows its solubility in waters of low pH. Its concentration is observed to be low in the samples from metamorphic rock and from mixed rock type. Higher iron concentration in the post-monsoon samples is consistent with the overall lower pH.

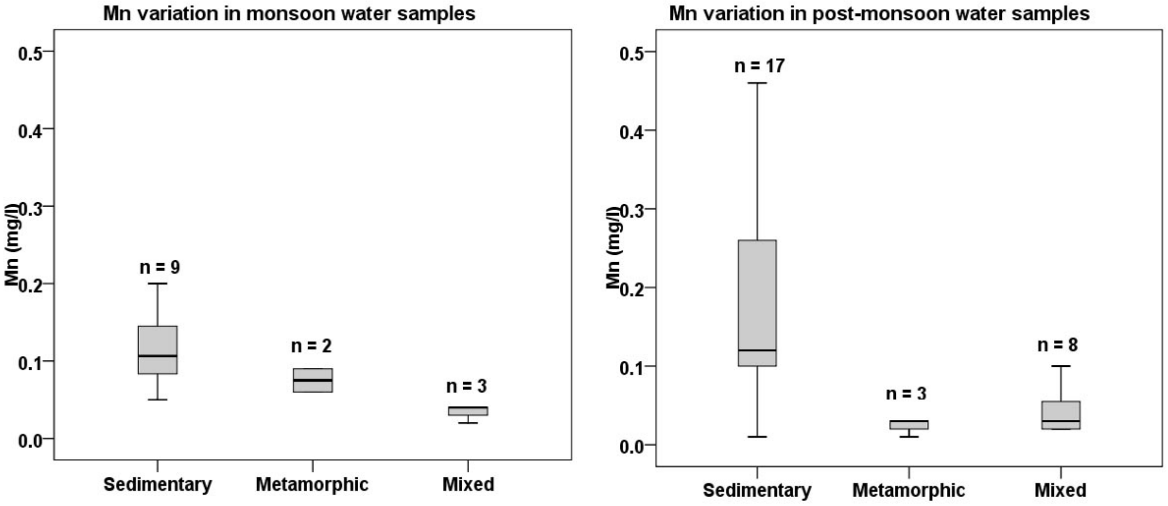

(a) (b)

**Figure 5.26: Variation of manganese in (a) monsoon (b) post-monsoon.**
**(Stream provenance is shown along X-axis. "n" denotes the number of valid samples)**

The solubility of manganese is also seen to have increased in the post-monsoon samples with pH being lower (Fig.5.26).

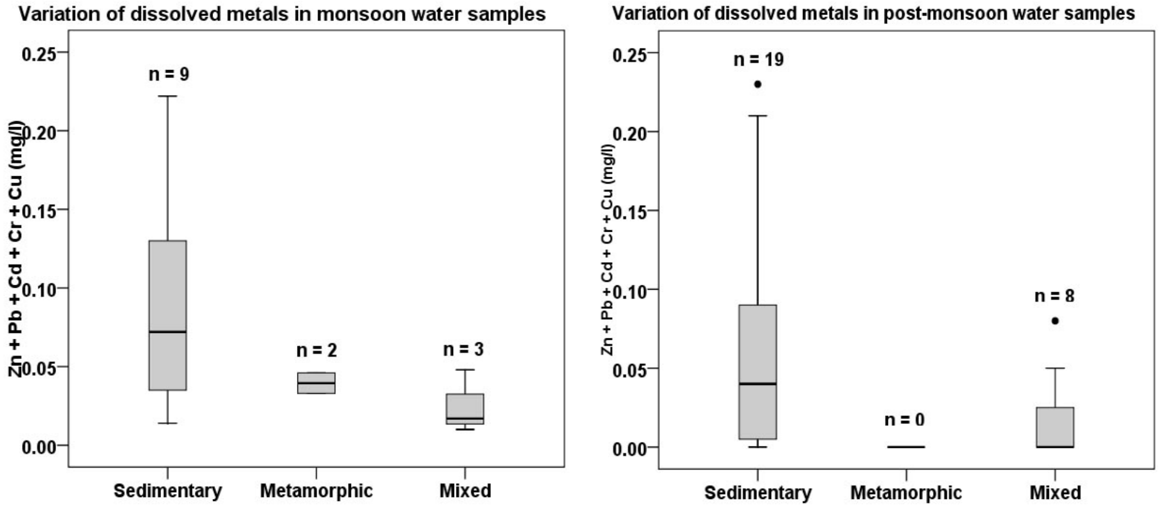

(a) (b)

**Figure 5.27: Variation of sum of trace metals in (a) monsoon (b) post-monsoon.**
**(Stream provenance is shown along X-axis. "n" denotes the number of valid samples)**

Trace metals can be seen to have been more dissolved in samples from sedimentary rock which has low pH vis-à-vis the samples from metamorphic rock and from mixed rock type (Fig.5.27). There was, however, only a slight seasonal variation in their concentration. The Meghalaya State Pollution Control Board (MSPCB, 1997) reported similar observations where they found very less variation in the monitored rivers in a study period of two years.

The distributions of a few pollutants in both monsoon and post-monsoon seasons have also been mapped and given below (Fig.5.28 to Fig.2.35).

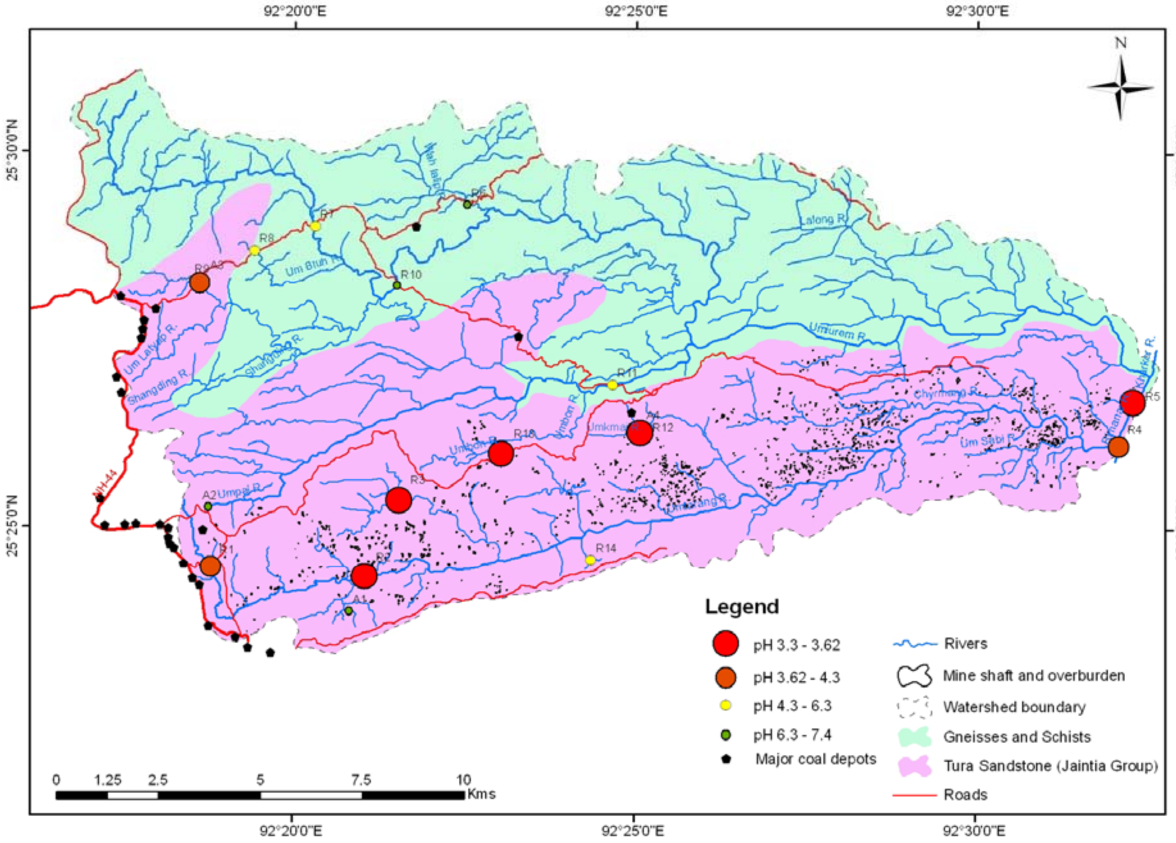

**Figure 5.28: Distribution of pH in monsoon samples.**
**(Symbol size based on Q1, Q2, Q3 from Table 5.4)**

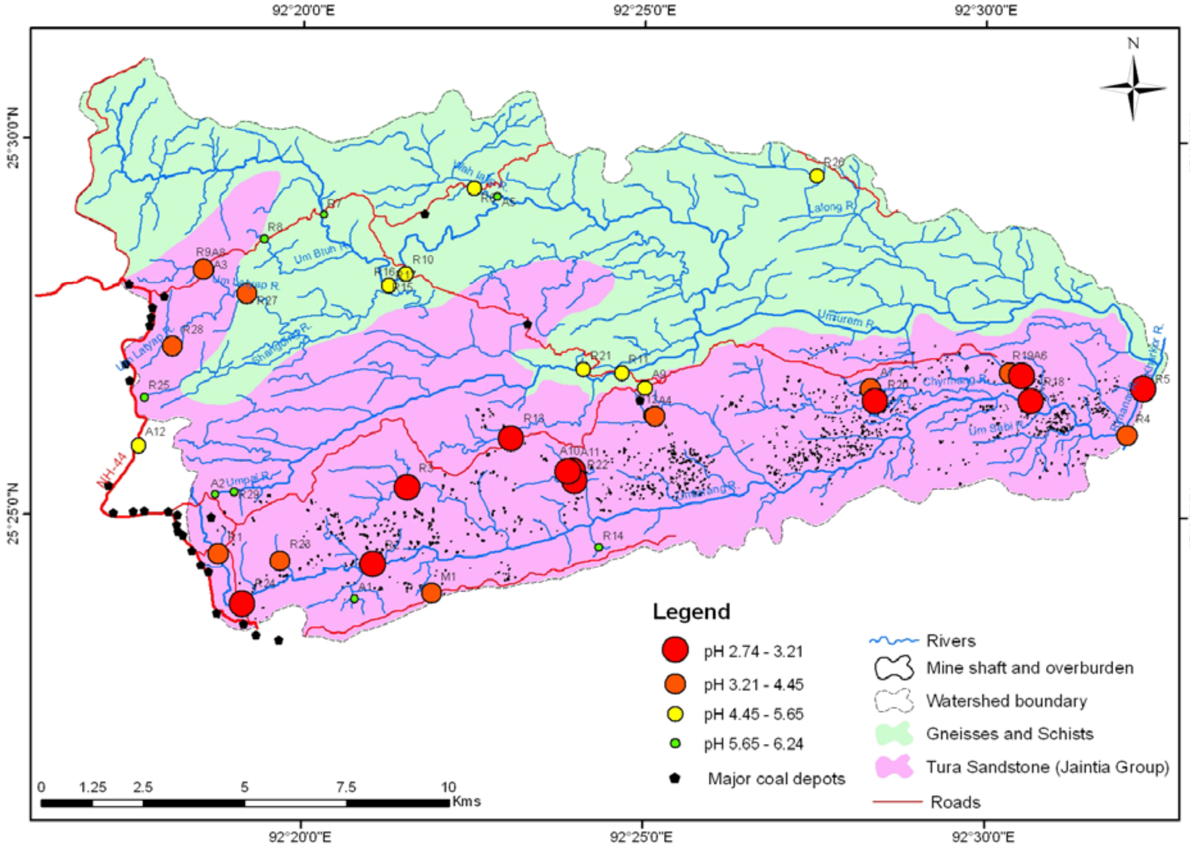

**Figure 5.29: Distribution of pH in post-monsoon samples.**
**(Symbol size based on Q1, Q2, Q3 from Table 5.5)**

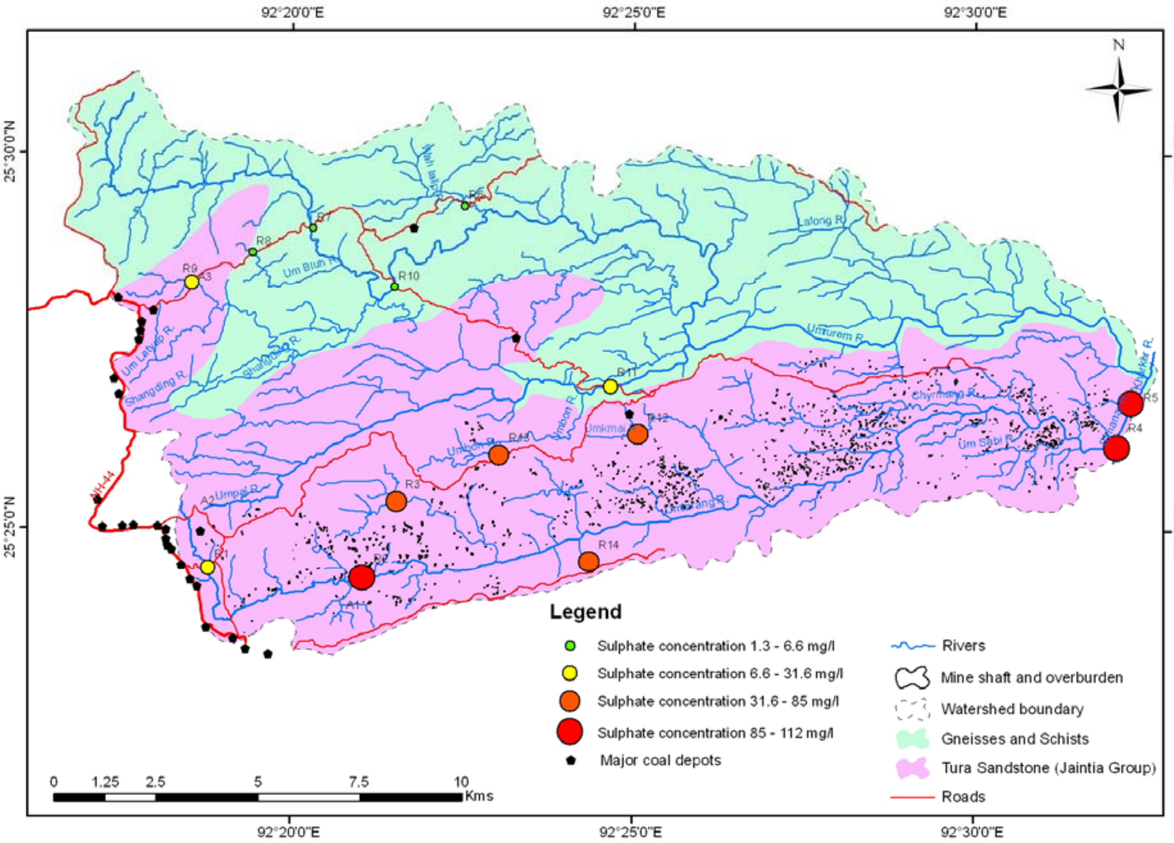

**Figure 5.30: Distribution of sulphate in monsoon samples.**
**(Symbol size based on Q1, Q2, Q3 from Table 5.4)**

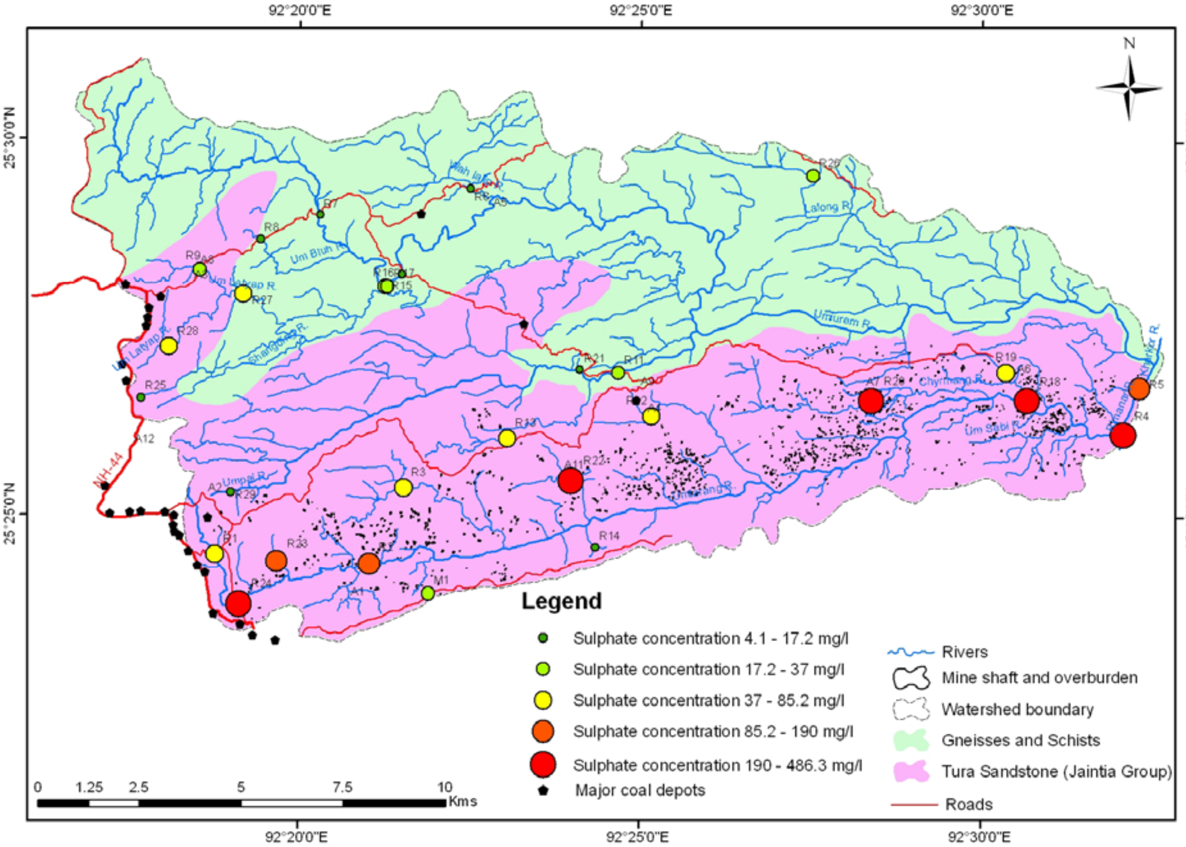

**Figure 5.31: Distribution of sulphate in post-monsoon samples.**
**(Symbol size based on Q1, Q2, Q3 from Table 5.5)**

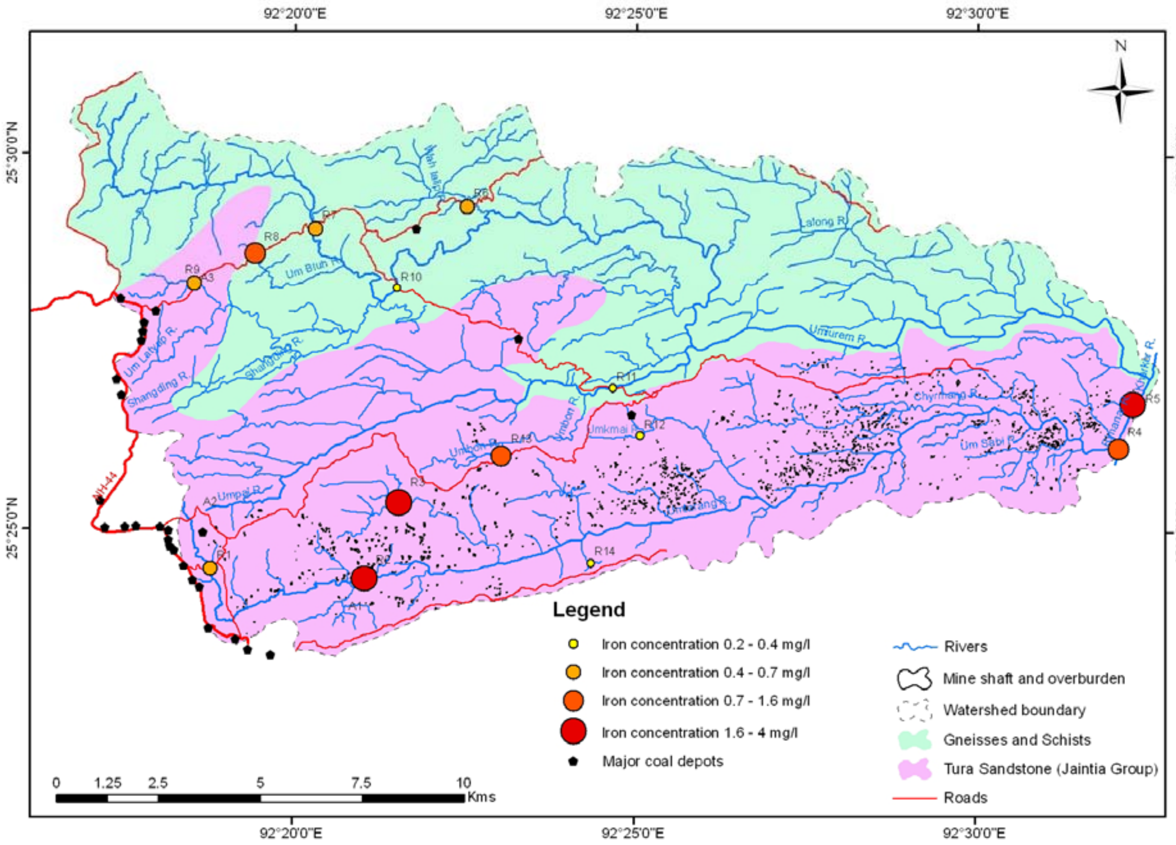

Figure 5.32: Distribution of iron in monsoon samples.
**(Symbol size based on Q1, Q2, Q3 from Table 5.4)**

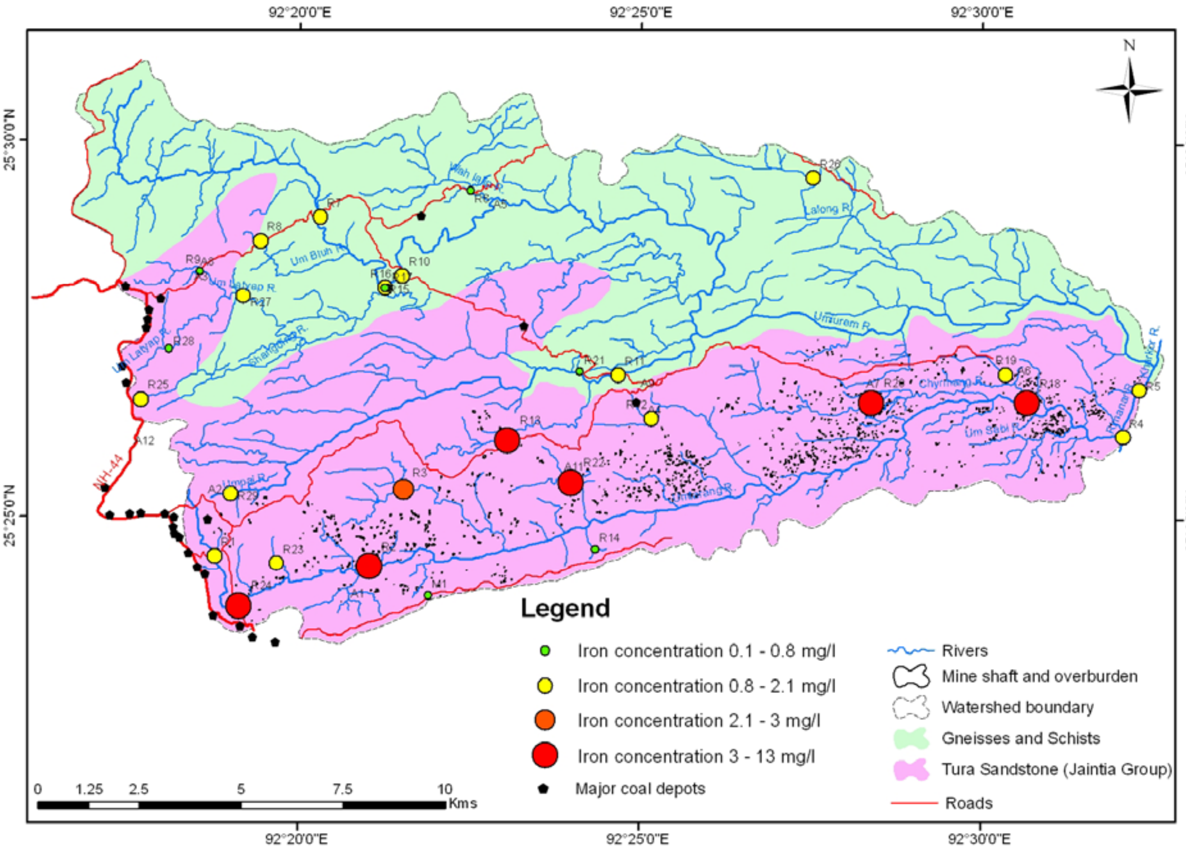

Figure 5.33: Distribution of iron in post-monsoon samples.
**(Symbol size based on Q1, Q2, Q3 from Table 5.5)**

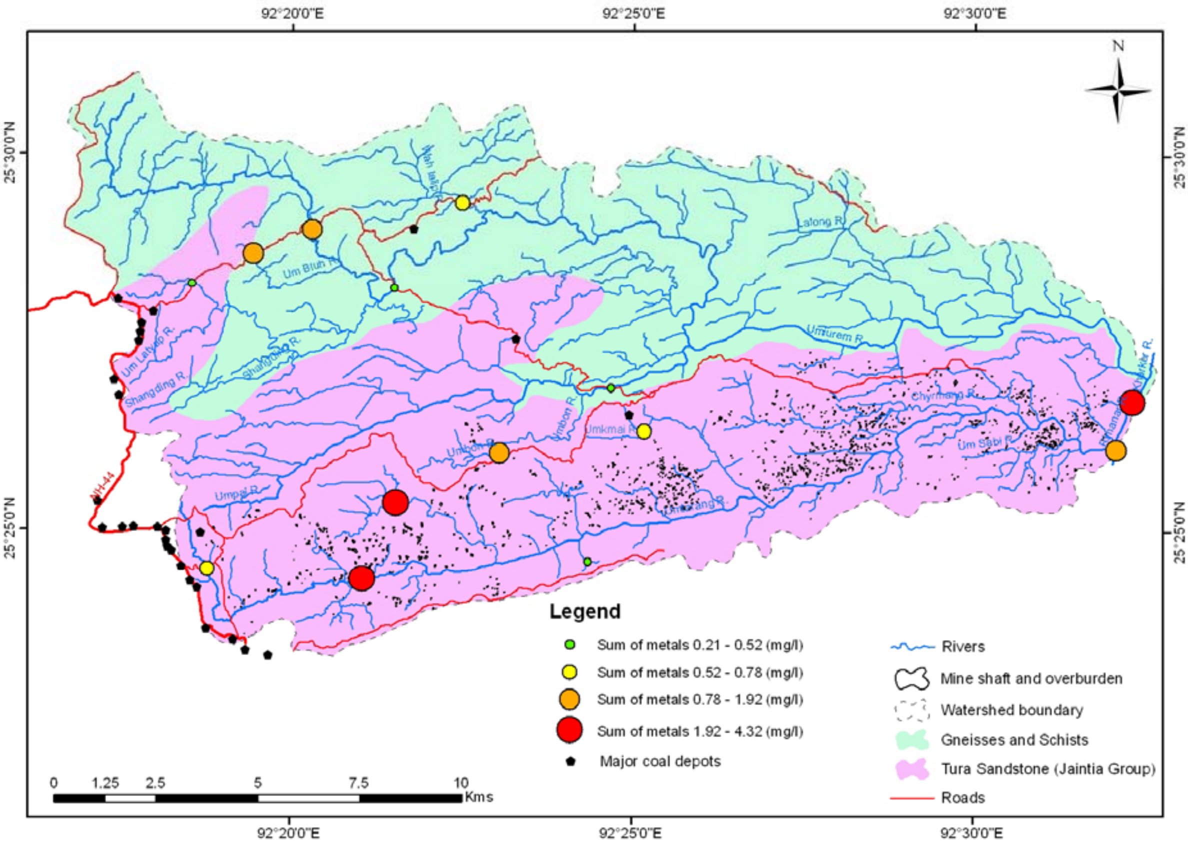

**Figure 5.34: Distribution of dissolved metals in monsoon samples.**
**(Symbol size based on Q1, Q2, Q3 from Table 5.4)**

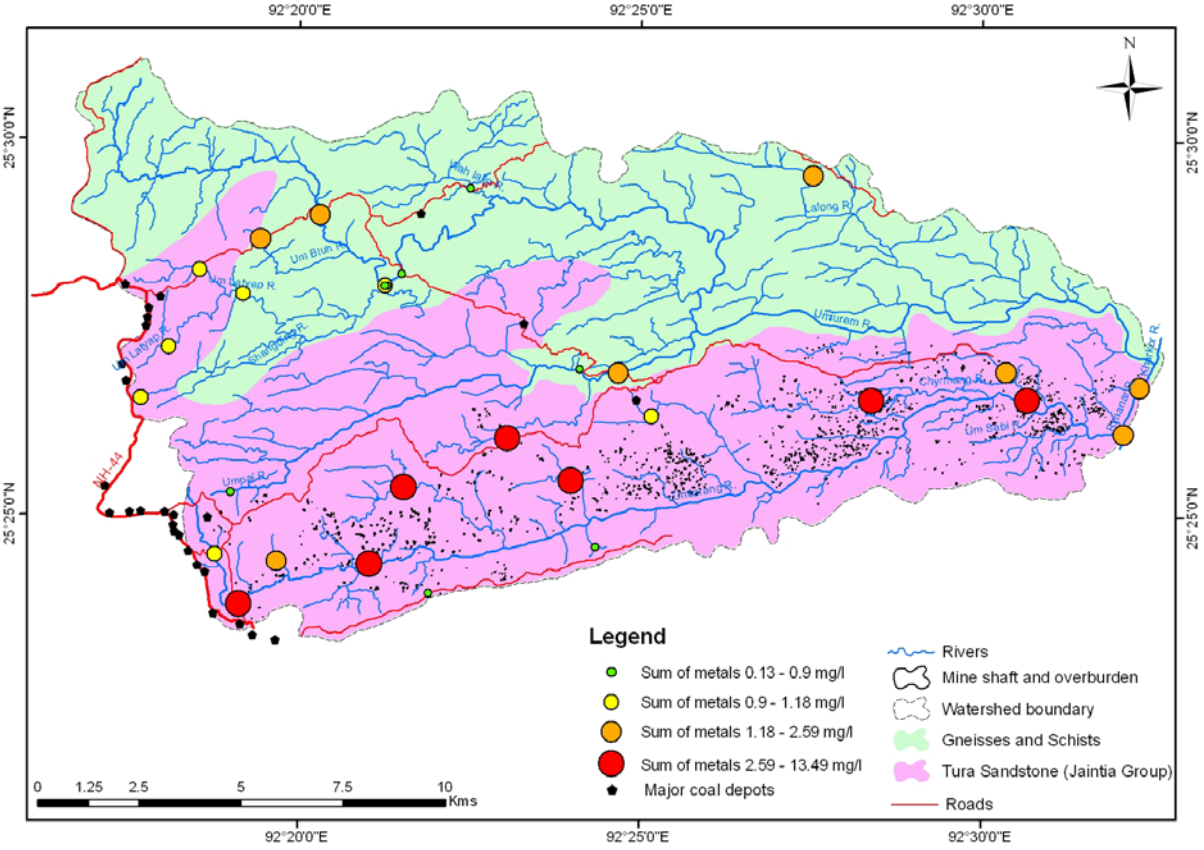

**Figure 5.35: Distribution of dissolved metals in post-monsoon samples.**
**(Symbol size based on Q1, Q2, Q3 from Table 5.5)**

From the above figures, it can clearly be seen that maximum contamination of the streams is happening in the southern sandstone part of the watershed. No doubt, the acidic soil from the surroundings has added to the stream water being slightly acidic all over the watershed. However, it was observed that stations located with provenance on metamorphic rocks are still unpolluted. Further, stations on sedimentary rocks but away from mining areas have been found to be unaffected also (R14, R25, R29, A1, A2). The major impact has been felt by stations located on sedimentary rocks that are being actively mined for coal. Clearly it can be seen that with the increase in density of mines, the impact on river water has been very high.

Another activity which has contributed to pollution in the study area, both to the air and water, is the existence of coal depots. Some of the major depots have been shown in the above Fig.5.28 to Fig.5.35 and photographs shown in Fig.5.36. The major depots are located along the length of the National Highway (NH-44) on the west of the study area and one each to the east of Shangpung and at Khlieh Rangnah. Depots at 8th Mile, Bapung and Mookhep lie within the watershed of the study area and have a direct influence on the water quality of the rivers downstream. These depots have made soils in their vicinity very acidic and unsuitable for plants except for a few resistant species (Das Gupta, 1999; Das Gupta *et al.*, 2002, Lyngdoh, 1995; Shankar *et al.*, 1993; Jeeva, 2007). Leachate and run-off from these depots enter the nearby water courses, which eventually reach the rivers and streams making them acidic. The stations R9, R27 and R28 have a direct impact from the depots located in and around 8th Mile which lie immediately upstream. These stations, though lying on sandstones, have no mining activity in their vicinity but it is observed that their water quality has deteriorated due to the presence of the depot upstream. The depots on both sides of the National Highway at Bapung and Mookhep have a major influence on water quality at station R1 and R24.

(a) 8th Mile. (b) Khlieh Rangnah. (c) Kongong.

(d) Bapung. (e) Tuber. (f) Narwan Road.

**Figure 5.36: Photographs of major coal depots in the study area.**

In conclusion, it can be said that the water quality analysis of the streams in the study area has revealed that those in the southern half, lying on coal-bearing sedimentary rocks, have been contaminated from the coal mining activity. The distribution of mines interpreted from the merged CARTOSAT-1/RESOURCESAT-1 image when overlaid on the study area clearly shows that the areas with high density of mines is the one that has been most affected by the presence of AMD. Precipitating iron hydroxide has left its mark on the stream beds with its distinctive orange-yellow color which can clearly be seen in the pan-sharpened QuickBird and Google Earth images in true color combination (Fig.4.2, Fig.4.3 and Fig.5.14).

### 5.3.2. Stream sediment quality

Sediment samples were collected from 8 locations during monsoon and from 22 locations during post-monsoon. Thirteen trace metals were analyzed at the ITC Laboratory by Drs. J. B. de Smeth. The summaries of the analytical results are given in Table 5.8 and Table 5.9 respectively, and the details in Appendix 6 and Appendix 9 respectively. As stated earlier, in India neither quality criteria nor standards have been prescribed for river sediments. In this study, the consensus-based threshold effect concentration (TEC), below which harmful effects are unlikely to be observed on benthic macro-invertebrates, after MacDonald *et al.* (2000) and da Silva *et al.* (2006), was used to describe the sediment quality (Refer Table 4.6).

**Table 5.8: Summary of analytical results of monsoon sediment samples.**

| Parameter | n | Min | Max | Mean | SD | Q1 | Q2 | Q3 |
|---|---|---|---|---|---|---|---|---|
| Antimony | 4 | 0.1 | 0.6 | 0.3 | 0.24 | 0.1 | 0.25 | 0.5 |
| Arsenic | 1 | 7.1 | 7.1 | 7.1 | - | 7.1 | 7.1 | 7.1 |
| Barium | 8 | 4.63 | 26.56 | 10.35 | 7.06 | 6.8 | 7.75 | 11.26 |
| Cadmium | 8 | 0.6 | 1.7 | 1.1 | 0.3 | 1.0 | 1.1 | 1.15 |
| Chromium | 8 | 13.45 | 29.74 | 21.50 | 5.65 | 17.85 | 20.45 | 26.09 |
| Cobalt | 8 | 1.04 | 4.93 | 2.38 | 1.25 | 1.48 | 2.15 | 2.92 |
| Copper | 8 | 8.28 | 23.46 | 15.08 | 4.58 | 12.54 | 14.43 | 17.46 |
| Iron (%) | 8 | 1.05 | 4.38 | 2.44 | 0.94 | 1.99 | 2.45 | 2.6 |
| Lead | 8 | 6.6 | 11.5 | 8.96 | 1.53 | 7.75 | 9.35 | 9.7 |
| Lithium | 8 | 2.26 | 9.38 | 4.88 | 2.38 | 3.58 | 4.11 | 6.02 |
| Manganese | 8 | 27.70 | 110.1 | 65.44 | 30.65 | 40.60 | 58.9 | 93.35 |
| Nickel | 8 | 2.85 | 12.27 | 7.17 | 3.15 | 5.05 | 6.93 | 9.15 |
| Zinc | 8 | 14.60 | 41.00 | 22.18 | 8.74 | 15.1 | 21.35 | 24.45 |

**Note:** n = Number of valid samples, SD = Standard deviation
Q1, Q2, Q3 = First, second and third quartiles of the each parameter distribution
All values are in mg/kg except where indicated

In the monsoon sediment samples, the single sample of arsenic was found to be below the TEC. Cadmium was found to be above the TEC in all but one sample. Chromium, copper, lead, manganese, nickel and zinc were found to be having concentrations well below the TEC. Iron was observed to be higher than the TEC in all but two samples.

**Table 5.9: Summary of analytical results of post-monsoon sediment samples.**

| Parameter | n | Min | Max | Mean | SD | Q1 | Q2 | Q3 |
|---|---|---|---|---|---|---|---|---|
| Antimony | 2 | 0.1 | 0.5 | 0.3 | 0.28 | 0.1 | 0.3 | 0.5 |
| Arsenic | 2 | 8.7 | 15.9 | 12.3 | 5.09 | 8.7 | 12.3 | 15.9 |
| Barium | 22 | 2.21 | 53.5 | 16.98 | 11.94 | 8.61 | 14.22 | 21.34 |
| Cadmium | 22 | 0.3 | 2.8 | 1.23 | 0.62 | 0.8 | 1.05 | 1.6 |
| Chromium | 22 | 5.73 | 81.39 | 24.89 | 16.7 | 13.5 | 21.03 | 32.6 |
| Cobalt | 22 | 0.41 | 7.15 | 2.9 | 1.92 | 1.64 | 2.26 | 4.66 |
| Copper | 22 | 4.09 | 35.02 | 16.03 | 7.64 | 10.16 | 15.35 | 20.2 |
| Iron (%) | 22 | 0.53 | 5.2 | 2.39 | 1.49 | 1.32 | 1.78 | 3.79 |
| Lead | 22 | 1.9 | 22.0 | 9.78 | 4.51 | 7.9 | 9.25 | 12.8 |
| Lithium | 21 | 1.13 | 17.3 | 7.95 | 4.48 | 4.52 | 7.17 | 11.11 |
| Manganese | 22 | 6.7 | 150.8 | 70.55 | 42.97 | 35.3 | 66.65 | 97.9 |
| Nickel | 22 | 1.21 | 14.02 | 7.05 | 3.61 | 4.77 | 6.01 | 10.38 |
| Zinc | 22 | 4.1 | 59.8 | 25.4 | 13.58 | 15.4 | 23.55 | 32.0 |

**Note:** n = Number of valid samples, SD = Standard deviation
Q1, Q2, Q3 = First, second and third quartiles of the each parameter distribution
All values are in mg/kg except where indicated

In the post-monsoon sediment samples, the two arsenic samples were observed to be one above and one below the TEC. Copper, lead, manganese, nickel and zinc were found to be having concentrations below the TEC. Iron and cadmium once again had most samples higher than the TEC. Chromium, too, was observed to have two of its samples above the TEC.

The sediment quality obtained was also used to calculate the predicted incidence of toxicity to benthic sediment-dwelling organisms by the method proposed by MacDonald *et al.* (2000). These toxicity levels were then mapped to show the extent of metal contamination in the study area.

In this study, comparison of the sediment quality between stations can be carried out only for the post-monsoon samples as they were more in number and fairly scattered around the study area. The background values for locations on sedimentary rocks can be taken from station R29 which was located in a broad valley with paddy fields all around and no mining activity observed in the vicinity. Similarly, R26 can be considered as the background station for those on gneisses and schists as this too, was located in a valley with paddy fields on its western back and fairly dense forest on its eastern bank.

When comparing the trace metal concentrations of the background stations and the downstream stations, it was observed that there was not much difference between them. In fact, the background values were higher than some of the downstream stations. In the background stations, the natural high acidity of the river water may leach metals into solution and these may have either precipitated or been adsorbed onto bed sediments. In the downstream stations, the very low pH of the water keeps the leached metals in dissolved state and bed sediments free from metal contamination. At the downstream most station (R5) on the Rimanar River with recorded pH of 3.55 and 3.08 during monsoon and post-monsoon respectively, some precipitation of iron and adsorption of metals has occurred. Some iron sulphides precipitate to their amorphous forms even at very low pH, e.g. jarosite forms at pH between 1.5 and 3 and schwertmannite forms at pH between 3 and 4 (Murad and Rojik, 2004). Since this was the boundary of the study area, sediments were not collected further downstream from this station. Further, the relatively low concentration of metals in water samples may also mean that there are lesser metals to precipitate out in waters of higher pH.

Only seven samples in post-monsoon were taken as repeat of monsoon samples and all, except R11, are located on sedimentary rock. Therefore, getting a clear picture of the seasonal variation at all sampling locations was not possible. Further, as the difference in the stream velocity during and after monsoon may have had consequences for the fines in the sediments, the results of the seven common locations are first normalized to 25,000 ppm or 2.5% iron which eliminates the stream velocity as a factor of variation and makes the results more comparable. The value of 2.5% iron was taken as it lies in the middle of the range and it is a common value in the stream sediments. Seasonal variation of trace metals in river bed sediment samples is given in the following Figures 5.37 to 5.47.

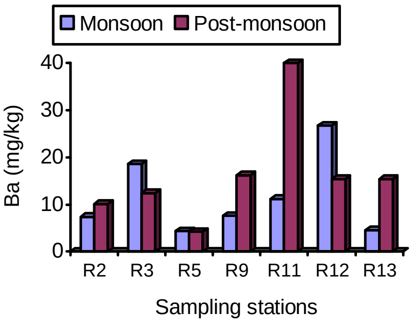

**Figure 5.37: Seasonal variation of barium.**
**(Normalized to 2.5% iron)**

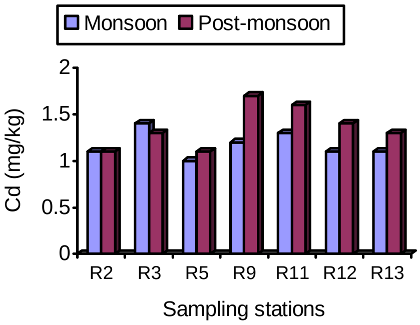

**Figure 5.38: Seasonal variation of cadmium.**
**(Normalized to 2.5% iron)**

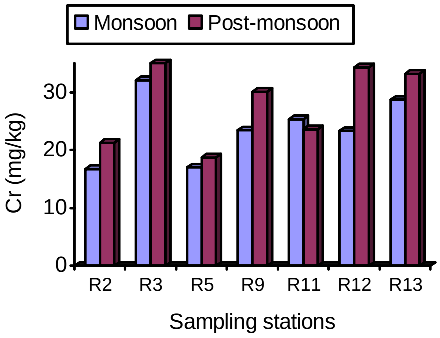

**Figure 5.39: Seasonal variation of chromium.**
**(Normalized to 2.5% iron)**

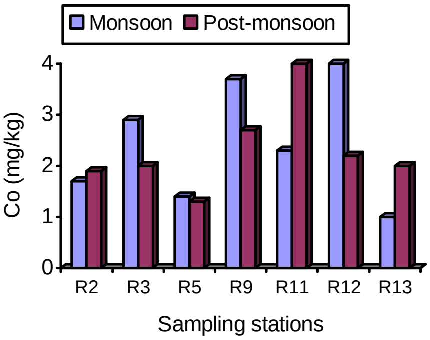

**Figure 5.40: Seasonal variation of cobalt.**
**(Normalized to 2.5% iron)**

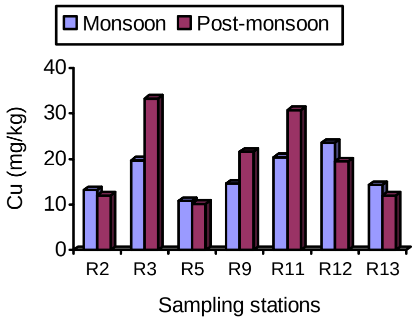

**Figure 5.41: Seasonal variation of copper.**
**(Normalized to 2.5% iron)**

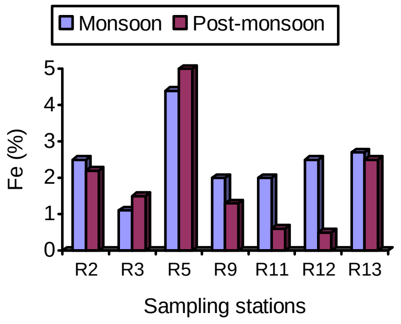

**Figure 5.42: Seasonal variation of iron.**

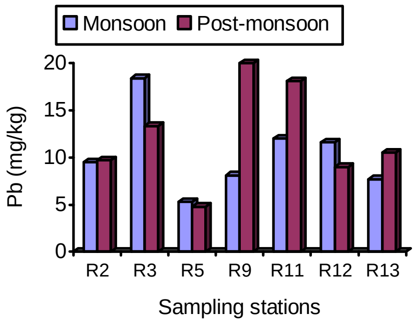

**Figure 5.43: Seasonal variation of lead.**
**(Normalized to 2.5% iron)**

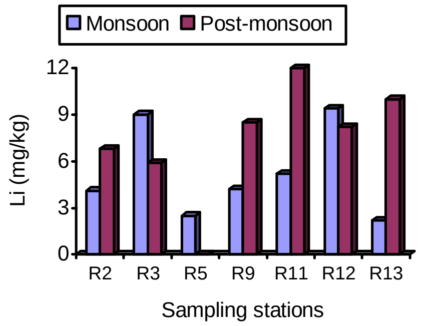

**Figure 5.44: Seasonal variation of lithium.**
**(Normalized to 2.5% iron)**

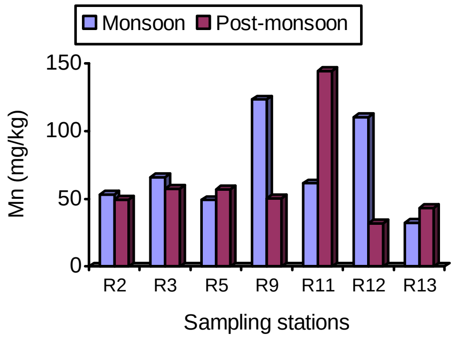

**Figure 5.45: Seasonal variation of manganese.**
**(Normalized to 2.5% iron)**

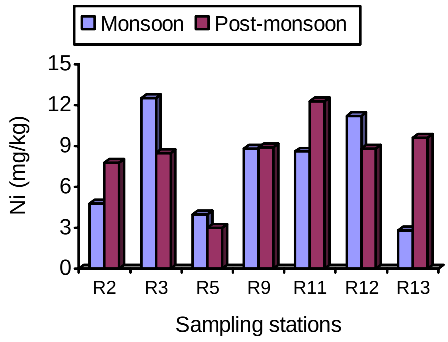

**Figure 5.46: Seasonal variation of nickel.**
**(Normalized to 2.5% iron)**

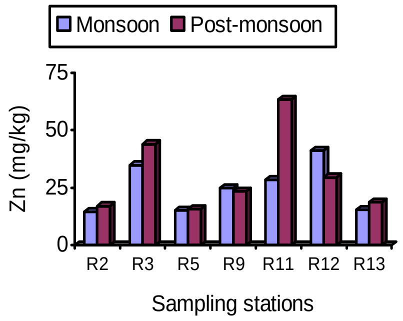

**Figure 5.47: Seasonal variation of copper.**
**(Normalized to 2.5% iron)**

From the above, it is observed that cadmium, chromium, cobalt and copper have very less seasonal variation. The other metals do not have a clear trend. Some show an increase at some stations and a decrease at others. However, with limited samples to compare from, no far reaching conclusions can be made from the seasonal variation of the trace metals.

The seasonal variation of iron, manganese and the sum of trace metals (barium, cadmium, chromium, cobalt, copper, lead, lithium, nickel and zinc) in the different lithology was also shown using box plots.

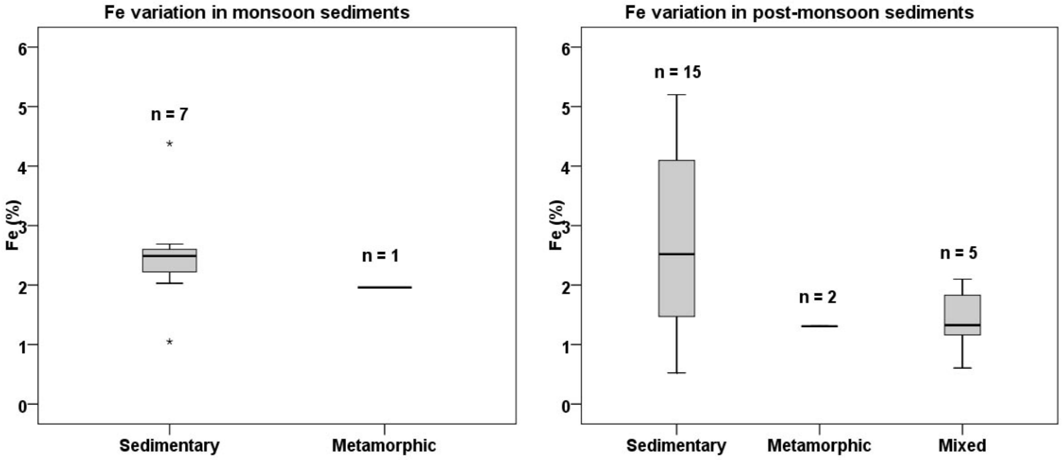

(a) (b)

**Figure 5.48: Variation of iron in stream sediments (a) monsoon (b) post-monsoon. (Stream provenance is shown along X-axis. "n" denotes the number of valid samples)**

From Fig.5.48 it is seen that in monsoon some precipitation of iron has occurred in R5, the downstream most sampling location while at R3, located near active coal mining areas in the mid-stream, iron is still dissolved in the water. In post-monsoon, with more number of samples, a bigger variation can be seen in the locations on sedimentary rock. Even with the pH slightly lower, precipitation of iron has occurred at several stations, perhaps, due to higher adsorption by stream particles. In locations on metamorphic rock and in mixed provenance, the precipitation of iron is seen to be still less due to lower pH.

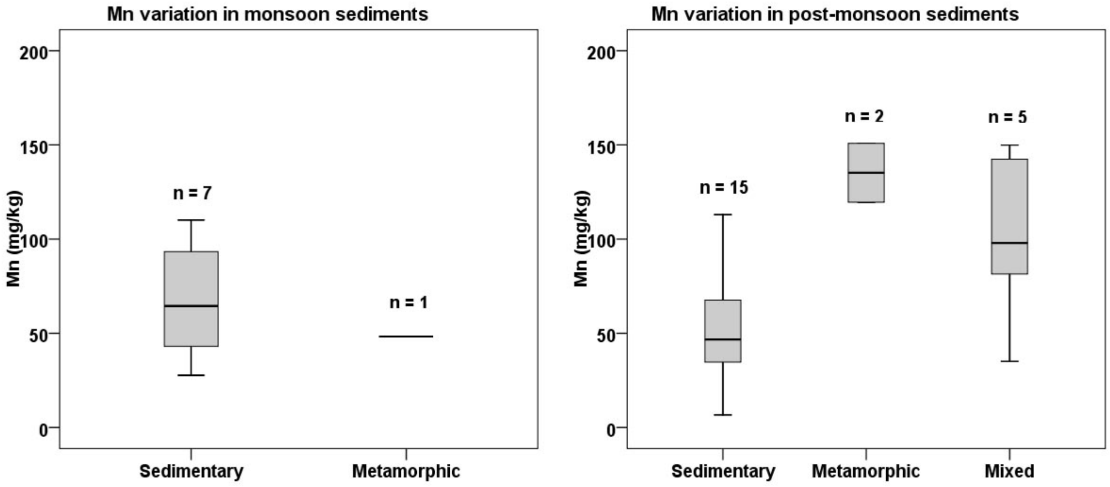

(a) (b)

**Figure 5.49: Variation of manganese in stream sediments (a) monsoon (b) post-monsoon. (Stream provenance is shown along X-axis. "n" denotes the number of valid samples)**

From Fig.5.49, it can be seen that in the metamorphic and mixed provenance, more precipitation of manganese has occurred because of the relatively higher pH in these locations than in the sedimentary.

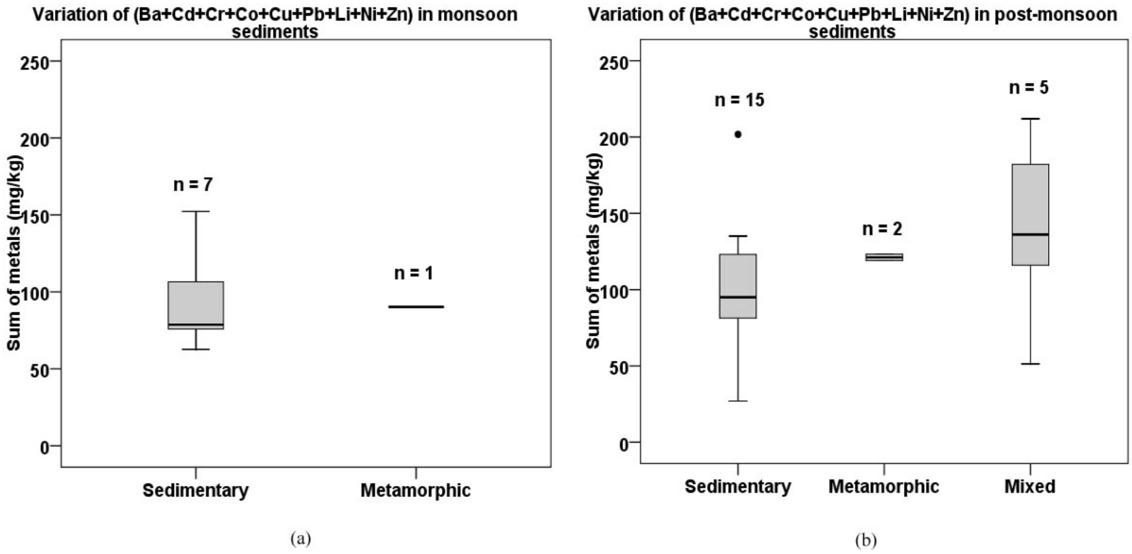

**Figure 5.50: Variation of heavy metals in stream sediments (a) monsoon (b) post-monsoon. (Stream provenance is shown along X-axis. "n" denotes the number of valid samples)**

Fig.5.50 also shows that with higher pH in the metamorphic and mixed provenance, more precipitation of the heavy metals has taken place than in the sedimentary locations. In sedimentary provenance, the upstream stations show more metal concentration in their sediments because higher pH allows for more ions to get adsorbed to the stream particles and sediments.

## 5.4. Pollutant distribution maps

The calculations to estimate the predicted incidence of toxicity to benthic sediment-dwelling micro-organisms after MacDonald *et al.* (2000) are shown in Tables 5.10 and 5.11. The locations have been divided as per the stream provenance. The predicted incidence of toxicity in the monsoon sediments varied from 9% (R3) to 23% (R5) which indicates low toxicity in all the 8 locations. Limited number of samples made it impossible to compare between locations of different lithology. Similarly the post-monsoon sediment toxicity ranged from 4% (R12) to 32% (A6) which show low impact on sediment-dwelling organisms.

**Table 5.10: Calculation of predicted incidence of toxicity in monsoon sediments.**

| | | | Location Code | R1 | R2 | R3 | R5 | R9 | R12 | R13 | R11 |
|---|---|---|---|---|---|---|---|---|---|---|---|
| | | | Lithology | S | S | S | S | S | S | S | M |
| Element | Unit | TEC | PEC | | | | | | | | |
| As | mg/kg | 9.79 | 33 | | | | | | | 7.1 | |
| Cd | mg/kg | 0.99 | 4.98 | 1.2 | 1.1 | 0.6 | 1.7 | 1.0 | 1.1 | 1.1 | 1.0 |
| Cr | mg/kg | 43.4 | 111 | 21.0 | 16.7 | 13.5 | 29.7 | 19.0 | 23.2 | 29.0 | 19.9 |
| Cu | mg/kg | 31.6 | 149 | 14.4 | 13.2 | 8.3 | 18.9 | 11.8 | 23.5 | 14.5 | 16.0 |
| Fe | (%) | 2* | 4* | 2.41 | 2.51 | 1.05 | 4.38 | 2.03 | 2.49 | 2.69 | 1.96 |
| Pb | mg/kg | 35.8 | 128 | 9.9 | 9.5 | 7.7 | 9.3 | 6.6 | 11.5 | 7.8 | 9.4 |
| Mn | mg/kg | 460* | 780* | 64.5 | 53.3 | 27.7 | 86.3 | 100.4 | 110.1 | 32.9 | 48.3 |
| Ni | mg/kg | 22.7 | 48.6 | 12.3 | 4.8 | 5.3 | 7.1 | 7.2 | 11.1 | 2.9 | 6.8 |
| Zn | mg/kg | 121 | 459 | 22.4 | 14.6 | 14.6 | 26.5 | 20.3 | 41.0 | 15.6 | 22.4 |
| Mean PEC-Q | | | | 0.18 | 0.15 | 0.09 | 0.25 | 0.15 | 0.20 | 0.18 | 0.14 |
| Predicted incidence of toxicity (%) | | | | **17** | **14** | **9** | **23** | **14** | **19** | **17** | **13** |

**N.B.**: No value cells indicate concentration below detectable limits; S = Sedimentary provenance, M = Metamorphic provenance;

* Values taken from da Silva *et al.* (2006). All others after MacDonald *et al.* (2000).

**Table 5.11: Calculation of predicted incidence of toxicity in post-monsoon sediments.**

| | | | Location Code | R2 | R3 | R5 | R9 | R12 | R13 | R18 | R19 | R20 | R22 | R23 | R24 | R29 | A6 | A11 | R6 | R26 | R11 | R15 | R17 | R21 | R27 |
|---|---|---|---|---|---|---|---|---|---|---|---|---|---|---|---|---|---|---|---|---|---|---|---|---|---|
| | | | Lithology | S | S | S | S | S | S | S | S | S | S | S | S | S | S | S | M | M | S+M | S+M | S+M | S+M | S+M |
| | Unit | TEC | PEC | | | | | | | | | | | | | | | | | | | | | | |
| As | mg/kg | 9.79 | 33 | | | 15.9 | | | | | | | | | 8.7 | | | | | | | | | | |
| Cd | mg/kg | 0.99 | 4.98 | 1 | 0.8 | 2.2 | 0.9 | 0.3 | 1.4 | 2.2 | 1 | 1.1 | 1.6 | 1.4 | 1.6 | 0.8 | 2.8 | 1.9 | 0.7 | 0.8 | 0.4 | 0.9 | 0.8 | 1.4 | 1.1 |
| Cr | mg/kg | 43.4 | 111 | 18.6 | 20.9 | 37.2 | 16.0 | 7.2 | 35.8 | 26.4 | 29.9 | 11.7 | 32.6 | 29.7 | 21.1 | 26.2 | 81.4 | 37.1 | 11 | 16 | 5.7 | 13.5 | 8.6 | 16.2 | 44.6 |
| Cu | mg/kg | 31.6 | 149 | 10.5 | 19.8 | 20.3 | 11.5 | 4.1 | 12.9 | 18.6 | 10.2 | 5.5 | 28.5 | 19.5 | 17.2 | 13.5 | 24.8 | 22.1 | 9.3 | 9.7 | 7.5 | 20.2 | 13.5 | 18.4 | 35 |
| Fe | (%) | 2* | 4* | 2.19 | 1.5 | 5.0 | 1.3 | 0.5 | 2.52 | 5.1 | 1.7 | 1.3 | 4.0 | 3.13 | 3.79 | 1.45 | 5.2 | 4.15 | 1.3 | 1.3 | 0.6 | 1.3 | 1.2 | 2.1 | 1.8 |
| Pb | mg/kg | 35.8 | 128 | 8.50 | 7.9 | 9.5 | 15.1 | 1.9 | 11.3 | 6.8 | 7.9 | 2.5 | 14.3 | 12.8 | 9 | 8.9 | 13.7 | 14.8 | 6.1 | 9.5 | 4.4 | 9.8 | 9.6 | 8.8 | 22 |
| Mn | mg/kg | 460* | 780* | 43.3 | 34.1 | 113 | 26.7 | 6.7 | 46.7 | 71.4 | 35.3 | 12.4 | 56.2 | 68.3 | 66.4 | 42 | 85.5 | 66.9 | 150.8 | 119.6 | 35.1 | 81.5 | 142.4 | 149.9 | 97.9 |
| Ni | mg/kg | 22.7 | 48.6 | 6.83 | 5.1 | 5.9 | 4.7 | 1.9 | 10.4 | 3.5 | 5.1 | 1.2 | 6.1 | 10.5 | 5.8 | 14.0 | 11.7 | 9.3 | 5.3 | 6.4 | 3 | 11.4 | 4.8 | 9 | 13.2 |
| Zn | mg/kg | 121 | 459 | 14.9 | 26.1 | 31.3 | 12.5 | 6.2 | 20 | 23.7 | 13.5 | 4.1 | 28 | 23.4 | 16.2 | 21.6 | 32 | 21 | 33.9 | 30.3 | 15.4 | 37.3 | 34 | 53.6 | 59.8 |
| Mean PEC-Q | | | | 0.14 | 0.12 | 0.34 | 0.11 | 0.04 | 0.19 | 0.3 | 0.13 | 0.08 | 0.24 | 0.21 | 0.24 | 0.15 | 0.37 | 0.26 | 0.12 | 0.12 | 0.06 | 0.14 | 0.12 | 0.18 | 0.22 |
| Predicted incidence of toxicity (%) | | | | **13** | **12** | **30** | **11** | **4** | **18** | **24** | **13** | **8** | **22** | **20** | **22** | **14** | **32** | **24** | **12** | **12** | **6** | **13** | **12** | **17** | **20** |

**N.B.**: No value cells indicate concentration below detectable limits; S = Sedimentary provenance, M = Metamorphic provenance, S + M = Mixed provenance

* Values taken from da Silva *et al.* (2006). All others after MacDonald *et al.* (2000).

The pollutant distribution maps based on the predicted incidence of toxicity for monsoon and post-monsoon are given in Fig.5.51 and Fig.5.52 respectively. The percentage values were classified into three classes using the ArcGIS software and graduated symbols were used to depict percent toxicity.

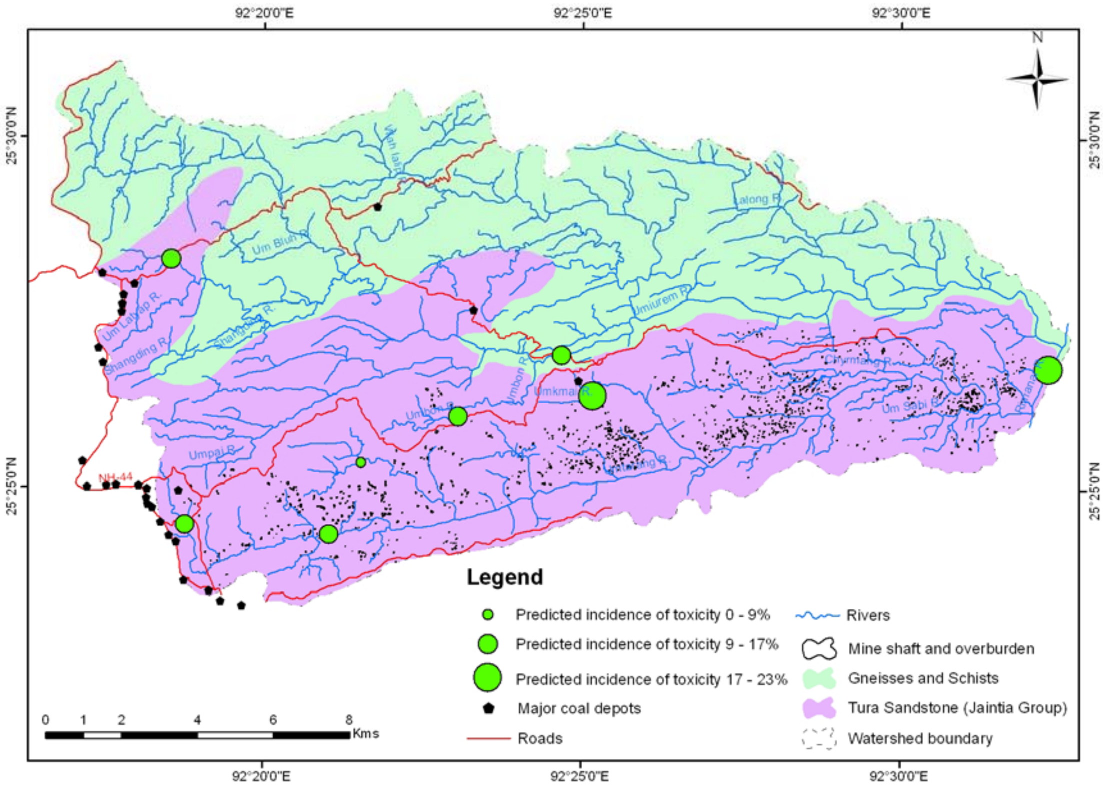

**Figure 5.51: Predicted incidence of toxicity for monsoon samples.**

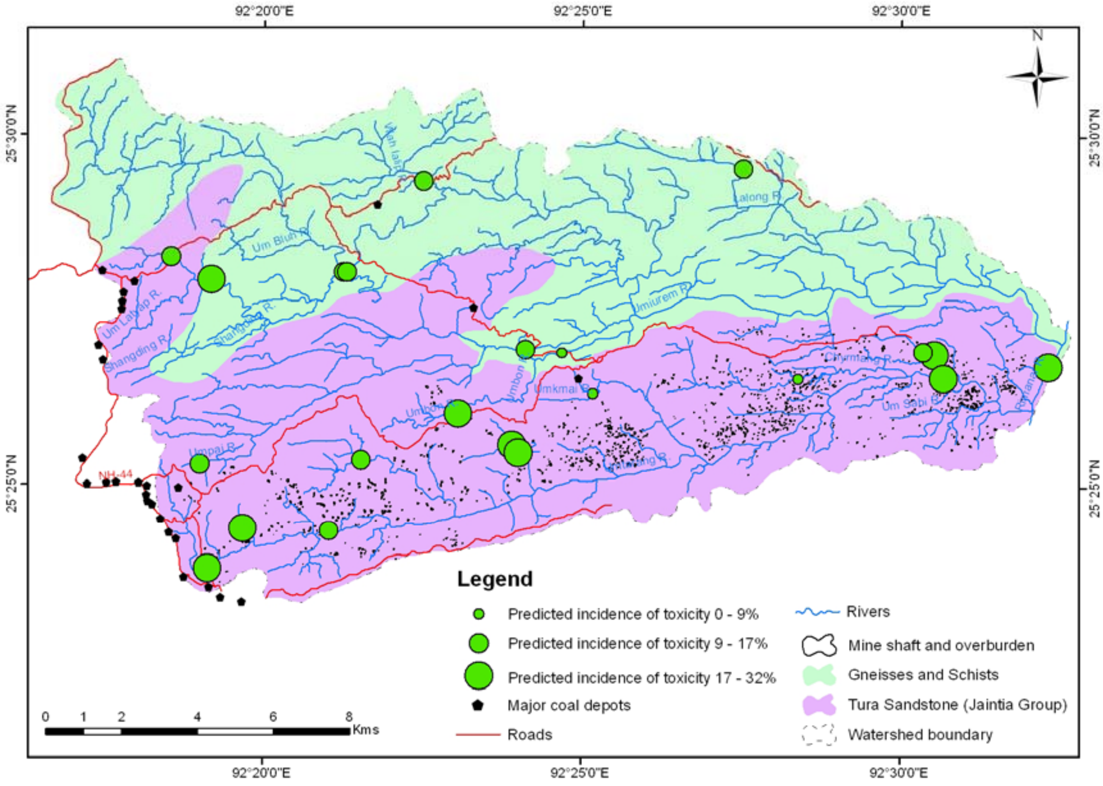

**Figure 5.52: Predicted incidence of toxicity for post-monsoon samples.**

It is observed that the predicted toxicity to benthic sediment-dwelling organisms is low for all stations and for both seasons. This may be because of high acidity in almost all the stations, the trace metal have either not yet precipitated or been adsorbed by the stream particles and remained in solution. Also, the fact that the metal concentration is less in the water samples means that the stream sediments are still relatively unpolluted. The highest predicted toxicity was observed to be at station R5 for both seasons. This, incidentally, is the downstream most station for this study and, therefore, indicates that some metal precipitation may have started due to a lower chemical mobility at high pH values. Comparing the post-monsoon incidence of toxicity with the distribution of dissolved metals (Fig.5.34 and Fig.5.35) also reveals that there is a slight decrease in dissolved metal load at this station as compared to the other upstream stations. It is also seen that at this station the concentration of iron in the sediments was highest for monsoon season (4.38%) and was second highest for post-monsoon season (4.96%). The highest was recorded at A6 (5.1%) which also had the highest toxicity of 32%. However, no more samples were collected further downstream, as that would have gone beyond the study area boundary.

# 6. Conclusions

The conclusions that can be drawn from this study are summed up by answering each research question to see if the research objectives have been met or not.

## 6.1. Answers to research questions

### 6.1.1. Question 1

*"Can the rat-hole mines be identified and mapped through RESOURCESAT-1-1 (IRS-P6) LISS-IV, CARTOSAT-1, ETM+ and ASTER images?"*

Identification and mapping of the artisanal "rat-hole" mines in the Umiurem-Umtarang (Myntriang) watershed of the Jaiñtia Hills district through ASTER image (VNIR bands, 15m spatial resolution) and Landsat ETM+ merged panchromatic and multi-spectral images (15m spatial resolution) is not possible because of the coarse spatial resolution of the sensors. With the sides of mine shafts measuring about 6 to 8 m, identification of individual mines through these images was completely ruled out. The RESOURCESAT-1 (IRS-P6) LISS-IV image, on its own, is not very clear to be used for identification of the mines. Bright spots can be identified, but as the mine shafts are not visible, it cannot be concluded that these are mines because even the roads and settlements have similar spectral signatures. Only after merging it with the 2.5 m spatial resolution panchromatic image of CARTOSAT-1, are the mines discernable. However, this has its own limitations in that older mines with darker overburden dump signatures merged with the background barren land or vegetation and cannot be discriminated. At several places, clusters of several small mines appear as a single big mine. When compared with the very high spatial resolution (61 cm) merged PAN and multi-spectral QuickBird image, the visual interpretation yield an overall accuracy of 46%, by taking a count of the number of polygons mapped through each image, and of 59% , through comparison in terms of area. However, an observation is made that almost all the mines that can visually be mapped, match in location with those on the QuickBird image, which means that despite the resolution limitation, what can be mapped is done so correctly. The low accuracy can be attributed to lower spatial resolution of the merged CARTOSAT-1/RESOURCESAT-1 image and also due to quality loss in the image when making the mosaic and during image fusion.

### 6.1.2. Question 2

*"Can the mines be identified using OOC?"*

An algorithm is developed to semi-automatically classify the coal mines through an OOC approach using the Definiens Developer 7 software. The algorithm developed on the merged CARTOSAT-1/RESOURCESAT-1 image for the whole study area proves to be capable of identifying the artisanal "rat-hole" mines. Where the technique of pixel-based supervised classification gave inconclusive and unclear results, OOC has proved its superiority. By incorporating spectral signatures along with textural, contextual and shape features, OOC is able to discriminate between the different features and finally isolate the mines with an overall accuracy of 67.4%. A limitation of the procedure is observed due to spectral and textural signatures of mine overburden dumps, roads and settlements being identical. Further, similarity in shape due to quadtree segmentation is also an important reason for this misclassification. Therefore, besides being able to discriminate the mines, several settlement and road objects are also classified as mines leading to a high error of commission (54%). Perhaps, the addition of another contextual layer which depicts the settlement boundaries may have reduced the high error of commission as this will help in correct classification of the settlements. Moreover, if it had been possible to run multi-resolution segmentation directly on the whole image, this error will have further reduced.

To validate the algorithm developed, it is tested on a subset of a pan-sharpened QuickBird image. The segmentation parameters and classification thresholds are suitably changed to match with the QuickBird data. The overall accuracy obtained is 72% with errors of commission and omission of 15% and 28% respectively.

Finally, the answer to the question is, yes, the mines can be identified through OOC, but in all, the mines are over-identified because of reasons stated above. A drawback of OOC is that the segmentation parameters and the threshold values used in the rule-set are area and data specific.

### 6.1.3. Question 3

*"What are the hydro-chemical characteristics of AMD in the watershed?"*

In general, the water throughout the watershed is acidic with a range of 3.3 to 7.4 in monsoon and 2.74 to 6.24 in post-monsoon samples respectively. A slightly acidic value would be normal due to the presence of acidic soils throughout the study area because of intense leaching. Acid rock drainage (ARD) and runoff from these soils lowers the pH of the stream waters which then leaches metals present in the surrounding rock. Pyrite from the surrounding coal gets quickly hydrolyzed in this slightly acidic water and in that process, releases further protons and sulphates, adding to the acidity and increasing the concentration of sulphate. With lower pH, trace metals mostly become more mobile and get leached into the stream water reducing its quality even further.

The water quality analysis suggests that many streams in the watershed are affected by AMD as manifested in the form of low pH and elevated values of EC, iron, sulphates and manganese. A very high correlation between EC and sulphates also indicates the presence of AMD in the river water. The dominance of sulphate ions seen in the Piper diagrams of both seasons indicates that oxidation and hydrolysis of pyrites has led to the presence of high acidity and iron concentration. When compared with the visually interpreted map, it is observed that water quality had deteriorated considerably in areas where the density of mines is very high, downstream of actively mined areas or downstream of major coal depots, but is still relatively good in other places.

Stream sediments, on the other hand, have not reached alarming concentration levels in the study area. High acidity in almost all the streams may have kept the metals in solution or is due to the low trace metal concentrations in the weathered sulphide minerals in the coal. Unfortunately there is no information on the chemical composition of the sulphide minerals in the study area. However, in the more downstream stations, the presence of iron precipitates can be observed on the stream beds. This fact is corroborated by seeing these locations in the pan-sharpened QuickBird image in true color combination with the distinctive yellow-orange coloration of iron precipitates. Field verification at these locations also confirmed it. Landsat ETM+ with its advantage of having six optical and infrared bands is used for detecting stream beds that are coated with iron precipitate through the process of band ratio calculation. Coarse spatial resolution made it possible to locate presence of iron precipitates only along the wider streams, but these locations match with those seen in the QuickBird image.

### 6.1.4. Question 4

*"Are the mines the main cause of AMD in the watershed or are there other plausible causes?"*

As stated above, the streams in the watershed are found to be slightly acidic throughout. This is basically due to ARD and runoff and leaching from surrounding acidic soils, a common feature throughout the state of Meghalaya. However, the contamination became elevated in the proximity of coal mines. Pyrite oxidation and hydrolysis quickly occurs in these slightly acidic waters reducing the pH drastically and increasing the concentrations of iron and sulphates. In locations having the same lithology, but away from the clusters of coal mines, it is observed that the acidity is low (i.e. the pH is relatively higher) and the presence of metals and other pollutants is minimal. The presence of coal depots within the study area also contributes to water pollution. These depots are seen to have affected the water quality at the sampling stations located immediately downstream to them. It can be concluded that though the mines may not be responsible for water acidity in the study area per se, their presence, along with related activities like coal depots, has exacerbated the situation to a large extent by adding AMD and increasing the contaminants in it.

### 6.1.5. Question 5

*"What is the extent of the presence of heavy metals in the watershed?"*

Heavy metals in the study area are present within permissible limits in the water samples, with iron and manganese being the only metals having concentrations above these limits. The stream sediments have heavy metal concentrations well below the Threshold Effect Concentrations (TEC's) given by MacDonald *et al.* (2000) and da Silva *et al.* (2006). Cadmium is the only metal with values consistently above the TEC's but well below the Probable Effect Concentrations (PEC's). Iron once again was above the TEC limit but below PEC in all cases. All the bigger streams in the watershed flow through deep valleys, so the lateral dispersion of heavy metal pollution into surrounding soils can be ruled out unless the water is used for irrigation purposes on the valley slopes. Some iron precipitation has occurred within the study area with several locations showing higher presence of metals in their sediments. However, the true picture of the extent of metal contamination in the stream sediments can only be known if more sampling was done further downstream.

## 6.2. Limitations

1. A major problem encountered during field work is accessibility within the study area. There are only a few paved roads which give access to the northern part which is of less interest because no mines are present there. The main mining area is accessible only through forest roads cut by the earth moving machines of the coal prospectors and miners. Heavy rain during the monsoon sampling programme turned these forest roads into pools of mud which became inaccessible even to a four-wheel driven vehicle.
2. The extent of the AMD problem cannot be conclusively determined by this study. To determine the change in water quality from headstream to downstream of all streams in the area, a more

detailed study has to be conducted. As stated above, due to accessibility problems, systematic sampling could not be carried out.

3. Heavy rain disrupted the monsoon sampling which resulted in having very few repeat samples to compare seasonal variability.
4. This study has been limited to only one watershed within the Bapung coalfield. To know the full extent of AMD problem and its impact on the environment, and also man-made features like the Kopili Dam, detailed studies have to be carried out in both upstream and downstream of the Rimanar and Kharkor Rivers and their tributaries. Other noted problem watersheds like that of the Lukha-Lunar and even watersheds lying in the coalfields where coal deposits have dwindled from over-exploitation, need to be thoroughly studied and results compared with control sites so that the source and extent of AMD can be positively ascertained in the district. This can then be used in formulating management and restoration strategies.
5. There was no information available on the chemical composition of the sulphide minerals and trace elements in the coal found in the study area and the facilities to determine them were not available at both Meghalaya State Pollution Control Board and IIRS.

## 6.3. Recommendations

1. It is observed from this study that most of the streams in proximity to coal mines have been affected by AMD to a considerable extent. Although the stream sediments have not been impacted within this watershed, the problem may exist further downstream of the last sampling station (R5). Regular monitoring of this area is recommended so that the AMD problem can be checked. This can be restricted to parameters that can be measured *in situ*. pH, EC and temperature can be easily measured using portable meters. pH can also be easily ascertained by using special pH paper. However, it is recommended that complete analysis of all parameters under the Uniform Protocol on Water Quality Monitoring Order, 2005 issued by the Ministry of Environment and Forests, Government of India through its Notification No. S.O. 2151 dated 17th June, 2005 has to be carried out as per given protocol. A map showing proposed locations for regular monitoring is given in Fig.6.1. These locations are chosen on the basis of accessibility with more emphasis on the streams on coal-bearing sedimentary rock.
2. Coal mining has brought about a lot of wealth to the Jaiñtia Hills, but has also resulted in environmental degradation at certain places as well. Ignorance about the impacts of haphazard and unorganized coal mining has led to streams/rivers becoming highly acidic. It is seen from literature that forests have dwindled in area, soil degradation has resulted in reduced agricultural yield and the scenic natural beauty has been destroyed. What needs to be done is to firstly, create awareness among the mine owners about the dangers of the prevailing system of mining. Limestone is found abundantly in Jaiñtia Hills. Perhaps, this can be used to neutralize mine drainage to some extent in constructed drains or ponds near mine shafts before releasing it to the receiving waters. This would increase the salt load of the waters but in view of the abundant rainfall in the area, this should not pose a problem.
3. Mine owners should be directed to backfill their abandoned mine shafts after either prospecting has been done or the mine shaft is abandoned. It is here that the local grass-root administration can play a very important role. The village headman and his council may be given the authority to penalize a mine owner who does not backfill abandoned mine shafts even if the mine lies in the individual's private property.

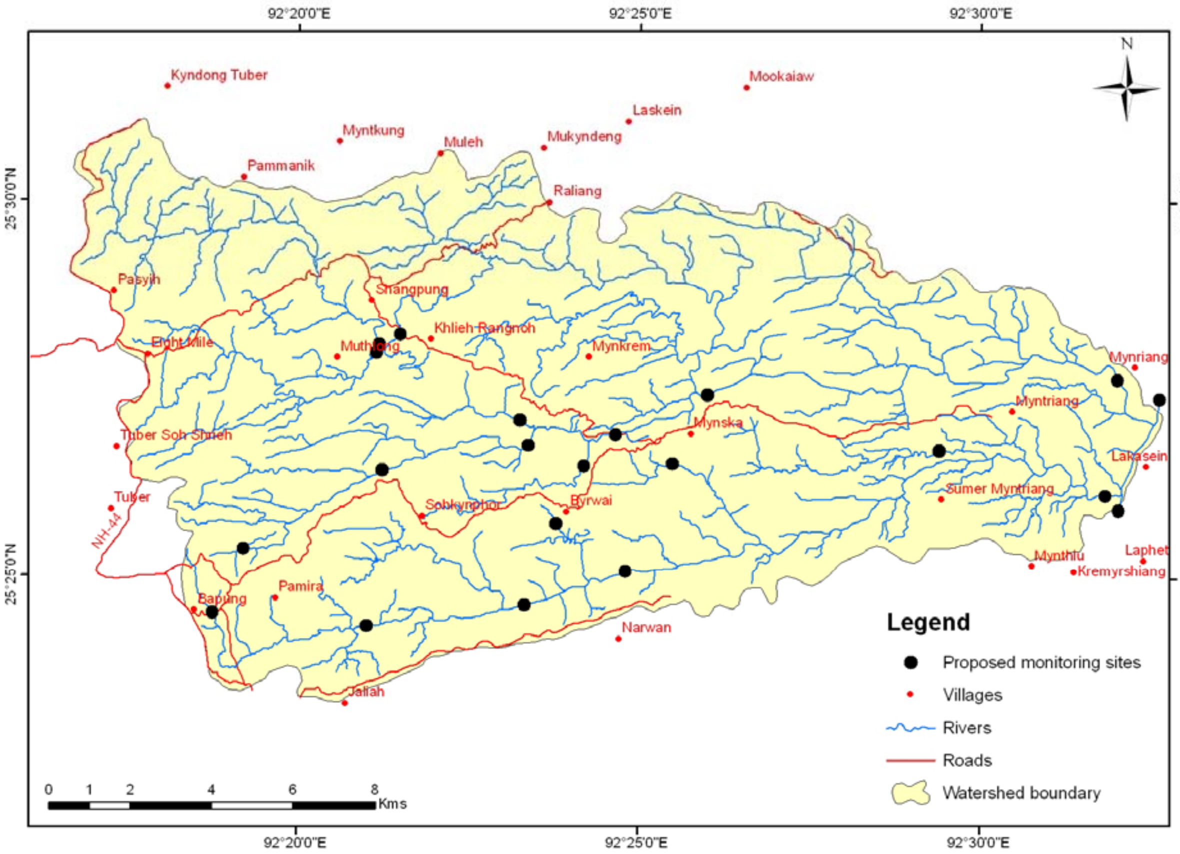

**Figure 6.1: Proposed locations for regular monitoring.**

4. Coal mining has made several people extremely wealthy but this wealth has not been utilized in developing the areas around the coal belts. The people there have remained as poverty stricken as before. These rich mine owners may be directed to start some sort of fund, which can be looked after by the village councils, and to be used to restore abandoned mining sites, to reforest barren areas and mine dumps, to provide educational and medical facilities to the people living in the mine areas and to develop roads and other infrastructure.
5. The Government of Meghalaya has introduced the Draft Mining Policy, 2009 which has been vehemently opposed from all quarters as it does not provide for protection of the rights of indigenous people, as laid down in the Sixth Schedule of the Indian Constitution. It has been accused of ushering in the big players and pushing the individual miner to the sidelines. The Policy is yet to be approved and implemented. As the debate goes on, it can be said that finally, the State government has taken a positive step to try and regulate this highly unorganized, environmentally unfriendly but very resourceful industry.
6. Chemical analysis is required to investigate the trace element composition of the coal and associated sulphide minerals. This would help to determine its toxicity.
7. Hyperspectral remote sensing can also be tried to determine the extent of presence of heavy metals in the mining areas and in dry stream beds. Indirect detection and mapping of heavy metals may be done by studying the spectral signatures of minerals that bind them in the soil or sediments (Choe *et al.*, 2008).

# References

Akcil, A. and Koldas, S. (2006) Acid Mine Drainage (AMD): causes, treatment and case studies" Journal of Cleaner Production 14:1139–1145.

APHA-AWWA-WEF (1998) "Standard Methods for the Examination of Water and Wastewater" 20th Edition, Eds. Clesceri, L.S., Greenberg, A.E. and Eaton, A.D., American Public Health Association, Washington D.C.

Bank, M.K. (1883) "Early coal mining" The Ohio Mining Journal 1(4):158–168.

Barille, V. and Bilotta, G. (2008) "An application of remote sensing: Object-oriented analysis of satellite data" The International Archives of the Photogrammetry, Remote Sensing and Spatial Information Sciences Vol.XXXVII Part B8, Beijing.

Barlow, J., Franklin, S.E. and Martin, Y. (2006) "High spatial resolution satellite imagery, DEM derivatives, and image segmentation for the detection of mass wasting processes" Photogrammetric Engineering and Remote Sensing 72(6): 687–692.

Barlow, J., Martin, Y. and Franklin, S.E. (2003) "Detecting translational landslide scars using segmentation of Landsat ETM+ and DEM data in the northern Cascade Mountains, British Columbia" Canadian Journal of Remote Sensing 29(4):510–517.

Bhattacharyya, N. N. (2002) "Environment, Land and People of Jaiñtia Hills" *In:* Jaiñtia Hills, A Meghalaya Tribe: Its Environment, Land and People (Eds. P.M. Passah and A.S. Sarma). Reliance Publishing House, New Delhi. pp:1–5.

Blake, L. (2005) "Acid rain and soil acidification" *In:* Encyclopedia of Soils in the Environment (Editor-in-Chief D. Hillel). Elsevier/Academic Press, New York, U.S.A. pp:1-11.

Blaschke, T., (2009) "Object based image analysis for remote sensing" ISPRS Journal of Photogrammetry and Remote Sensing, doi:10.1016/j.isprsjprs.2009.06.004.

Bolan, N.S., Curtin, D. and Adriano, D.C. (2005) "Acidity" *In:* Encyclopedia of Soils in the Environment (Editor-in-Chief D. Hillel). Elsevier/Academic Press, New York, U.S.A. pp:11-17.

Borrego, J., Morales, J.A., de la Torre, M.L. and Grande, J.A. (2002) "Geochemical characteristics of heavy metal pollution in surface sediments of the Tinto and Odiel river estuary (southwestern Spain)" Environmental Geology 41:785–796.

Boult, S., Collins, D.N., White, K.N. and Curtis, C.D. (1994) "Metal transport in a stream polluted by acid mine drainage – the Afon Goch, Anglesey, U.K." Environmental Pollution 84:279–284.

Bureau of Indian Standards (BIS) (2003) "Indian Standard: Drinking water – Specification (First Revision)" IS 10500: 1991 Edition 2.2, Bureau of Indian Standards, New Delhi.

Centre for Streamside Studies (CSS) (2000) "Environmental Impacts of Hardrock Mining in Eastern Washington" (Fact Sheet #8) College of Forest Resources and Ocean and Fishery Sciences, University of Washington, Seattle, WA.

Chatterjee, R.S., Bannerjee, D., Roy, J. and Bhattacharya, A.K. (1994) "Landsat TM data processing techniques for identifying and delineating environmental impacts of coal mining" ITC Journal 2:155–162.

Chica–Olmo, M., Rodriguez, F., Abarca, F., Rigol–Sanchez, J.P., deMiguel, E., Gomez, J.A., and Fernandez–Palacios, A. (2004) "Integrated remote sensing and GIS techniques for biogeochemical characterization of the Tinto–Odiel estuary system, SW Spain" Environmental Geology 45:834–842.

Choe, E., van der Meer, F., van Ruitenbeek, F., van der Werff, H., de Smeth, B. and Kim, K-W (2008) "Mapping of heavy metal pollution in stream sediments using combined geochemistry, field spectroscopy, and hyperspectral remote sensing: A case study of the Rodalquilar mining area, SE Spain" Remote Sensing of Environment 112:3222–3233.

Chon H–T and Hwang J–H (2000) "Geochemical Characteristics of the Acid Mine Drainage in the water system in the vicinity of the Dogye Coal Mine in Korea" Environmental Geochemistry and Health 22: 155–172.

Coal mining (2009) in *Encyclopædia Britannica*. Retrieved August 22, 2009, from Encyclopædia Britannica Online: www.britannica.com/EBchecked/topic/122975/coal–mining. Access date 15th September 2009.

Cotter, J. and Brigden, K. (2006) "Acid Mine Drainage: the case of the Lafayette mine, Rapu Rapu (Philippines)" Greenpeace Research Laboratories Technical Note 09/2006 downloaded from www.greenpeace.to/publications/acid–mine–drainage.pdf . Access date 17th November 2009.

da Silva, E.F., Patinha, C., Reis, P., Fonseca, E.C., Matos, J. X., Barrosinho, J. and Oliveira, J.M.S. (2006) "Interaction of acid mine drainage with waters and sediments at the Corona stream, Lousal mine (Iberian Pyrite Belt, Southern Portugal)" Environmental Geology 50:1001–1013.

Das Gupta, S. (1999) "Studies on vegetational and microbiological processes in coal mining affected areas" PhD Thesis, North Eastern Hill University, Shillong, Meghalaya, India.

Das Gupta, S., Tiwari, B.K. and Tripathi, R.S. (2002) "Coal mining in Jaintia hills, Meghalaya: An ecological perspective" *In:* Jaiñtia Hills, A Meghalaya Tribe: Its Environment, Land and People (Eds. P.M. Passah and A.S. Sarma). Reliance Publishing House, New Delhi. pp:121–128.

de Zwart, D. and Trivedi, R.C. (1994) "Manual on Integrated Water Quality Evaluation", Central Pollution Control Board, Delhi.

De, U. K. (2007) "Dynamics of coal and Limestone extraction in Meghalaya: a comparative Analysis". Presented in the International Econference on Issues in Development Economics: Environment, Culture & Society, organised by the University of Burdwan, West Bengal, India during 28–29 January, 2006 downloaded from www.mpra.ub.uni–muenchen.de/5678/1/MPRA_paper_5678.pdf. Access date 12th February 2009.

Definiens (2008a), Definiens Developer 7 Reference Book, Definiens AG, München, Germany.

Definiens (2008b), Definiens Developer 7 User Guide, Definiens AG, München, Germany.

Department of Agriculture (DoA) (2006) "Meghalaya soil profile" 3rd Edition, Department of Agriculture, Government of Meghalaya.

Department of Environment and Forests (DEF), Government of Meghalaya (2005) "State of the Environment Report, 2005 – Meghalaya", Shillong, Meghalaya.

Devereux, B.J., Amable, G.S. and Posada, C.C. (2004) "An efficient segmentation algorithm for landscape analysis" International Journal of Applied Earth Observation and Geoinformation 6:47-61.

Directorate of Economics and Statistics (DES) (2007) "District Level Statistics", Government of Meghalaya.

Directorate of Economics and Statistics (DES) (2009) "Statistical Handbook Meghalaya 2008–2009", Government of Meghalaya.

Drever, J.I. (1997) “The Geochemistry of Natural Waters – Surface and Groundwater Environments” 3rd Edition, Prentice Hall, Upper Saddle River, New Jersey, 436 pp.

Durieux, L., Lagabrielle, E. and Nelson, A. (2008) “A method for monitoring building construction in urban sprawl areas using object-based analysis of SPOT 5 images and existing GIS data” ISPRS Journal of Photogrammetry and Remote Sensing 63:399-408.

Eby, G.N. (2004) “Principles of Environmental Geochemistry” Brooks/Cole-Thomson Learning, California, U.S.A., 514pp.

ENVIS (2003) “Evolution of environmental management in mining industry in India” Monograph No.11, Environmental Information System (ENVIS) Centre on Mining Environment, Indian School of Mines, Dhanbad.

EPA (1995a) “Human health and environmental damages from mining and mineral processing wastes” Office of Solid Waste, U.S. Environmental Protection Agency.

EPA (1995b) “Profile of the Metal Mining Industry” (EPA/310–R–95–008) Office of Compliance, Office of Compliance and Assurance, U.S. Environmental Protection Agency.

Ezeigbo, H. I. and Ezeanyim, B. N. (1993) “Environmental pollution from coal mining activities in the Enugu area Anambka state Nigeria” Mine Water and the Environment 112:53–62

Garg, D.K., Goyal, R.N. and Agarwal, V.P. (1990) “Correlation among water quality parameters of ground water – Roorkee City” Indian Journal of Environmental Protection 10(5):355–359.

Geldenhuis, S. and Bell, F. G. (1998) “Acid mine drainage at a coal mine in the eastern Transvaal, South Africa” Environmental Geology 34 (2/3):234–242.

Gemici, Ü. (2008) “Evaluation of the water quality related to the acid mine drainage of an abandoned mercury mine (Alaşehir, Turkey)” Environmental Monitoring and Assessment 147:93–106.

Geological Survey of India (GSI) (1974) “Geology and Mineral Resources of the States of India Part IV – Arunachal Pradesh, Assam, Manipur, Meghalaya, Mizoram, Nagaland and Tripura”, Miscellaneous Publication No. 30.

Geological Survey of India (GSI) (1981) “Coalfields of India (Vol.1) – Coalfields of North Eastern India”, Bulletin Series A, No.45.

Ghose, M.K. and Sinha, D.K. (1990) “Surface water quality monitoring programme and status of water quality in coal mining areas” Indian Journal of Environmental Protection 10(6):459–461.

Grande, J.A., Borrego, J., Morales, J.A., and de la Torre M.L. (2003) “A description of how metal pollution occurs in the Tinto–Odiel rias (Huelva–Spain) through the application of cluster analysis” Marine Pollution Bulletin 46:475–480.

Gray, N. F. (1996) “Field assessment of acid mine drainage contamination in surface and ground water” Environmental Geology 27:358–361.

Gray, N. F. (1997) “Environmental impact and remediation of acid mine drainage: a management problem” Environmental Geology 30 (1/2):62–71.

Gray, N. F. (1998) “Acid mine drainage composition and the implications for its impact on lotic systems” Water Research 32(7):2122–2134.

Harries, J. (1997) Acid mine drainage in Australia: Its extent and potential future liability” Supervising Scientist Report 125, Supervising Scientist, Canberra, Australia.

Harris, D.L., Lottermoser, B.G., and Duchesne, J. (2003) “Ephemeral acid mine drainage at the Montalbion silver mine, north Queensland” Australian Journal of Earth Sciences 50:797–809.

Hounslow, A.W. (1995) “Water Quality Data Analysis and Interpretation” Lewis Publisher, U.S.A., 397 pp.

Jeeva, S. (2007) “Impact of mining on plant diversity and community structure of aquatic and terrestrial ecosystems of Jaiñtia Hills, Meghalaya” PhD Thesis, North Eastern Hill University, Shillong, Meghalaya, India.

Jennings, S.R., Neuman, D.R. and Blicker, P.S. (2008). “Acid Mine Drainage and Effects on Fish Health and Ecology: A Review”. Reclamation Research Group Publication, Bozeman, MT.

Jensen, J.R. (1996) “Introductory Digital Image Processing: A Remote Sensing Perspective” 2nd Edition, Prentice Hall, Upper Saddle River, New Jersey, 316 pp.

Johnson, D. B. and Hallberg, K. B. (2005) “Acid mine drainage remediation options: a review” Science of the Total Environment 338:3–14.

Kim, J–Y and Chon H–T (2001) “Pollution of a water course impacted by acid mine drainage in the Imgok creek of the Gangreung coalfield, Korea” Applied Geochemistry 16: 1387–1396.

Lee, C.G., Chon, H-T, and Jung, M.C. (2001) “Heavy metal contamination in the vicinity of the Daduk Au-Ag-Pb-Zn mine in Korea” Applied Geochemistry 16:1377-1386.

Lee, C.H. and Lee, H.K. (2001) “Hydrochemical monitoring and heavy metal contaminations at the Narim Mine Creek in the Sulcheon District, Republic of Korea” Environmental Geochemistry and Health 23:347–372.

Lillesand, T.M. and Kiefer, R.W. (2000) “Remote Sensing and Image Interpretation” 4th Edition, John Wiley and Sons (Asia) Pte. Ltd., Singapore, 696 pp.

Lottermoser, B.G., Ashley, P.M., and Lawie, D.C. (1999) “Environmental geochemistry of the Gulf Creek copper mine area, north–eastern New South Wales, Australia” Environmental Geology 39(1):61–74.

Lyngdoh, T. (1995) “Community dynamics and edaphic changes in relation to coal mining in Jaiñtia Hills, Meghalaya” PhD Thesis, North Eastern Hill University, Shillong, Meghalaya, India.

MacDonald D.D., Ingersoll, C.G. and Berger, T.A. (2000) “Development and evaluation of consensus-based sediment quality guidelines for freshwater ecosystems” Archives of Environmental Contamination and Toxicology 39:20–31.

McGinness, S. (1999) “Treatment of Acid Mine Drainage” Research Paper 99/10, Science and Environment Section, U.K. House of Commons Library.

Meghalaya State Pollution Control Board (MSPCB) (1997) “Environmental Impact of Coal Mining in Jaiñtia Hills District”, Shillong, Meghalaya.

Ministry of Coal, Govt. of India: http://coal.nic.in/abtcoal.htm. Access date 28th July 2009.

Moine, M., Puissant, A. and Malet, J.-P., (2009) “Detection of landslides from aerial and satellite images with a semi-automatic method. Application to the Barcelonnette basin (Alpes-de-Haute-Provence, France)” *In:* Malet, J.-P., Remaitre, A. and Bogaard, T. (Eds.), “Landslide Processes: from geomorphological mapping to dynamic modeling”. CERG, Strasbourg, France, pp.63-68.

Montero S., I.C., Brimhall, G.H., Alpers, C.N. and Swayze, G.A. (2005) “Characterization of waste rock associated with acid drainage at the Penn Mine, California, by ground-based visible to short-wave infrared reflectance spectroscopy assisted by digital mapping” Chemical Geology 215:453–472.

Mukherjee, K. N., Dutta, D., Chandra, D. and Singh, M. P. (1992) “Geochemistry of trace elements of Tertiary coals of India” International Journal of Coal Geology 20:99–113.

Murad, E. and Rojik, P. (2004) “Jarosite, schwertmannite, goethite, ferrihydrite and lepidocrocite: the legacy of coal and sulfide ore mining” SuperSoil 2004: 3rd Australian New Zealand Soils Conference, 5-9 December 2004, University of Sydney, Australia. Downloaded from http://www.regional.org.au/au/asssi/supersoil2004/s1/oral/1088_murade.htm. Access date 19th December 2009.

Nasipuri, P. and Chatterjee, A. (2009) "Land use around Maithon reservoir: a study from high-rsolution ASTER data" Current Science 97(10):25-27.

NBSSLUP (1996) Meghalaya Soils Map, National Bureau of Soil Survey and Land Use Planning (ICAR), Regional Centre, Jorhat.

NEERI (1987) "Laboratory Manual on Water Analysis" National Environmental Engineering Research Institute, Nagpur.

North Eastern Council (NEC), Ministry of Home Affairs (1991) "Compendium on the coal occurrences of North Eastern India Volume III D – Coalfields of Jaiñtia Hills, Meghalaya" prepared by Central Mine Planning and Design Institute Limited.

Olías, M., Nieto, J.M., Sarmiento, A.M., Cerón, J.C., and Cánovas, C.R. (2004) "Seasonal water quality variations in a river affected by acid mine drainage: the Odiel River (South West Spain)" Science of the Total Environment 333:267–281.

Pandey, P.K., Sharma, R., Roy, M. and Pandey, M. (2007) "Toxic mine drainage from Asia's biggest copper mine at Malanjkhand, India" Environmental Geochemistry and Health 29:237–248.

Payal, G. (2002) "Land system in Jaiñtia Hills District" *In:* Jaiñtia Hills, A Meghalaya Tribe: Its Environment, Land and People (Eds. P.M. Passah and A.S. Sarma). Reliance Publishing House, New Delhi. pp.23–27.

Peters, D.C. and Hauff, P.L. (2000) "Multispectral remote sensing to characterize mine waste (Cipple Creek and Goldfield, U.S.A.)" *In*: Remote Sensing for Site Characterization, Methods in Environmental Geology (Eds. Kuehn, F., King, T.V.V., Hoerig, B. and Peters, D.C.) Berlin: Springer-Verlag. pp.113–164.

Rahman, Md. Mahbub (1997) "Identification of Land use and Land cover using band ratio calculation technique" Department of Geoscience, Murray State University. Downloaded from www.murraystate.edu/qacd/cos/geo/gsc641/1997/rahman/ .Access date 11th August 2009.

Rajendran, B. P. G. S. and Thirunavukkarasu, A. (2007) "Analysis of uncertainties in visualizing remote sensing and spatial data" Proceedings of 5th International Symposium on Spatial Data Quality (ISSDQ 2007), International Institute of Geo-Information Science and Earth Observation (ITC), The Netherlands. Downloaded from www.itc.nl/ISSDQ2007/proceedings/Postersession/poovalinga.pdf. Access date 4th September 2009.

Rathore, C.S. and Wright, R. (1993) "Monitoring environmental impacts of surface coal mining" International Journal of Remote Sensing 14(6):1021-1042.

Rawat, N.S. and Singh, G. (1982) "Occurrence of Acid Mine Drainage in Northeastern Coal Mines of India" 1982 Symposium on Surface Mining Hydrology, Sedimentology and Reclamation, University of Kentucky, Lexington, Kentucky.

Repic, R. L., Lee, J. K., Mausel, P. W., Escobar, D. E. and Everitt, J. H. (1991) "An analysis of selected water parameters in surface coal mines using multispectral videography" Photogrammetric Engineering and Remote Sensing 57(12):1589–1592.

Robb, G. A. and Robinson, J. D. F. (1995) "Acid drainage from mines" The Geographical Journal 161(1):47–54.

Rukezo, G. (2003) "Drainage geochemistry of the Recsk–Lahoca Mining Area, Matra Mountains, Hungary" M.Sc. Thesis, International Institute for Geo-Information Science and Earth Observation (ITC), the Netherlands.

Sabins Jr., F.F. (1987) "Remote Sensing – Principles and Interpretation" 2nd Edition, W.H. Freeman and Co., New York, 449 pp.

Sadashivaiah C., Ramakrishnaiah, C.R. and Ranganna, G. (2008) "Hydrochemical analysis and Evaluation of groundwater quality in Tumkur Taluk, Karnataka State, India" International Journal of Environmental Research and Public Health 5(3):158–164.

Saha, A.K., Arora, M.K., Csaplovics, E. and Gupta, R.P. (2005) "Land cover classification using IRS LISS III image and DEM in a rugged terrain: A case study in Himalayas" Geocarto International 20(2):33–40.

Sainz, A., Grande, J.A., and de la Torre, M.L. (2003) "Odiel River, acid mine drainage and current characterisation by means of univariate analysis" Environment International 29:51–59.

Sainz, A., Grande, J.A., and de la Torre, M.L. (2005) "Application of a systemic approach to the study of pollution of the Tinto and Odiel rivers (Spain)" Environmental Monitoring and Assessment 102: 435–445

Salem, H.M. and El-Fouly, A.A. (2000) "Minerals reconnaissance at Saint Catherine Area, Southern Central Sinai, Egypt and their environmental impacts on human health" International Conference for Environmental Hazard Mitigation (ICEHM 2000), Cairo University, Egypt, pp 586–598.

Sares, M.A., Hauff, P.L., Peters, D.C., Coulter, D.W., Bird, D.A., Henderson III, F.B. and Prosh, E.C. (2004) "Characterizing Sources of Acid Rock Drainage and Resulting Water Quality Impacts Using Hyperspectral Remote Sensing – Examples from the Upper Arkansas River Basin, Colorado". Presented at the 2004 Advanced Integration of Geospatial Technologies in mining and Reclamation, December 7 – 9, 2004, Atlanta, GA.

Sarma, K. (2005) "Impacts of Coal Mining on Vegetation: A Case Study in Jaiñtia Hills District of Meghalaya, India" M.Sc. Thesis, International Institute for Geo-Information Science and Earth Observation (ITC), the Netherlands and Indian Institute of Remote Sensing (IIRS), India.

Sarmiento, A.M., Nieto, J.M., Olías, M., and Cánovas, C.R. (2009) "Hydrochemical characteristics and seasonal influence on the pollution by acid mine drainage in the Odiel river Basin (SW Spain)" Applied Geochemistry (24):697–714.

Sen, T.K., Nayak, D.C., Singh, R.S., Dubey, P.N., Maji, A.K., Chamuah, G.S. and Sehgal, J. (1997) "Pedology and edaphology of benchmark acid soils of north-eastern India" Journal of the Indian Society of Soil Science 43(4):782–790.

Shankar, U., Boral, L., Pandey, H.N. and Tripathi, R.S. (1993) "Degradation of land due to coal mining and its natural pattern" Current Science 65(9):680–686.

Sharma, Y.C., Aggarwal, P., and Singh, T.N. (2009) "Economic liabilities of environmental pollution by coal mining: Indian scenario" Environment, Development and Sustainability 11:589–599.

Singer, P.C. and Stumm, W. (1970) "Acidic Mine Drainage: The Rate–Determining Step" Science, New Series, Vol. 167(3921):1121–1123.

Singh, G. (1987) "Mine Water quality deterioration due to Acid Mine Drainage" International Journal of Mine Water, Vol. 6(1):49–61.

Singh, R.S., Maji, A.K., Sehgal, J. and Velayutham, M. (1999) "Soils of Meghalaya: Their kinds, distribution, characterization and interpretations for optimizing land use" NBSS Publication 52, National Bureau of Soil Survey and Land Use Planning (ICAR), Nagpur, 42pp.

Soe, M., Kyaw, T.A. and Takashima, I. (2005) "Application of Remote Sensing Techniques on Iron Oxide Detection from ASTER and Landsat Images of Tanintharyi Coastal Area, Myanmar"

Scientific and Technical Reports of Faculty of Engineering and Resource Science, Akita University 26:21-28.

Song, M., Civco D.L. and Hurd, J.D. (2005) "A competitive pixel-object approach for land cover classification" International Journal of Remote Sensing 26(22):4981–4997.

Suchiang, F. "The Jaiñtia Hills: Land, People and its Environment" *In:* Jaiñtia Hills, A Meghalaya Tribe: Its Environment, Land and People (Eds. P.M. Passah and A.S. Sarma). Reliance Publishing House, New Delhi. pp:17–21.

Swer, S. and Singh, O. P. (2003) "Coal mining impacting water quality and aquatic biodiversity in Jaiñtia Hills District of Meghalaya" ENVIS Bulletin Himalayan Ecology 11(2):26–33.

Swer, S. and Singh, O. P. (2004) "Status of water quality in coal mining areas of Meghalaya, India" In: Proceedings of the National Seminar on Environmental Engineering with special emphasis on Mining Environment, NSEEME–2004, Indian School of Mines, Dhanbad, 19–20 March 2004. (Eds. I. N. Sinha, M. K. Ghose and G. Singh).

The Constitution of India (COI), modified upto 1st December 2007, Ministry of Law and Justice, Government of India.

Tiwary, R.K. (2001) "Environmental impact of coal mining on water regime and its management" Water, Air, and Soil Pollution 132:185–199.

Tiwary, R.K. and Dhar, B.B. (1994) "Environmental pollution from coal mining activities in Damodar River Basin, India" Mine Water and the Environment 13:1-10.

Trinh, M.V., Duong, N.D. and Van Keulen, H. (2005) "Using Landsat images for studying land use dynamics and soil degradation – Case study in Tamduong District, Vinhphuc Province, Vietnam" International Journal of Geoinformatics 1(1):157–164.

Tutu, H., McCarthy, T.S., and Cukrowska, E. (2008) "The chemical characteristics of acid mine drainage with particular reference to sources, distribution and remediation: The Witwatersrand Basin, South Africa as a case study" Applied Geochemistry 23:3666–3684.

Vandeberg, G.S. (2003) "Identification and characterization of mining waste using Landsat Thematic Mapper imagery Cherokee County, Kansas" presented at the 2003 National Meeting of the American Society of Mining and Reclamation and the 9th Billings Land Reclamation Symposium, Billings, MT. Downloaded from http://dept.ca.uky.edu/asmr/W/Full%20Papers%202003/1329-Vandeberg.pdf . Access date 7th December, 2009.

Wangdi, T. (2004) "Importance of EIA in relation to Rat Hole Coal Mines of Meghalaya". Environmental Management Capacity Building Technical Assistance Project: Mining Sub–component. 14–25 June 2004 at UNSW, Sydney, Australia. Downloaded from www.mining.unsw.edu.au/KCMI/Presentations/ParticipantWangdi.pdf. Access date 22nd January 2009.

Williams, D.J., Bigham, J.M., Cravotta III, C.A., Traina, S.J., Anderson, J.E. and Lyon, J.G. (2002) "Assessing mine drainage pH from the color and spectral reflectance of chemical precipitates" Applied Geochemistry 17:1273–1286.

Yan, G., Mas, J-F., Maathuis, B.H.P., Xiangmin, Z. and Van Dijk, P.M. (2006) "Comparison of pixel-based and object-oriented image classification approaches—a case study in a coal fire area, Wuda, Inner Mongolia, China" International Journal of Remote Sensing 27(18):4039—4055.

Younger, P.L. (2001) "Mine water pollution in Scotland: nature, extent and preventative strategies" The Science of the Total Environment 265:309–326.

## Internet references:

http://en.wikipedia.org/wiki/Acid_mine_drainage
http://jaintia.nic.in – Jaiñtia Hills District official website
http://meghalaya.nic.in/naturalres/mineral.htm – Meghalaya State official website
http://meghalaya.nic.in/policy/mining%20policy%202009.pdf
http://megspcb.gov.in/PublicHearing.html – Meghalaya State Pollution Control Board website
http://www.cpcb.nic.in/Water_Quality_Criteria.php

## Appendix 1: Statement of coal production in Meghalaya, 1994-95 to 2008-09.

| | PRODUCTION ( in Metric tonnes) | | | |
|---|---|---|---|---|
| YEAR | JAIÑTIA HILLS | GARO HILLS | KHASI HILLS | TOTAL (Col.2+3+4) |
| 1994-1995 | 2389714 | 752831 | 122552 | 3265097 |
| 1995-1996 | 2159474 | 899173 | 188062 | 3246709 |
| 1996-1997 | 2273550 | 803315 | 164086 | 3240951 |
| 1997-1998 | 2514577 | 599454 | 119462 | 3233493 |
| 1998-1999 | 3246111 | 807118 | 184569 | 4237798 |
| 1999-2000 | 2935932 | 907011 | 217158 | 4060101 |
| 2000-2001 | 2839800 | 1017727 | 207375 | 4064902 |
| 2001-2002 | 3869323 | 977502 | 302529 | 5149354 |
| 2002-2003 | 3084393 | 916374 | 405140 | 4405907 |
| 2003-2004 | 3918037 | 1058440 | 462791 | 5439268 |
| 2004-2005 | 3610603 | 1101088 | 633499 | 5345190 |
| 2005-2006 | 3879738 | 1120525 | 565451 | 5565714 |
| 2006-2007 | 4045710 | 1174635 | 566307 | 5786652 |
| 2007-2008 | 4359878 | 1370263 | 811004 | 6541145 |
| 2008-2009 | 2890865 | 1594170 | 1003613 | 5488648 |

Source: DMR, Govt. of Meghalaya

## Appendix 2: Rule set used in OOC of the merged CARTOSAT-1/ RESOURCESAT-1 image of the entire study area

- classification_full
  - qt6
    - quadtree: 6 creating 'New Level'
  - background
    - unclassified with Mean Layer 1 = 0 at New Level: background
    - loop: background at New Level
  - clouds
    - unclassified with Mean Layer 9 = 1 at New Level: clouds
    - loop: clouds at New Level
  - shadows
    - unclassified with Mean Layer 9 = 3 at New Level: shadows
    - loop: shadows at New Level
  - river
    - unclassified with Mean Layer 5 <> 255 at New Level: rivers
    - loop: rivers at New Level
  - mrs7
    - at New Level: 7 [shape:0.2 compct.:0.1]
  - slope
    - unclassified with Mean Layer 6 > 16 at New Level: steep slope
    - loop: steep slope at New Level
  - vegetation
    - unclassified with Mean Layer 4 > -0.18 at New Level: vegetation1
    - loop: vegetation1 at New Level
  - vegetation
    - unclassified with Mean Layer 8 < 60 at New Level: vegetation2
    - loop: vegetation2 at New Level
  - barren
    - unclassified with Mean Layer 8 < 95 at New Level: barren & fallow land
    - loop: barren & fallow land at New Level
  - roads
    - unclassified with Length/Width > 2 at New Level: roads
    - loop: roads at New Level
  - roads
    - unclassified with Shape index > 1.9 at New Level: roads2
    - loop: roads2 at New Level
  - settlements
    - unclassified with Mean Layer 10 = 0 at New Level: settlements
    - loop: settlements at New Level
  - settlements
    - unclassified with GLCM Dissimilarity Layer 7 (all dir.) < 32 at New Level: settlements
    - loop: settlements at New Level
  - mines
    - unclassified at New Level: mines
    - mines at New Level

## Appendix 3: Daily rainfall in Jowai (June-October 2009)

| DATE | RAINFALL IN JOWAI (mm) | | | | |
|---|---|---|---|---|---|
| | **Jun 2009** | **Jul 2009** | **Aug 2009** | **Sep 2009** | **Oct 2009** |
| 1 | 31.75 | 157.48 | 2.79 | 2.79 | 0.00 |
| 2 | 83.82 | 114.30 | 8.89 | 0.00 | 0.00 |
| 3 | 0.00 | 81.02 | 21.08 | 0.00 | 0.00 |
| 4 | 0.00 | 58.16 | 6.60 | 0.00 | 0.00 |
| 5 | 0.00 | 17.52 | 0.00 | 4.06 | 2.54 |
| 6 | 36.83 | 10.16 | 0.00 | 2.54 | 23.36 |
| 7 | 3.81 | 7.87 | 5.58 | 33.02 | 17.01 |
| 8 | 0.00 | 11.68 | 3.04 | 0.00 | 56.89 |
| 9 | 0.00 | 7.62 | 4.31 | 3.55 | 161.54 |
| 10 | 0.00 | 12.70 | 2.79 | 0.00 | 4.32 |
| 11 | 7.62 | 12.19 | 18.03 | 9.14 | 2.29 |
| 12 | 8.89 | 3.55 | 61.46 | 6.35 | 0.00 |
| 13 | 172.72 | 0.00 | 29.21 | 0.00 | 0.00 |
| 14 | 9.14 | 0.00 | 60.45 | 13.20 | 0.00 |
| 15 | 2.03 | 5.08 | 45.21 | 0.00 | 0.00 |
| 16 | 0.00 | 12.70 | 34.03 | 0.00 | 6.10 |
| 17 | 0.00 | 4.57 | 40.89 | 2.54 | 0.00 |
| 18 | 0.00 | 4.06 | 57.65 | 0.00 | 0.00 |
| 19 | 0.00 | 0.00 | 35.56 | 15.74 | 0.00 |
| 20 | 8.89 | 2.03 | 67.31 | 26.92 | 0.00 |
| 21 | 4.31 | 0.00 | 21.08 | 4.57 | 0.00 |
| 22 | 0.00 | 10.66 | 93.72 | 0.00 | 0.00 |
| 23 | 7.11 | 4.82 | 12.44 | 37.08 | 0.00 |
| 24 | 16.51 | 31.75 | 93.72 | 14.73 | 0.00 |
| 25 | 2.54 | 0.00 | 9.90 | 8.89 | 0.00 |
| 26 | 0.25 | 5.84 | 0.00 | 0.00 | 0.00 |
| 27 | 2.51 | 3.04 | 23.36 | 0.00 | 0.00 |
| 28 | 5.33 | 56.38 | 7.36 | 0.00 | 0.00 |
| 29 | 73.23 | 48.51 | 0.00 | 0.00 | 0.00 |
| 30 | 82.55 | 63.24 | 17.78 | 0.00 | 0.00 |
| 31 | | 9.65 | 4.06 | | 0.00 |
| **TOTAL** | **214.40** | **756.58** | **788.30** | **185.12** | **274.05** |

Source: Meghalaya State Electricity Board

# Appendix 4: Sampling locations and field measurements for monsoon samples

(Coordinates are in UTM/WGS84 Zone 46N, electrical conductivity (EC) in µS/cm and temperature in °C)

| Location Code | X-coordinate | Y-coordinate | Altitude (m) | Water temperature | pH | EC |
|---|---|---|---|---|---|---|
| R1 | 430934.93 | 2810214.62 | 1296 | 21.4 | 3.8 | 126.8 |
| R2 | 434688.68 | 2809949.75 | 1234 | 21.7 | 3.3 | 402 |
| R3 | 435522.19 | 2811883.70 | 1225 | 21.7 | 3.5 | 264 |
| R4 | 453265.46 | 2813169.81 | 773 | 22.1 | 4.24 | 180 |
| R5 | 453615.51 | 2814239.07 | 753 | 23.4 | 3.55 | 335 |
| R6 | 437238.04 | 2819169.16 | 1168 | 23.8 | 6.5 | 29 |
| R7 | 433488.43 | 2818630.48 | 1270 | 24.3 | 6.3 | 14.6 |
| R8 | 432011.03 | 2818013.43 | 1304 | 26.9 | 6.2 | 19.1 |
| R9 | 430566.09 | 2817221.03 | 1339 | 28.6 | 4.4 | 53.5 |
| R10 | 435536.07 | 2817094.67 | 1228 | 22.3 | 6.73 | 18.9 |
| R11 | 440831.34 | 2814738.51 | 1223 | 22.4 | 4.35 | 53 |
| R12 | 441538.04 | 2813477.27 | 1147 | 24.5 | 3.62 | 248 |
| R13 | 438108.68 | 2813022.01 | 1204 | 23 | 3.39 | 392 |
| R14 | 440259.02 | 2810397.54 | 1211 | 22.9 | 5.96 | 10.2 |
| A1 | 434193.02 | 2809149.29 | 1287 | 21.3 | 7.4 | 14.5 |
| A2 | 430841.91 | 2811682.44 | 1303 | 21 | 7.02 | 6 |
| A3 | 430702.73 | 2817183.41 | 1322 | 26 | 4.15 | 42 |
| A4 | 441488.25 | 2813588.23 | 1150 | 23.9 | 4.2 | 36 |

## Appendix 5: Analytical results of monsoon water samples

(in mg/l except where indicated, BDL = Below Detectable Limits, NM = Not measured)

| Location Code | Turb (NTU) | DO | TDS | TSS | T H | Acid. | Alk. | Ca | Mg | Na | K | $Cl^-$ | $NO_3^-$ | $SO_4^{2-}$ | Fe | Zn | Pb | Cd | Cr | Cu | Mn |
|---|---|---|---|---|---|---|---|---|---|---|---|---|---|---|---|---|---|---|---|---|---|
| R1 | 0.7 | 5.8 | 113.4 | 10 | 20 | 30 | NM | 6 | 1.2 | 6 | 5 | 5 | 1.5 | 30.1 | 0.66 | 0.034 | BDL | BDL | 0.002 | BDL | 0.077 |
| R2 | 0.8 | 3.2 | 361.8 | 10 | 22 | 80 | NM | 9 | 0.5 | 7 | 8 | 4 | 1.75 | 100.1 | 4 | 0.22 | BDL | BDL | 0.002 | BDL | 0.093 |
| R3 | 2.9 | 4 | 190.08 | 5 | 18 | 60 | NM | 6 | 0.7 | 8 | 6 | 4 | 1.7 | 57.2 | 2.2 | 0.03 | BDL | BDL | 0.005 | BDL | 0.05 |
| R4 | 3.9 | 8.7 | 129.6 | 15 | 60 | 108 | NM | 2 | 14.5 | 7 | 5 | 5 | 1.9 | 89.2 | 1.6 | 0.16 | 0.02 | BDL | BDL | BDL | 0.14 |
| R5 | 3.8 | 9.44 | 241.2 | 20 | 52 | 90 | NM | 9 | 12.8 | 8 | 9 | 6 | 1.2 | 112 | 3.4 | 0.12 | 0.01 | BDL | BDL | BDL | 0.15 |
| R6 | 2.1 | 9.2 | 25.1 | 5 | 20 | NM | 12 | NIL | 3.1 | 5 | 3 | 9 | 1.8 | 6.6 | 0.64 | 0.02 | 0.01 | BDL | 0.003 | BDL | 0.06 |
| R7 | 2.1 | 8.7 | 12.7 | 10 | 6 | NM | 6 | NIL | 0.2 | 4 | 5 | 8 | 1.7 | 2.5 | 0.66 | 0.02 | 0.02 | BDL | 0.006 | BDL | 0.09 |
| R8 | 0.9 | 8 | 16.7 | 5 | 8 | NM | 0.8 | 2 | 0.7 | 7 | 4 | 7 | 1.6 | 1.3 | 0.74 | 0.03 | 0.01 | BDL | 0.008 | BDL | 0.04 |
| R9 | 1.3 | 8 | 47.2 | 5 | 16 | 16 | NM | 6 | 0.2 | 6 | 4 | 5 | 1.6 | 17.5 | 0.4 | 0.01 | 0.01 | BDL | 0.010 | BDL | 0.09 |
| R10 | 0.7 | 7.8 | 17 | 5 | 4 | NM | 8 | NIL | 1.6 | 5 | 6 | 9 | 1.3 | 6 | 0.22 | 0.006 | BDL | BDL | 0.010 | 0.001 | 0.04 |
| R11 | 0.8 | 7.2 | 47.7 | 15 | 8 | 20 | NM | 2 | 0.2 | 9 | 7 | 7 | 1.4 | 16 | 0.2 | BDL | BDL | BDL | 0.010 | BDL | 0.02 |
| R12 | 0.7 | 6.8 | 223.2 | 10 | 116 | 58 | NM | 2 | 23.5 | 6 | 6 | 8 | 1.6 | 85 | 0.36 | 0.06 | BDL | BDL | 0.010 | 0.002 | 0.12 |
| R13 | 0.3 | 6.6 | 352.8 | 10 | 56 | 74 | NM | 6 | 9.9 | 14 | 14 | 9 | 1.5 | 72 | 1.6 | 0.06 | 0.01 | BDL | 0.010 | BDL | 0.2 |
| R14 | 0.6 | 7.2 | 9.2 | 10 | 16 | NM | 4 | 6 | 0.24 | 2 | 3 | 6 | BDL | 33 | 0.2 | 0.004 | BDL | BDL | 0.010 | BDL | BDL |

**Key:**

Turb : Turbidity
DO : Dissolved oxygen
TDS : Total Dissolved Solids
TSS : Total Suspended Solids

T H : Total hardness
Acid. : Acidity
Alk. : Alkalinity

| **Element** | **Detection limit (mg/l)** |
|---|---|
| Zinc | 0.003 |
| Lead | 0.010 |
| Cadmium | 0.010 |
| Chromium | 0.001 |
| Copper | 0.001 |
| Manganese | 0.010 |
| Nickel | 0.030 |

## Appendix 6: Analytical results of monsoon sediment samples

(in mg/kg except where indicated, BDL = Below Detectable Limits)

| Location Code | Sb | As | Ba | Cd | Cr | Co | Cu | Fe (%) | Pb | Li | Mn | Ni | Zn |
|---|---|---|---|---|---|---|---|---|---|---|---|---|---|
| R1 | BDL | BDL | 13.7 | 1.2 | 21 | 2.9 | 14.4 | 2.41 | 9.9 | 7.7 | 64.5 | 12.3 | 22.4 |
| R2 | 0.1 | BDL | 7.4 | 1.1 | 16.7 | 1.7 | 13.2 | 2.51 | 9.5 | 4.1 | 53.3 | 4.8 | 14.6 |
| R3 | BDL | BDL | 7.8 | 0.6 | 13.5 | 1.2 | 8.3 | 1.05 | 7.7 | 3.8 | 27.7 | 5.3 | 14.6 |
| R5 | 0.6 | BDL | 7.7 | 1.7 | 29.7 | 2.5 | 18.9 | 4.38 | 9.3 | 4.4 | 86.3 | 7.1 | 26.5 |
| R9 | BDL | BDL | 6.2 | 1 | 19 | 3 | 11.8 | 2.03 | 6.6 | 3.4 | 100.4 | 7.2 | 20.3 |
| R11 | 0.1 | BDL | 8.8 | 1 | 19.9 | 1.8 | 16 | 1.96 | 9.4 | 4.1 | 48.3 | 6.8 | 22.4 |
| R12 | 0.4 | BDL | 26.6 | 1.1 | 23.2 | 4.9 | 23.5 | 2.49 | 11.5 | 9.4 | 110.1 | 11.1 | 41 |
| R13 | BDL | 7.1 | 4.6 | 1.1 | 29 | 1 | 14.5 | 2.69 | 7.8 | 2.3 | 32.9 | 2.9 | 15.6 |

| **Element** | **Detection limit (mg/l)** |
|---|---|
| Zinc | 0.003 |
| Lead | 0.010 |
| Cadmium | 0.010 |
| Chromium | 0.001 |
| Copper | 0.001 |
| Manganese | 0.010 |
| Nickel | 0.030 |

## Appendix 7: Sampling locations and field measurements for post-monsoon samples

(Coordinates are in UTM/WGS84 Zone 46N, electrical conductivity (EC) in µS/cm and temperature in °C)

| Location Code | X-coordinate | Y-coordinate | Altitude (m) | Water temperature | pH | EC |
|---|---|---|---|---|---|---|
| R1 | 430934.93 | 2810214.62 | 1296 | 23.6 | 3.8 | 103.6 |
| R2 | 434688.68 | 2809949.75 | 1234 | 24.3 | 2.74 | 623 |
| R3 | 435522.19 | 2811883.70 | 1225 | 22.5 | 3.21 | 265 |
| R4 | 453265.46 | 2813169.81 | 773 | 24.7 | 3.57 | 315 |
| R5 | 453615.51 | 2814239.07 | 753 | 26.1 | 3.08 | 542 |
| R6 | 437238.04 | 2819169.16 | 1168 | 25.3 | 5.45 | 29.7 |
| R7 | 433488.43 | 2818630.48 | 1270 | 20.3 | 6.2 | 12 |
| R8 | 432011.03 | 2818013.43 | 1304 | 27.3 | 6.22 | 26.2 |
| R9 | 430566.09 | 2817221.03 | 1339 | 21.8 | 4.25 | 41.6 |
| R10 | 435536.07 | 2817094.67 | 1228 | 21.9 | 5.58 | 17.8 |
| R11 | 440831.34 | 2814738.51 | 1223 | 22.1 | 4.62 | 37.4 |
| R12 | 441538.04 | 2813477.27 | 1147 | 23 | 3.56 | 188.3 |
| R13 | 438108.68 | 2813022.01 | 1204 | 21.5 | 3.11 | 299 |
| R14 | 440259.02 | 2810397.54 | 1211 | 26.2 | 5.78 | 6.5 |
| R15 | 435089.92 | 2816765.22 | 1207 | 22.6 | 5.7 | 16.6 |
| R16 | 435152.06 | 2816796.30 | 1202 | 22.9 | 5.65 | 14.6 |
| R17 | 435148.71 | 2816796.31 | 1198 | 22.4 | 5.85 | 13.3 |
| R18 | 450858.06 | 2814025.58 | 847 | 23.8 | 2.88 | 925 |
| R19 | 450307.66 | 2814730.80 | 914 | 26 | 3.48 | 210 |
| R20 | 446933.14 | 2813988.86 | 994 | 24.3 | 3.1 | 472 |
| R21 | 439949.94 | 2814749.20 | 1109 | 22.1 | 5.14 | 17.7 |
| R22 | 439689.74 | 2812037.21 | 1163 | 24.3 | 2.9 | 988 |
| R23 | 432428.77 | 2810032.30 | 1302 | 20.1 | 3.39 | 211 |
| R24 | 431491.25 | 2808962.85 | 1280 | 23.1 | 2.79 | 1143 |
| R25 | 429002.85 | 2813951.83 | 1351 | 21.7 | 5.93 | 41.5 |
| R26 | 445888.30 | 2819183.07 | 1133 | 20 | 5.46 | 19.7 |
| R27 | 431589.24 | 2816670.05 | 1297 | 19.9 | 4.42 | 45.4 |
| R28 | 429640.88 | 2815454.58 | 1231 | 23.2 | 3.84 | 125.4 |
| R29 | 430809.49 | 2811679.54 | 1301 | 24.6 | 6.24 | 9.4 |
| M1 | 436140.16 | 2809305.40 | 1291 | 21.8 | 3.91 | 37.3 |
| A1 | 434193.02 | 2809149.29 | 1287 | 23.1 | 5.93 | 19.9 |
| A2 | 430841.91 | 2811682.44 | 1303 | 24.5 | 6.2 | 9.1 |
| A3 | 430702.73 | 2817183.41 | 1322 | 20.8 | 4.82 | 29.8 |
| A4 | 441488.25 | 2813588.23 | 1150 | 23.4 | 5.5 | 29 |
| A5 | 437843.18 | 2819011.30 | 1140 | 23.1 | 5.98 | 20.6 |
| A6 | 450613.54 | 2814519.27 | 903 | 26.3 | 2.98 | 734 |
| A7 | 446930.97 | 2814287.86 | 1022 | 24.3 | 3.5 | 215 |

Appendix 7 contd…

| **Location Code** | **X-coordinate** | **Y-coordinate** | **Altitude (m)** | **Water temperature** | **pH** | **EC** |
|---|---|---|---|---|---|---|
| A8 | 430588.71 | 2817275.06 | 1328 | 20.8 | 4.9 | 26 |
| A9 | 441410.85 | 2814285.01 | 1167 | 25.2 | 4.48 | 9.2 |
| A10 | 439643.67 | 2812229.37 | 1170 | 21.2 | 3.14 | 469 |
| A11 | 439630.26 | 2812229.43 | 1168 | 23 | 2.87 | 1085 |
| A12 | 428945.60 | 2812951.75 | 1319 | 20 | 5.45 | 26.4 |

## Appendix 8: Analytical results of post-monsoon water samples

(in mg/l except where indicated, BDL = Below Detectable Limits, NM = Not measured)

| Location Code | Turb (NTU) | DO | TDS | TSS | T H | Acid. | Alk. | Ca | Mg | Na | K | $Cl^-$ | $NO_3^-$ | $SO_4^{2-}$ | Fe | Zn | Pb | Cd | Cr | Cu | Mn | Ni |
|---|---|---|---|---|---|---|---|---|---|---|---|---|---|---|---|---|---|---|---|---|---|---|
| R1 | 2.3 | N M | 72.1 | 15 | 20 | 26 | NIL | 2 | 4.4 | 11 | 7 | 8 | 2 | 44.91 | 1 | BDL | BDL | BDL | BDL | BDL | 0.11 | BDL |
| R2 | 1.3 | N M | 568 | 10 | 117.1 | 79 | NIL | 60 | 13.9 | 7 | 4 | 70 | 3.9 | 127.41 | 9.8 | 0.03 | BDL | BDL | BDL | BDL | 0.13 | BDL |
| R3 | 5.7 | N M | 219.7 | 15 | 13 | 38 | NIL | 4 | 2.2 | 11 | 5 | 5 | 2.5 | 46.62 | 3 | BDL | BDL | BDL | BDL | BDL | 0.05 | BDL |
| R4 | 0.4 | N M | 272 | 5 | 94 | 32 | NIL | 24 | 17 | 15 | 11 | 3 | 2.5 | 190.42 | 2.1 | 0.13 | 0.01 | BDL | BDL | 0.01 | 0.31 | 0.03 |
| R5 | 0.6 | N M | 497 | 5 | 95 | 68 | NIL | 27 | 16.5 | 13 | 11 | 5 | 2.7 | 190 | 1.1 | 0.18 | 0.01 | BDL | 0.01 | BDL | 0.28 | 0.05 |
| R6 | 0.7 | 7.2 | 24.2 | 5 | 7 | NIL | 16 | 2 | 1.2 | 7 | 4 | 2 | 1.2 | 14.23 | 0.68 | BDL | BDL | BDL | BDL | BDL | 0.03 | BDL |
| R7 | 0.6 | N M | 13.1 | 5 | 5 | NIL | 14 | 1 | 1 | 8 | 5 | 3 | 1.2 | 16.16 | 1.8 | BDL | BDL | BDL | BDL | BDL | 0.03 | BDL |
| R8 | 2.7 | N M | 24.2 | 10 | 6.1 | 6 | 16 | 0.05 | 1.5 | 6 | 3 | 3 | 1 | 4.07 | 1.1 | 0.05 | BDL | BDL | BDL | BDL | 0.1 | BDL |
| R9 | 0.8 | N M | 37.1 | 5 | 8 | 12 | 8 | 2 | 1.5 | 8 | 6 | 4 | 3 | 21.83 | 0.78 | 0.05 | BDL | BDL | BDL | BDL | 0.1 | BDL |
| R10 | 6.2 | N M | 12.7 | 10 | 13 | 6 | 18 | 1 | 2.9 | 11 | 7 | 8 | 1.5 | 17.15 | 0.88 | BDL | BDL | BDL | BDL | BDL | 0.02 | BDL |
| R11 | 0.9 | 7.2 | 29.2 | 5 | 6 | 12 | 4 | 1 | 1.2 | 9 | 5 | 6 | 1.2 | 21.82 | 1.36 | BDL | BDL | BDL | BDL | BDL | 0.03 | BDL |
| R12 | 0.9 | 6.2 | 167.1 | 5 | 35 | 36 | NIL | 15 | 4.9 | 7 | 4 | 6 | 1.2 | 76.79 | 0.9 | 0.04 | BDL | BDL | BDL | BDL | 0.1 | 0.03 |
| R13 | 1.9 | N M | 262 | 10 | 24 | 51 | NIL | 14 | 2.4 | 11 | 6 | 7 | 2.3 | 66.38 | 4.6 | 0.01 | BDL | BDL | BDL | BDL | 0.06 | BDL |
| R14 | 3.3 | N M | 16.7 | 15 | 7 | 6 | 12 | 1 | 1.5 | 7 | 3 | 5 | 1 | 11.38 | 0.48 | BDL | BDL | BDL | BDL | BDL | BDL | BDL |
| R15 | 0.3 | 7.2 | 17.2 | 5 | 8 | 6 | 14 | 2 | 1.5 | 8 | 7 | 4 | 1 | 22.72 | 0.1 | BDL | BDL | BDL | BDL | BDL | 0.03 | BDL |
| R16 | 0.3 | 7.8 | 16.7 | 5 | 7 | 6 | 12 | 2 | 1.2 | 10 | 6 | 4 | 1.1 | 26.69 | 0.88 | 0.08 | BDL | BDL | BDL | BDL | 0.02 | BDL |
| R17 | 0.4 | 7.6 | 11.1 | 5 | 6 | 4 | 13 | 1 | 1.2 | 9 | 6 | 3 | 1.2 | 22.52 | 0.7 | BDL | BDL | BDL | BDL | BDL | 0.02 | BDL |
| R18 | 0.6 | 8 | 789.2 | 10 | 140.1 | 160 | NIL | 138 | 0.5 | 12 | 7 | 10 | 3.5 | 383.56 | 8.4 | 0.16 | 0.02 | BDL | 0.01 | 0.02 | 0.22 | 0.10 |
| R19 | 0.4 | 7.4 | 187 | 5 | 58 | 32 | NIL | 15 | 10.4 | 14 | 11 | 39 | 2.1 | 82.21 | 1.2 | 0.03 | 0.01 | BDL | BDL | BDL | 0.46 | 0.02 |
| R20 | 0.5 | 7.2 | 397 | 5 | 182.1 | 48 | NIL | 91 | 22.1 | 9 | 5 | 37 | 3.3 | 295.12 | 7 | 0.03 | 0.01 | BDL | BDL | 0.01 | 0.17 | 0.04 |
| R21 | 0.8 | 7.2 | 16.2 | 5 | 5 | 6 | 12 | 1 | 1 | 8 | 5 | 5 | 1 | 15.96 | 0.28 | BDL | BDL | BDL | BDL | BDL | 0.03 | BDL |
| R22 | 4.2 | N M | 872 | 15 | 177 | 306 | NIL | 107 | 17 | 14 | 6 | 62 | 4.6 | 293.10 | 13 | 0.19 | 0.01 | BDL | 0.01 | 0.02 | 0.12 | 0.14 |
| R23 | 1.4 | N M | 182 | 5 | 35 | 28 | NIL | 11 | 5.8 | 11 | 7 | 6 | 2.2 | 87.15 | 1.8 | 0.05 | BDL | BDL | BDL | BDL | 0.10 | BDL |

Appendix 8 contd…

| Location Code | Turb (NTU) | DO | TDS | TSS | T H | Acid. | Alk. | Ca | Mg | Na | K | $Cl^-$ | $NO_3^-$ | $SO_4^{2-}$ | Fe | Zn | Pb | Cd | Cr | Cu | Mn | Ni |
|---|---|---|---|---|---|---|---|---|---|---|---|---|---|---|---|---|---|---|---|---|---|---|
| R24 | 2.1 | N M | 998 | 10 | 271 | 386 | NIL | 205 | 16 | 17 | 8 | 91 | 4.5 | 486.30 | 11.4 | 0.1 | 0.01 | BDL | 0.01 | 0.01 | 0.29 | 0.07 |
| R25 | 1.7 | N M | 38.2 | 10 | 31 | 6 | 24 | 7 | 5.8 | 5 | 2 | 5 | 1.7 | 16.65 | 1 | 0.01 | BDL | BDL | BDL | BDL | 0.01 | BDL |
| R26 | 1.7 | N M | 20.1 | 5 | 20 | 6 | 16 | 1 | 4.6 | 10 | 8 | 3 | 1.4 | 28.74 | 1.26 | BDL | BDL | BDL | BDL | BDL | 0.01 | BDL |
| R27 | 1.7 | N M | 40 | 10 | 31 | 8 | 16 | 5 | 6.3 | 9 | 3 | 8 | 1.2 | 39.43 | 0.9 | BDL | BDL | BDL | BDL | BDL | 0.08 | BDL |
| R28 | 2.8 | N M | 98.2 | 10 | 34 | 36 | NIL | 3 | 7.5 | 10 | 5 | 8 | 1.5 | 53.57 | 0.84 | BDL | BDL | BDL | BDL | BDL | 0.26 | BDL |
| R29 | 1.1 | N M | 8 | 5 | 3 | 8 | 12 | 0.05 | 0.7 | 9 | 3 | 2 | 1.2 | 10.91 | 0.9 | BDL | BDL | BDL | BDL | BDL | BDL | BDL |
| M1 | 3.3 | N M | 41.2 | 15 | 16.1 | 20 | NIL | 4 | 2.9 | 11 | 6 | 4 | 1.5 | 34.65 | 0.52 | 0.02 | BDL | BDL | BDL | BDL | 0.03 | 0.01 |

**Key:**

Turb : Turbidity
DO : Dissolved oxygen
TDS : Total Dissolved Solids
TSS : Total Suspended Solids

T H : Total hardness
Acid. : Acidity
Alk. : Alkalinity

| Element | Detection limit (mg/l) |
|---|---|
| Zinc | 0.003 |
| Lead | 0.010 |
| Cadmium | 0.010 |
| Chromium | 0.001 |
| Copper | 0.001 |
| Manganese | 0.010 |
| Nickel | 0.030 |

## Appendix 9: Analytical results of post-monsoon sediment samples

(in mg/kg except where indicated, BDL = Below Detectable Limits)

| Location Code | Sb | As | Ba | Cd | Cr | Co | Cu | Fe (%) | Pb | Li | Mn | Ni | Zn |
|---|---|---|---|---|---|---|---|---|---|---|---|---|---|
| R 02 | BDL | BDL | 8.8 | 1 | 18.7 | 1.7 | 10.5 | 2.189 | 8.5 | 6 | 43.3 | 6.8 | 14.9 |
| R 03 | BDL | BDL | 7.3 | 0.8 | 20.9 | 1.2 | 19.8 | 1.484 | 7.9 | 3.5 | 34.1 | 5.1 | 26.1 |
| R 05 | 0.1 | 15.9 | 8.3 | 2.2 | 37.2 | 2.6 | 20.3 | 4.962 | 9.5 | BDL | 113 | 5.9 | 31.3 |
| R 06 | BDL | BDL | 34.5 | 0.7 | 11 | 5.1 | 9.3 | 1.3 | 6.1 | 17.3 | 150.8 | 5.3 | 33.9 |
| R 09 | BDL | BDL | 8.6 | 0.9 | 1 | 1.5 | 11.5 | 1.3 | 15.1 | 4.5 | 26.7 | 4.7 | 12.5 |
| R 11 | BDL | BDL | 10.1 | 0.4 | 5.7 | 1.7 | 7.5 | 0.606 | 4.4 | 3.2 | 35.1 | 3 | 15.4 |
| R 12 | BDL | BDL | 3.2 | 0.3 | 7.2 | 0.5 | 4.1 | 0.526 | 1.9 | 1.7 | 6.7 | 1.9 | 6.2 |
| R 13 | BDL | BDL | 16.6 | 1.4 | 35.8 | 2.2 | 12.9 | 2.519 | 11.3 | 10.7 | 46.7 | 10.4 | 20 |
| R 15 | BDL | BDL | 29.2 | 0.9 | 13.5 | 6.7 | 20.2 | 1.326 | 9.8 | 7.2 | 81.5 | 11.4 | 37.3 |
| R 17 | BDL | BDL | 27.9 | 0.8 | 8.6 | 4.8 | 13.5 | 1.162 | 9.6 | 12.1 | 142.4 | 4.8 | 34 |
| R 18 | BDL | BDL | 8.8 | 2.2 | 26.4 | 1.5 | 18.6 | 5.069 | 6.8 | 3.4 | 71.4 | 3.5 | 23.7 |
| R 19 | BDL | BDL | 12.4 | 1 | 30 | 1.8 | 10.2 | 1.735 | 7.9 | 5.9 | 35.3 | 5.1 | 13.5 |
| R 20 | BDL | BDL | 2.2 | 1.1 | 11.7 | 0.4 | 5.5 | 1.291 | 2.5 | 1.1 | 12.4 | 1.2 | 4.1 |
| R 21 | BDL | BDL | 53.5 | 1.4 | 16.2 | 7.2 | 18.4 | 2.1 | 8.8 | 14.1 | 149.9 | 9 | 53.6 |
| R 22 | BDL | BDL | 13.1 | 1.6 | 32.6 | 1.6 | 28.5 | 4.038 | 14.3 | 7.2 | 56.2 | 6.1 | 28 |
| R 23 | BDL | BDL | 16.7 | 1.4 | 29.7 | 2.6 | 19.5 | 3.133 | 12.8 | 8.3 | 68.3 | 10.5 | 23.4 |
| R 24 | BDL | 8.7 | 8.4 | 1.6 | 21.1 | 1.7 | 17.2 | 3.793 | 9 | 4.8 | 66.4 | 5.8 | 16.2 |
| R 26 | BDL | BDL | 27.4 | 0.8 | 16 | 4.7 | 9.7 | 1.315 | 9.5 | 14.3 | 119.6 | 6.4 | 30.3 |
| R 27 | BDL | BDL | 21.3 | 1.1 | 44.6 | 5.4 | 35 | 1.829 | 22 | 9.5 | 97.9 | 13.2 | 59.8 |
| R 29 | BDL | BDL | 19.8 | 0.8 | 26.2 | 3.4 | 13.5 | 1.461 | 8.9 | 8.7 | 42 | 14 | 21.6 |
| A 06 | 0.5 | BDL | 19.7 | 2.8 | 81.4 | 3.3 | 24.8 | 5.2 | 13.7 | 12.4 | 85.5 | 11.7 | 32 |
| A 11 | BDL | BDL | 15.3 | 1.9 | 37.2 | 2.4 | 22.1 | 4.151 | 14.8 | 11.1 | 66.9 | 9.3 | 21 |

| **Element** | **Detection limit (mg/l)** |
|---|---|
| Zinc | 0.003 |
| Lead | 0.010 |
| Cadmium | 0.010 |
| Chromium | 0.001 |
| Copper | 0.001 |
| Manganese | 0.010 |
| Nickel | 0.030 |

# Appendix 10: Specification for Drinking Water (BIS: 10500 - 1991)

### Bureau of Indian Standard
### Specification for Drinking Water (BIS: 10500 - 1991)

| Sl. No. | Substance or characteristic | Requirement Desirable limit | Undesirable effect outside the desirable | Permissible limit in the absence of alternate source | Remarks |
|---|---|---|---|---|---|
| | **Essential Characteristic** | | | | |
| 1. | Turbidity (NTU) Max | 5 | Above 5, consumer acceptance decreases | 10 | - |
| 2. | pH value | 6.5 to 8.5 | Beyond this range the water will after the mucous membrane and/or water supply system | No relaxation | - |
| 3. | Total Hardness (mg/L) CaCO3 | 300 | Encrustation in water supply structure and adverse effects on domestic use | 600 | - |
| 4. | Iron (mg/L Fe) Max | 0.3 | Beyond this limit taste/appearance are affected; has adverse effects on domestic uses and water supply structure and promotes iron bacteria | 1.0 | - |
| 5. | Chlorides 250 (mg/L, Cl) Max | 250 | Beyond effects outside the desirable limit | 1000 | - |
| | **Desirable Characteristics** | | | | |
| 6. | Dissolved solids mg/L. Max | 500 | Beyond this, palatability decreases and may cause gastrointestinal irritation. | 2000 | - |
| 7. | Calcium (mg/L, Ca) Max. | 75 | Encrustation in water supply structure and adverse effects on domestic use. | 200 | - |
| 8. | Magnesium (mg/L, Mg) Max | 30 | Encrustation in water supply structure and adverse effects on domestic use. | 100 | - |
| 9. | Copper (mg/L, Cu) Max | 0.05 | Astringent taste dis-coloration and corrosion of pipes fittings and utensils | 1.5 | - |

| **Sl. No.** | **Substance or characteristic** | **Requirement Desirable limit** | **Undesirable effect outside the desirable** | **Permissible limit in the absence of alternate source** | **Remarks** |
|---|---|---|---|---|---|
| | | | will be caused beyond this. | | |
| 10. | Manganese (mg/L, Mn) Max | 0.1 | Beyond this limit taste/appearance are affected, has adverse effect on domestic use and water supply structure | 0.3 | - |
| 11. | Sulphate (mg/L, SO4) Max. | 200 | Beyond this causes gastro intestinal irritation when magnesium or sodium are present | 400 | May be extended upto 400 provided magnesium (as Mg) does not exceed 30 |
| 12. | Nitrate (mg/L, NO3) Max. | 45 | Beyond this methaemo-globinemia takes place. | 100 | - |
| 13. | Cadmium (mg/L, Cd) Max | 0.01 | Beyond this the water becomes toxic | No Relaxation. | To be tested when pollution is suspected |
| 14. | Lead (mg/L Pb) Max. | 0.05 | Beyond this the water becomes toxic | No Relaxation | To be tested when pollution is suspected |
| 15. | Zinc (mg/L, Zn) Max. | 5 | Beyond this limit it can cause astringent taste and an opalescence in water | 15 | To be tested when pollution is suspected |
| 16. | Chromium (mg/L, Cr6+ | 0.05 | May be carcinogenic above this limit | - | - |